From subduction to extension: The tectonomagmatic evolution of the Bulgarian Rhodopes

Inaugural-Dissertation

zur

Erlangung des Doktorgrades

der Mathematisch-Naturwissenschaftlichen Fakultät

der Universität zu Köln

vorgelegt von

Maria Kirchenbaur

aus Nördlingen

– Köln 2012 –

Prüfer:	Prof. Dr. C. Münker
Zweiter Referent:	Prof. Dr. N. Froitzheim
Vorsitzender der Prüfungskommission:	Prof. Dr. T. Mansfeldt
Beisitzer:	Dr. D. Hezel
Tag der mündlichen Prüfung:	25.01.2012

- Contents -

- Abstract -

The Bulgarian Rhodopes provide an unique opportunity to study processes that take place at convergent continental margins. Ophiolite complexes incorporated in the Rhodopean nappe stack as well as the directly overlying post-collisional volcanism allow the investigation of processes from subduction, collision, and subsequent lithospheric extension triggering lithospheric mantle melting that leads to volcanism in collisional orogens.

The first part of this dissertation investigates the high-pressure (HP) metamorphic history of ophiolite complexes incorporated in different levels of the Rhodopean nappe stack. The determination of the exact timing of these HP events as well as the characterization of the metamorphic protoliths is crucial for reconstructing the geodynamic evolution of the Rhodopes. In this context, the Lu-Hf isotope system has already been proven useful to date HP mineral assemblages in other Alpine units and was therefore applied to four eclogite samples from different units of the nappe stack of the Bulgarian Rhodopes. The Lu-Hf garnet dating revealed a metamorphic event during the Cretaceous (~ 126 Ma) affecting the highest nappe unit investigated (Upper Allochthon) and an Eocene event (~ 43 Ma) for the Middle Allochthon. These results provide evidence for two separate subduction events in the Rhodopes, in support of previous findings. Moreover, thrusting of the Middle over the Lower Allochthon can be narrowed down to the time span 42 - 34 Ma.

The second and third part of this dissertation provides an extensive dataset on the post-collisional volcanism in the Bulgarian Rhodopes as well as for arc lavas from Santorini, which are used as a comparative suite throughout the text. The Bulgarian post-collisional volcanism is characterized by a high magnitude of incompatible trace element enrichment, which is particularly shown by its affiliation to the high-K and shoshonite series. Two petrogenetic models that were previously proposed for the generation of high-K magmas involve the melting of ancient, enriched lithospheric mantle sources (*single-stage model*) or melting triggered by young refertilization of subduction-related components derived from subducted sediments or oceanic crust (*multi-stage model*). These two models are tested for the Bulgarian K-rich rocks, based on new major, trace element and Sr-Nd-Hf-Pb isotope compositions. The *single-stage model* is evaluated by Sr-Nd isotope modelling assuming the presence of ancient lithospheric mantle domains whereas the *multi-stage model* is assessed by comparing compositions of the Bulgarian lavas with those of lavas from Santorini. Santorini Island lavas are thought to sample the current trace element and isotope inventory of the long-

lived Aegean subduction-zone system. This northward facing system has been active since late Jurassic/Early Cretaceous and was potentially involved in refertilizing the mantle sources of the Bulgarian lavas. In addition to the Bulgarian lavas, we present new major, trace element and Sr-Nd-Hf-Pb isotope data for Santorini. Modelling of Sr-Nd isotope compositions of the Bulgarian lavas argues for a young (Meso- to Cenozoic) source enrichment. Therefore, *single-stage* models involving melting of ancient, > 1 Ga old lithospheric mantle can be confidently ruled out, in agreement with tectonic models for the region. The enriched isotope signatures found in the Bulgarian lavas, coupled with a pronounced enrichment in incompatible elements, instead indicate mantle refertilization by subduction components similar to presently subducted continent-derived sediments. Notably, the Bulgarian lavas record a predominant influx of fluid-like subduction components when compared to the Santorini lavas. Collectively, the data presented for the Bulgarian lavas are thus clearly in favour of a *multi-stage model*.

The last part of this dissertation focuses on extended high-field-strength element (HFSE) systematics in the Bulgarian and Santorini lavas. The extended HFSE (Nb, Ta, Zr, Hf, W, Mo, and Sb) are of particular interest in magmatic rocks as their fractionations hint towards specific residual phases in their source regions, such as rutile, allanite, zircon, micas, and sulphides. Tungsten, Sb, and Mo are of particular importance in that they are mobilized in subduction zones by fluids and melts at distinct temperatures and redox conditions and might provide important insights into the conditions and magnitude of source enrichment. However, no significant fractionation of the HFSE ratios (Nb/Ta, Zr/Hf, Zr/Nb) compared to MORB were observed in the Santorini lavas and in the Bulgarian high-K rocks. An influence on the HFSE budget by residual phases like allanite, zircon, or phengite can be largely ruled out, whereas trace amounts of residual rutile in the source may account for the slightly lower Nb/Ta observed in the dataset than expected for bulk sediment addition. The W-Sb-Mo systematics of both sample suites furthermore confirm the predominance of subducted sediments on the incompatible trace element budget, which is dominated by more fluid-like components in the Bulgarian lavas and melt-like in the Santorini lavas.

- *Zusammenfassung* -

Der bulgarische Teil der Rhodopen stellt eine einzigartige Möglichkeit dar, Prozesse an konvergenten Kontinentalrändern zu studieren. Ophiolithkomplexe, die in den Deckenkomplex der Rhodopen mit eingegliedert wurden, sowie der direkt aufliegende post-kollisionale Vulkanismus ermöglichen die Untersuchung der Prozesse von Subduktion, Kollision bis hin zur anschließenden Lithosphärenextension, die das Aufschmelzen des lithosphärischen Mantels bedingt und damit zu Vulkanismus in kollisionalen Orogenen führt.

Der erste Teil der vorliegenden Dissertation befasst sich mit der Hochdruck-metamorphen Entwicklung der Ophiolithkomplexe, die sich in unterschiedlichen Stockwerken des Rhodopen-Deckenstapels befinden. Die genaue zeitliche Bestimmung dieser Hochdruck-Ereignisse als auch die Charakterisierung der metamorphen Ausgangsgesteine ist entscheidend für die Rekonstruktion der geodynamischen Entwicklung der Rhodopen. In diesem Zusammenhang hat sich das Lu-Hf Isotopensystem als äußerst nützlich erwiesen, um Hochdruck-Mineralparagenesen in anderen alpinen Einheiten zu datieren. Es wurde deshalb an vier Eklogitproben aus unterschiedlichen Einheiten des Deckenstapels der bulgarischen Rhodopen angewandt. Die Lu-Hf Granatdatierung bestimmte ein metamorphes Ereignis während der Kreide (~ 126 Ma) für die oberste studierte Einheit (Oberes Allochthon) und eine weitere Hochdruckmetamorphose während des Eozäns (~ 43 Ma) für das Mittlere Allochthon. Diese Resultate belegen und unterstützen schon vorhandene Forschungsergebnisse, dass zwei unterschiedliche Subduktionsereignisse in den Rhodopen stattgefunden haben. Des weiteren kann die Überschiebung des Mittleren über das Untere Allochthon auf eine Zeitspanne zwischen 42 – 34 Ma eingegrenzt werden.

Der zweite und dritte Teil dieser Dissertation stellt einen extensiven Datensatz über den post-kollisionalen Vulkanismus in den bulgarischen Rhodopen sowie für Inselbogenvulkanite von Santorin bereit. Letztere werden als Vergleichssuite für die bulgarischen Vulkanite benutzt. Der bulgarische post-kollisionale Vulkanismus zeichnet sich insbesondere durch einen hohen Anreicherungsgrad von inkompatiblen Spurenelementen aus, was vor allem durch die Zugehörigkeit zu Kalium-angereicherten ('high-K') und shoshonitischen Vulkanitserien Ausdruck findet. Für die Entstehung von Kalium-reichen Vulkaniten werden gegenwärtig zwei unterschiedliche petrogenetische Modelle vorgeschlagen: partielles Aufschmelzen von altem lithosphärischem Mantel (*Einstufenmodell*) oder die Entstehung aus Mantelquellen, die durch ein junges Subduktionsereignis mit Sediment- oder ozeanischer Krustenkomponenten

angereichert wurden (*Mehrstufenmodell*). Diese beiden Modelle werden anhand neuer Haupt- und Spurenelementdaten und Sr-Nd-Hf-Pb Isotopenzusammensetzungen für die bulgarischen Vulkanite getestet. Die Validität des *Einstufenmodells* wird anhand von Sr-Nd Isotopenmodellierungen beurteilt, wohingegen das Mehrstufenmodell durch den Vergleich mit den Santorin-Laven evaluiert wird, welche das gegenwärtige Endglied der ägäischen Subduktionszone darstellen und für die neue Haupt-, Spurenelement und Sr-Nd-Hf-Pb Isotopendaten vorgestellt werden. Die nach Norden einfallende ägäische Subduktionszone ist seit dem späten Jura/frühe Kreide aktiv und war potenziell auch schon an der Quellenanreicherung der bulgarischen Laven beteiligt. Die Modellierung von Sr-Nd Isotopenzusammensetzungen für die bulgarischen Laven ergibt ein eher junges Alter für die Quellenanreicherung (meso- bis känozoisch). Deshalb kann das *Einstufenmodell*, bei dem alter lithosphärischer Mantel aufschmilzt (älter als 1 Ga), ausgeschlossen werden, was auch mit gängigen tektonischen Modellen für die Region übereinstimmt. Die angereicherten Isotopensignaturen der bulgarischen Laven, sowie deren ausgeprägte Anreicherung inkompatibler Spurenelemente sprechen für die Anreicherung der Magmenquellen durch klastische Sedimente, wie sie gegenwärtig in der Ägäis subduziert werden. Im Vergleich mit den Santorin-Laven sind die bulgarischen Magemenquellen eher durch Fluide angereichert worden. Zusammenfassend sprechen diese Resultate eindeutig für ein *Mehrstufenmodell* für die Entstehung der bulgarischen K-reichen Vulkanite.

Der letzte Teil dieser Dissertation konzentriert sich auf die erweiterte Gruppe der high-field-strength Elemente (HFSE) in den bulgarischen und Santorin Laven. Die erweiterten HFSE (Nb, Ta, Zr, Hf, W, Mo, und Sb) sind besonders in magmatischen Systemen von Bedeutung, da ihre jeweiligen Fraktionierungen auf spezifische residuale Phasen in den Mantelquellen hinweisen, wie zum Beispiel Rutil, Allanit, Zirkon, Glimmer und Sulfide. Wolfram, Sb und Mo sind besonders interessant, da diese Elemente in Subduktionszonen durch Fluide und Schmelzen bei unterschiedlichen Temperaturen und Redox-Bedingungen mobilisiert werden und dadurch Einblicke in den Grad und die Bedingungen der Quellenanreicherungen geben können. In dieser Studie konnte keine signifikante Fraktionierung der HFS Elementverhältnissen wie Nb/Ta, Zr/Hf und Zr/Nb in Bezug auf MORB in den bulgarischen und Santorin Laven festgestellt werden. Deshalb kann ein Einfluss residualer Phasen wie Allanit, Zirkon oder Phengit auf das HFSE Budget ausgeschlossen werden. Geringe Mengen an residualem Rutil in den subduzierten Sedimenten können dahingegen für die geringfügig niedrigere Nb/Ta verantwortlich sein, die so nicht erwartet würden für eine Quellenanreicherung durch Rutil-freie Sedimente. Desweiteren untermauert die W-Sb-Mo

Systematik der beiden Probensuiten die Dominanz von subduzierten Sedimenten auf das Budget der inkompatiblen Elemente, welche in den bulgarischen Laven hauptsächlich durch Fluide und in den Santorin Laven durch Schmelzen angereichert wurden.

- Chapter 1 -

Introduction

Subduction and subsequent collision of oceanic and continental crust can be confidently considered as THE most important surface-shaping geological process currently occurring on Earth. Collisional orogens or their deeply eroded roots are found throughout most of Earth's history and on all continents (*Pan-African orogeny*, Black *et al*., 1979; *Variscan orogeny*, Tait *et al*., 1997; *Alpine orogeny*, Dewey *et al*., 1973; Schmid *et al*., 1996), providing evidence that the amalgamation of continental crust fragments is a major process contributing to the assemblage of larger continents. However, collisional orogens are also the site where crust is destroyed and eventually in part recycled back into the mantle (von Huene & Scholl, 1991; Plank & Langmuir, 1998; Clift & Vannucchi, 2003).

Subduction of oceanic crust precedes the collision of two crustal fragments. Remnants of the consumed oceanic crust can subsequently mark the suture zone between the two continental slivers, either as entire ophiolite complexes or as dismembered meta-basaltic sequences (e.g., *Vardar suture*; Ricou *et al*., 1998; *Oman ophiolite*; Coleman, 1981, Hacker, 1994; *Appalachian ophiolites*; Dewey & Bird, 1971; *Isua ophiolite complex*; Furnes *et al*., 2007). Three different types of collisional orogens can be distinguished, based on the lithologies involved. (1) The collision of two island arcs *(arc-arc collision)*, as it presently occurs, for example, in Central Japan (*Izu collision zone*; Tani *et al*., 2010). (2) *Arc-continent collision* as it is currently found in Taiwan (collision of the Luzon arc with the Asian continent; e.g., Teng, 1990; Wang *et al*., 2004), and (3) *continent-continent collision* (e.g., *Caledonides*; Griffin *et al*., 1985; *Alpine-Himalayan belt*; Dewey *et al*., 1973; McKenzie, 1978; Schmid *et al*., 1996). Whereas types (1) and (2) are important types for the growth and destruction of continental crust throughout Earth's history, continent-continent collisions, however, might be considered as the processes creating the most extensive mountain belts (e.g., *Caledonides*; Smith, 1984; *Alpine-Himalayan mountain belt*; Stampfli & Borel, 2002). Being typical of the last step of the Wilson cycle, such collisions create supercontinents like Pangea or Gondwana (Wilson, 1966). Hence, the detailed investigation of convergent margins and collisional orogens is of paramount importance in understanding processes and timescales

that ultimately lead to the amalgamation of larger continents.

Generally, the tectonic processes in collisional orogens are dominated by nappe stacking along low-angle detachment faults, thrusting and faulting in the early stages of collision, whereas late- to post-collision is mainly dominated by unroofing, extension and graben formation (Bott, 1976; Lister *et al*., 1986), as well as post-collisional volcanism (Turner *et al*., 1996; Miller *et al*., 1999; Aldanmaz *et al*., 2000; Sajona *et al*, 2000; Williams *et al*., 2004). Furthermore, collisional orogens are also the place where continental crust can be subducted to ultra-high pressure (UHP) conditions into the mantle, (~ 150 – 200 km) before being exhumed (e.g., *Dora Maira Massif*, Chopin, 1984; *Caledonides*, Smith, 1984; *Kokchetav Massif,* Sobolev & Shatsky, 1990; *Dabieshan*, Xu *et al*., 1992). The subsequent orogenic collapse of the piled up nappe stacks triggers melting in the mantle, while mafic underplating further facilitates extension and the exhumation of deeper portions of the nappe stack, which can afterwards be exposed in metamorphic core complexes (e.g., *D'Entrecasteaux Islands*, Davies & Warren, 1988; *Colorado River, USA*, Lister & Davis, 1989; *Arabian-Nubian Shield*, Blasband *et al*., 2000).

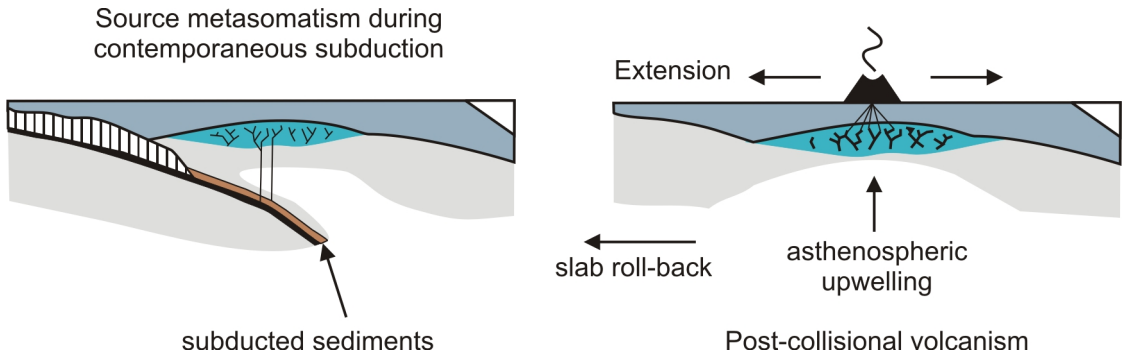

Fig. 1.1: Schematic sketch of the assumed genetic evolution of post-collisional volcanism, where (a) the lithospheric mantle source is enriched by subduction, and (b) at a later stage melts in response to a change in the P-T regime of the mantle source.

Commonly, magmatism in collisional orogens is virtually entirely controlled by syn- to late-stage tectonic processes, i.e., lithospheric thickening, crustal heating and orogenic collapse. Combined with lithospheric thinning and asthenospheric upwelling, orogenic collapse might lead to extensive lithospheric mantle melting in some collisional orogens (e.g., *Tibet*; Turner *et al*., 1996, Williams *et al*., 2004). The ensuing volcanism is thus described as "post-collisional". Bulk compositions of post-collisional volcanic rocks are usually bimodally distributed, i.e., predominantly basaltic and rhyolitic/phonolitic compositions (e.g., Gill,

1981). Although major element compositions of volcanic rocks in post-collisional settings can be highly variable, a common feature is the strong enrichment in incompatible elements and the large abundance of high-K or shoshonitic series (e.g., Peccerillo & Taylor, 1976; Turner *et al*., 1996; Williams *et al*., 2004; Wang *et al*., 2004; Prelević *et al*., 2005; Gao *et al*., 2009; Conticelli *et al*., 2009b). From early studies on, geochemical or experimental, it has been recognized that the petrogenesis of these rock suites involves hybrid mantle sources, with contributions from asthenospheric, lithospheric and crustal sources (Tatsumi & Koyagushi, 1986; Meen, 1987; Foley, 1992; Edgar & Vukadinovic, 1992; Conceição & Green, 2004; Holbig & Grove, 2008). Typically, the subduction-related geochemical characteristics of post-collisional lavas are interpreted to be inherited from the mantle source that has been metasomatized during prior subduction (*multi-stage model*; see Fig. 1.1a; e.g., Hawkesworth & Vollmer, 1979). However, highly enriched isotope signatures (e.g., Sr-Nd-Pb) recorded in post-collisional and high-K lavas were also interpreted to result from melting of an ancient lithospheric mantle (*single-stage model*; e.g., Varne, 1985; McKenzie, 1989; Turner *et al*., 1996). This model implies that the mantle sources of post-collisional lavas may have been modified by subduction zone processes up to hundreds of million years before being tapped by decompression melting or astenospheric upwelling (see Fig. 1.1b).

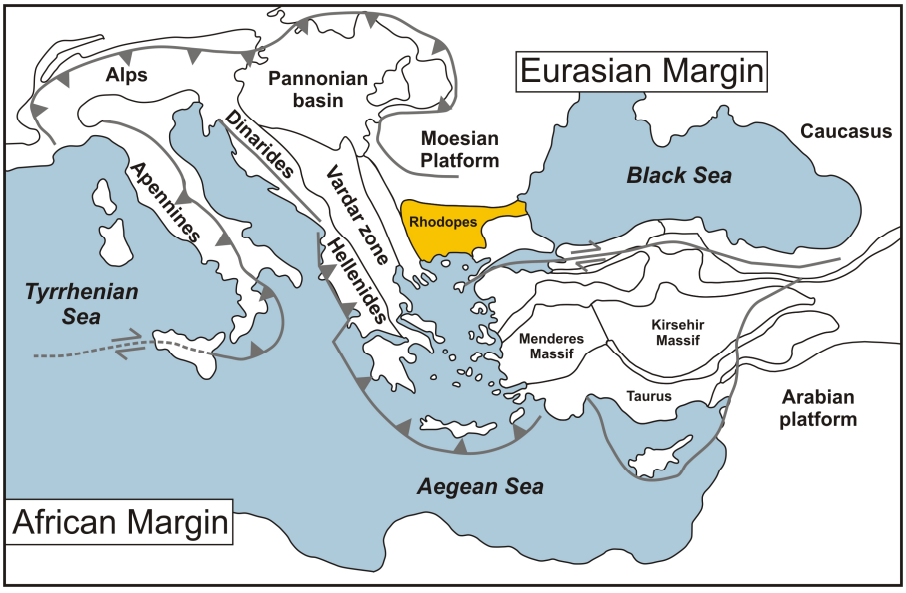

Fig. 1.2.:
Overview of the Mediterranean with its most important tectonic structures (grey lines) and the location of the Rhodopes in relation to other major crustal fragments and accretionary units. Modified after Barr *et al*. (1999), and Wortel & Spakman (2000).

The Eastern Mediterranean and especially the Rhodopes provide an excellent opportunity to study tectono-magmatic processes along convergent margins and in collisional orogens. During the Alpine orogeny, microcontinents as well as ocean basins formerly located between Africa and Eurasia, were assembled along the Eurasian continental margin, thus forming a large-scale thrust wedge (Ricou *et al*., 1998; van Hinsbergen *et al*., 2005; Nagel *et al*., 2011). Moreover, subduction is still ongoing south of the Hellenic Trench (see Fig. 1.2) with currently active subduction zone volcanism located in the Aegean island-arc (*Santorini*; Zellmer et al., 2000; Bailey et al., 2009; *Kos*; Pe-Piper & Moulton, 2008). The Rhodopes, located in Bulgaria and northern Greece, represent a key area within the Alpine-Himalayan orogenic belt in the Eastern Mediterranean in that they form the link between the Hellenides and the Eurasian continental margin (see Fig. 1.2). They consist of a nappe stack of continental and oceanic units, where the deeper nappe units are exposed in large scale extensional domes. These domes, or metamorphic core complexes, are directly overlain by volcanoclastic sediments and post-collisional lavas. The direct succession of subduction, nappe stacking, lithospheric extension, and subsequent volcanism allows a detailed investigation of the kinematics of subduction-exhumation and mass fluxes triggering volcanism in post-collisional settings.

Within the Rhodopes, ophiolite complexes have been reported that occur at different levels of the nappe stack (Kolčeva *et al*., 1986; Liati & Mposkos, 1991). They might constitute potential remnants of an ancient subduction zone: either remnants of subducted oceanic crust or, alternatively, mafic associations within continental crust that were subducted together with continental lithologies. In the Rhodopes, especially in the Greek part, eclogites have previously been reported and described by Kolčeva *et al*. (1986), Liati & Seidel (1996), Liati & Gebauer (1999), and Liati (2005). Increasing attention has been drawn on these assemblages after the discovery of ultra-high-pressure (UHP) assemblages in these rocks as well as in metapelites and mélange zone rocks (microdiamonds, coesite relics, and supersilicic garnet; Mposkos & Kostopoulos, 2001; Perraki *et al*., 2006; Cornelius, 2008; Schmidt *et al*., 2010; Janák *et al*., 2011). Although petrological and geochronological investigations were carried out on eclogites and ultramafic rocks in separate studies (e.g., Liati & Seidel, 1996; Wawrzenitz & Mposkos, 1997), no combination of both together with a detailed geochemical investigation was performed so far.

Within this thesis work, eclogites from two different structural entities of the Rhodopean nappe stack (Middle and Upper Allochthon; after Janák *et al*., 2011) were sampled and a systematic petrological, geochemical, and geochronological study was carried

out, which is here reported in **Chapter 2**. The petrological study involving pseudosection calculations, carried out in collaboration with Dr. Jan Pleuger and Dr. Thorsten Nagel, revealed peak metamorphic conditions of ca. 700°C/20-25 kbar. In order to provide a robust time constraint on this high-pressure (HP) metamorphic event, Lu-Hf and Sm-Nd garnet chronometry were applied during the course of this thesis, which is particularly useful to date peak metamorphism in garnet-bearing mafic lithologies (Vance & O'Nions, 1990; Duchêne *et al*., 1997; Scherer *et al*., 1997, 2000; Blichert-Toft & Frei, 2001; Thöni, 2002; Lapen *et al*., 2003; Lagos *et al*., 2007; Herwartz *et al*., 2008, 2011). By employing these techniques, two HP metamorphic events could be revealed: (1) a Lower Cretaceous event in the Upper Allochthon (126.0 ± 1.7 Ma) and (2) an Eocene event in the Middle Allochthon of the Rhodopes (44.6 ± 0.7 Ma; 43.5 ± 0.4 Ma; 42.8 ± 0.5 Ma). In combination with whole-rock trace element and Hf-Nd isotope analyses it could furthermore been shown, that the eclogites do not represent remnants of an oceanic basin. They rather exhibit island-arc basaltic trace element signatures and hence were most likely subducted intimately associated with the continental units. Based on these results, a new interpretation for the crustal architecture of the Rhodopes is proposed in **Chapter 2,** showing that subduction and high-P metamorphism are younger than previously assumed, in support of the view that the Rhodopes represent a large scale tectonic window that exposes the deepest nappe units of the Hellenides (see also Nagel *et al*., 2011).

The post-collisional volcanism in the Rhodopes directly post-dates the exhumation of the metamorphic core complexes (e.g., Bonev *et al*., 2006) and is later followed by alkaline intraplate volcanism (28 – 26 Ma; Marchev *et al*., 1998a, b). This provides a unique opportunity to study the change in mantle composition beneath the Rhodopes, following collision and nappe emplacement. In contrast to island-arc volcanism, where the K-enrichment is attributed to the breakdown of hydrous minerals in the subducting oceanic slabs with increasing depth of the Benioff zone beneath the island-arc ('K-h relationship'; Dickinson & Hatherton, 1967; Schmidt & Poli, 1998), there are two different models proposed for source enrichment in post-collisional settings (*single-stage* and *multi-stage*; see Fig. 1.1 and explanation in text). The Bulgarian post-collisional rocks and the currently active Aegean island-arc are connected by the same subduction zone, which is active since at least the Late Jurassic (van Hinsbergen *et al*., 2005), and involved compositionally similar sediments in the source refertilization of both sample suites. This genetic relationship consequently permits the evaluation of both models.

In **Chapter 3** the petrogenetic evolution of the Bulgarian post-collisional lavas is thus tested using an extensive data set of major and trace element concentrations as well as Sr-Nd-Hf-Pb isotope compositions, all measured during the course of this thesis work. The *single-stage model* is evaluated by comparing the Sr-Nd isotope compositions of Bulgarian lavas with modelled compositions of putative ancient lithospheric domains. As alternative, the *multi-stage model* is assessed by comparing compositions of the Bulgarian lavas with those of calc-alkaline lavas from Santorini (Aegean arc) that originate from presently active subduction zone processes. In addition to the Bulgarian lavas, **Chapter 3** therefore includes new major, trace element and Sr-Nd-Hf-Pb isotope data for lavas from Santorini. These are evaluated together with literature data to infer the mode of source enrichment in the Aegean realm.

The Bulgarian lavas exhibit an unusually broad range from medium-K to high-K and shoshonitic compositions, exhibiting radiogenic $^{87}Sr/^{86}Sr$ (0.706 – 0.709), and unradiogenic εNd (-5.7 to -1.9) and εHf isotope signatures (-3 to +3). The trace element and isotope budget of the lavas clearly mirrors mantle source processes as it was apparently well-buffered against shallow level assimilation as documented by major element and Sr-Nd isotope systematics. Modelling of these Sr-Nd isotope compositions of the Bulgarian lavas argues for a young (Meso- to Cenozoic) source enrichment. Therefore *single-stage* models involving melting of ancient, > 1 Ga old lithospheric mantle can be confidentially ruled out, in agreement with tectonic models for the region. The enriched isotope signatures together with a pronounced enrichment of incompatible elements rather indicate mantle refertilization by subduction zone processes closely related in time to eruption of the lavas. The subduction components are similar to those present in the sources of Santorini lavas, involving large amounts of continent-derived sediments. Collectively, the data presented for the Bulgarian lavas are therefore clearly in favour of a *multi-stage model*.

Trace element analyses carried out via quadrupole-ICPMS on the Bulgarian lavas in **Chapter 3** suggest high concentrations of the high-field-strength elements (HFSE). The group of HFSE comprises elements with a high charge/size ratio like Nb, Ta, Zr, and Hf and also elements like W, Sb, Mo that are defined as "extended" HFSE group. High-field-strength elements are of particular interest in magmatic systems, as e.g., Nb-Ta and Zr-Hf are considered geochemical twins and display similar compatibility during mantle melting. However, recent work has shown that the silicate portion of the Earth is depleted in Nb with respect to Ta, leading to subchondritic Nb/Ta (< 20) in the mantle and the crust (see Fig. 1.3a; Münker *et al*., 2003). Several hypothesis have been proposed to explain this so-called 'Nb-

paradox': (1) a hidden reservoir with high Nb/Ta (Rudnick *et al*., 2000; Kamber & Collerson, 2000), (2) the preferential partitioning of Nb in the core during the conditions of core formation (Wade & Wood, 2001), (3) collisional erosion of a high Nb/Ta protocrust (e.g., O'Neill & Palme, 2008), and (4) an inherited feature from distinct groups of carbonaceous chondrites (CV group, Münker *et al*., 2003). Most recently it has been proposed that up to 30 % of the 'missing Nb' may potentially be stored in the sublithospheric mantle owing to widespread carbonatite metasomatism (high Nb/Ta) recorded in the sources of continental basalts (Pfänder *et al*., 2011).

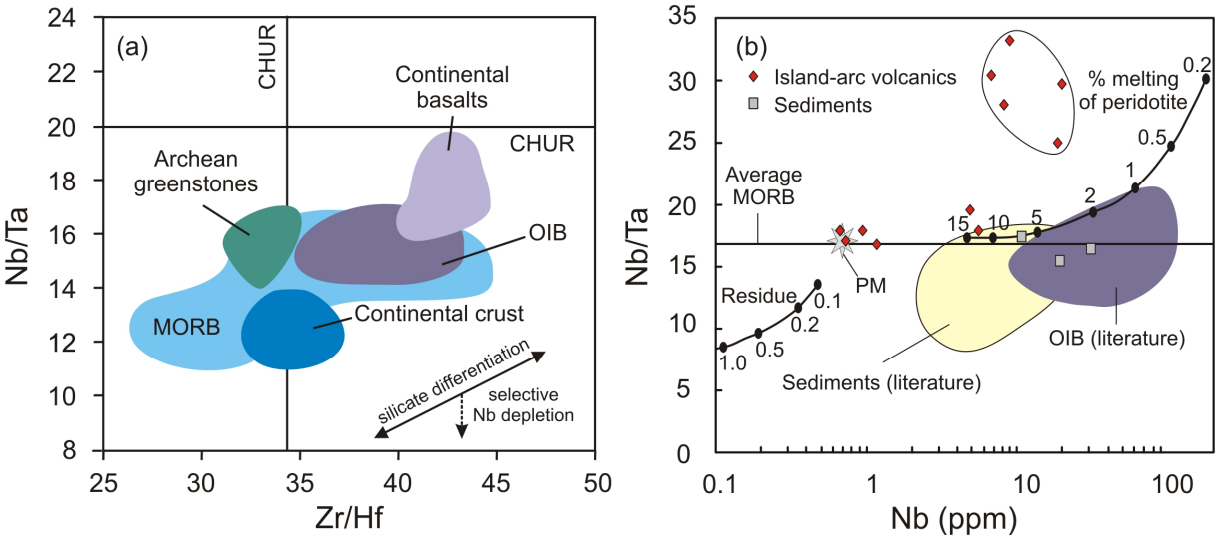

Fig. 1.3.:
(a) Major terrestrial silicate reservoirs in Nb/Ta - Zr/Hf space (modified after Münker *et al*., 2003), illustrating the subchondritic Nb/Ta of all reservoirs.
(b) Nb/Ta vs. Nb concentration modified after Stolz *et al*., 1996; some high-K island-arc basalts from Indonesia show Nb/Ta up to 33, which suggests that these lavas might tap a high Nb-Ta source in the mantle.

K-rich lavas are of particular interest in this respect, as they might tap mantle reservoirs with elevated Nb/Ta ratios. Stolz *et al*. (1996) reported HFSE data for K-rich rocks from Indonesia using spark source mass spectrometry (SSMS), yielding Nb/Ta of up to 33 (see Fig. 1.3b), suggesting that such potassic rocks might tap a high-Nb/Ta source in the upper mantle. The Bulgarian lavas are uniquely suited to test this hypothesis in that the entire spectrum of K-enrichment found elsewhere in subduction zone systems is present in the sample suite. The HFSE patterns of Bulgarian lavas can subsequently be compared to the island-arc lavas of Santorini that represent the youngest volcanic suite of the Aegean subduction system. Furthermore, the extended HFSE W, Mo, and Sb are important proxies for the sediment flux in subduction zones due to their high concentrations in terrigeneous and pelagic sediments and their mobility in subduction zone fluids and hydrothermal systems (see

König *et al*., 2008). Different mobilities of W, Mo, and Sb at reducing or oxidizing conditions further enables to place constraints on redox conditions during slab dehydration and melting.

In **Chapter 4** the first high-precision measurements of the HFSE and W for mafic K-rich volcanic rocks are reported. The analyses were carried out via isotope dilution and multi-collector-ICPMS. Although concentrations of the HFSE are consistently high, no significant fractionations of Nb/Ta and Zr/Hf were observed, compositions of the samples rather overlap with values found for MORB (Büchl *et al*., 2002). The group of absarokites, however, displays near chondritic Nb-Ta ratios (~ 20; Münker *et al*., 2003), which can be attributed to the fractionation of phlogopite and does not mirror source processes. Employing HFSE ratios like Zr/Nb, $^{176}Lu/^{177}Hf$, and Zr/Hf in combination with the Hf isotope compositions reported in **Chapter 3** confirms a strong source overprint by sediment-derived melts, controlling the elemental budgets of all HFSE. HFSE ratios indicative for significant fractionation by residual phases like rutile (Nb/Ta), zircon (Zr/Hf) or allanite (Nb/La) rule out any major control of such phases on the Nb-Ta-Zr-Hf budget of the K-rich rocks.

The elemental budget of the extended HFSE (W, Mo, Sb) is stronger enriched in the Bulgarian K-rich lavas than in the Santorini lavas, while both suites are considerably enriched compared to intra-oceanic island arcs (e.g., König *et al*., 2008; 2010). Whereas the W, Sb, and Mo budgets in the Bulgarian lavas are primarily controlled by dehydration of the slab and sediments (Sb) and mobilization from subducted terrigenous sediments by partial melts (W, Mo), the W budget in the Santorini lavas is dominated by hydrous sediment-melts. Small amounts of residual rutile might buffer the W budget to a small degree, which is the cause for the slightly lower W/Th of the Santorini lavas compared to MORB. A relative mobility order during sediment-melt mediated source overprint of Th > W > Ba > Nb was established, which is in contrast to fluid-dominated intra-oceanic island-arcs, where Ba has been shown to be more mobile than W. The difference is possibly caused by residual phengite in the subducted sediments. The Sb and Mo budget in the Santorini lavas is primarily controlled by the sediment-derived melts, which is less efficient than fluid-mobilization as recorded for the Bulgarian lavas, resulting in the mobility order W > Mo > Sb. Altogether, the W-Mo-Sb systematics of both sample suites argue for a source overprint by terrigeneous sediments rather than pelagic clays, which is in contrast to other island-arcs with low W/Mo like the Solomon Islands or Tonga.

Collectively, the high precision HFSE data reported in **Chapter 4** provide no evidence for a volumetrically important high Nb/Ta reservoir in the sources of the Mediterranean high-K magmas. However, the extended HFSE systematic of the K-rich rocks emphasize the

exceptionally high magnitude of incompatible element enrichment compared to other island-arcs, owing to selective source enrichment by sediment-derived melts.

- Chapter 2 -

Timing of high-pressure metamorphic events in the Bulgarian Rhodopes from Lu-Hf garnet geochronology

2.1. Introduction

The convergence between Africa and the Eurasian continent since the Jurassic led to the closure of the Tethyan realm in a protracted succession of subduction and collision events involving several micro-plates (Stampfli & Borel, 2002; van Hinsbergen *et al*., 2005). In this context, rock units of both oceanic and continental affinity were subducted and metamorphosed at high-pressure (HP) and even ultra-high pressure (UHP) conditions (e.g., Gebauer *et al*., 1997; Mposkos & Kostopoulos, 2001), and subsequently they were exhumed and incorporated into the evolving Alpine orogen. Constraining the exact timing of these events as well as characterization of the protoliths involved is crucial for reconstructing the geodynamic evolution of the Eastern Mediterranean realm. The Rhodopes, which are exposed in Southern Bulgaria and Northern Greece (Fig. 2.1, 2.2), are a key locality to understand the succession of HP events in the eastern Mediterranean as they represent the link between the Hellenic-Dinaric thrust belt and the Eurasian continental margin.

In the Rhodopes, evidence for the presence of deeply subducted oceanic and continental fragments reaching up to UHP conditions has been discovered in eclogites, metapelites and mélange-zone rocks (Mposkos & Kostopoulos, 2001; Perraki *et al*., 2006; Cornelius, 2008; Schmidt *et al*., 2010; Janák *et al*., 2011). However, only limited geochronological and geochemical data for the eclogite-facies rocks are available so far and the results are inconsistent. Based on zircon dating, Liati (2005) postulated four episodes of HP to UHP metamorphism whereas Krenn *et al*. (2010) argue that UHP metamorphism was confined to ca. 180 Ma, followed by decompression.

In the last two decades, direct dating of HP metamorphic events in Alpine or older metamorphic rocks has been improved by the application of the Lu-Hf (and Sm-Nd) geochronometers to metamorphic garnet (e.g., Vance & O'Nions, 1990; Duchêne *et al*., 1997; Amato *et al*., 1999; Scherer *et al*., 1997, 2000; Blichert-Toft & Frei, 2001; Thöni, 2002;

Lapen *et al*., 2003; Lagos *et al*., 2007; Herwartz *et al*., 2008, 2011; Smit *et al*., 2010). The major advantages of this approach are: (1) high Lu/Hf (and Sm/Nd) ratios in garnet, (2) the additional information from initial Hf-Nd isotope compositions about the nature of the protolith and (3) the fact that garnet ages can be tied to specific P-T conditions. New analytical approaches (e.g., Lagos *et al*., 2007) also allow the selective digestion of garnet, thus minimizing effects of inclusions that are in isotopic disequilibrium with the host garnet.

In this study, we present Lu-Hf and Sm-Nd isotope data for whole rocks and omphacite/garnet mineral separates for four eclogite samples from two different tectonic units of the Bulgarian Rhodopes. These data are complemented by element profiles of garnet obtained by LA-ICP-MS and electron microprobe, whole rock major and trace element analyses and are furthermore combined with petrological observations and phase diagram calculations. The results lead to a fundamental tectonic re-interpretation of the Rhodopes as the most internal portion of the Hellenides rather than an independent older orogen.

2.2. Geological overview

The Rhodopes are tectonically sandwiched between the Hellenic-Dinaric thrust belt in the southwest and the Eurasian continental margin, including the Balkanides, to the North (Fig. 2.1). To the south, the Rhodopes extend into Greece and are partially covered by the Aegean Sea. The present study focuses on the Bulgarian part of the Rhodopes, which is built of several metamorphic thrust units that were re-structured by intense extension in the Eocene and Miocene (e.g., Burg *et al*., 1996; Kilias *et al*., 1999; Krohe & Mposkos, 2002; Bonev *et al*., 2006; Pleuger *et al*., 2011). The extensive nomenclature for individual, local units so far lacks a consistent classification scheme. Here, we follow the approach of Janák *et al*. (2011), referring to four large superunits: the Lower, Middle, Upper, and Uppermost Allochthon (Fig. 2.1, 2.2). The nomenclature introduced by Janák *et al*. (2011) also allows a direct tectonic correlation between the Rhodopes in the strict sense and the Serbo-Macedonian Massif further southwest. A short description of the respective units along with the most important available geochronological data is given in Table 2.1.

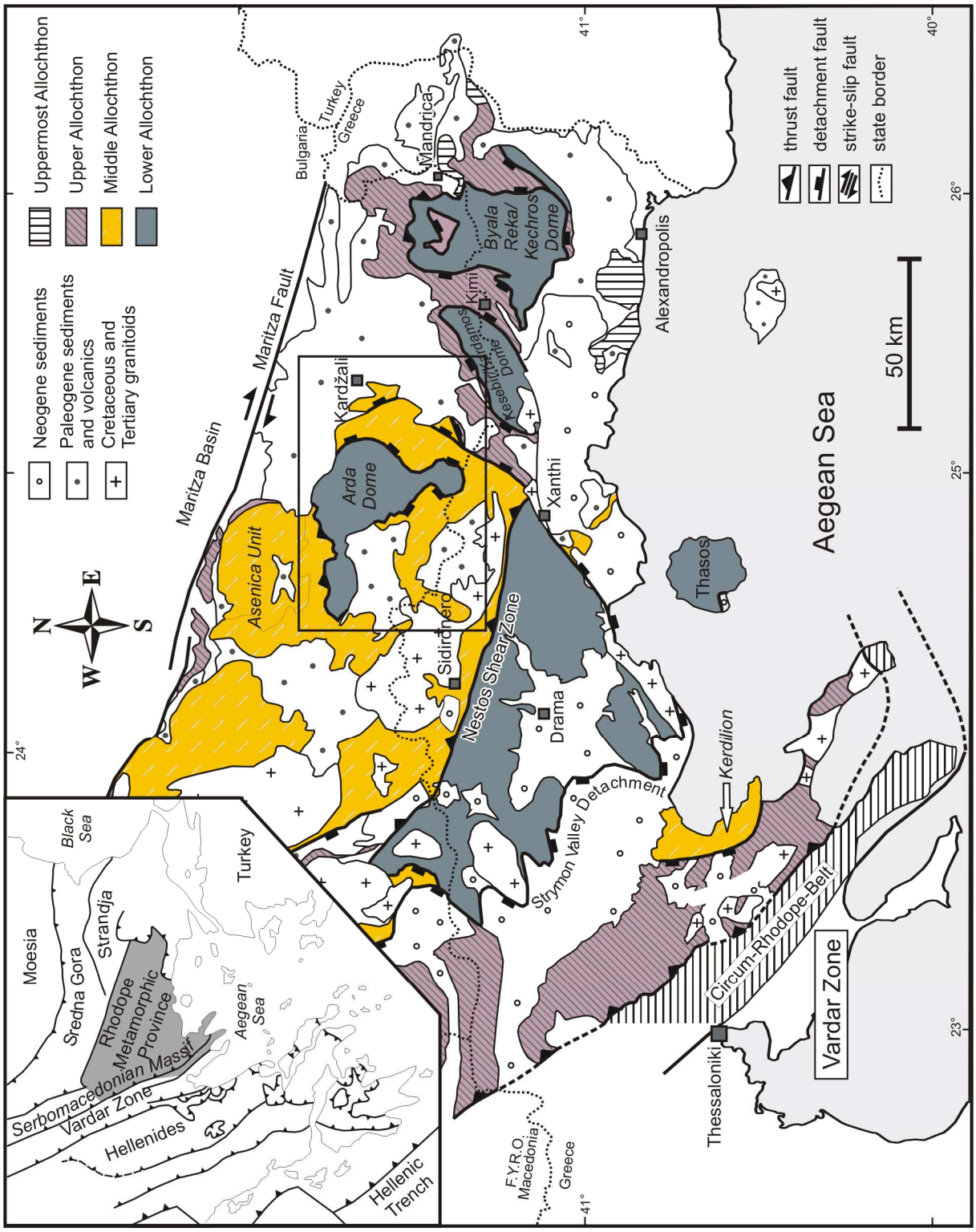

Fig. 2.1:

Geological overview of the Bulgarian and Greek Rhodopes; modified after Tückmantel *et al*. (2008) and Jahn-Awe *et al*. (2010). Marked field illustrates map shown in Fig. 2.2.

The ***Lower Allochthon*** is exposed south of the Nestos Shear Zone ("Rhodope Metamorphic Core Complex" or "Pangaion-Pirin Complex"; Dinter & Royden, 1993; Dinter, 1998; Georgiev *et al*., 2010; Jahn-Awe *et al*., 2010) as well as in three metamorphic core complexes (Arda – Byala Reka/Kechros – Kesebir/Kardamos) that form extensive domes in the eastern part of the Rhodopes (Fig. 2.1, 2.2). The Lower Allochthon is composed of Variscan basement (e.g., Wawrzenitz & Mposkos, 1997; Peytcheva *et al*., 2004; Ovtcharova *et al*., 2004; Turpaud & Reischmann, 2010) and a meta-sedimentary sequence, reaching greenschist- to amphibolite-facies metamorphism in the Pangaion-Pirin Complex and migmatisation in the Arda, Byala Reka/Kechros, and Kesebir/Kardamos complexes. Migmatisation in the Arda dome took place at 37.8 ± 1.5 Ma (Cherneva *et al*., 2002).

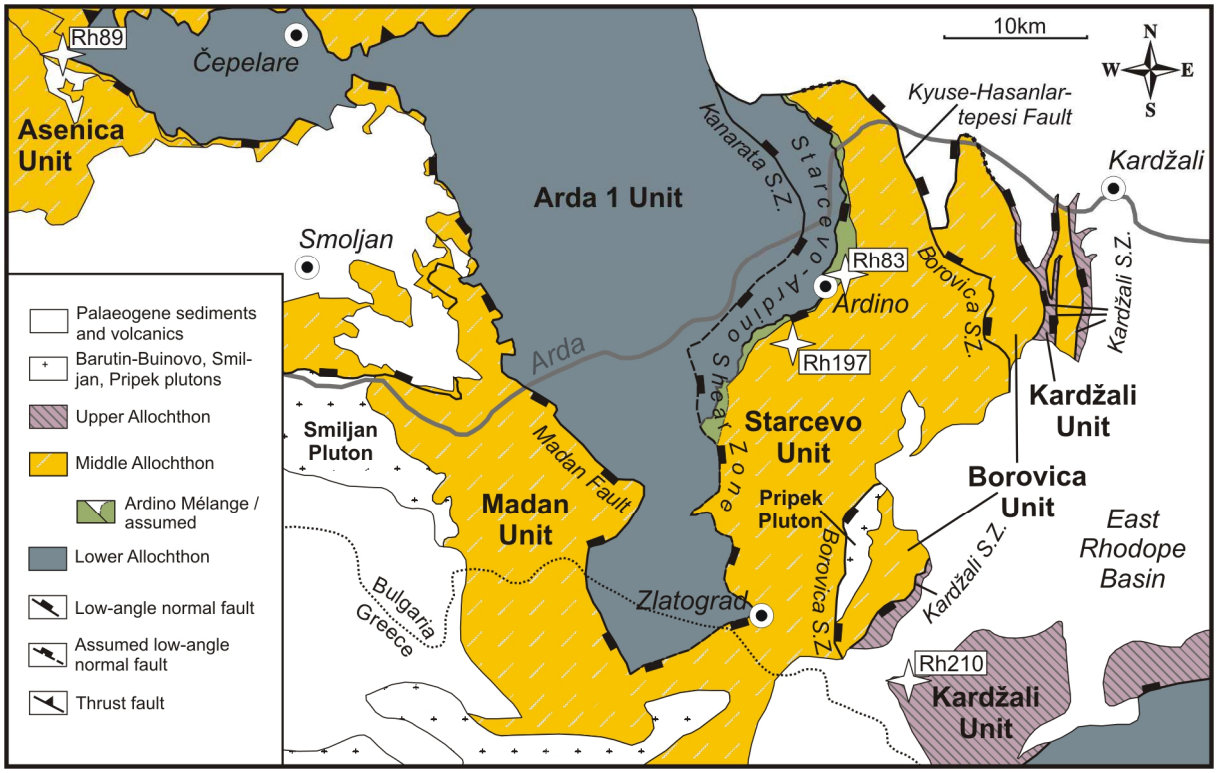

Fig. 2.2:
Sample localities of the four studied eclogite samples: Rh-83, Rh-89 and Rh-197 from the Middle Allochthon (Starcevo Unit and Chepelare suture) and Rh-210 from the Upper Allochthon (Kardzali Unit). Modified after Jahn-Awe *et al*. (2011).

Table 2.1: Compilation of geochronological data of the Rhodope thrust units

	Lower Allochthon	Middle Allochthon	Upper Allochthon
Corresponds to	Pangaion-Pirin-Complex [1] Thracia terrane [2]	Sidironero-Mesta Unit Starcevo Unit Asenica Unit Madan Unit Borovica Unit Arda 2 Unit	Kimi Complex (Eastern Rhodopes) Vertiskos/Ograzhden unit (SMM)[12] Kardžali Unit
Exposure	Metamorphic core complexes South of Nestos Shear zone	North of Nestos Shear zone around core complexes	Eastern Rhodopes around core complexes Western Rhodopes
Lithologies	Composite unit Variscan basement (orthogneisses) metasedimentary sequence	Mixed unit (continental and oceanic) intruded by arc granitoids	Composite unit metapelites, gneisses, amphibolites ultramafics (dunites, pyroxenites) marbles hosting eclogite boudins
Metamorphic grade	greenschist to amphibolite facies	Up to eclogite-facies Locally reaching UHP (microdiamonds)	Eclogite-facies Locally reaching UHP (microdiamonds)
Felsic rocks/Metapelites			
Inherited components *		**3200-500 – 410 – 356** [2],[6],[14] **330 - 250** [2]	**298** [7] **3000-2370 – 451 - 290** [7],[10]
Protolith crystallization	**32** [1]; **334 – 266** [2],[3],[9],[13],	**294** [4],[6]; **170 – 134** [1],[2],[13]	**151** [10]; **232** [11]; **430** [12]
Metamorphism	Eocene (?) [13]	**Eocene** [4],[6],[1],[13], + **145/148** (?)[14],[6]	**170 – 160** [7] **82 – 65** (amphibolite-facies ?) [7],[8]
Cooling – Uplift - Extension	**35 – 38 - 56** [3],[9],[13]	**52.8 - 45 - 36 - 32** [4],[13],[15]	**65 - 62** [8],[5]
Mafic rocks	***none reported***		
Protolith crystallization		**Min. 77.4 bis max. 294 (245 – 294)** [4],[6] Inherited: **430** [6]	**117.4 (?)**[5]; **288 – 200** [7]
Metamorphism		**42.2 – 51** [4],[6]	**160** (HT) [7] **120-115** (HP) [7],[9] **82 – 73.5** (Low-grade) [7],[5]

* mostly zircon cores in metapelites and gneisses, interpreted to be inherited from sedimentary precursor or from assimilated material

[1] Jahn-Awe et al. (2010)
[2] Turpaud & Reischmann (2010)
[3] Peytcheva et al. (2004)
[4] Liati & Gebauer (1999)
[5] Liati et al. (2002)
[6] Liati (2005)
[7] Bauer et al. (2007)
[8] Mposkos & Wawrzenitz (1995)
[9] Wawrzenitz & Mposkos (1997)
[10] Cornelius (2008)
[11] Himmerkus et al. (2009a)
[12] Himmerkus et al. (2009b)
[13] Ovtcharova et al. (2004)
[14] Krenn et al. (2010)
[15] Lips et al. (2000)

The ***Middle Allochthon*** corresponds to the Sidironero-Mesta Unit in the broad sense and includes the Madan, Arda 2, Starcevo, Borovica and Asenica Units in the Central Rhodopes (Table 2.1; Fig. 2.1, 2.2). The Middle Allochthon is equivalent to the "Rhodope Terrane" of Turpaud & Reischmann (2010) and Jahn-Awe *et al.* (2010) and is a mixed unit of continental and oceanic affinity, including orthogneisses derived from Jurassic to Early Cretaceous arc granitoids, and intruded by Eocene granitoids (U-Pb on zircons; Ovtcharova *et al*., 2004; Turpaud & Reischmann, 2010; Jahn-Awe *et al*., 2010). The metamorphic grade reached up to eclogite-facies (e.g., Kolčeva *et al*., 1986; Liati & Mposkos, 1990; Liati & Seidel, 1996). Furthermore, mineral relics and -compositions indicating UHP metamorphic conditions have been reported from several different localities from the base of the Middle Allochthon (microdiamond inclusions in garnet of metapelites; Mposkos & Kostopoulos, 2001; Perraki *et al*., 2006; Schmidt *et al*., 2010). The timing for thrusting of the Middle on the Lower Allochthon along the top-to-the-southwest Nestos Shear Zone was recently confined by Jahn-Awe *et al*. (2010) to 55 - 32 Ma. An Eocene activity of the Nestos Shear Zone is also constrained by ca. 42 - 38 Ma old pegmatite veins affected by mylonitisation along the Nestos Shear Zone (Liati, 2005; Bosse *et al*., 2009).

The ***Upper Allochthon*** is composed of the Kardžali Unit and the Kimi Complex in the Eastern Rhodopes and the Vertiskos/Ograzhden Unit in the Serbo-Macedonian Massif, which is regarded as the western continuation of the Rhodopes (Table 2.1 and Fig. 2.1, 2.2; Burg *et al*., 1996; Ricou *et al*., 1998; Himmerkus *et al*., 2009a, b). The Upper Allochthon is a composite unit made up of metapelites, gneisses, amphibolites, marbles, and boudins of eclogites and ultramafic rocks. The latter have previously been interpreted as melting residues and cumulates emplaced at the base of a thickened crust (Baziotis *et al*., 2008). A metamorphic grade of eclogite-facies up to UHP conditions has been documented for the Kimi Complex (Mposkos & Kostopoulos, 2001). Recently, microdiamond inclusions in zircons were also reported from the mélange zone at the base of the Upper Allochthon by Cornelius (2008). So far, the timing of UHP metamorphism in the Upper Allochthon could only be constrained between 200 and 41 Ma and is still a matter of debate for the Kimi Complex. Most recently an Early Jurassic age (~180 Ma) was suggested by Krenn *et al*. (2010).

The ***Uppermost Allochthon*** consists of the Circum-Rhodope Belt as well as the Mandrica and Alexandropolis greenschists. These units consist of low-grade metamorphic

sedimentary and volcanic rocks, partly of oceanic affinity and were thrust northwards over the Eurasian margin in the Late Jurassic to Early Cretaceous (Bonev & Stampfli, 2003).

2.3. Sample localities

Three eclogite samples (Rh-83, Rh-89 and Rh-197) were taken from key localities in the Middle Allochthon and one sample (Rh-210) from the Upper Allochthon (GPS coordinates see Table 2.2). Rh-83 and Rh-197 were sampled near to each other, within the same sub-unit (Starcevo Unit of the Middle Allochthon; see Fig. 2.2).

Sample Rh-83 is of particular importance, in that it is a sapphirine-bearing kyanite eclogite. It has been collected in a small creek bed ~300 m northeast of the town of Ardino, located at the top of the Ardino Mélange (Fig. 2.2). This mélange forms the basal part of the Starcevo Unit (Middle Allochthon) and is characterized by ortho- and para-gneisses, marbles, amphibolites and minor ultramafic rocks and eclogites. On top of the mélange towards east follow mixed gneisses of the Starcevo Unit proper. As sample Rh-83 was part of a stream boulder, it is not clear whether its original tectonic position was in the uppermost part of the mélange or upstream in the hanging-wall of the mélange within the mixed gneisses of the Starcevo Unit that also contain eclogites.

Eclogite Rh-197 has been collected ~700 m to the northeast of Sransko village (southwest of Ardino; Fig. 2.2). It originates from lenses of amphibolite and eclogite enclosed in migmatitic gneisses of the Starcevo Unit.

Eclogite sample Rh-89 originates from the so-called “Čepelare Shear Zone” (Fig. 2.2; Burg *et al*., 1990; Bosse *et al*., 2009; Gerdjikov *et al*., 2010), a mixed zone at the base of the Arda 2 Unit (Middle Allochthon). The sample has been collected ~1 km southeast of Beden village. At this locality, fine-grained eclogites and surrounding garnet-amphibolites form a 25 m long and 10 m thick boudin embedded in gneiss.

Eclogite sample Rh-210 originates from the Kardžali Unit, which is part of the Upper Allochthon (see Table 2.1). The sample has been collected ~3 km WNW of Drangovo village (Fig. 2.2). The sample originates from an eclogite boudin hosted by garnet-micaschists. More

eclogite outcrops can be found towards north-northeast and south-southwest in a thin band on top of a west-northwest-dipping extensional shear zone.

Table 2.2: Major and trace element analyses

Sample ID	Rh-83	Rh-89	Rh-197	Rh-210
Unit	Middle Allochthon	Middle Allochthon	Middle Allochthon	Upper Allochthon
Sub-Unit	Starcevo Unit	Chepelare suture	Starcevo Unit	Kimi Complex
UTM coordinates	E345379 N4606164	E290760 N4620157	E341746 N4601344	E349781 N4578464
Major elements (wt.%)				
SiO_2	48.4	47.8	51.1	45.8
Al_2O_3	16.7	15.4	17.0	14.0
Fe_2O_3	10.3	12.4	9.2	14.0
MnO	0.17	0.21	0.18	0.25
MgO	8.32	7.84	6.71	7.43
CaO	10.2	9.34	9.86	12.9
Na_2O	3.35	3.37	4.11	3.14
K_2O	0.47	0.52	0.02	0.02
TiO_2	1.63	2.38	1.18	2.29
P_2O_5	0.15	0.28	0.20	0.17
SO_3	0.41	0.27	0.010	0.27
L.O.I.	0.00	0.19	0.00	0.00
Sum	100.2	100.2	99.6	99.9
Trace elements (ppm)				
Li	8.72	17.2	4.02	17.1
Sc	40.2	37.9	36.0	52.5
V	221	285	203	395
Cr	320	286	264	182
Co	43.4	45.2	32.9	45.6
Ni	94.1	142	54.2	62.0
Cu	35.1	44.7	41.3	74.0
Zn	81.5	106	95.9	103
Ga	17.7	22.8	17.9	18.4
Rb	12.4	15.1	0.986	0.594
Sr	194	151	166	86.6
Y	29.0	47.8	26.5	45.1
Zr	152	200	113	123
Nb	3.37	5.43	5.83	3.54
Mo	0.692	0.858	0.249	0.266
Sn	1.23	2.14	3.07	1.45
Sb	0.0768	0.178	0.0939	0.0487
Cs	0.788	0.464	0.107	0.0176
Ba	94.4	106	6.18	9.36
La	8.57	10.1	19.1	0.894
Ce	22.7	27.4	40.4	3.33
Pr	3.36	4.23	5.22	0.701
Nd	15.7	21.0	21.8	4.73
Sm	4.24	6.34	5.18	2.86
Eu	1.52	2.07	1.58	1.31
Gd	4.91	7.76	5.16	5.61
Tb	0.826	1.33	0.773	1.14
Dy	5.32	8.67	4.70	7.91
Ho	1.10	1.80	0.989	1.69
Er	3.03	4.97	2.86	4.78
Tm	0.445	0.731	0.435	0.719
Yb	2.94	4.81	2.89	4.75
Lu	0.435	0.706	0.432	0.709
Hf	3.42	4.92	2.82	3.24
Ta	0.232	0.371	0.381	0.264
W	0.209	0.545	0.461	0.355
Tl	0.174	0.154	0.0201	0.024
Pb	2.63	1.94	5.32	0.727
Th	0.585	0.927	4.01	0.0573
U	0.132	0.195	0.914	0.194

Table 2.3: Lu-Hf and Sm-Nd isotope compositions

Sample ID		weight (mg)	ppm Lu	ppm Hf	$^{176}Lu/^{177}Hf$	2σ	$^{176}Hf/^{177}Hf$	2σ	ppm Sm	ppm Nd	$^{147}Sm/^{144}Nd$	2σ	$^{143}Nd/^{144}Nd$	2σ
Rh-83	*Whole rock*	80.3	0.437	3.39	0.01830	± 6	0.282918	± 6	3.79	13.9	0.1645	± 3	0.512759	± 17
Rh-83_Gt-1	*garnet*	80.9	1.75	0.117	2.126	± 7	0.284670	± 35						
Rh-83_Gt-2	*garnet*	34.1	1.91	0.119	2.280	± 7	0.284768	± 23						
Rh-83_Gt-3	*garnet*	52.8	1.69	0.150	1.599	± 5	0.284251	± 17						
Rh-83_Gt-4	*garnet*	12.7	1.82	0.0906	2.853	± 9	0.285340	± 76						
Rh-83_Gt-5	*garnet*	9.85	1.81	0.0889	2.892	± 11	0.285396	± 78						
Rh-89	*Whole rock*	79.8	0.713	4.78	0.02118	± 7	0.283017	± 4	5.98	20.1	0.1799	± 4	0.512863	± 12
Rh-89_Gt-1	*garnet*	119	1.89	0.0789	3.398	± 11	0.285765	± 17						
Rh-89_Gt-2	*garnet*	47.2	1.90	0.0904	2.993	± 9	0.285418	± 30						
Rh-89_Gt-3	*garnet*	62.4	1.87	0.107	2.470	± 8	0.284998	± 19						
Rh-197	*Whole rock*	81.1	0.432	2.92	0.02096	± 7	0.282821	± 6	4.71	20.0	0.1425	± 3	0.512514	± 15
Rh-197_Gt-1	*garnet*	92.2	1.59	0.0599	3.779	± 12	0.285830	± 23						
Rh-197_Gt-2	*garnet*	52.0	1.65	0.0624	3.760	± 12	0.285802	± 29						
Rh-197_Gt-3	*garnet*	50.4	1.70	0.0688	3.519	± 11	0.285611	± 27						
Rh-197_Gt-4	*garnet*	32.9	1.66	0.0567	4.151	± 13	0.286096	± 72						
Rh-210	*Whole rock*	80.1	0.714	2.92	0.03468	± 11	0.283098	± 6	2.60	4.3	0.3664	± 7	0.513129	± 23
Rh-210_Gt-1	*garnet*	108	1.82	0.0854	3.029	± 9	0.290157	± 11						
Rh-210_Gt-2	*garnet*	63.6	1.89	0.0799	3.368	± 10	0.290960	± 17						
Rh-210_Gt-3	*garnet*	67.5	1.80	0.104	2.448	± 8	0.288735	± 16						
Rh-210_Gt-4	*garnet*	50.8	1.83	0.0863	3.016	± 9	0.290099	± 25	2.35	1.96	0.7261	± 15	0.513389	± 20
Rh-210_Px-1	*pyroxene*	47.3	0.00964	1.10	0.001245	± 7	0.283011	± 19	1.22	1.67	0.4400	± 9	0.513193	± 20

2.4. Analytical techniques

Sample preparation, separation and digestion

Four eclogite samples (Rh-83, Rh-89, Rh-197, Rh-210) were analyzed for their whole rock major and trace element concentrations as well as for Lu-Hf and Sm-Nd isotope compositions. The results along with GPS coordinates of sample localities are listed in Table 2.2 and 2.3.

After removing the weathering crusts with a rock saw, the samples (total weight ca. 2-3 kg) were crushed in a steel mortar. A representative aliquot was then ground in an agate mill and the powder was subsequently used for bulk rock analyses. For trace element analyses, the sample powder was digested in a 1:1 mixture of HNO_3-HF in Parr bombs for three days to ensure complete sample digestion and was subsequently dried down with one mL of perchloric acid. A second aliquot of the crushed sample was sieved and the fractions > 63 µm were purified with a Frantz magnet separator. In order to prevent a selective separation of either garnet rim or core, the settings were adjusted to remove non-magnetic minerals only. Subsequently, three to five garnet separates per sample were hand-picked under a binocular lens. Both visibly inclusion-free and inclusion-bearing garnet fractions were separated in order to avoid biasing the results towards either garnet rims or cores. For sample Rh-210 an additional omphacite fraction was separated. Nine to 120 mg of mineral fractions were used for Lu-Hf and Sm-Nd measurements (see Table 2.3). Prior to digestion, the whole rock powders and mineral separates were spiked with a mixed ^{176}Lu-^{180}Hf and ^{149}Sm-^{150}Nd tracer. The digestion procedures employed for whole rocks (bomb digestion) and mineral separates (tabletop digestion) were described in detail by Lagos *et al*. (2007) and Herwartz *et al*. (2008). The Lu-Hf separation as well as an additional clean-up step for the Hf fraction was carried out using the method of Münker *et al*. (2001). Samarium-Nd separation was carried out using the REE-rich matrix cut left over from the Hf separation, using BioRad® AG50W-X8 cation resin (200 – 400 mesh) and Eichrom Ln-spec resin (Pin & Zalduegui, 1997). Procedural blanks were less than 50 pg for both Hf and Nd.

Measurements

Major element whole rock analyses were carried out using a PANalytical ProTrace XRF at Universität Bonn, Germany. The whole rock trace element contents were determined

by quadrupole ICPMS using an Agilent 7500cs mass spectrometer at Universität Kiel, Germany. Analytical procedures followed those of Garbe-Schönberg (1993). Lutetium, Hf, Sm and Nd were measured using the Thermo-Finnigan Neptune MC-ICP-MS at the Steinmann-Institut Bonn, operated in static mode. Values of $^{143}Nd/^{144}Nd$ and $^{176}Hf/^{177}Hf$ were corrected for mass fractionation using the exponential law and $^{146}Nd/^{144}Nd = 0.7219$ and $^{179}Hf/^{177}Hf = 0.7325$, respectively. Measured $^{143}Nd/^{144}Nd$ and $^{176}Hf/^{177}Hf$ values of the samples are reported relative to $^{143}Nd/^{144}Nd = 0.511859$ for the La Jolla Nd standard (measured value = 0.511836 ± 47 (2SE); n = 2) and $^{176}Hf/^{177}Hf = 0.282160$ for the Münster Ames Hf standard (measured value = 0.282161 ± 44 (2SE); n = 27) that is isotopically identical to the JMC-475 standard.

Several garnet grains were also analyzed in situ by laser ablation mass spectrometry along line profiles (Fig. 2.5), in order to measure their Mn and Lu abundances. Laser ablation of these garnet grains was carried out using a Resonetics M50-E ATL Excimer 193 nm laser system coupled to a Thermo-Finnigan X-series 2 quadrupole ICP-MS (Steinmann-Institut Bonn). Spot sizes were set between 33 and 75 μm depending on the size of the garnets analyzed, as well as the amount of mineral inclusions found in the cores of the individual grains. Laser fluence at the sample surface was measured at 7 J/cm^{-2}, and the laser repetition rate was set to 15 Hz. Count rates were normalized using ^{29}Si as the internal standard, and one external standard (NIST-610 glass, Pearce *et al*., 1997). The isotopes ^{29}Si, ^{43}Ca, ^{57}Fe, ^{55}Mn and ^{175}Lu were monitored. Data reduction and evaluation was carried out following the procedure laid out by Longerich *et al*. (1996). Electron microprobe BSE images of the garnets before and after LA-ICP-MS analyses are enclosed in the Appendix material.

Mineral major element abundances were analyzed by spot analysis using a JEOL superprobe JXA-8900 microprobe (Universität zu Köln) and a JEOL superprobe JXA-8200 microprobe (Steinmann-Institut Bonn) in wavelength dispersive mode (WDS) employing 15kV acceleration voltage and 15 nA beam current. Calibrations for Mg, Al, Si, Ti, Ca, Fe, Na, K, Cr, and Mn were carried out on andradite, rutile, basaltic glass (VG2 – USNM 111240/52), and Jadeite-Diopside synthetic glass. In addition, high-resolution X-ray maps were made for selected garnet grains of all four samples, in order to identify and characterize their zonations with respect to Ca, Fe, Mg, and Mn (see Fig. 2.4, 2.5). X-ray maps were performed using a JEOL superprobe JXA-8200 microprobe (Steinmann-Institut Bonn), with 15kV acceleration voltage and 100nA beam current over 24 hours.

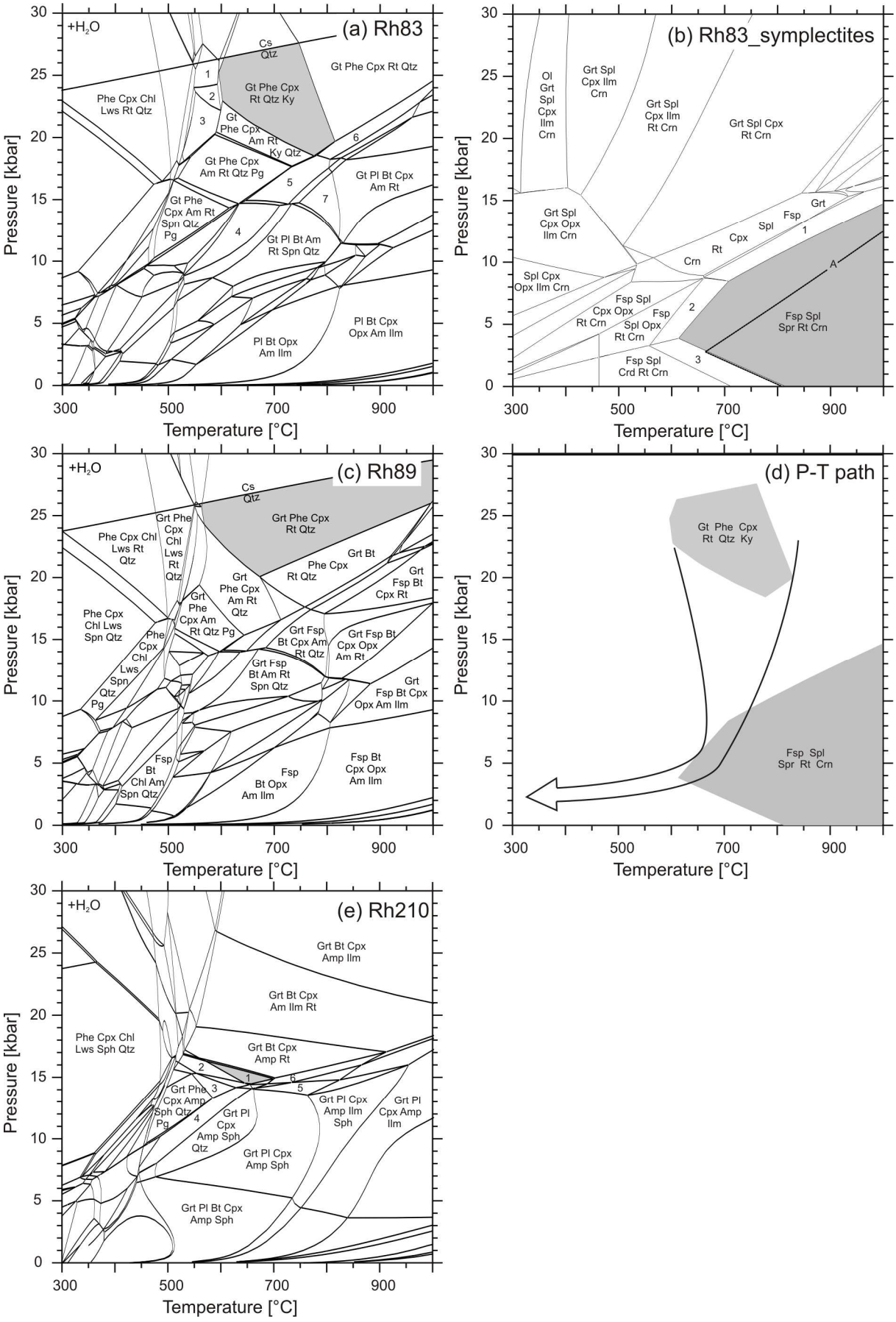
(a) Rh83
+H2O
Cs
Qtz
Gt Phe Cpx Rt Qtz
Gt Phe Cpx Rt Qtz Ky
Phe Cpx Chl Lws Rt Qtz
Gt Phe Cpx Am Rt Ky Qtz
Gt Phe Cpx Am Rt Qtz Pg
Gt Pl Bt Cpx Am Rt
Gt Phe Cpx Am Rt Spn Qtz Pg
Gt Pl Bt Am Rt Spn Qtz
Pl Bt Cpx Opx Am Ilm
Pl Bt Opx Am Ilm
(b) Rh83_symplectites
Ol Grt Spl Cpx Ilm Crn
Grt Spl Cpx Ilm Crn
Grt Spl Cpx Ilm Rt Crn
Grt Spl Cpx Rt Crn
Grt Spl Cpx Opx Ilm Crn
Spl Cpx Opx Ilm Crn
Fsp Spl Cpx Opx Rt Crn
Fsp Spl Spr Rt Crn
Fsp Spl Opx Rt Crn
Fsp Spl Crd Rt Crn
(c) Rh89
Grt Phe Cpx Rt Qtz
Phe Cpx Chl Lws Rt Qtz
Grt Bt
Phe Cpx Rt Qtz
Grt Fsp Bt Cpx Rt
Grt Phe Cpx Am Rt Qtz
Phe Cpx Chl Lws Spn Qtz
Grt Phe Cpx Am Rt Qtz Pg
Grt Fsp Bt Cpx Am Rt Qtz
Grt Fsp Bt Cpx Opx Am Rt
Grt Fsp Bt Am Rt Spn Qtz
Grt Fsp Bt Cpx Opx Am Ilm
Fsp Bt Chl Am Spn Qtz
Fsp Bt Opx Am Ilm
Fsp Bt Cpx Opx Am Ilm
(d) P-T path
Gt Phe Cpx Rt Qtz Ky
Fsp Spl Spr Rt Crn
(e) Rh210
Grt Bt Cpx Amp Ilm
Grt Bt Cpx Am Ilm Rt
Phe Cpx Chl Lws Sph Qtz
Grt Bt Cpx Amp Rt
Grt Phe Cpx Amp Sph Qtz Pg
Grt Pl Cpx Amp Sph Qtz
Grt Pl Cpx Amp Ilm Sph
Grt Pl Cpx Amp Ilm
Grt Pl Cpx Amp Sph
Grt Pl Bt Cpx Amp Sph
Pressure [kbar]
Temperature [°C]

Fig. 2.3:

Results of the calculation of equilibrium phase diagrams for the samples Rh-83, Rh-89 and Rh-197.

a: Equilibrium assemblage diagram for the bulk composition of Rh-83 (Table 2.2) in an Si-Al-Ti-Fe-Mn-Mg-Ca-Na-K system with excess H_2O. Grey-shaded area corresponds to the observed high-pressure assemblage. (1) Grt + Phe + Cpx + Ctd + Lws + Rt + Qtz; (2) Grt + Phe + Cpx + Ctd + Rt + Qtz; (3) Grt + Phe + Cpx + Ctd + Am + Rt + Qtz; (4) Grt + Fsp + Phe + Am + Rt + Spn + Qtz; (5) Grt + Fsp + Phe + Am + Spn + Qtz; (6) Grt + Fsp + Phe + Cpx + Am + Rt + Qtz; (7) Grt + Fsp + Phe + Cpx + Rt + Qtz; (8) Grt + Fsp + Bt + Cpx + Am + Rt + Qtz; (9) Grt + Fsp + Bt + Am + Spn + Qtz.

b: Equilibrium assemblage diagram for the estimated composition of Al-rich coronae around decomposing kyanite in Rh-83 (Table 2.2) in an Si-Al-Ti-Fe-Mg-Ca-Na system. Grey-shaded area corresponds to the observed assemblage. (1) Grt + Fsp + Spl + Spr + Rt + Crn; (2) Fsp + Spl + Opx + Spr + Rt + Crn; (3) Fsp + Spl + Crd + Spr + Rt + Crn; (A) Boundary of stability field of Fsp + Spl + Spr + Rt + Crn with excess H_2O.

c: Equilibrium assemblage diagram for the bulk composition of Rh-89 (Table 1.2) in an Si-Al-Ti-Fe-Mn-Mg-Ca-Na-K system with excess H_2O. Grey-shaded area corresponds to the observed high-pressure assemblage

d: Pressure-temperature path for the exhumation of the lower, eclogite-bearing part of the Middle Allochthon constrained by the high-pressure assemblage (see Fig. a) and Al-rich coronae (Pl + Spl + Rt + Spr + Crn; see Fig. b) observed in Rh-83, and Al-rich coronae (Pl + Ky + Spl + Spn + Crn) observed in Rh-197.

e: Equilibrium assemblage diagram for the bulk composition of Rh-210 (Table 2) in an Si-Al-Ti-Fe-Mn-Mg-Ca-Na-K system with excess H_2O. Grey-shaded area corresponds to the observed high-pressure assemblage. (1) Grt + Phe + Cpx + Am + Rt + Qtz; (2) Grt + Fsp + Cpx + Am + Rt + Spn; (3) Grt + Fsp + Cpx + Am + Rt.

2.5. Petrography and Equilibrium Phase Diagrams

Mineral compositions of garnet, omphacite, amphibole, phengite, plagioclase and sapphirine were analyzed by electron microprobe, the results of which are listed in Tables 2.4 and 2.5. Using these data, we calculated equilibrium assemblage diagrams (Fig. 2.3) for the samples Rh-83, Rh-89, and Rh-210 using the whole rock compositions obtained by XRF (Table 2.2), the Domino-Theriak program package (de Capitani & Petrakakis, 2010) and a modified JUN92 database (Berman, 1988; upgrade 1992). The database was modified with non-ideal solid solution models for garnet (Berman, 1990), phengite (Massonne & Szpurka, 1997), and feldspar (Fuhrman & Lindsley, 1988) and ideal approximations for clinopyroxene (endmembers: diopside-hedenbergite-jadeite), clinoamphibole (tremolite, pargasite, Fe-pargasite, glaucophane, tschermakite), spinel (spinel-hercynite), biotite (phlogopite-annite-Mn-biotite), chlorite (chlinochlore-daphnite-Mn-chlorite), and sapphirine. For sapphirine, we chose Mg-sapphirine $Mg_{3.5}AL_9Si_{1.5}O_{20}$ and Fe-sapphirine $Fe_{3.5}AL_9Si_{1.5}O_{20}$ as end-members, as these are compositionally close to the sapphirine observed in sample Rh-83. ΔfH_0 and S_0 of

the sapphirine and daphnite end-members were adopted from Holland & Powell (1998) and slightly adjusted so that the internal consistency of the database was maintained.

Table 2.4: Electron microprobe analyses

	Rh83 Grt core	Rh83 Grt rim	Rh83 Omp1	Rh83 Omp2 sympl	Rh83 Amp	Rh197 Grt core	Rh197 Grt rim	Rh197 Cpx	Rh197 Amp	Rh89 Grt core	Rh89 Grt rim	Rh89 Omp	Rh89 Cpx	Rh89 Amp	Rh89 Phengite	Rh210 Grt core	Rh210 Grt rim	Rh210 Omp	Rh210 Amp	Rh210 Phengite
SiO_2	39.9	39.5	55.0	53.1	39.0	38.6	40.0	54.9	39.9	39.0	38.3	54.2	52.4	42.0	52.8	39.6	39.7	54.6	43.9	50.7
TiO_2	0.03	0.03	0.09	0.27	0.56	0.09	0.01	0.04	1.71	0.09	0.03	0.10	0.35	0.67	0.70	0.01	0.07	0.21	0.55	1.44
Al_2O_3	22.4	22.0	11.2	8.0	17.8	21.1	22.7	1.4	17.7	21.3	21.2	10.4	4.7	13.8	26.6	21.9	22.4	9.82	16.1	28.0
FeO	21.2	22.8	3.37	5.12	12.7	22.2	23.6	8.26	10.3	23.1	23.9	5.58	4.76	11.2	1.30	20.4	20.5	6.69	11.6	2.48
MnO	0.65	0.26	0.00	0.09	0.08	4.20	0.65	0.05	0.06	0.59	0.39	0.04	0.01	0.06	0.00	1.50	0.46	0.07	0.04	0.00
MgO	9.43	7.89	9.67	11.9	12.1	3.08	8.77	14.2	12.8	8.46	9.57	9.50	13.8	14.4	3.95	4.96	6.63	8.72	11.7	3.33
CaO	7.22	8.31	14.4	18.6	10.4	11.1	6.71	21.0	10.9	7.86	5.69	15.7	20.9	11.4	0.00	11.8	10.2	14.7	9.64	0.02
Na_2O	0.00	0.00	6.45	3.55	3.25	0.03	0.00	2.14	3.29	0.00	0.01	5.38	2.70	3.09	0.51	0.04	0.01	6.23	4.13	0.40
K_2O	0.02	0.00	0.01	0.00	0.69	0.00	0.01	0.01	0.20	0.00	0.00	0.01	0.01	0.71	10.2	0.01	0.01	0.02	0.15	10.1
Cr_2O_3	0.04	0.01	0.00	0.02	0.04	0.08	0.00	0.05	0.04	0.00	0.04	0.02	0.06	0.08	0.00	0.00	0.03	0.04	0.01	0.00
total	100.9	100.8	100.1	100.6	96.6	100.5	102.5	102.0	96.9	100.4	99.1	100.9	99.7	97.5	96.1	100.2	100.1	101.1	97.9	96.4
Si	6.01	6.00	1.96	1.92	5.83	6.04	5.97	2.00	5.87	5.97	5.94	1.94	1.93	6.19	3.47	6.08	6.05	1.96	6.37	3.34
Ti	0.00	0.00	0.00	0.01	0.06	0.01	0.00	0.00	0.19	0.01	0.00	0.00	0.01	0.07	0.03	0.00	0.01	0.01	0.06	0.07
Al	3.94	3.97	0.47	0.34	3.14	3.90	4.00	0.06	3.07	3.85	3.87	0.44	0.20	2.40	2.06	3.97	4.02	0.42	2.74	2.17
Fe	2.90	2.66	0.10	0.15	1.59	2.91	2.95	0.25	1.26	2.96	3.10	0.17	0.15	1.38	0.07	2.62	2.61	0.20	1.41	0.14
Mn	0.03	0.08	0.00	0.00	0.01	0.56	0.08	0.00	0.01	0.08	0.05	0.00	0.00	0.01	0.00	0.19	0.06	0.00	0.01	0.00
Mg	1.79	2.11	0.51	0.64	2.71	0.72	1.95	0.77	2.81	1.93	2.21	0.51	0.75	3.16	0.39	1.13	1.51	0.47	2.53	0.33
Ca	1.35	1.16	0.55	0.72	1.66	1.86	1.07	0.82	1.71	1.29	0.95	0.60	0.82	1.80	0.00	1.94	1.67	0.56	1.50	0.00
Na	0.00	0.00	0.45	0.25	0.94	0.01	0.00	0.15	0.94	0.00	0.00	0.37	0.19	0.88	0.065	0.01	0.00	0.43	1.16	0.05
K	0.00	0.003	0.00	0.00	0.13	0.001	0.002	0.00	0.04	0.001	0.00	0.00	0.00	0.13	0.86	0.00	0.00	0.00	0.03	0.85
Cr	0.00	0.01	0.00	0.00	0.00	0.01	0.00	0.00	0.00	0.00	0.00	0.00	0.00	0.00	0.00	0.00	0.00	0.00	0.00	0.00
total	16.0	16.0	4.03	4.03	16.1	16.0	16.0	4.05	15.9	16.1	16.1	4.03	4.06	16.0	6.93	15.9	15.9	4.05	15.8	6.95
O	24	24	6	6	23	24	24	6	23	24	24	6	6	23	11	24	24	6	23	11

Table 2.4:
Representative microprobe analyses of eclogite phases in weight % and p.f.u.. All Fe is calculated as Fe^{2+}. See also Table 2.5.

Table 2.5: Electron microprobe analyses

	Rh83 Spr sympl. core	Rh83 Spl sympl. core	Rh83 Pl sympl. core	Rh83 Pl sympl. rim	Rh197 Grt core	Rh197 Amphibole	Rh197 Spl sympl. core	Rh197 Ilm sympl. core	Rh197 Pl sympl. core	Rh197 Pl sympl. rim
Proportion in corona [%]	***8***	***30***	***60***			***13.5***	***4.5***	***2***	***48***	
SiO_2	10.7	0.04	57.5	64.1	38.6	39.9	0.05	0.53	55.7	61.7
TiO_2	0.02	0.05	0.01	0.04	0.09	1.71	0.08	44.8	0.00	0.03
Al_2O_3	69.7	66.3	27.6	23.2	21.1	17.7	61.2	0.16	27.8	23.4
FeO	3.94	16.2	0.19	0.09	22.2	10.3	23.7	43.7	0.12	0.14
MnO	0.06	0.08	0.03	0.00	4.20	0.06	0.06	0.46	0.02	0.00
MgO	16.2	17.0	0.04	0.00	3.08	12.8	11.3	0.45	0.01	0.00
CaO	0.19	0.08	9.01	4.09	11.1	10.9	0.11	0.22	9.37	4.53
Na_2O	0.09	0.00	6.37	8.68	0.03	3.29	0.00	0.08	5.94	8.72
K_2O	0.00	0.00	0.08	0.19	0.00	0.20	0.00	0.02	0.02	0.06
Cr_2O_3	0.09	0.12	0.01	0.00	0.08	0.04	0.18	0.04	0.02	0.03
total	101.0	99.8	100.9	100.3	100.5	96.9	96.6	90.5	99.0	98.6
Si	1.25	0.00	2.56	2.81	6.04	5.87	0.00	0.02	2.52	2.77
Ti	0.00	0.00	0.00	0.00	0.01	0.19	0.00	0.95	0.00	0.00
Al	9.58	2.00	1.45	1.20	3.90	3.07	1.99	0.01	1.49	1.24
Fe	0.35	0.35	0.01	0.00	2.91	1.26	0.55	1.03	0.01	0.01
Mn	0.01	0.00	0.00	0.00	0.56	0.01	0.00	0.01	0.00	0.00
Mg	2.82	0.65	0.00	0.00	0.72	2.81	0.46	0.02	0.00	0.00
Ca	0.02	0.00	0.43	0.19	1.86	1.71	0.00	0.01	0.46	0.22
Na	0.02	0.00	0.55	0.74	0.01	0.94	0.00	0.00	0.52	0.76
K	0.00	0.00	0.00	0.01	0.00	0.04	0.00	0.00	0.00	0.00
Cr	0.01	0.00	0.00	0.00	0.01	0.00	0.00	0.00	0.00	0.00
total	14.1	3.00	5.00	4.96	16.0	15.9	3.00	2.04	4.99	4.99
O	20	4	8	8	24	23	4	3	8	8

	Rh83 Corona	Rh197 Corona	
Si	26.9	38.6	
Ti	1.81	0.94	
Al	46.4 *	43.8	*: 2% TiO2 (Rutile) added
Fe	4.72	3.05	to corona composition
Mn	0	0	
Mg	10.1	3.18	
Ca	4.42	5.24	
Na	5.62	5.17	
K	0	0	
Cr	0	0	
H	0	1.70 **	**: Assuming 2OH for the amphibole
total	100	101.7	
O	149.1	159.7	

The equilibrium assemblage diagrams were calculated for water-saturated Si-Al-Ti-Fe-Mn-Mg-Ca-Na-K bulk rock compositions (see Table 2.2). In order to constrain the retrograde P-T path, we also calculated one diagram in a Si-Al-Ti-Fe-Mn-Mg-Ca-Na-K system for a retrograde corona forming around decomposing kyanite (sample Rh-83). The composition was estimated from the proportions and compositions of the minerals constituting the coronae (see Table 2.5).

Sample Rh-83 from the Middle Allochthon (Starcevo Unit) is a sapphirine-bearing kyanite eclogite, from the same unit as and similar to those described by Kolčeva *et al*. (1986), and Liati & Seidel, (1996) It contains the high-pressure assemblage garnet-omphacite1 (Jd_{37-43})-kyanite-quartz-rutile-zoisite-apatite, corresponding to 600-830°C/19-27.5 kbar in the equilibrium assemblage diagram (Fig. 2.3a). Phengite was not observed, probably because it was completely consumed during retrograde growth of amphibole and biotite. Most of the omphacite was replaced during several stages of retrograde overprint, starting with the growth of pargasitic amphibole (mostly around garnet) and omphacite2 (Jd_{17-26})-plagioclase symplectites (mostly at the expense of omphacite1) that show ambiguous textural relations with the pargasitic hornblende. Symplectites of plagioclase ($Ab_{29-57}An_{41-69}$), spinel, and sometimes rutile, sapphirine and/or corundum formed around decomposing kyanite (see BSE images in the Appendix). Biotite is locally pseudomorphic after amphibole and together with plagioclase forms patches after the sapphirine-bearing symplectite coronae. Garnets in Rh-83 are several millimeter large, corroded grains that display a complex chemical zonation (Fig. 2.4a). A wide rim domain displays patches enriched in Fe and Ca and depleted in Mg. The inclusion-rich core has a composition similar to the outermost rim with respect to Fe, Mg, and Ca, but shows a higher Mn content than the rest of the grain. This Mn-rich domain preserves an edgy euhedral shape in some garnet grains (Fig. 2.4a) and a more diffuse shape in others (Fig. 2.5a). We interpret this compositional pattern to result from partial resetting (resorption) of the garnet rims that also result in an increase in abundance of trace elements like Lu in the resorbed rims (Fig. 2.5a and discussion below).

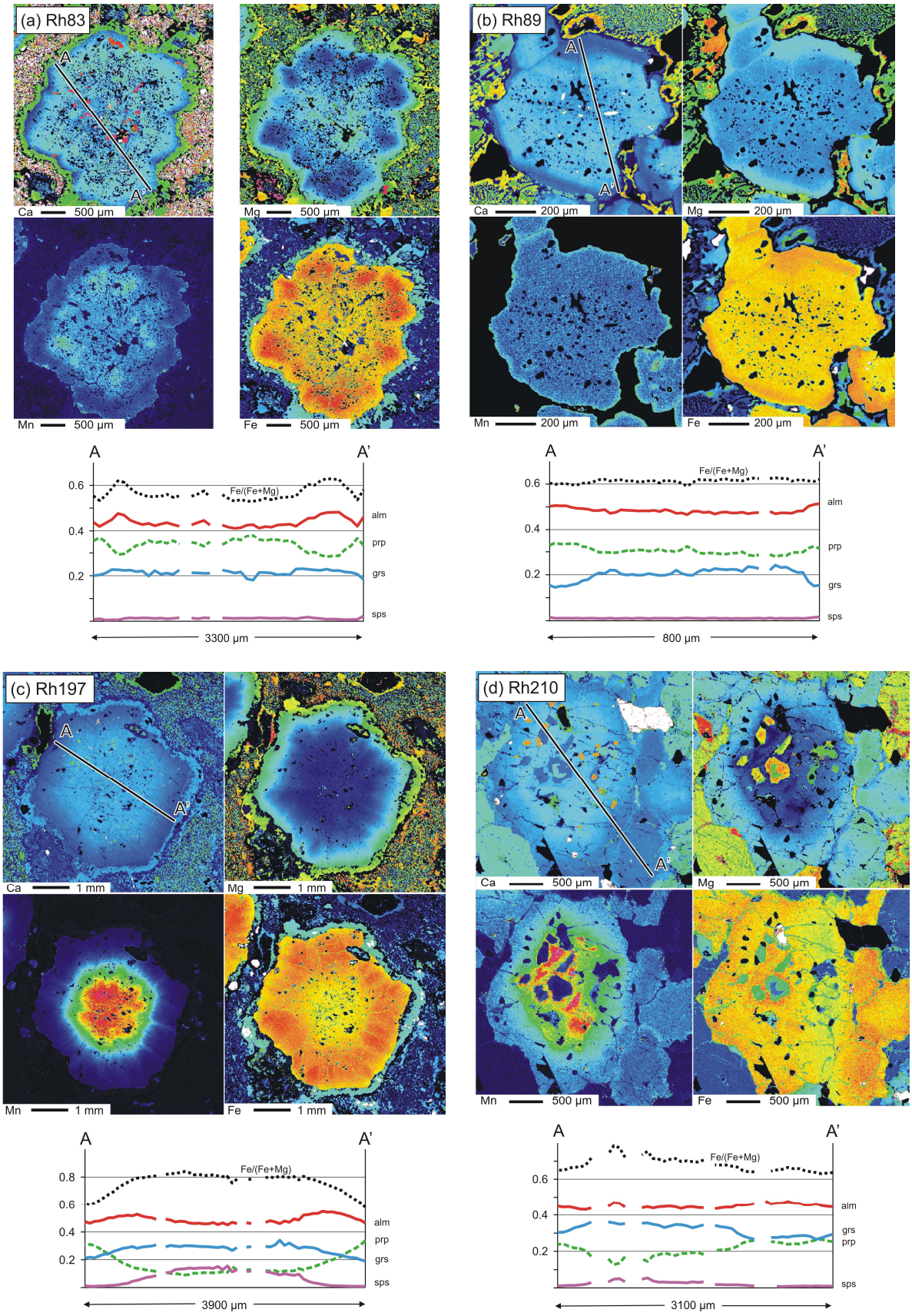

Fig. 2.4 a-d:

Major element distribution maps and cross sections through representative garnets from the four eclogite samples obtained by electron microprobe analyses.

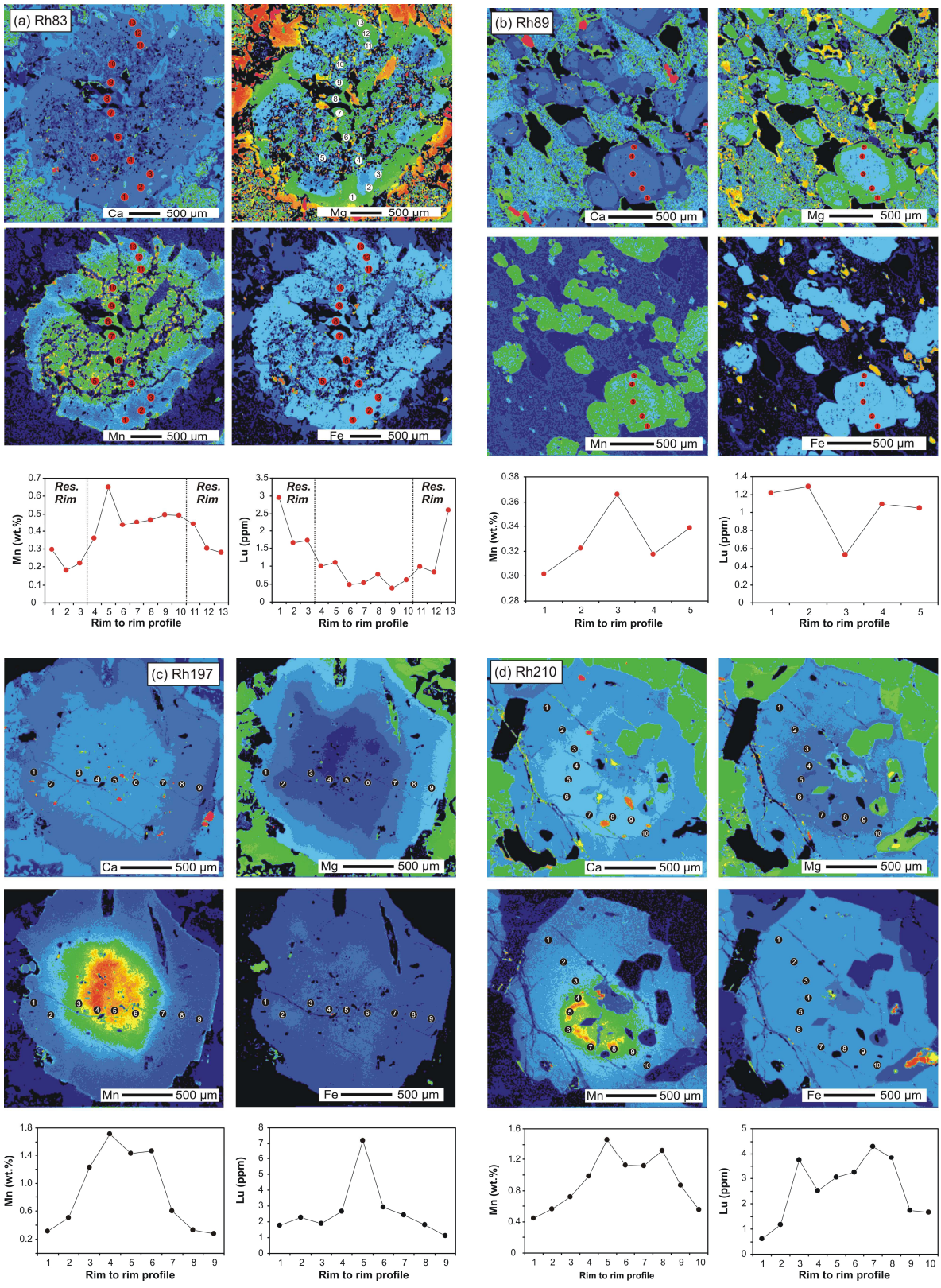

Fig. 2.5 a-d:

Major element distribution map of the garnets analyzed by LA-ICP-MS as well as the element profiles obtained by LA-ICP-MS for Lu and Mn. BSE images of the selected garnet grains before and after laser ablation are enclosed in the Appendix. Note that “Res. Rim” in the Lu and Mn profiles of c) corresponds to resorbed garnet rim domains.

Based on chemical and textural evidence we propose that the growth of the plagioclase-spinel-sapphirine symplectites around kyanite was controlled by local chemical equilibria. Therefore, we used a composition estimated as described above (Table 2.5) as input for the calculation of the equilibrium assemblage diagram (Fig. 2.3b). For a dry composition, the observed assemblage plagioclase-spinel-sapphirine-corundum-rutile is predicted to be stable in the grey-shaded field of Fig. 2.3b, i.e. above 610°C. Adding excess water to the same composition leads to a shift of the plagioclase-spinel-sapphirine-corundum-rutile stability field to higher temperatures, i.e. above 670°C. The maximum pressure is constrained by the boundary of the plagioclase-spinel-sapphirine-corundum-rutile stability field toward garnet stability and increases from c. 8 kbar at 710°C to c. 12.5 kbar at 900°C. It is therefore realistic to assume that the sapphirine-bearing coronae formed at temperatures around or even below 700°C, i.e., roughly at the same temperatures where the orthogneissic country rocks underwent migmatisation (Georgieva *et al*., 2002). Likewise, if calculated for a broader compositional range, the absence of garnet from the observed assemblage requires pressures significantly below those of a high-pressure granulite-facies overprint above 12 kbar, which was previously postulated by various authors (Liati & Seidel, 1996, Carrigan *et al*., 2002).

The matrix assemblage of sample Rh-197 (Starcevo Unit) is much more strongly affected by retrogression than documented for sample Rh-83. However, large garnet porphyroblasts are much better preserved, are euhedral and clearly exhibit growth zonation (Figs. 2.4c, 2.5c). Manganese, Ca, and the Fe to (Fe+Mg) ratio show the classic bell-shaped distribution. Zonations of Fe and particularly Mn are edgy, discontinuous and parallel to the grain boundaries. Nevertheless, garnets in Rh-197 also display thin channels, along which transport and some re-equilibration might have occurred (Fig. 2.4c). However, Lu element profiles (Fig. 2.5c) strongly indicate that garnets in Rh-197 preserve their original trace element zonation displayed by the high Lu concentration in the core and decreasing concentrations towards the rims (see also discussion below). Clinopyroxene ($Di_{62-79}Hd_{6-23}Acm_{5-15}Jd_{1-4}$) is abundant in symplectites with plagioclase. Pargasitic amphibole grew along the rims of garnet and within the matrix. Rh-197 also contains Al-rich symplectite patches comprising plagioclase ($Ab_{46-57}An_{43-53}$), kyanite, amphibole, spinel, ilmenite and sometimes corundum (see BSE images in the Appendix). Unlike in Rh-83, we did not observe specific mineral relicts within the symplectite patches.

Sample Rh-89 contains the high-pressure assemblage garnet-omphacite (Jd_{27-35})-quartz-phengite-rutile, corresponding to the grey-shaded stability field in the phase diagram (Fig. 2.3c). Garnets occur as slightly corroded, euhedral grains and are much smaller than in the two previous samples (Fig. 2.4b, 2.5b). They show distinct Ca-poor and Fe- and Mg-rich rims. The Fe to (Fe+Mg) ratio is slightly elevated in the core. However, the distribution of Mn is flat (Fig. 2.4b, 2.5b).and indicates resorption of garnet. Altogether, the chemical zoning, at least of Fe, Mg, and Mn appear to be strongly reset in sample Rh-89, which is also documented by the enrichment of Lu in the rim domains (Fig. 2.5b). Metamorphic retrogression caused growth of pargasitic amphibole, plagioclase-clinopyroxene ($Di_{70-83}Hd_{0-18}Acm_{0-12}Jd_{8-12}$) symplectites, and biotite together with plagioclase. Al-rich symplectites as in Rh-83 and Rh-197 were not observed in Rh-89.

The overlapping stability fields of the high-pressure assemblages in samples Rh-83 and Rh-89 and the Al-rich symplectites in both Rh-83 and Rh-197 allow to roughly constrain a pressure-temperature path for the exhumation of the lower part of the Middle Allochthon (Fig. 2.3d).

The observed high-pressure assemblage in Rh-210 is garnet-omphacite (Jd_{32-41})-amphibole-phengite-rutile. Mica is scarce (<1%) due to the low potassium content of the sample (0.02 wt.%). Garnets are again large (> 2 mm) and show original growth zonation with humps of Ca, Mn and the Fe to (Fe+Mg) ratio (Fig. 2.4d) and Lu (Fig. 2.5c) in the core. In the equilibrium assemblage diagram (Fig. 2.3e), this assemblage is predicted to be stable under somewhat lower pressures (15-19 kbar) than those estimated from the high-pressure assemblages of the samples from the Middle Allochthon (20 to 25 kbar). Sample Rh-210 exhibits little evidence of retrogression other than the growth of chlorite along isolated cracks.

2.6. Geochemical results

2.6.1. Major and trace elements

The major and trace element concentrations of all four eclogite samples are given in Table 1.2. The four analyzed samples yield basaltic whole rock compositions (SiO_2 = 45.8 – 51.1 wt. %; MgO = 6.71 – 8.32 wt. %; Al_2O_3 = 14.0 – 17.0 wt. %), with both high Zr (113 – 200 ppm) and compatible element contents (e.g., Cr = 182 – 320 ppm; Ni = 54.2 – 142 ppm).

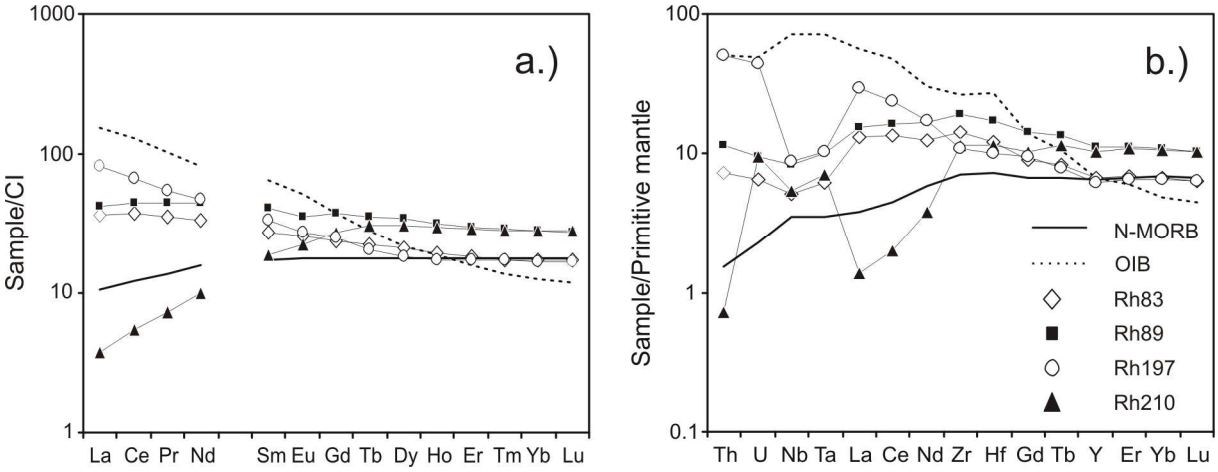

Fig. 2.6:

Trace element composition of the four eclogite samples studied.

a: CI-normalized trace element pattern of the four eclogite samples as well as OIB and N-MORB (after Sun & McDonough, 1989).

b: Primitive-mantle normalized multi-element diagram of the four eclogite samples along with values for OIB and N-MORB for comparison (after Sun & McDonough, 1989).

With the exception of sample Rh-210, all samples are LREE-enriched (La_N/Yb_N = 1.4, 2.0, 4.5 for Rh-83, Rh-89 and Rh-197, respectively), but exhibit similar magnitudes of HREE abundances as N-MORB (Fig. 2.6a). Sample Rh-210 from the Upper Allochthon is characterized by a strong LREE depletion and a slight enrichment of the HREE with respect to N-MORB (La_N/Yb_N = 0.13). In the primitive mantle-normalized trace element diagram (Fig. 2.6b) sample Rh-210 is depleted in Th and La, Ce and Nd and displays positive anomalies of high field strength elements (HFSE) like Nb, Ta, Zr and Hf. In contrast, sample Rh-197 displays a striking negative Nb-Ta anomaly and Th-U enrichment. Samples Rh-83 and Rh-89 are enriched with respect to N-MORB (Fig. 2.6b), especially with regard to U and Th. All four samples display similar Nb/Ta ranging from 13.4 to 15.3 at high Zr/Hf (37.9 -

44.5), broadly overlapping the range of values found in MORBs and island-arc basalts (Büchl *et al*., 2002; Münker *et al*., 2004).

2.6.2. Lu-Hf and Sm-Nd geochronology

We analyzed the four eclogite samples for their Lu-Hf and Sm-Nd isotope compositions, using one whole rock aliquot as well as three to five mineral separates per sample (garnets and pyroxenes). The results of the Lu-Hf and Sm-Nd measurements are given in Table 2.3 and are illustrated in Fig. 2.7. Isochron regressions were calculated using ISOPLOT v.2.49 (Ludwig, 2001) and $\lambda\ ^{176}Lu = 1.867 \times 10^{-11}\ yr^{-1}$ (Scherer *et al*., 2001; Söderlund *et al*., 2004). The external reproducibilities of the isochron calculations were estimated by the empirical relationship 2σ external reproducibility $\approx 4\sigma_m$ (σ_m = standard error of a single analysis; Bizzarro *et al*., 2003).

The Hf contents of the whole rock samples range from 2.92 to 4.78 ppm and those of the garnets from 60 to 150 ppb. The $^{176}Lu/^{177}Hf$ of the garnets range from 1.60 to 3.78 and the pyroxenes from sample Rh-210 display a $^{176}Lu/^{177}Hf$ of 0.00124. For each sample, mineral separates and whole rock aliquots define statistically significant isochrons (MSWDs of 0.1 to 0.7; Fig. 2.7), also suggesting full sample-spike equilibrium during tabletop digestion. The Lu-Hf ages of the samples from the Middle Allochthon are 44.6 ± 0.7 Ma for Rh-83 (n = 6), 43.5 ± 0.4 Ma for Rh-89 (n = 4) and 42.8 ± 0.5 Ma for Rh-197 (n = 5). The sample from the Upper Allochthon (Rh-210) yields a Lu-Hf age of 126.0 ± 0.7 Ma (n = 6).

The Nd contents of the whole rock samples range from 4.28 to 20.1 ppm with $^{147}Sm/^{144}Nd$ of 0.14 to 0.37. The garnet (Gt-4) and the pyroxene (Px-1) fractions of sample Rh-210 display Nd concentrations of 1.96 and 1.67 ppm with $^{147}Sm/^{144}Nd$ of 0.726 and 0.440, respectively. The Sm-Nd age determined for sample Rh-210 is 109 ± 11 Ma (n = 3). Samarium-Nd garnet analyses of the other three samples were hampered by the presence of inclusions with low Sm/Nd in garnet.

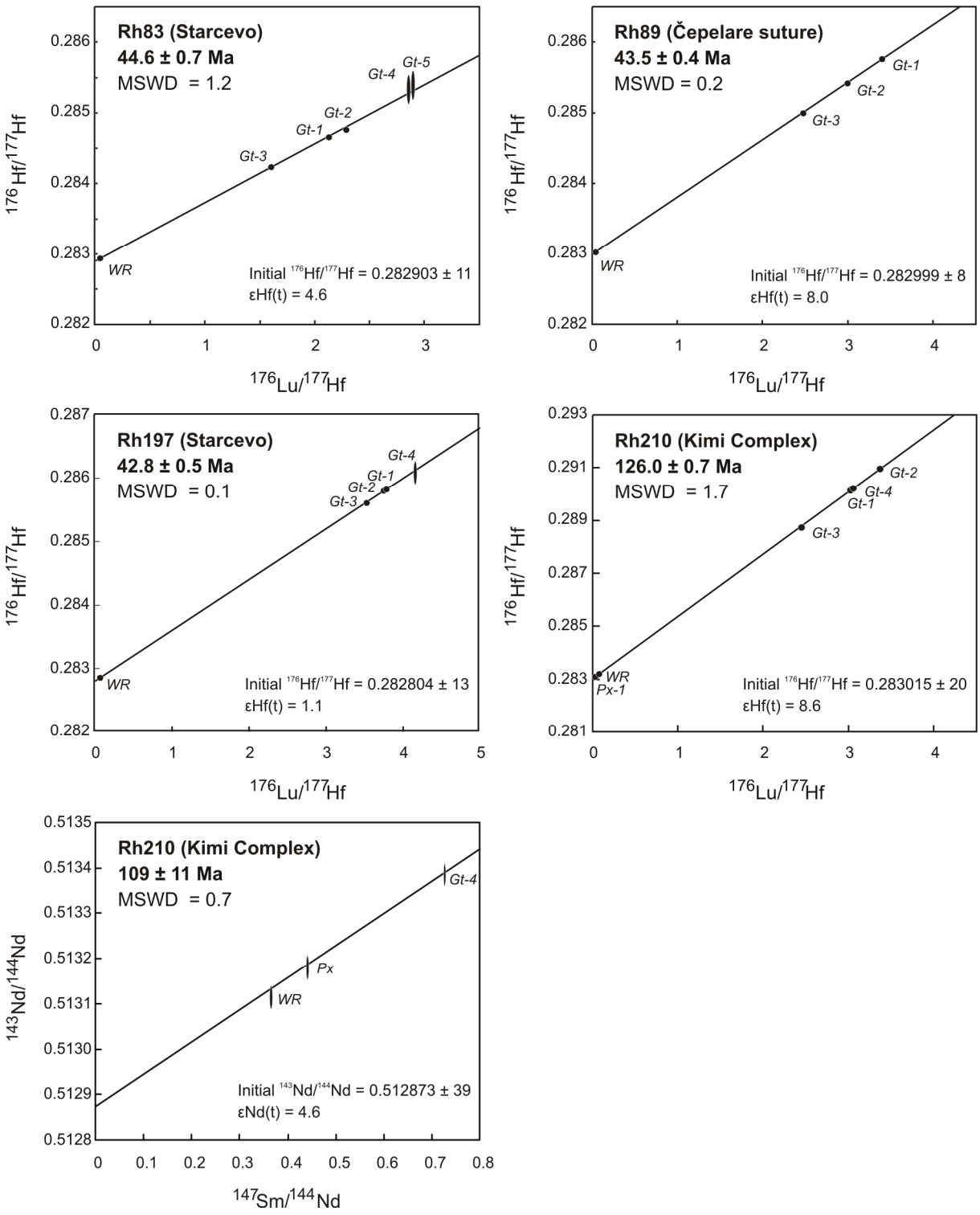

Fig. 2.7:

Lu-Hf isochrons for the four eclogite samples and a Sm-Nd isochron of sample Rh-210 from the Upper Allocthon. The elevated errors on sample splits Rh-83 Gt-4 and Gt-5 as well as Rh-197 Gt-4 reflect the smaller amount of analyzed Hf in these splits (see also Table 2.3).

2.7. Discussion

2.7.1. Significance of the Lu-Hf geochronological results

In order to adequately interpret the age information from the analyzed garnet populations, several important issues have to be addressed first. Two major points addressed here in detail are the representative sampling of garnet as well as protracted metamorphism and garnet growth.

(a) Representative sampling of bulk garnet and the problem of inclusions

The mineral separation technique employed in this study allows to test for any possible bias in the analyzed garnet separates. Pure garnet fractions (without visible inclusions; Gt-1, Gt-4, Gt-5 of each sample) as well as garnet fractions with a high density of inclusions were separated (Gt-2, Gt-3; see also Fig. 2.4 and 2.5, garnet major element distribution maps) and used for the Lu-Hf/Sm-Nd geochronological study. As illustrated in Fig. 2.7, all garnet separates define isochrons with considerably low MSWDs (< 1.7).

Furthermore, inclusions in garnet may significantly compromise the measured Hf isotope composition (e.g., Scherer *et al*., 2000). This issue is readily avoided by the employed tabletop digestion technique, which prevents the dissolution of Hf-rich phases like rutile or zircon (e.g., Scherer *et al*., 2000; Lagos *et al*., 2007). In contrast to the Lu-Hf isotope system, the Sm-Nd system is very sensitive to inclusions of apatite and monazite (Scherer *et al*., 2000) that are abundant as inclusions in garnet in samples Rh-83, Rh-89 and Rh-197, lowering the $^{147}Sm/^{144}Nd$ of the garnet separates. Hence, no meaningful Sm-Nd age could be determined for the samples from the Middle Allochthon.

(b) Constraints on protracted metamorphism and garnet growth

The good fit of all isochrons (MSWDs ≤ 1.7) strongly suggests that the Lu-Hf isotope system was not disturbed at a later stage, i.e., that garnets and whole rocks remained closed systems after formation. This is especially interesting for sample Rh-210 from the Upper Allochthon, which yields a Lu-Hf age of 126 ± 0.7 Ma. Based on U-Pb geochronology on zircons, Bauer *et al*. (2007) and Liati *et al*. (2002) infer a metamorphic event at ca. 74 – 77 Ma for the Kimi Complex, which supposedly reached amphibolite-facies conditions (Bauer *et*

al., 2007) or even eclogite- to UHP metamorphic conditions (Liati *et al*., 2002). Considering the results of the Lu-Hf and Sm-Nd geochronology of sample Rh-210 as well as similar results by Wawrzenitz & Mposkos (1997; 117 ± 3.5 Ma; Sm-Nd of gt-cpx-whole rock of a garnet-pyroxenite), it appears rather unlikely that a high-grade (eclogite- or UHP) post-Barremian metamorphic event affected sample Rh-210. To a certain degree, similar conclusions can be drawn with regard to older metamorphic events affecting the rocks from the Middle Allochthon as suggested from U-Pb zircon geochronology (~ 148 Ma, for the Nestos Shear Zone; Liati, 2005; Krenn *et al*., 2010). If garnet relicts from this Late Jurassic high-grade event had been preserved in the studied eclogite samples, then a mixture of old (radiogenic $^{176}Hf/^{177}Hf$; = garnet cores) and young (unradiogenic $^{176}Hf/^{177}Hf$; = garnet rims) garnet domains would be expected. Such observations have recently been made by Herwartz *et al*. (2011) for the Adula Nappe in the Central Alps.

Consequently, the Lu-Hf isochrons defined by the studied Rhodopean eclogites argue either (1) for a pervasive nature of both the Eocene and Cretaceous HP events in the Starcevo Unit and the Kardžali Unit, respectively or (2) for the absence of relictic garnet associated with previous metamorphic events in the respective unit. Moreover, the low MSWDs and the generally good fit between three (Rh-83, Rh-89 and Rh-197) of the four Lu-Hf isochrons provide strong evidence for a relatively short duration of garnet growth during the Eocene metamorphic cycle. This is also in line with the phase diagrams (Fig. 2.3) that predict garnet growth over a relatively small P-T interval just before reaching peak-pressure conditions, i.e., only above 500 °C. If garnet grew over a period of several tens of Myr, the data points would show a higher scatter, i.e. a higher MSWD (e.g., Kohn, 2009).

2.7.2. Prograde growth ages versus cooling ages

During the nucleation and subsequent growth of garnets along a prograde P-T path, minerals such as garnet develop a growth zonation, which can be approximated by a Rayleigh process (or fractional crystallization and thermodynamic equilibrium; after Kohn, 2003). Of fundamental interest here is the preservation of undisturbed distribution patterns for Lu-Hf (and Sm-Nd) in the garnets. Especially during the thermal peak of metamorphism diffusion of these elements would get enhanced. These effects may reset the Lu-Hf and Sm-Nd isotope systems, and the ages defined by the isochrons may then reflect cooling ages. Element diffusivity in garnet depends on a variety of other factors in addition to temperature, e.g., grain size, peak temperature, garnet composition, matrix composition, oxygen fugacity (fO_2),

duration of prograde metamorphism, cooling rate and ionic charge (e.g., Chakraborty & Rubie, 1996; Ganguly *et al*., 1998; van Orman *et al*., 2002; Skora *et al*., 2006, Caddick *et al*., 2010). A useful proxy to assess the effects of diffusion is the major element zonation found in garnets (Fig. 2.4, 2.5). As shown by experimental studies (e.g., van Orman *et al*., 2002) the ionic charge of an element exerts a major control on its diffusivity, where 2+ ions diffuse by orders of magnitude faster than 3+ (e.g. Lu), and presumably 4+ ions, (e.g., Hf). Furthermore, it appears that the Lu-Hf system is more resistant to diffusion compared to the Sm-Nd system, as relatively higher closure temperatures have been proposed for Lu-Hf (e.g., Scherer *et al*., 2000; Lapen *et al*., 2003).

The bell-shaped distributions of Mn, Ca and Fe/(Fe+Mg) in garnet in combination with elevated Lu concentrations in the garnet cores as it is shown for samples Rh-197 (Fig. 2.4c, 2.5c) and Rh-210 (Fig. 2.4d, 2.5d) can therefore be readily regarded as evidence for the preservation of the prograde growth zonation patterns for Lu-Hf. In these two cases, the Lu-Hf ages clearly reflect the time of garnet growth (e.g., Lapen *et al*., 2003). Based on mass balance arguments, however, Skora *et al*. (2009) pointed furthermore out, that the Lu-Hf ages reflect peak metamorphic conditions due to volumetrically higher abundance of garnet rims relative to garnet cores.

The large garnets in sample Rh-83 show a certain degree of garnet rim resorption (~30 % of the garnet radius). However, the very cores still show elevated Mn (and to a certain degree also Lu) contents. Considering the near-identical Lu-Hf age of Rh-83 (44.6 ± 0.7 Ma) with that of Rh-197 (42.8 ± 0.5 Ma), it is evident that resorption of the garnet rims is geochronologically barely resolvable and must have occurred at near-peak metamorphic conditions. Otherwise the Lu that diffused back into the garnet rims would have compromised the fit of the Lu-Hf isochron and biased the isochron towards an apparently younger age (see Kelly *et al*., 2011).

The more or less homogeneous major element composition of the small garnets in sample Rh-89 (Fig. 2.4b, 2.5b) probably results from diffusive reequilibration of formerly prograde zoned garnets. However, this feature may not necessarily indicate a concurrent diffusive mobilization of REEs, in line with findings by Dutch & Hand (2010), who reported garnets with flat equilibrated major element zonations but preserved primary REE zonations. Major element distribution maps shown in Fig. 2.4b and 2.5b in combination with the Lu concentration data obtained by LA-ICP-MS (Fig. 2.5b), however, also suggest the diffusion of Lu and resorption of large parts of the garnets. Considering the small garnet diameters of Rh-89 (less than 600 μm) compared to Rh-83 (2 - 3 mm), garnets in Rh-89 might have been more

susceptible to complete resorption and equilibration than the larger garnets in Rh-83. Furthermore, as all three eclogites from the Middle Allochthon (Rh-83, Rh-89 and Rh-197) display virtually identical Lu-Hf ages, it seems likely that the same near-peak metamorphism affecting sample Rh-83 also affected sample Rh-89.

Collectively, the Lu-Hf age of Rh-197 can be interpreted as closest representing the age of the peak metamorphic event affecting the Middle Allochthon. Samples Rh-83 and Rh-89 were affected by different degrees of garnet resorption close to the timing of the metamorphic peak. The Lu-Hf age in sample Rh-210 furthermore can be readily regarded as representative of the age of HP metamorphism in the Kardžali Unit. As mentioned above, the Sm-Nd isotope system of sample Rh-210 has been affected by element mobility during the metamorphic cycle. Therefore, we interpret the Sm-Nd age of 109 ± 11 Ma as only representing a minimum age for garnet growth.

2.7.3. Constraints on exhumation rates

Considering the Lu-Hf results discussed above, we can now place a robust age constraint on the P-T path of the investigated samples, in particular on the prograde flank towards peak pressure conditions (Fig. 2.3). Combining these results with published stratigraphic and geochronological data from the retrograde path allows to roughly estimate the orders of magnitudes of the cooling and exhumation rates. For the timing of prograde metamorphism we use the Lu-Hf age of sample Rh-197 (42.8 ± 0.5 Ma), as it represents the youngest garnet growth age and we therefore place minimum constraints on the exhumation rate. The depth of formation inferred from phase relationships corresponds to ca. 70 km. From Ar-Ar geochronology carried out on rocks from nearby units of the Middle Allochthon, the timing of cooling below 380-320°C is constrained by ages of 37.1 ± 2.4, and 36.1 ± 0.4 Ma (Lips *et al*., 2000), which might be considered as minimum ages due to a relatively low blocking temperature applied by the authors (350 ± 30 °C). Following Liati & Gebauer (1999) we assume a mean depth of c. 10 km for this phase of retrograde cooling. Complete exhumation of the Middle Allochthon to the surface is robustly constrained by unmetamorphosed marine sediments of Priabonian age that are unconformably resting on top of the Starcevo Unit northeast of Ardino (Yordanov *et al*., 2007). Hence, vertical exhumation from 70 kilometers depth had to be accomplished within less than 8 Myr and exhumation rates are therefore around 1 cm/year, similar to values estimated for the exhumation of the

Arda 1 and Starcevo Unit by Pleuger *et al*. (2011). This is clearly a minimum rate because the maximum subduction depths were probably reached somewhat later than the determined Lu-Hf age (< 42.8 ± 0.5 Ma). Moreover, exhumation and cooling in the study area may have occurred successively, the lithologies may have been exhumed isothermally first and then cooled (Fig. 2.3). Collectively, the actual exhumation may probably have occurred much faster, even before cooling started. Independent of this uncertainty, our results suggest higher exhumation rates than those proposed by Liati & Gebauer (1999), in the order of 5.7 – 11.8 mm/year (mean of 7.7 mm/year), nevertheless the order of magnitude is similar between both studies.

2.7.4. Constraints on the magmatic protolith

In developing a paleotectonic model for the Rhodopes, it is essential to constrain the nature of the eclogite protoliths, i.e., the tectonic environment in which the eclogite precursors formed. Of importance for the present study is the distinction between a divergent (MORB), a convergent (island-/continental- or back-arc), and an intra-plate setting (e.g., OIB). In this regard, the whole rock trace element budget as well as the Hf-Nd isotope compositions serve as a valuable tool to identify the original composition of the magmatic precursor (e.g., Becker *et al*., 2000; John *et al*., 2004; Zack & John, 2007; Zhao *et al*., 2007).

The mobility/immobility of trace elements during blueschist to eclogite transition has been the subject of extensive research over the past years where, for example, it has been shown that many trace elements are easily mobilized from the slab to the overlying mantle wedge during dehydration reactions (e.g., John *et al*., 2004, 2008; Zack & John, 2007; Beinlich *et al*., 2010). However, these processes are likely limited to zones with a high fluid flux (veins, channels and other fluid pathways). Other authors proposed a decoupling of fluid and trace element flux during subduction, i.e. only very limited amounts of trace elements are released from the subducting slab during prograde metamorphism (Spandler *et al*., 2003; 2004; 2007). Considering these interpretations, the bulk trace element patterns of the studied eclogite samples (Fig. 2.6a and b) may mirror element-loss of a more LREE-enriched precursor, like arc-related basalts or even OIBs, or may be considered as representative of the original magmatic protolith composition.

Sample Rh-210 from the Upper Allochthon appears to be affected by a selective loss

of LILE (Cs, Rb, Ba) and LREE (La, Ce, Pr, Nd), leaving behind positive anomalies of the HFSE and HREE (see Fig. 2.6a and b). Evidence for either a dehydration- or partial melt-mediated dissipation of Nd and Hf in sample Rh-210 is provided by increased $^{147}Sm/^{144}Nd$ (0.3664) and $^{176}Lu/^{177}Hf$ (0.03468) when compared to the other three samples (see Fig. 2.8a). This feature has also major implications for the interpretation of the Sm-Nd age determined for Rh-210 (see below). In any case, the consistently low $^{147}Sm/^{144}Nd$ and $^{176}Lu/^{177}Hf$ of the samples Rh-83, Rh-89 and Rh-197 might provide some evidence that these samples preserved their original magmatic REE and HFSE compositions.

A further tool to discriminate possible tectonic settings of metamorphic protoliths are the HFSE, which are considered as relatively immobile during subduction-zone metamorphism and subsequent retrograde overprint (e.g., Kogiso *et al*., 1997; Becker *et al*., 2000; Spandler *et al*., 2004; Schmidt *et al*., 2009). Ratios like Nb/Ta and Zr/Hf (13.4 – 15.3 and 37.9 – 44.5, respectively) of the four eclogites broadly overlap the fields of N-MORB, OIB and subduction-related basaltic rocks. The derivation of the protoliths from an enriched OIB-type source however can be excluded based on the high Zr/Nb (19.4 – 45.1) and low Nb concentrations (< 6 ppm), which would be expected to be higher if an OIB-type protolith is considered (Pfänder *et al*., 2007, Spandler *et al*., 2004). Furthermore, the negative Nb-Ta anomaly in sample Rh-197 (and to a lesser degree also in Rh-83 and Rh-89) are tentatively regarded as reflecting the derivation from a source with an island-arc setting.

Whole rock Hf (and to a lesser degree also the Nd) isotope compositions can be highly useful to constrain the nature of the eclogite protoliths due to the particular robustness of the Lu-Hf isotope system with respect to metamorphic overprints (e.g., Blichert-Toft *et al*., 1999; Polat *et al*., 2003). However, for the studied eclogites this approach is hampered by uncertainties in the protolith formation age, which is required to calculate initial isotope compositions. Therefore we assume a similar protolith formation age as was determined for eclogites near Sidironero by Liati (2005), reporting U-Pb SHRIMP ages for zircons of ~ 250 Ma (= t_1). Furthermore, a second protolith formation age (t_2) of 500 Ma was employed as a maximum estimate, as the presence of (possibly inherited) ~ 430 Ma old zircon domains (Liati, 2005) might indicate even older formation ages. Independent of the protolith age assumed, calculated εHf(t) and εNd(t) values for Rh-83 and Rh-197 are consistently low (see Fig. 2.8b), and they rather agree with the characteristics of a more enriched magmatic protolith than MORB. Conversely, initial values for Rh-89 well overlap the field for MORB.

Due to the near-chondritic $^{176}Lu/^{177}Hf$ of 0.03468, the whole rock εHf value of sample Rh-210 (εHf (i) ~ +10) is rather independent of the protolith age and overlaps the lower limit of the MORB field (Fig. 2.8b). However, back-calculated Hf and Nd isotopes of samples Rh-83 and Rh-197 unambiguously indicate a more enriched protolith than MORB (Fig. 2.8b).

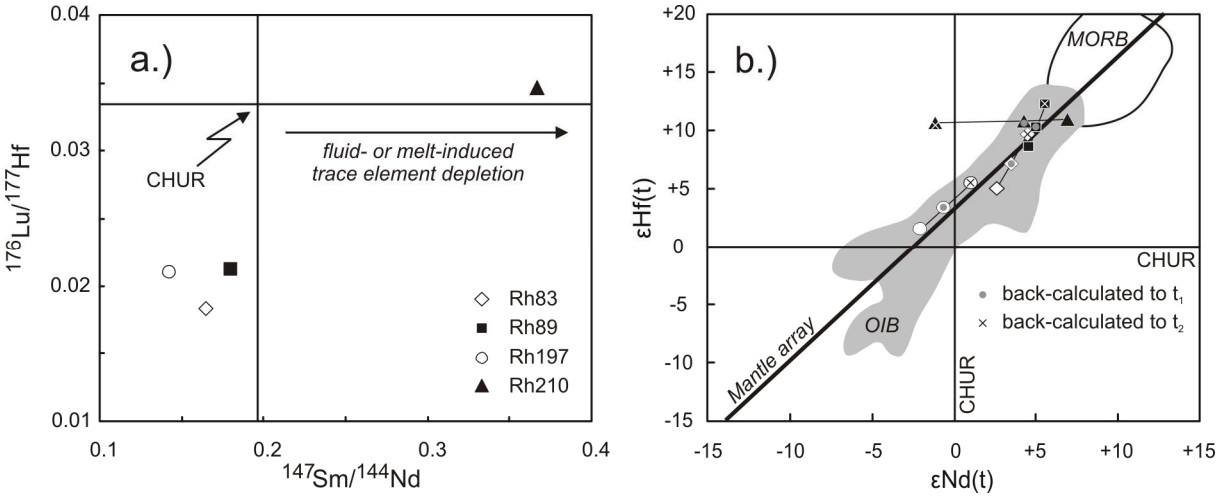

Fig. 2.8:

Constraints on the whole rocks of the four eclogites inferred by Lu-Hf and Sm-Nd isotope systematics.

a: $^{176}Lu/^{177}Hf$ vs. $^{147}Sm/^{143}Nd$ of the four eclogite samples, illustrating the effect of fluid-induced LREE depletion as it is especially important for sample Rh-210. After John *et al*. (2004).

b: εHf(t) - εNd(t) of the four samples in comparison to a compilation of global OIB and MORB (MORB after Pearce *et a*l., 1999; Woodhead *et al*., 2001; Chauvel & Blichert-Toft, 2001 and Kempton *et al*., 2002; OIB field after Nowell *et al*., 1998). Each sample is shown with εHf-εNd at present day, and also back-calculated to t_1 = 250 Ma and to t_2 = 500 Ma.

Collectively, our trace element and Hf-Nd isotope data for the four eclogites indicate significant element-loss for sample Rh-210 and possibly preserved original magmatic trace element signatures for samples Rh-83, Rh-89 and Rh-197. We can furthermore confidently exclude an OIB-type source for all four eclogites. The protoliths of samples Rh-83, Rh-89 and Rh-197 most likely originate from an island-arc setting based on the negative Nb-Ta anomalies and the rather unradiogenic Hf-Nd isotope systematics that are inconsistent with a MORB-setting. For sample Rh-210 we propose that the modified trace element pattern (loss of LREE, Th and also low K content) as well as the elevated $^{147}Sm/^{144}Nd$ and $^{176}Lu/^{177}Hf$ are the result of a partial melting event affecting the protolith somewhat before the closure of the Lu-Hf and Sm-Nd chronometers.

2.7.5. Implications for the tectonics of the Rhodopes and Hellenides

Our results show that two subduction events of different age are recorded in different structural levels of the Rhodopean nappe stack: Early Cretaceous in the Upper Allochthon and Eocene in the basal part of the Middle Allochthon. Such a distribution, older ages in the structurally higher nappes and younger ages in the deeper levels, is typical for collisional orogens and is also seen, for example, in the Alps (e.g., Gebauer, 1999) and the Norwegian Caledonides (e.g., Brueckner & Van Roermund, 2004). Our geochronological study confirms the results of Liati & Gebauer (1999) and Liati (2005) from U-Pb zircon dating, in that subduction-related metamorphism in the Rhodopes occurred more than once. In earlier studies, however, the geochronological results were rather assigned to specific areas (e.g., Western Rhodopes, Central Rhodopes – Liati, 2005) and not to specific structural levels in the Rhodopean nappe stack. In the present study we connect the results of the geochronology with the respective tectonostratigraphy, an approach that has emerged in the last few years (Krohe & Mposkos, 2002). It is also important to emphasize that our data actually support two metamorphic events (Early Cretaceous and Eocene), but do not preclude the existence of other subduction events, e.g., in the Jurassic (Liati, 2005; Bauer *et al*., 2007; Krenn *et al*., 2010; Nagel *et al*., 2011), at a more regional scale.

Significance of the Eocene ages from the Middle Allochthon

According to the most widely accepted evolutionary models for the Hellenic-Aegean orogenic system (van Hinsbergen *et al*., 2005; Papanikolaou, 2009; Jolivet & Brun, 2010), subduction and related metamorphism and deformation migrated progressively southward during the Mesozoic and Cenozoic. These models have assumed that the stacking of the Rhodopean nappes is Cretaceous in age. It has also been assumed that from the end of the Cretaceous onward, the Rhodopes were already in the hinterland of the southward retreating subduction zone (e.g., von Quadt *et al*., 2005) and thus were only affected by HT metamorphism, magmatism, and exhumation. However, this view cannot be maintained any longer. Instead, the basal part of the Middle Allochthon records subduction in the Eocene. Eocene ages for the peak pressure were already determined by U-Pb zircon SHRIMP dating of kyanite-eclogites from the area of Thermes in northern Greece (42.2 ± 9 Ma; Liati & Gebauer, 1999).

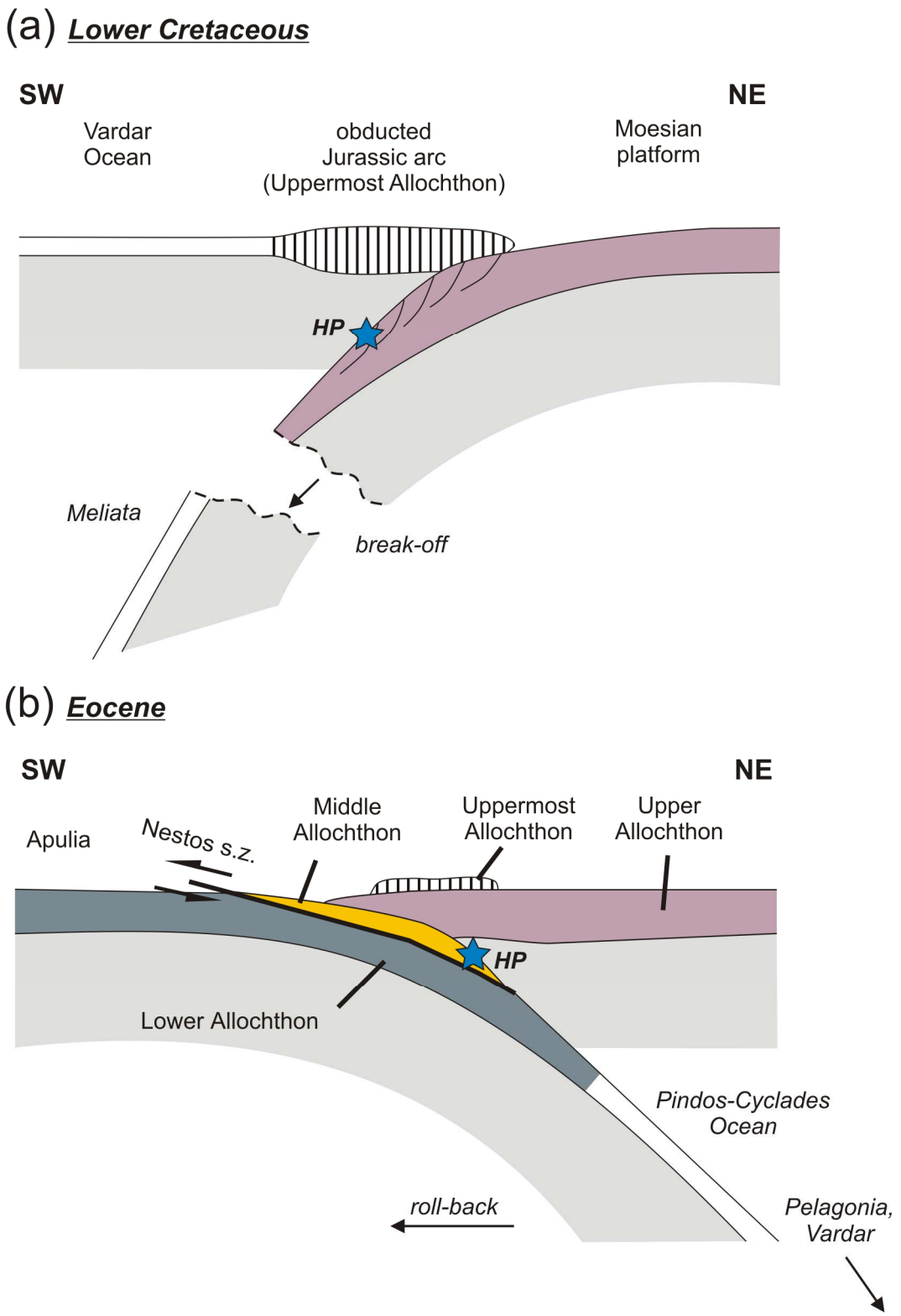

Fig. 2.9:

Schematic sketch illustrating the proposed paleotectonic reconstruction of the Rhodope nappe stack for (a) the Lower Cretaceous and (b) the Eocene. Modified after Jahn-Awe *et al*. (2011).

The results presented in our study thus confirm the inferences of Liati & Gebauer (1999). In the Nestos Shear Zone near Sidironero, further west but still in the same structural level, Liati (2005) dated the HP stage of an amphibolitized eclogite to 51.0 ± 1.0 Ma. Our new Eocene ages (44.6 ± 0.7 Ma, 43.5 ± 0.4 Ma, 42.8 ± 0.5 Ma) partially fill the gap between the ages from Thermes and from Sidironero. Hence, we assume that the ages from Thermes and Sidironero do not represent different metamorphic events, as suggested by Liati (2005), but rather point to protracted subduction lasting at least between 51 and 42 Ma. During the course of this subduction episode, different parts of the Middle Allochthon appear to have reached their peak pressure at different times.

Given the age constraints above, the question arises in which subduction zone system, from a paleogeographic point of view, the Eocene eclogites of the Rhodopes formed. All of the Eocene eclogites are from the lower part of the Middle Allochthon. This tectonic unit disappears beneath the Upper Allochthon towards the southwest. It is unlikely that the Middle Allochthon re-emerges in the ophiolite-bearing Vardar Zone, adjacent to the Rhodopes to the SW, as no Eocene HP metamorphism is known from that area. In the Cycladic Blueschist Unit, however, which is derived from the more southwesterly located Pindos-Cyclades Ocean, eclogite-facies metamorphism is also Eocene in age (U-Pb zircon and Lu-Hf garnet ages from 50 to 52 Ma; Tomaschek *et al*., 2003; Lagos *et al*., 2007). From stratigraphic evidence, ophiolites from the Pindos-Cyclades ocean were emplaced towards southwest onto continental crust of the Apulian continent during the Middle to Late Eocene (Papanikolaou, 2009). The emplacement of the Middle on the Lower Allochthon of the Rhodopes is also of Middle to Late Eocene age, as it postdates ca. 43 Ma old eclogite-facies metamorphism in the Middle Allochthon (this study, Nagel *et al*., 2011), and predates granitoid intrusions at 32 Ma (Jahn-Awe *et al*., 2010). Therefore, we suggest that the base of the Middle Allochthon in the Rhodopes represents the continuation of the Pindos-Cyclades suture towards deeper levels. In consequence, the underlying Lower Allochthon is correlated with the continental crust of Apulia (External Hellenide carbonate platform), as suggested by Dinter (1998), Krohe & Mposkos (2002), Jahn-Awe *et al*. (2010), and as illustrated in a paleotectonic sketch map in Fig. 2.9b. The Rhodopes are therefore interpreted as a large-scale tectonic window, exposing in its core the deepest nappe units of the Hellenides (see also Mposkos & Krohe, 2000). The sutures of both the Vardar and Pindos-Cyclades oceans are rooted along the northern border of the Rhodopes, north of the metamorphic domes (Arda etc.).

Significance of the Early Cretaceous age from the Upper Allochthon

The new 126.0 ± 0.7 Ma age for the eclogite from the Upper Allochthon is similar to published ages from the Kimi Complex (119.0 ± 3.5 Ma, Sm-Nd age for a garnet-pyroxenite; Wawrzenitz & Mposkos, 1997; and 117.4 ± 1.9, U-Pb zircon SHRIMP age for a garnet-rich mafic rock; Liati *et al*., 2002), and indicates that the Upper Allochthon in the Eastern Rhodopes was subducted during the Early Cretaceous. We assume that the Upper Allochthon represents the continental margin of Europe (Moesia), which collided with a Jurassic arc formed above a southwest-dipping subduction zone that consumed the Meliata Ocean (Bonev & Stampfli, 2008; Jahn-Awe *et al*., 2010; see Fig. 2.9a). During and after this collision, the European margin entered the subduction zone and was affected by eclogite-facies metamorphism. Between the Lower Cretaceous and the Eocene HP metamorphism, a subduction polarity switch occurred and the kinematic framework changed fundamentally.

2.8. Conclusions

New combined petrological and geochronological data for metamorphic rocks from the Bulgarian section of the Rhodopes can place new constrains on the tectonic evolution of the Eastern Mediterranean region. Lu-Hf garnet geochronological results for four eclogites from the Middle and Upper Allochthon reveal two high-pressure metamorphic events, (1) in the Lower Cretaceous (126 Ma) for the Upper Allochthon and (2) in the Eocene (45 – 42 Ma) for the Middle Allochthon. Geothermobarometry can place the peak metamorphic conditions in the Middle Allochthon at c. 700°C/20 – 25 kbar. Major and trace element analyses of the whole rocks point to an island-arc origin of the samples from the Middle Allochthon and clearly exclude OIB-like protoliths. Our data furthermore support previous findings that the Rhodopes represent a large-scale tectonic window, emphasizing a key role of the Rhodopes to understand the tectonic evolution of the Hellenides.

- Chapter 3 -

Tectonomagmatic Constraints on Magma Sources of Eastern Mediterranean K-rich Lavas

3.1. Introduction

Potassium-enriched (high-K) volcanic rocks occur in a variety of tectonic settings like active island arcs (e.g., *Indonesia;* Varne, 1985; Stolz *et al.*, 1990), or continental rifts (e.g., *East African rift*; Rosenthal *et al.*, 2009). High-K rocks are furthermore typical for syn- to post-collisional continental settings such as Italy (e.g., Conticelli *et al.*, 2002; 2009a, b; Gasperini *et al.*, 2002), Taiwan (e.g., Wang *et al.*, 2004), Serbia (e.g., Prelević *et al.*, 2005, Cvetković *et al.*, 2004), Tibet (e.g., Turner *et al.*, 1996; Williams *et al.*, 2004), and Tasmania (e.g., Crawford *et al.*, 1997). Regardless of age and setting, all of these rock suites tend to share geochemical similarities such as a strong enrichment in incompatible elements, as well as isotope compositions including low εNd and radiogenic $^{87}Sr/^{86}Sr$ (e.g., Hawkesworth & Vollmer, 1979; Conticelli *et al*., 2002). In most cases, shallow level assimilation of continental crust can be excluded as a major process due to the lack of coupled variations of major elements and isotope compositions (e.g., Mg-number vs. $^{87}Sr/^{86}Sr$). Thus, for mantle-derived high-K magmas, these features are generally assumed to mirror compositions of their source regions (e.g., Hawkesworth & Vollmer, 1979; Stolz *et al.*, 1990; Nelson, 1992b; Prelević *et al.*, 2008). In this context, two major models have been developed to explain the geochemical features of source regions of high-K magmas:

(1) Low-degree partial melting of ancient lithospheric mantle, producing melt compositions extremely enriched in incompatible trace elements together with large variations in radiogenic isotope compositions (*single stage model*; Varne, 1985; McKenzie, 1989; Foley, 1992b; Turner *et al.*, 1996).

(2) Subduction-related source enrichment by an enhanced flux of fluid- and/or melt-like components originating from mafic oceanic crust and subducted sediments (*multi-stage model*; Hawkesworth & Vollmer, 1979; Stolz *et al.*, 1990; Nelson, 1992b).

The metasomatized domains produced by any of these two mechanisms subsequently melt in

response to contemporary subduction or during later episodes of extension-decompression or asthenospheric upwelling.

In the present study we test these two genetic models using K-rich lavas from Bulgaria that comprise medium-K, high-K and shoshonitic suites after Peccerillo & Taylor (1976) (see Chapter 3.4). These lavas were emplaced in a post-collisional tectonic setting related to the closure of the Tethyan realm during the Alpine orogeny. The *single stage model* is assessed here by modelling the isotope evolution of ancient lithospheric mantle domains. In order to evaluate the role of young source enrichment by contemporary subduction (*multi-stage model*), we compare the compositions of the Bulgarian lavas to those of lavas from Santorini Island. The currently active volcanism on Santorini unambiguously taps mantle domains that have recently been overprinted by components derived from the subducting African plate (Francalanci *et al*., 2005; Bailey *et al*., 2009).

A close tectonomagmatic relationship of the currently active Aegean arc with the older (Eo-Oligocene) volcanism in Bulgaria is supported on the basis of recent P-wave tomographic models for the Eastern Mediterranean realm (Bijwaard *et al.* 1998; see also Fig. 3.2c). These models illustrate a continuous northward subduction of the Aegean slab since the Mesozoic (see also Wortel & Spakman, 2000; Faccenna *et al.* 2003; van Hinsbergen *et al.* 2005; Papanikolaou, 2009; Jolivet & Brun, 2010). Older models claiming several independent north-dipping subduction zones, e.g., Dercourt *et al.* (1986) and Gealey (1988), are not supported by the more recent tomographic studies. The persistent northward subduction in a single subduction zone system resulted in the consumption of an estimated 2100 – 2500 km of crust since the late Jurassic (van Hinsbergen *et al*., 2005). The proposed decoupling of the upper crustal parts from the subducting mafic lithosphere results in a nappe stack of terranes assembled along the European continental margin (van Hinsbergen *et al*., 2005). The inferred collision of the various Mediterranean terranes (Pelagonia – Apulia) along the Eurasian margin assembled diverse associations of subduction-related magmatic suites ranging in age from Jurassic to Quaternary (Pe-Piper, 1998; Pe-Piper & Piper, 2001; Marchev *et al.*, 2004, 2009; Bonev & Stampfli, 2008; Georgiev *et al.*, 2009; Vaggelli *et al.*, 2009). Therefore, the different volcanic arcs that formed during the progressive south-ward migration of the Hellenic trench can be related to the activity of one single subduction zone. It can be assumed that sediments derived from the African continental margin were continously subducted beneath the Eastern Mediterranean arcs (Pe-Piper & Piper, 2001). For South Aegean arc lavas this has been shown on the basis of Pb isotope compositions (e.g., Pe-Piper, 1994; Pe-Piper & Piper, 2001; Weldeab *et al*., 2002).

Here we present major and trace element as well as new Sr-Nd-Hf-Pb isotope data for mafic medium-K, high-K and shoshonite suites from Bulgaria as well as for mafic medium-K calc-alkaline lavas from Santorini. In addition, we report data for alkaline basalts from Bulgaria that represent the youngest stage of anorogenic magmatism in Bulgaria (28 – 26 Ma), tapping compositions of upwelling asthenospheric mantle during crustal extension.

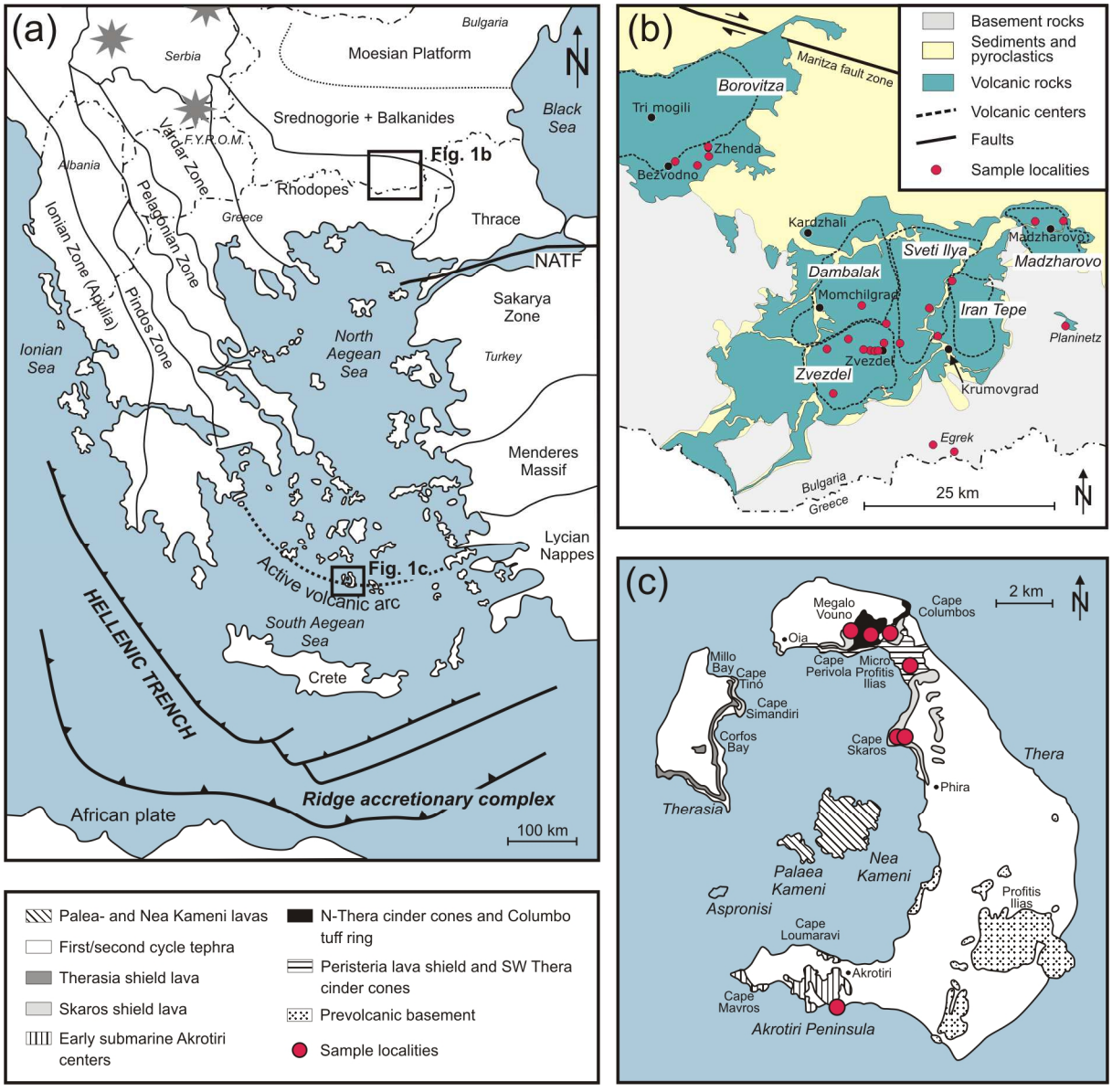

Fig. 3.1:

(a) Overview of the Eastern Mediterranean, modified after Barr *et al.* (1999) and van Hinsbergen *et al.* (2008). The grey stars denote major localities of post-collisional ultrapotassic rocks studied by Prelević *et al.* (2005), the stippled line indicates political borders. (b) Overview of Eastern Bulgaria showing the major volcanic centers and sample localities, modified after Ricou *et al.* (1998) and Marchev *et al.* (2004). (c) Map of Santorini illustrating major volcanic complexes and sample localities; after Druitt *et al.* (1999), and Bailey *et al.* (2009).

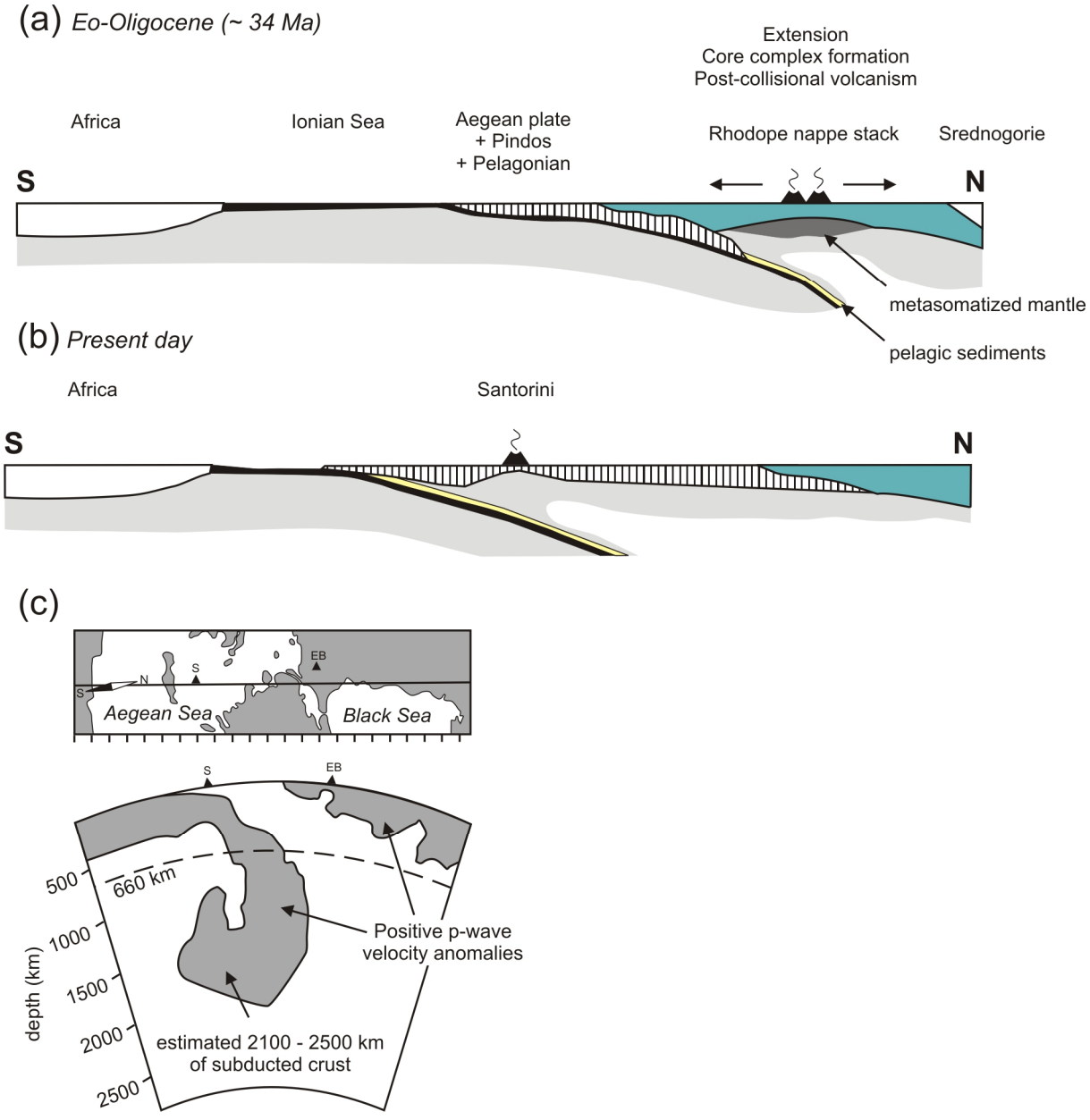

Fig. 3.2:

N-S cross sections from the Ionian Sea to the Rhodopes at (a) 34 Ma and (b) present day. Panel (c) illustrates a tomographic cross-section from the Hellenic Trench to the Eurasian platform modified after Bijwaard *et al.* (1998), van Hinsbergen *et al.* (2005) and Jolivet & Brun (2010). Black triangles denote location of Santorini (S) and Eastern Bulgaria (EB).

3.2. Geological background

3.2.1. Rhodopes – Bulgaria

The East Bulgarian Rhodope Massif is regarded as a pile of syn-metamorphic nappe stacks that were assembled at an active continental margin during the Alpine orogeny (e.g., Ricou *et al.*, 1998; Dinter, 1998; Schmid *et al.*, 2004; Turpaud & Reischmann, 2010; Jahn-Awe *et al*., 2010). The Rhodope Massif is bound to the north by the Maritza strike-slip fault, to the west by the Vardar zone and to the east by the Thrace and Maritza basins (Fig. 3.1a, b). The Southern part of the Rhodopes is covered by the Aegean Sea (see Fig. 3.1a). During the course of the Alpine orogeny, the eastern Mediterranean region was affected by successive episodes of oceanic basin formation and repeated collisions with continental fragments derived from the African margin with Eurasian crust (Ricou *et al.*, 1998; Dinter, 1998; van Hinsbergen *et al*., 2005; Jolivet & Brun, 2010). These tectonic episodes are intimately related to the magmatic pulses recorded around the Aegean Sea (e.g., Pe-Piper, 1998; Bailey *et al.*, 2009). In Bulgaria, subduction-related volcanic activity is recorded from the Jurassic - early Cretaceous (*Evros-Thrace*, Bonev & Stampfli, 2008), the Upper Cretaceous (*Srednogorie Zone*, Marchev *et al.*, 2009; Georgiev *et al.*, 2009) and the Eocene-Oligocene (*Rhodopes,* Yanev *et al.*, 1998; Marchev *et al.*, 1998a, b, 2004). The youngest subduction-related volcanism in the Eastern Mediterranean is represented by the active Aegean island-arc (e.g., Zellmer *et al.*, 2000; Bailey *et al.*, 2009; Vaggelli *et al.*, 2009).

The Eocene-Oligocene volcanism in the Eastern Rhodopes is considered post-collisional (see also Fig. 3.2a). Compressional episodes in the Rhodopes are documented for the Lower Cretaceous (~ 120 Ma; Warwzenitz & Mposkos, 1997; Liati *et al.*, 2002), probably early Paleocene (~ 65 Ma; Liati *et al*., 2002), and Eocene (~ 42 Ma; Liati & Gebauer, 1999). In the Late Cretaceous, an extensional episode was triggered by reorganization of plate boundaries, gravitational collapse and the retreat of the subduction zone further south (Burg *et al.*, 1996; Mposkos & Krohe, 2000; Bonev *et al.*, 2006) or, as recently suggested, by a reversal of the subduction zone polarity (Jahn-Awe *et al*., 2010). After a further episode of HP metamorphism during the Eocene (Liati & Gebauer, 1999), which was related to the amalgamation of the Rhodopean nappe stack to the Eurasian platform, the subsequent extensional episode was linked to the formation of metamorphic core complexes and sedimentary basins (Sokoutis *et al.*, 1993; Boyanov & Goranov, 2001; Bonev *et al*., 2006; Siemes *et al.*, 2009). This extensional process was furthermore accompanied by two distinct

episodes of magmatic pulses in the Rhodopes: (1) Paleocene-Early Eocene intrusion of granitoids (70-42 Ma), which is regarded as the direct continuation of the magmatism from the Srednogorie Zone, and (2) Eocene-Oligocene acid-intermediate and basic volcanism (ca. 34-30 Ma; Krohe & Mposkos, 2002; Marchev *et al*., 2004, 2005; Bonev *et al.*, 2006), which is the focus of our study. This post-collisional high-K volcanism in the Eastern part of the Rhodopes lasted from the late Eocene (Priabonian, ca. 34 Ma) to the Oligocene (ca. 30 Ma*;* Singer & Marchev, 2000; Marchev & Singer, 2002). After a hiatus of several Myrs, the emplacement of alkaline mafic intraplate lavas is recorded from 28 - 26 Ma (e.g., Marchev *et al.*, 1998a, b), similar in age to other Cenozoic provinces with intraplate volcanism in Europe (e.g., Lustrino & Wilson, 2007).

3.2.2. Santorini – Aegean Sea

After the collision between the Eurasian continental margin and crustal fragments related to Africa (Dinter, 1998, van Hinsbergen *et al*., 2005), an extensional period followed during Paleogene time. Subsequently, active subduction has been re-located since the mid-Miocene in the Aegean region with the Eastern Mediterranean sea floor subducting towards the northeast beneath the Aegean microplate (see Fig. 3.1a and 3.2b; e.g., Ninkovich & Hays, 1972; Jolivet & Brun, 2010). Presently, subduction takes place south of Crete along the Hellenic Trench (see Fig. 3.1a; e.g., Lepichon & Angelier, 1979; Wortel & Spakman, 2000). Santorini is located in an extensional tectonic regime on thinned and stretched continental crust of the Aegean plate (20-32 km thick), consisting of metamorphic basement of late Palaeozoic/early Mesozoic age that is mainly composed of metapelites, limestones and various other metamorphic lithologies of the Cycladic Crystalline Complex (see Druitt *et al.*, 1999 and references therein). Volcanism at Santorini is active since ~ 750 ka, including 12 major explosive and over 100 smaller eruption cycles (Druitt *et al.*, 1999). The last eruption has been recorded in 1950 and Santorini is currently regarded as dormant. Explosive eruptions on Santorini are of plinian-type with andesitic to rhyodacitic products as well as lava flows and cinder cones of basaltic to andesitic compositions (Nicholls, 1971; Druitt *et al.*, 1999; Bailey *et al.*, 2009). A detailed description of the volcanism on Santorini is given in Druitt *et al.* (1999) and Bailey *et al.* (2009).

3.2.3. Sample suite

(a) Bulgarian lavas from the Eastern Rhodopes

The samples analyzed in our study represent the most mafic volcanic rocks found in the Eastern Rhodopes of Bulgaria and they originate from five discrete volcanic centres, located in close proximity to the border of Greece (see Fig. 3.1b). These volcanic centres include shield and stratovolcanoes, composed of lava flows, domes and dikes as well as large amounts of epiclastic and pyroclastic material. The volcanic structures are part of a Cenozoic magmatic belt that extends toward the NW into Macedonia and Serbia (see Cvetković *et al*., 2004; Prelević *et al*., 2005), crossing the Vardar zone, and continues to the SE in the Thracian Basin and Western Anatolia. The sample locations are illustrated in Fig. 3.1b. The Borovitza caldera (1) is the largest volcanic edifice in the Eastern Rhodopes. Its tectono-magmatic evolution can be divided into six major absarokitic-shoshonitic-latitic episodes dated between 34 and 30 Ma (Marchev *et al.*, 2004; Dhont *et al.*, 2008). Further shoshonitic to high-K calc-alkaline volcanoes are, from W to E: (2) Sveti Ilya, (3) Zvezdel, (4) Iran Tepe and (5) Madzharovo. An additional volcanic edifice (Dambalak) was not sampled during the course of this study but is also shown in Fig. 3.1b. The younger alkaline basalts (28 – 26 Ma old) examined in this study originate from two localities SSE of Krumovgrad close to the village of Egrek (reported as "Krumovgrad alkaline basalts" by Marchev *et al.*, 1998a, b; 2004; Fig. 3.1b). They occur as N-S to NW-SE striking dikes of 0.5 – 50 m thickness. Detailed field and petrographic descriptions of the different volcanic centres are given by Marchev *et al.* (2004).

The Bulgarian samples were collected in fresh outcrops and, except for the absarokites from Borovitza, generally lack major alteration features. The absarokites were collected at two different localities: (1) close to the village of Zhenda (Borovitza caldera) and (2) close to the village of Planinetz, located ca. 20 km east of Krumovgrad (Fig. 3.1b). Absarokites from the Borovitza caldera (Zhenda) are silica-undersaturated (nepheline-normative) and characterized by olivine, clinopyroxene and relict leucite phenocrysts, the latter are virtually entirely replaced by analcime, probably during low-grade alteration. The impact of analcime formation on the geochemistry of high-K, shoshonitic and lamproitic rocks was already discussed in detail by Prelević *et al*. (2005) and our observations are generally in accord with their interpretations. Planinetz absarokites are silica-saturated (hypersthene-normative) and characterized by clinopyroxene and olivine phenocrysts, and phlogopite was observed in the groundmass. The common phenocryst mineral assemblage in the silica-saturated medium-K

and high-K rock suite usually comprises olivine, clinopyroxene, plagioclase as well as minor phlogopite, amphibole and apatite in a groundmass comprising plagioclase, clino-/orthopyroxene and a glassy/sanidine matrix in the shoshonitic rocks. The alkaline basalts are characterized by a glassy matrix with olivine, clinopyroxene, and plagioclase phenocrysts. Furthermore, some rare occurrences of micro-xenoliths (<1.5 mm) were observed in the alkaline basalts. The xenoliths exclusively consist of quartz, either as single crystals or as aggregates. A more detailed petrographic description of the alkaline basalts is given by Marchev *et al.* (1998b).

(b) Santorini

Samples analyzed in this study are from four different volcanic centers on Santorini: (1) Akrotiri, (2) Therasia, (3) Megalo Vouno and (4) Skaros (see Fig. 3.1c). All samples are characterized by the phenocryst assemblage olivine-clinopyroxene-plagioclase in a glassy/Pl-rich matrix. Where available, the GPS coordinates of the sample localities are given in Table 3.1.

3.3. Analytical techniques

A total set of 33 mafic samples was analyzed for major and trace element concentrations (Table 3.1) as well as for Sr-Nd-Hf-Pb isotope compositions (Table 3.2 and 3.3). The major element contents were determined on $Li_2B_4O_7$-flux fusion discs by X-ray fluorescence (XRF) using a PANalytical Axios X-ray spectrometer at Universität Bonn, Germany. Trace element analyses were performed by quadrupole inductively-coupled plasma mass spectrometry (ICP-MS) using an Agilent 7500cs at Universität Kiel, Germany. Analytical procedures followed those of Garbe-Schönberg (1993) involving multi-step multi-acid digestions of 100 mg aliquots of powdered samples with HF-HNO_3-$HClO_4$ in either high-pressure Parr bombs (JA-1), or PFA vials (BHVO-II and samples). Typical analytical precision as estimated from replicate measurements and sample duplicate digests was better than 1.5 %RSD for all trace elements, except Mo, W, Tl, Pb (< 3 % RSD) and Sb (<15%). The accuracy of the results can be inferred from measured values for the JA-1 and BHVO-2 reference materials that were analyzed along with the samples (Table 3.1).

Chemical separation of Sr-Nd-Hf was carried out on one split of ca. 100 mg of sample

powder that was spiked with a mixed ^{176}Lu-^{180}Hf tracer and subsequently digested in a 1:1 mixture of concentrated HF-HNO_3. The chemical separation of Hf and Lu from the matrix follows the procedure reported by Münker *et al.* (2001). Strontium and Nd were separated from the matrix left-over from the Hf separation, using BioRad® AG50W-X8 cation resin (200 – 400 mesh) and Ln-Spec resin (see Pin & Zalduegui, 1997). Lead isotope measurements were carried out on hand-picked, 3-4 mm sized whole rock chips. About 250 mg of the sample chips were subsequently leached in warm 3 M and 6 M HCl for one hour, respectively. After digestion in 3: 1 HF-HNO_3, a HCl-HBr chemistry was employed for Pb purification (after Korkisch & Hazan, 1965) using BioRad® AG1X8 (100 – 200 mesh) anion resin. The procedure was repeated to ensure a clean Pb fraction. Yields were always better than 97%.

The Sr-Nd-Hf-Pb isotope compositions as well as Lu and Hf concentrations were determined via a Thermo-Finnigan Neptune multi-collector ICP-MS at Universität Bonn, operated in static mode. Values of ^{87}Sr/^{86}Sr, ^{143}Nd/^{144}Nd and ^{176}Hf/^{177}Hf were corrected for mass fractionation using the exponential law and ^{86}Sr/^{88}Sr = 0.1194, ^{146}Nd/^{144}Nd = 0.7219 and ^{179}Hf/^{177}Hf = 0.7325, respectively. For Pb analyses, mass fractionation correction was carried out using the Tl-doping method employing the NBS 997 thallium standard (e.g., Hirata, 1996; Rehkämper & Mezger, 2000; Albarède *et al.,* 2004). Repeated analyses of the standards NBS 987 for Sr, La Jolla for Nd, JMC-475 for Hf and NBS 981 for Pb yield mean values of ^{87}Sr/^{86}Sr = 0.710269 (n = 29), ^{143}Nd/^{144}Nd = 0.511803 (n = 5), ^{176}Hf/^{177}Hf = 0.282149 (n = 21), and ^{206}Pb/^{204}Pb = 16.917, ^{207}Pb/^{204}Pb = 15.470, ^{208}Pb/^{204}Pb = 36.640 (n = 40). The external long-term reproducibility is ca. ±40 ppm for Sr, Nd, Hf, and better than ±130 ppm for all Pb isotope ratios (2 r.s.d.). Reported values are given relative to 0.710240 for NBS 987, 0.511859 for La Jolla, and 0.282160 for JMC-475. Lead isotope data are given relative to NBS 981 values of ^{206}Pb/^{204}Pb = 16.9405, ^{207}Pb/^{204}Pb = 15.4963 and ^{208}Pb/^{204}Pb = 36.7219 as reported by Galer & Abouchami (1998). Procedural blanks were typically <70 pg for Hf and Nd, <200 pg for Sr and <30 pg for Pb. The external precision of Sr-Nd-Hf measurements was further assessed by multiple digestions of six selected samples and three replicate analyses were carried out for Pb isotopes (see Table 3.2). External precision (2 r.s.d.) for the replicates was better than 30 ppm for ^{87}Sr/^{86}Sr and ^{143}Nd/^{144}Nd, 40 ppm for ^{176}Hf/^{177}Hf and 100 - 300 ppm for ^{206}Pb/^{204}Pb, 50 - 400 ppm for ^{207}Pb/^{204}Pb and 100 - 500 ppm for ^{208}Pb/^{204}Pb.

Table 3.1: Whole rock major and trace element analyses

Sample ID	BG-99a	BG-102	BG-99b	BG-101	BG-109a	BG-109b	BG-60	BG-103	BG-113	BG-46
Rock type	Abs	Abs	Abs	Abs	Abs	Abs	Sho	Sho	Sho	Banakite
Locality	Borovitza	Borovitza	Borovitza	Borovitza	Planinetz	Planinetz	Zvezdel	Borovitza	Madjarovo	Madjarovo
GPS (N)	41° 46.627'	41° 46.388'	41° 46.627'	41° 46.388'	41° 30.002'	41° 30.002'		41° 45.508'	41° 39.350'	
GPS (E)	025° 10.884'	025° 11.325'	025° 10.884'	025° 11.325'	025° 53.959'	025° 53.959'		025° 08.883'	025° 53.715'	
wt %										
SiO_2	48.1	50.4	48.7	49.6	48.6	48.3	53.0	53.6	53.0	56.9
Al_2O_3	10.8	11.2	10.9	9.09	11.9	11.6	16.3	15.3	17.2	17.5
MgO	7.35	7.13	6.91	5.40	8.77	8.51	2.84	4.73	4.25	2.19
Fe_2O_3	7.59	6.23	7.54	6.08	9.01	9.02	7.53	6.56	8.33	6.52
FeO	6.83	5.61	6.78	5.47	8.11	8.12	6.78	5.90	7.50	5.87
TiO_2	0.860	0.860	0.860	0.720	0.910	0.900	0.940	0.830	1.05	1.14
Na_2O	2.62	2.71	2.85	2.31	1.71	1.88	2.70	2.26	2.60	3.46
K_2O	3.30	3.27	3.10	2.57	3.74	3.56	3.15	3.98	2.65	3.77
CaO	12.8	12.8	12.5	15.3	10.6	10.8	5.87	6.60	8.47	5.90
P_2O_5	1.28	1.35	1.33	1.14	0.715	0.723	0.260	0.690	0.494	0.560
MnO	0.150	0.190	0.210	0.160	0.140	0.180	0.190	0.110	0.130	0.130
L.O.I.	4.32	3.71	4.06	6.90	2.98	3.27	6.78	4.74	1.01	1.42
Summe	99.5	100	99.3	99.6	99.3	99.1	99.8	99.8	99.5	99.8
ppm										
Li	24.1	14.6	18.9	19.1	18.5	14.7	14.5	56.8	10.0	6.37
Sc	34.9	36.0	34.6	28.9	47.0	48.2	21.6	25.1	25.0	16.2
V	186	193	191	155	227	229	186	186	213	141
Cr	452	460	439	382	354	360	14.1	75.1	39.5	8.39
Co	33.5	30.2	29.5	23.4	39.0	39.6	18.4	19.4	24.2	11.3
Ni	110	93.6	104	88.3	55.7	56.5	4.05	18.4	15.0	1.97
Cu	77.3	131	67.2	41.3	112	117	2.22	27.4	35.0	6.93
Zn	62.2	71.5	65.0	55.0	61.0	70.5	76.2	70.2	83.8	70.0
Ga	12.4	12.8	12.7	10.5	13.1	13.0	17.7	16.9	18.7	19.2
Rb	88.9	78.8	94.2	75.3	333	323	120	186	89.7	143
Sr	590	692	610	591	379	367	347	1189	693	992
Y	17.4	18.1	17.7	14.6	15.5	15.7	27.0	21.9	21.6	24.9
Zr	128	133	128	107	87.8	87.5	177	176	150	239
Nb	8.92	9.02	8.73	7.44	5.14	5.12	8.61	10.7	12.2	19.3
Mo	1.02	0.648	1.14	0.802	1.39	1.38	0.680	0.835	1.51	2.49
Sn	3.06	3.11	3.39	3.31	3.45	4.07	2.15	3.01	4.20	6.79
Sb	1.32	0.0990	2.00	0.318	0.0562	0.0864	0.163	0.343	0.117	0.789
Cs	278	212	378	134	18.9	7.79	15.0	5.69	243	456
Ba	1334	1573	1364	1324	970	953	882	2180	1257	1665
La	18.3	19.1	18.5	15.8	12.0	12.2	32.2	36.2	23.9	29.8
Ce	39.3	40.8	39.2	33.4	28.4	28.5	57.3	72.4	49.0	61.3
Pr	5.12	5.26	5.07	4.29	3.99	3.98	7.27	8.24	6.02	7.50
Nd	21.7	22.6	21.6	18.3	17.7	17.6	28.2	31.4	24.5	30.2
Sm	4.88	5.03	4.88	4.10	4.08	4.08	5.59	6.10	5.35	6.47
Eu	1.24	1.28	1.25	1.04	1.13	1.12	1.37	1.41	1.39	1.60
Gd	4.25	4.44	4.29	3.57	3.80	3.79	5.23	5.16	4.84	5.66
Tb	0.593	0.615	0.594	0.500	0.546	0.549	0.768	0.733	0.713	0.824
Dy	3.36	3.47	3.38	2.83	3.11	3.11	4.53	4.12	4.10	4.76
Ho	0.649	0.674	0.654	0.545	0.591	0.589	0.903	0.798	0.797	0.924
Er	1.76	1.81	1.76	1.48	1.54	1.55	2.50	2.17	2.16	2.53
Tm	0.256	0.263	0.257	0.216	0.218	0.219	0.367	0.320	0.315	0.371
Yb	1.68	1.71	1.69	1.41	1.39	1.41	2.40	2.12	2.05	2.46
Lu	0.252	0.254	0.251	0.213	0.206	0.207	0.360	0.315	0.303	0.367
Hf	3.25	3.33	3.22	2.74	2.39	2.41	4.42	4.46	3.83	5.91
Ta	0.488	0.492	0.478	0.406	0.345	0.343	0.620	0.750	0.867	1.39
Tl	1.28	0.522	1.90	0.472	1.35	1.18	1.01	1.62	1.03	1.43
Pb	21.6	22.6	22.3	18.2	17.2	20.4	17.6	33.6	28.0	40.7
Th	7.69	7.93	7.67	6.54	5.99	6.02	11.6	17.2	12.8	22.0
U	1.86	2.77	1.76	2.37	2.98	3.03	3.46	4.97	5.97	11.9

Table 3.1: continued

Sample ID	BG-62	BG-58	BG-78	BG-56	BG-67	BG-59	BG-82	BG-52	BG-92	BG-117
Rock type	MK-HK	MK-HK	MK-HK	MK-HK	MK-HK	MK-HK	MK-HK	MK-HK	MK-HK	MK-HK
Locality	Zvezdel	Zvezdel	Zvezdel	Zvezdel	Zvezdel	Zvezdel	Iran Tepe	Zvezdel	Sveti Ilya	Sveti Ilya
GPS (N)	41° 28.903'		41° 24.708'		41° 31.825'		41° 34.698'	41° 28.317'	41° 32.189'	41° 29.211'
GPS (E)	025° 31.508'		025° 25.673'		025° 28.411'		025° 40.088'	025° 32.438'	025° 38.057'	025° 37.690'
wt %										
SiO_2	55.4	53.1	55.5	55.4	53.2	55.6	55.3	55.2	54.1	53.2
Al_2O_3	17.4	16.7	17.4	16.6	16.6	17.0	16.8	16.7	16.3	16.0
MgO	3.40	4.91	3.36	2.87	4.90	3.74	3.88	4.25	4.82	5.33
Fe_2O_3	8.30	9.22	7.87	7.40	8.94	7.51	7.54	7.84	7.42	8.37
FeO	7.47	8.30	7.08	6.66	8.04	6.76	6.78	7.05	6.68	7.53
TiO_2	1.00	1.00	0.91	0.99	0.97	0.81	0.99	0.89	0.84	0.96
Na_2O	3.45	2.67	2.99	2.50	2.52	2.85	3.49	3.16	2.91	2.77
K_2O	1.98	2.33	3.07	2.81	2.30	2.57	1.72	2.17	1.67	1.68
CaO	7.16	8.56	7.03	7.02	8.55	7.09	7.03	7.34	8.48	8.71
P_2O_5	0.280	0.290	0.250	0.280	0.270	0.200	0.280	0.270	0.270	0.280
MnO	0.220	0.180	0.130	0.160	0.150	0.150	0.140	0.150	0.130	0.120
L.O.I.	0.790	0.440	0.770	3.32	0.890	1.31	1.65	1.13	2.01	1.85
Summe	99.6	99.6	99.5	99.5	99.5	99.3	99.0	99.3	99.2	99.5
ppm										
Li	6.77	4.77	7.95	11.4	8.74	6.04	5.88	6.69	11.0	11.0
Sc	23.4	30.4	22.5	22.5	31.4	24.8	23.7	24.5	27.9	30.9
V	204	239	205	182	237	200	185	189	195	219
Cr	22.9	52.8	24.2	19.5	56.4	16.9	45.9	46.3	71.6	119
Co	20.0	28.1	23.0	18.8	27.9	20.9	22.5	22.3	25.0	27.0
Ni	5.04	15.6	15.1	5.90	17.4	5.66	14.9	11.7	23.9	30.7
Cu	19.1	28.9	62.7	32.2	46.0	18.2	33.1	18.8	39.3	58.5
Zn	79.1	84.7	71.5	76.0	76.2	72.4	71.2	71.8	66.3	71.9
Ga	18.9	18.2	18.5	18.6	18.1	18.3	18.5	18.2	17.3	17.0
Rb	102	88.2	126	66.4	109	80.2	154	105	75.5	64.2
Sr	535	516	484	496	523	500	482	507	487	620
Y	25.4	22.0	22.1	24.8	22.2	21.5	24.3	22.5	21.4	23.4
Zr	187	121	181	232	149	148	191	183	139	162
Nb	8.95	7.49	9.26	10.9	7.52	8.40	9.81	8.56	7.46	8.68
Mo	1.71	1.35	1.51	2.05	1.30	1.53	1.38	1.50	1.11	1.19
Sn	2.44	2.33	2.65	2.60	2.36	1.97	2.87	2.61	2.70	2.84
Sb	0.107	0.0925	0.114	0.149	0.0896	0.206	0.0984	0.0988	0.108	0.107
Cs	4.18	5.11	3.42	1.32	4.88	4.28	7.18	5.22	4.59	6.18
Ba	836	843	865	1076	822	869	868	853	937	858
La	29.4	25.2	29.4	34.6	25.3	32.0	29.9	28.2	23.9	24.3
Ce	60.1	51.5	58.3	71.7	51.9	62.7	60.5	57.1	47.8	49.2
Pr	7.15	6.23	6.74	8.25	6.24	7.29	7.15	6.77	5.72	5.87
Nd	27.7	24.7	25.6	31.4	24.6	27.2	27.7	26.2	22.5	23.2
Sm	5.63	5.16	5.10	6.16	5.15	5.17	5.63	5.29	4.79	5.00
Eu	1.37	1.30	1.21	1.35	1.26	1.24	1.34	1.27	1.18	1.21
Gd	5.19	4.76	4.65	5.44	4.72	4.58	5.10	4.81	4.42	4.69
Tb	0.782	0.706	0.690	0.799	0.710	0.678	0.765	0.712	0.668	0.722
Dy	4.66	4.17	4.07	4.67	4.19	3.99	4.52	4.23	4.00	4.31
Ho	0.929	0.814	0.806	0.913	0.824	0.782	0.894	0.837	0.792	0.861
Er	2.58	2.23	2.22	2.52	2.27	2.18	2.47	2.31	2.21	2.37
Tm	0.381	0.326	0.335	0.374	0.334	0.326	0.366	0.345	0.327	0.354
Yb	2.55	2.13	2.22	2.43	2.20	2.16	2.39	2.28	2.17	2.32
Lu	0.38	0.315	0.333	0.362	0.329	0.322	0.358	0.342	0.322	0.342
Hf	4.66	3.06	4.60	5.77	3.88	3.78	4.83	4.58	3.56	4.05
Ta	0.649	0.550	0.700	0.784	0.561	0.627	0.789	0.632	0.584	0.679
Tl	1.12	0.621	0.673	0.516	0.770	0.410	1.632	0.868	1.05	0.522
Pb	20.3	17.8	23.3	24.0	19.2	19.7	24.9	20.2	23.7	25.8
Th	11.9	10.4	16.4	16.1	10.9	12.6	14.4	12.4	11.7	12.2
U	3.53	3.33	4.92	4.66	3.42	3.17	4.70	3.89	4.23	4.26

Table 3.1: continued

Sample ID	BG-107	BG-61	BG-64	BG-72	BG-49	BG-110	BHVO-II
Rock type	MK-HK	MK-HK	MK-HK	MK-HK	Alkaline dikes	Alkaline dikes	Standard
Locality	Borovitza	Zvezdel	Zvezdel	Zvezdel	Egrek	Egrek	Tabletop digestion
GPS (N)	41° 45.159'	41° 28.261'	41° 30.785'	41°.29.597'	41° 18.761'	41° 19.106'	
GPS (E)	025° 09.467'	025° 31.285'	025° 32.749'	025° 24.432'	025° 38.347'	025° 37.595'	
wt %							
SiO_2	56.4	58.4	56.3	53.5	46.5	46.0	
Al_2O_3	16.2	18.0	16.7	16.8	16.4	16.8	
MgO	4.01	0.74	3.64	4.06	7.33	7.51	
Fe_2O_3	6.19	6.87	7.79	8.99	8.74	8.96	
FeO	5.57	6.18	7.01	8.09	7.86	8.06	
TiO_2	0.770	1.05	0.990	1.00	2.03	2.07	
Na_2O	3.02	2.99	3.47	3.14	3.78	2.02	
K_2O	2.97	3.28	2.16	1.27	1.97	2.31	
CaO	7.11	6.32	6.63	8.36	9.48	10.1	
P_2O_5	0.440	0.250	0.260	0.180	0.687	0.579	
MnO	0.120	0.0600	0.140	0.170	0.160	0.140	
L.O.I.	1.70	1.45	0.99	1.73	1.93	2.96	
Summe	99.4	99.7	99.3	99.3	99.3	99.7	
ppm							
Li	5.42	17.0	6.85	10.2	9.31	13.3	4.70 (4.60)
Sc	21.1	21.4	23.2	28.6	23.4	25.1	34.7 (31.8)
V	156	177	184	226	200	226	327 (317)
Cr	72.4	16.6	23.5	31.3	183	151	310 (289)
Co	18.3	15.0	19.8	26.8	32.7	32.3	45.9 (45.0)
Ni	21.3	5.01	5.82	8.05	109	76.2	120 (119)
Cu	28.7	16.9	24.8	21.1	42.2	52.3	130 (127)
Zn	65.0	72.9	79.8	81.7	73.1	74.5	107 (103)
Ga	17.9	17.4	18.8	18.3	19.9	19.3	21.6 (21.7)
Rb	120	113	124	85.0	71.4	58.2	9.01 (9.20)
Sr	973	357	528	515	803	692	400 (395)
Y	21.4	22.0	24.2	24.8	24.0	23.9	25.0 (25.5)
Zr	189	167	236	150	213	190	173 (174)
Nb	11.9	8.04	10.3	7.24	65.8	63.6	17.2 (18.0)
Mo	1.69	0.880	1.97	1.21	3.18	3.14	3.58 (4.00)
Sn	3.23	1.66	2.59	1.75	1.64	1.71	1.64 (1.80)
Sb	0.101	0.164	0.124	0.0855	0.127	0.0879	0.110 (0.130)
Cs	108	51.9	4.97	2.94	2.12	3.43	0.100 (0.110)
Ba	1967	1453	852	605	680	715	123 (130)
La	38.9	30.8	34.1	23.4	43.0	40.5	15.3 (15.2)
Ce	77.9	60.6	70.6	47.9	80.9	77.1	37.6 (38.0)
Pr	8.67	6.97	8.07	5.78	9.27	8.93	5.35 (5.30)
Nd	32.2	26.2	30.8	23.0	36.2	35.0	24.6 (25.0)
Sm	6.17	5.10	6.04	4.93	7.03	6.93	6.09 (6.20)
Eu	1.39	1.20	1.37	1.28	2.16	2.11	2.06 (2.06)
Gd	5.18	4.58	5.36	4.80	6.31	6.21	6.15 (6.30)
Tb	0.730	0.677	0.783	0.744	0.885	0.873	0.925 (0.930)
Dy	4.07	3.98	4.55	4.54	4.89	4.85	5.29 (5.25)
Ho	0.781	0.796	0.893	0.914	0.901	0.899	0.967 (0.990)
Er	2.15	2.20	2.45	2.54	2.35	2.35	2.42 (2.50)
Tm	0.317	0.329	0.366	0.378	0.329	0.328	0.325 (0.340)
Yb	2.12	2.20	2.37	2.51	2.12	2.09	1.97 (2.00)
Lu	0.319	0.328	0.359	0.376	0.310	0.307	0.276 (0.280)
Hf	4.80	4.10	5.83	3.83	4.62	4.16	4.37 (4.20)
Ta	0.940	0.600	0.740	0.512	3.86	3.77	1.13 (1.13)
Tl	1.28	0.936	0.945	0.445	0.119	0.142	0.0277 (-)
Pb	49.3	13.0	22.3	14.4	4.71	4.91	1.49 (1.70)
Th	19.4	13.0	15.9	8.12	7.49	7.65	1.25 (1.21)
U	5.26	3.26	4.40	1.92	2.01	1.84	0.409 (0.410)

Table 3.1: continued

Sample ID	SA-1	SA-3	SA-4	SA-6	SA-9	SA-10	SA-11
Rock type	Basalt	MK-Andesite	HK bas. And.	MK bas. And.	MK-Andesite	MK bas. And	MK bas. And.
Locality	Therasia	Vouno Cone	Therasia	Akrotiri	Skaros	Skaros	Skaros
GPS (N)	36° 27.820'	36 ° 27.959'	36° 27.303'	36° 20.832'	36° 25.940'	36° 25.918'	36° 27.904'
GPS (E)	025° 24.056	025° 24.411'	025° 25.302'	025° 23.725'	025° 25.146'	025° 25.095'	025° 24.758'
wt %							
SiO_2	51.5	56.5	54.5	54.5	56.8	52.5	55.2
Al_2O_3	18.5	17.3	18.3	17.3	16.1	16.9	17.9
MgO	6.26	4.24	3.87	5.79	3.96	7.17	3.88
Fe_2O_3	9.22	8.55	8.73	8.32	9.77	8.97	8.20
FeO	8.30	7.69	7.86	7.49	8.79	8.07	7.38
TiO_2	0.88	0.88	1.02	0.88	1.25	0.85	0.84
Na_2O	2.76	3.2	3.58	3.08	3.55	2.65	3.37
K_2O	0.550	1.45	1.68	1.21	1.45	0.750	0.960
CaO	10.5	8.45	8.24	9.19	7.49	10.5	9.18
P_2O_5	0.0830	0.114	0.178	0.120	0.181	0.0910	0.122
MnO	0.160	0.160	0.160	0.150	0.200	0.170	0.170
L.O.I.	0.0600	-0.170	0.170	0.040	-0.200	-0.280	-0.208
Summe	101	101	101	101	101	100	99.7
ppm							
Li	7.48	13.2	14.6	11.9	13.8	10.2	7.46
Sc	43.0	35.5	27.0	39.9	39.0	47.1	40.0
V	335	286	256	281	280	285	252
Cr	84.3	15.3	23.8	148	100	286	38.6
Co	37.8	29.9	26.6	32.3	27.0	38.4	26.1
Ni	51.8	16.3	13.3	52.2	23.1	75.3	15.1
Cu	74.8	50.7	40.4	64.0	74.8	64.7	60.2
Zn	74.2	75.4	84.8	76.5	95.6	76.6	81.8
Ga	17.9	18.5	20.3	17.7	18.8	16.7	18.7
Rb	15.4	62.0	57.8	45.3	58.4	27.9	31.7
Sr	242	210	309	195	191	192	229
Y	20.9	27.1	28.9	26.0	37.4	23.8	28.3
Zr	77.0	141	188	139	193	104	126
Nb	3.29	5.27	8.28	5.29	5.99	3.09	3.82
Mo	0.514	1.23	1.02	0.92	1.64	0.773	0.932
Sn	0.736	1.50	1.57	1.18	1.69	0.877	1.01
Sb	0.0658	0.139	0.0794	0.0959	0.178	0.0874	0.0986
Cs	0.422	1.83	1.80	1.15	1.86	0.882	0.829
Ba	130	209	386	219	230	128	187
La	8.03	14.8	24.7	15.4	17.1	9.07	12.1
Ce	17.2	30.8	51.5	31.5	37.3	20.1	26.5
Pr	2.33	3.83	5.93	3.87	4.81	2.65	3.46
Nd	10.4	15.8	23.2	15.6	20.5	11.7	14.9
Sm	2.80	3.89	5.01	3.72	5.23	3.16	3.86
Eu	0.943	1.05	1.29	1.03	1.37	0.949	1.17
Gd	3.31	4.32	5.04	4.15	5.93	3.74	4.43
Tb	0.576	0.749	0.844	0.711	1.03	0.649	0.770
Dy	3.75	4.79	5.20	4.53	6.66	4.26	4.99
Ho	0.793	1.01	1.08	0.963	1.41	0.905	1.07
Er	2.26	2.90	3.07	2.75	3.99	2.57	3.05
Tm	0.343	0.447	0.470	0.418	0.613	0.390	0.468
Yb	2.29	3.01	3.15	2.83	4.15	2.61	3.16
Lu	0.349	0.458	0.482	0.435	0.629	0.400	0.483
Hf	1.98	3.56	4.32	3.29	4.69	2.59	3.10
Ta	0.237	0.436	0.533	0.394	0.455	0.247	0.289
Tl	0.0242	0.166	0.0946	0.145	0.110	0.0586	0.0721
Pb	3.67	9.35	12.2	7.93	8.42	4.32	5.73
Th	2.33	8.83	7.39	6.77	9.00	4.13	5.07
U	0.679	2.89	2.05	1.99	2.74	1.27	1.54

3.4. Results

3.4.1. Major and trace elements

Major and trace element data for the mafic to intermediate potassium-rich volcanic rocks of Eastern Bulgaria as well as for seven mafic calc-alkaline rocks of Santorini (<57 wt. % SiO_2) are listed in Table 3.1. Following the classification scheme of Peccerillo & Taylor (1976; Fig. 3.3a) the samples are grouped into the following suites: The Bulgarian samples comprise a medium- to high-K suite (15 samples) as well as a shoshonitic-banakitic group (four samples). Six absarokite samples that represent the most mafic samples of the shoshonite series are grouped separately on the basis of their distinct major and trace element composition. The Bulgarian dataset is complemented by two samples from alkaline basalt dikes, representing the youngest volcanic episode in Bulgaria (28 – 26 Ma).

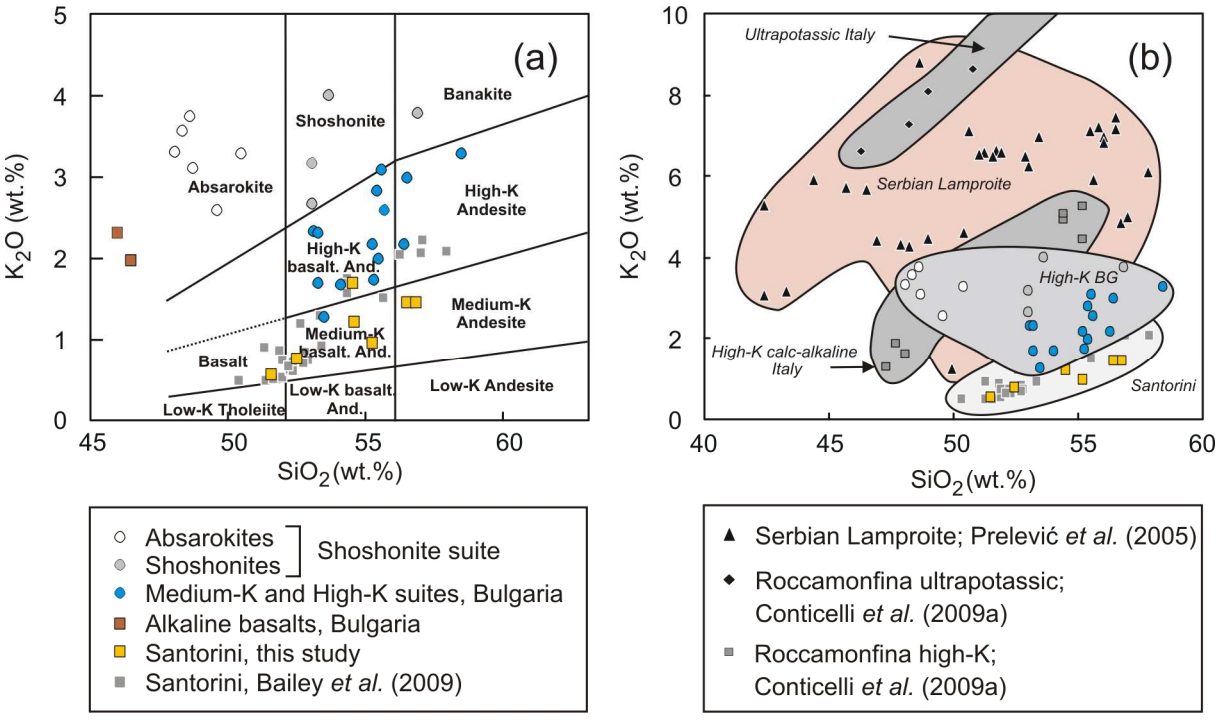

Fig. 3.3:

K_2O vs. SiO_2 systematic of lavas from Bulgaria and Santorini. (a) Classification diagram after Peccerillo & Taylor (1976). (b) Comparison of Bulgarian, Santorini, Serbian and Italian K-rich rocks in SiO_2 vs. K_2O space.

On the basis of the classification diagram of Peccerillo & Taylor (1976) the samples from Santorini from this study as well as from Bailey *et al*. (2009) can be classified as a low-

to medium-K calc-alkaline suite (see also Zellmer *et al*., 2009), comprising basaltic andesites and andesites (seven samples; see Fig. 3.3a). A comparison to other K-rich rocks from Serbia and Italy is shown in Fig. 3.3b.

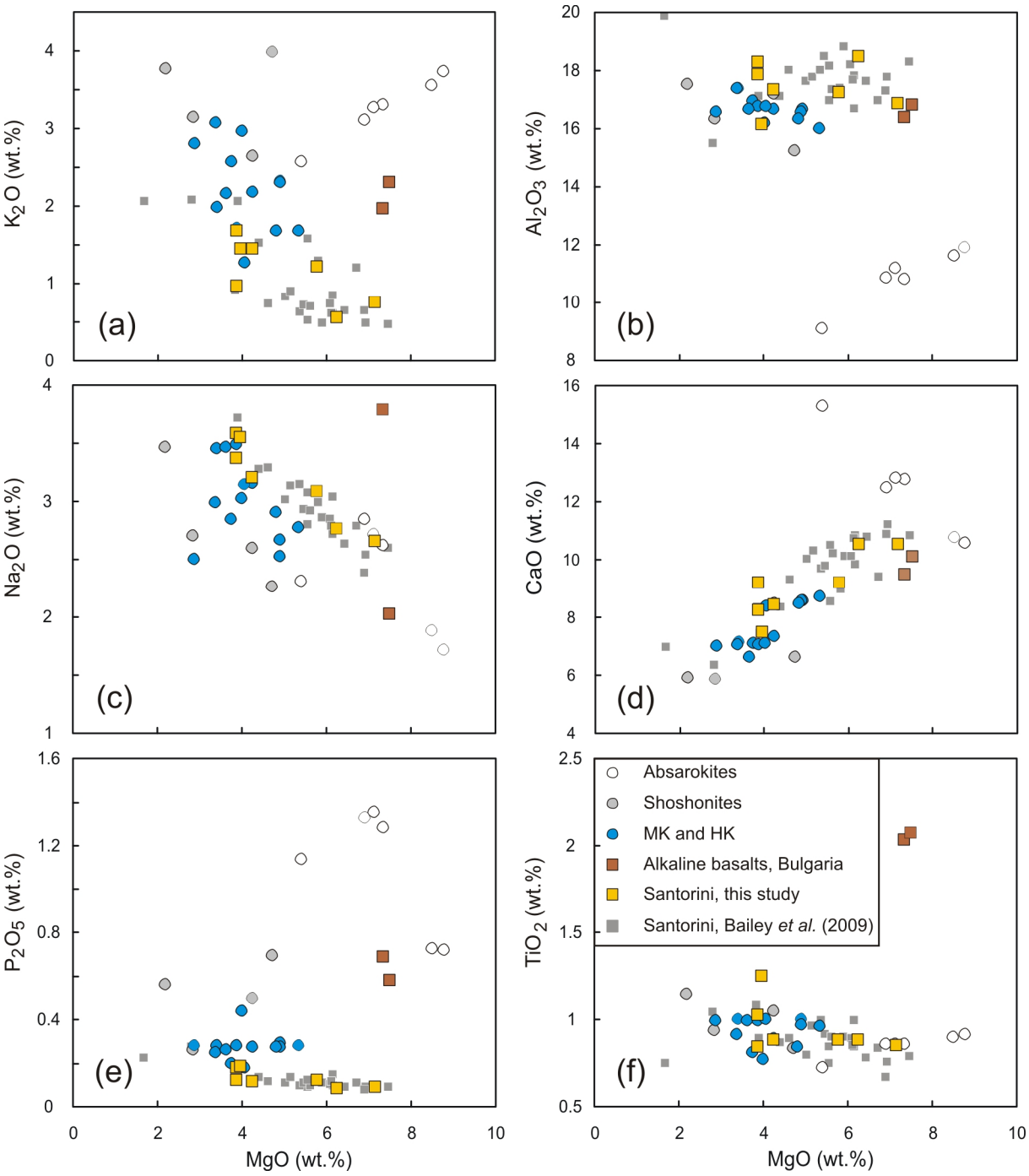

Fig. 3.4:

Major element variation diagrams for the sample suites from Bulgaria (medium- to high-K, shoshonitic, absarokitic and alkaline basalts), and Santorini (low- to medium-K).

The most primitive end-member of the studied K-rich sample suites is the absarokitic group with MgO = 5.4 - 8.8 wt. %, Cr = 350 - 460 ppm, Ni = 56 - 110 ppm and relatively high Mg-numbers of 50-56. Notably, the absarokites are relatively Ca-rich with CaO/Al_2O_3 from 0.9 – 1.7. Harker variation diagrams for the absarokites (Fig. 3.4 a-f and 3.5 a-c) generally show trends inverse to those expected for olivine fractionation, possibly reflecting fractionation of clinopyroxene and/or a K-Mg rich phase like phlogopite. Although phlogopite abundances in the studied rocks are rather low (< 5 vol. %), the Mg-numbers of subduction zone phlogopites can reach up to 94 (Coltorti *et al.*, 2007; Grégoire *et al.*, 2008), and therefore can be considered as an early phase to fractionate.

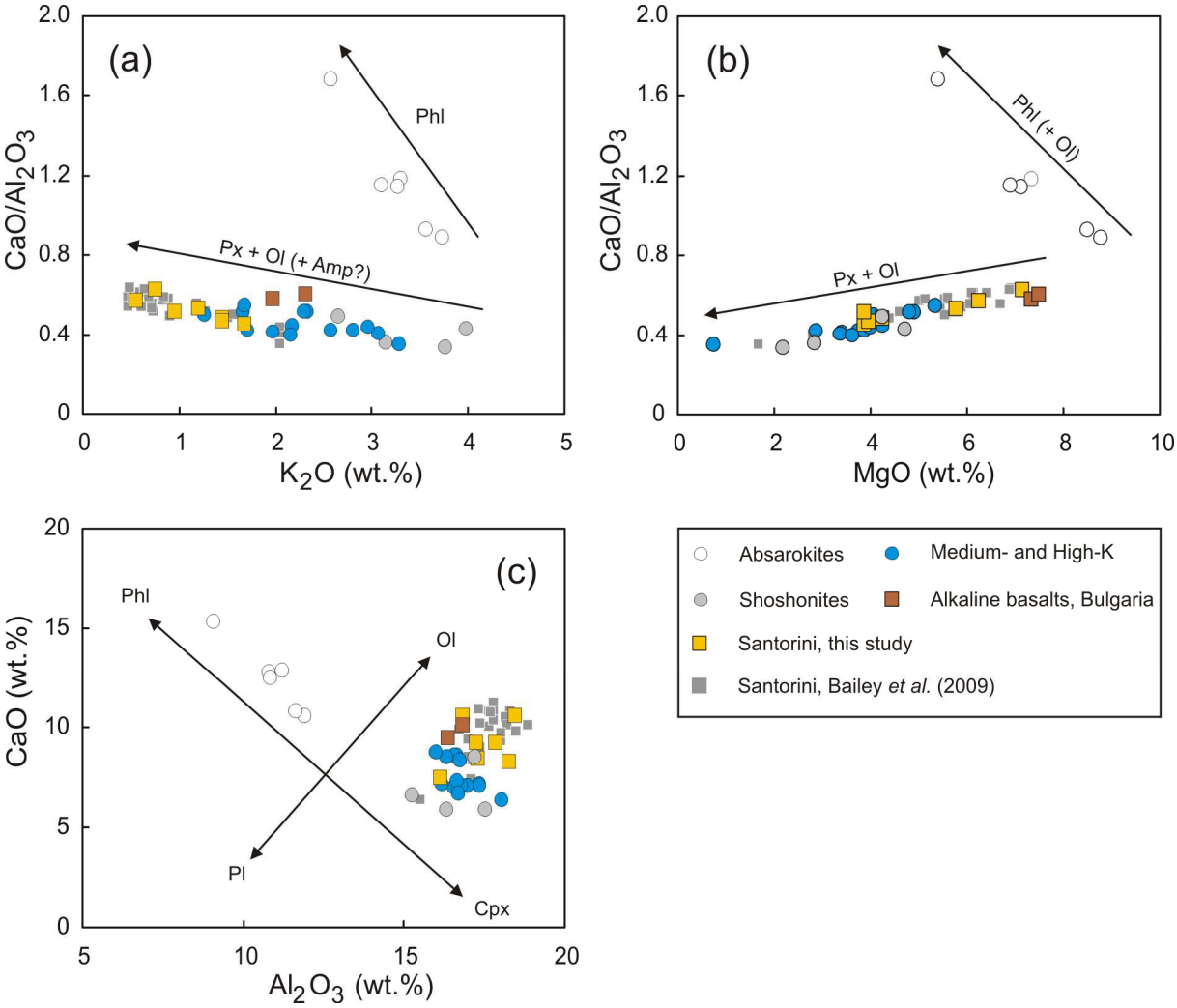

Fig. 3.5 a-c:

Major element variation diagrams indicating the major fractionating phases for the different sample suites (illustrated by vectors). Compositions of the Santorini and most Bulgarian lavas are controlled by olivine-pyroxene fractionation. As an exception, the Bulgarian absarokites were influenced by phlogopite fractionation.

The CI-normalized REE patterns of the absarokites (see inlet Fig. 3.6a) indicate a less pronounced LREE enrichment than for K-rich rocks from Serbia (lamproite-affinity group, see figure captions of Fig. 3.6 for details; Prelević *et al*., 2005) and from Italy (Roccamonfina high-K rocks; Conticelli *et al*., 2009a). Furthermore, in a primitive mantle normalized multi-element diagram (Fig. 3.6a) the absarokites from Bulgaria display enrichments in LILE, Pb and P and depletions of Nb and Ta. As for REE, the Bulgarian absarokites are less enriched in HFSE than the K-rich samples from Italy and Serbia. Compositions obtained here for the Bulgarian absarokites (and also the other compositional groups) are in excellent agreement with previously published trace element data for absarokites from Borovitza and Planinetz by Marchev *et al.* (2004; see stippled lines in Fig. 3.6).

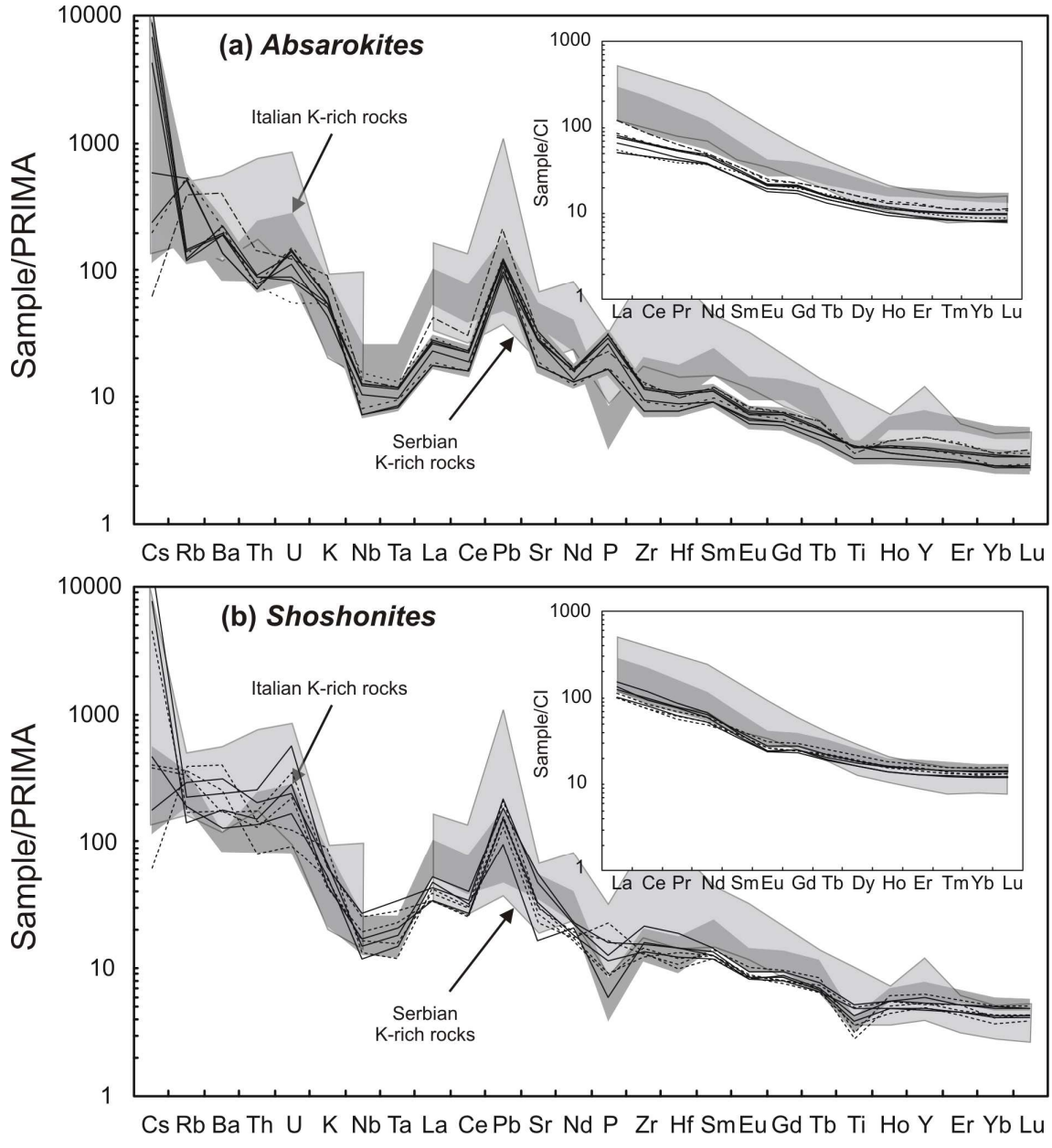

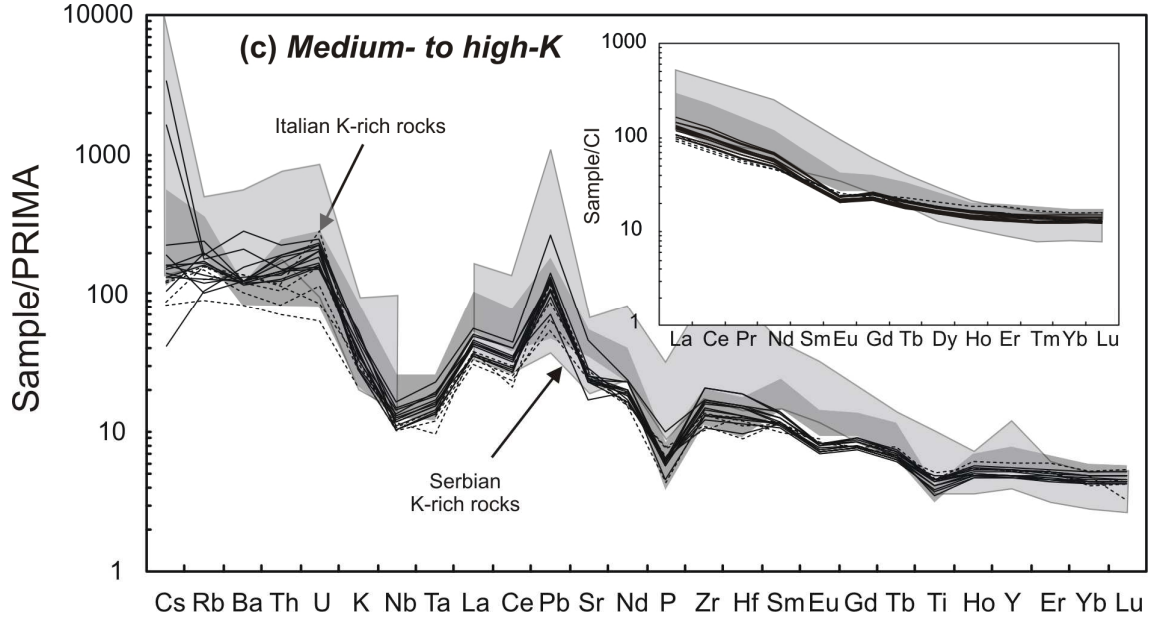
(c) Medium- to high-K
Italian K-rich rocks
Serbian
K-rich rocks
Sample/PRIMA
Sample/CI
10000
1000
100
10
1
Cs Rb Ba Th U K Nb Ta La Ce Pb Sr Nd P Zr Hf Sm Eu Gd Tb Ti Ho Y Er Yb Lu
La Ce Pr Nd Sm Eu Gd Tb Dy Ho Er Tm Yb Lu

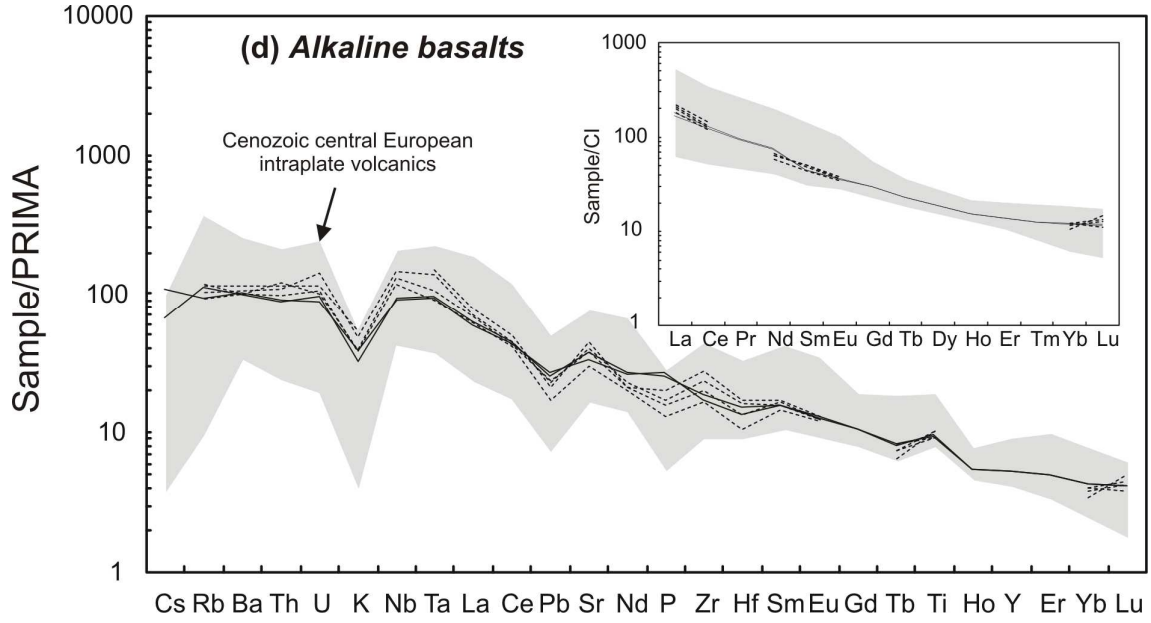
(d) Alkaline basalts
Cenozoic central European
intraplate volcanics
Sample/PRIMA
Sample/CI
10000
1000
100
10
1
Cs Rb Ba Th U K Nb Ta La Ce Pb Sr Nd P Zr Hf Sm Eu Gd Tb Ti Ho Y Er Yb Lu
La Ce Pr Nd Sm Eu Gd Tb Dy Ho Er Tm Yb Lu

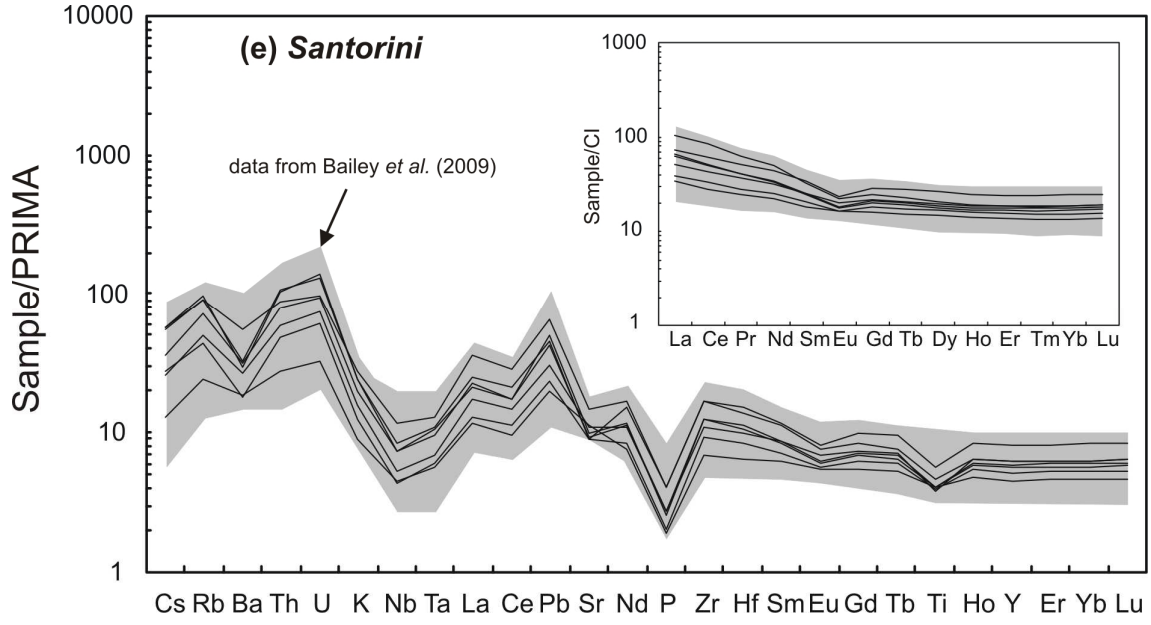

Fig. 3.6 a-e:

PRIMA-normalized multi-element diagrams and REE patterns for the three K-rich subgroups of the E-Bulgarian volcanic rocks, the Bulgarian alkaline basalts, and the calc-alkaline Santorini lavas. PRIMA and CI normalization values after Sun & McDonough (1989). For better comparability, Serbian LAG rocks (lamproite affinity group, after Prelević *et al.*, 2005) were screened for SiO_2 < 58 wt. % and K_2O < 6 wt. %. The Roccamonfina sample suite from Conticelli *et al.* (2009a) is shown without ultrapotasssic rocks. Compilation of Cenozoic central European intraplate volcanics are based on the online database http://georoc.mpch-mainz.gwdg.de. The stippled lines represent data of the same volcanic centres of the Eastern Rhodopes by Marchev *et al.* (2004).

With higher SiO_2 and MgO from 2.8 – 7.2 wt. %, Cr from 8.4 – 286 ppm, Ni from 4.1 – 75.3 ppm, Mg# from 11 – 44, the shoshonites and medium- to high-K samples from Bulgaria are less primitive than the Bulgarian absarokites. In Harker variation diagrams, the suites follow trends as expected for olivine-clinopyroxene dominated fractionation (Fig. 3.5). Incompatible trace element systematics for the shoshonites (Fig. 3.6b) and medium- to high-K samples from Bulgaria (Fig. 3.6c) are overlapping compositions of both the Serbian lamproites, the Italian (Roccamonfina volcano, Roman Magmatic Province) K-rich rocks in CI normalized and primitive mantle normalized diagrams.

The two (anorogenic) alkaline basalts from Bulgaria exhibit a narrow compositional range (MgO = 7.3 and 7.5 wt. %, Mg# = 48, SiO_2 = 46 and 46.5 wt. %). The samples are rich in TiO_2 (2.0 wt. %), and display Cr contents of 151 and 183 ppm and Ni contents of 76 and 109 ppm, respectively. The La_N-Yb_N ratios for the Bulgarian alkaline basalts range from 13.9 and 14.6. Figure 3.6d illustrates compositions of the Bulgarian alkaline basalts in comparison

to a compilation of Cenozoic central European intraplate volcanics and previously published data on the Bulgarian alkaline basalts by Marchev *et al.* (2004; stippled lines in Fig. 3.6e). Samples from all localities display similar CI-normalized REE patterns. In the primitive mantle (PRIMA) normalized diagram all suites show elevated Nb-Ta and Ti values.

The calc-alkaline samples from Santorini are characterized by MgO contents from 3.9 – 7.1 wt. %, resulting in Mg# from 31 – 47. Likewise, the compatible element contents are highly variable (Cr = 15 – 286 ppm and Ni = 13 – 75 ppm). In contrast to the Bulgarian lavas, the samples from Santorini are less enriched in LREE, yielding La_N/Yb_N from 2.4 – 7.3 (Fig. 3.4), and also display lower abundances of fluid mobile elements like Ba, Cs, and Pb. As for the Bulgarian suite, Santorini lavas are characterized by high LILE-HFSE ratios with a variable enrichment of fluid-mobile elements and marked HFSE depletions. As illustrated in Fig. 3.6e (grey field), compositions of the samples analyzed in this study cover the range of previously published REE data for Santorini lavas by Bailey *et al*. (2009) and can therefore be regarded as being representative for volcanism on Santorini.

Table 3.2:

Sample	age (Ma)	$^{87}Sr/^{86}Sr$ measured	± 2σ	$^{87}Rb/^{86}Sr$	$^{87}Sr/^{86}Sr$ (i)	$^{143}Nd/^{144}Nd$ measured	± 2σ	$^{147}Sm/^{144}Nd$	$^{143}Nd/^{144}Nd$ (i)	εNd(i)	± 2σ
absarokites											
BG-99a	32	0.708462	± 15	0.4359	0.708264	0.512463	± 10	0.1758	0.512426	-4.0	± 0.4
BG-102	32	0.708405	± 11	0.3296	0.708255	0.512450	± 9	0.1739	0.512414	-4.2	± 0.4
BG-99b	32	0.708454	± 13	0.4465	0.708251	0.512448	± 10	0.1769	0.512411	-4.3	± 0.4
BG-101	32	0.708438	± 16	0.3685	0.708271	0.512449	± 9	0.1757	0.512412	-4.3	± 0.3
BG-109a	32	0.707730	± 17	2.542	0.706574	0.512560	± 10	0.1809	0.512522	-2.1	± 0.4
BG-109b	32	0.707580	± 13	2.545	0.706423	0.512553	± 13	0.1812	0.512515	-2.2	± 0.5
BG-109b*	32	0.707562	± 12	2.545	0.706405	0.512557	± 9	0.1812	0.512519	-2.2	± 0.4
shoshonites											
BG-60	32	0.707715	± 12	0.9992	0.707261	0.512488	± 12	0.1554	0.512456	-3.4	± 0.5
BG-103	32	0.708518	± 12	0.4535	0.708312	0.512359	± 11	0.1519	0.512327	-5.9	± 0.4
BG-103*	32	0.708516	± 16	0.4535	0.708310	0.512356	± 11	0.1519	0.512324	-6.0	± 0.4
BG-113	32	0.708217	± 12	0.3745	0.708046	0.512502	± 10	0.1712	0.512466	-3.2	± 0.4
BG-46	32	0.708270	± 14	0.4180	0.708080	0.512483	± 9	0.1673	0.512448	-3.6	± 0.3
medium- and high-K											
BG-62	32	0.707365	± 11	0.5535	0.707114	0.512478	± 10	0.1587	0.512445	-3.6	± 0.4
BG-58	32	0.707448	± 11	0.4946	0.707223	0.512484	± 9	0.1634	0.512449	-3.5	± 0.3
BG-78	32	0.707298	± 13	0.7541	0.706955	0.512496	± 11	0.1559	0.512463	-3.3	± 0.4
BG-78*	32	0.707277	± 11	0.7542	0.706934	0.512490	± 13	0.1559	0.512457	-3.4	± 0.5
BG-56	32	0.707050	± 14	0.3876	0.706874	0.512463	± 10	0.1532	0.512431	-3.9	± 0.4
BG-67	32	0.707494	± 12	0.6050	0.707219	0.512470	± 11	0.1638	0.512436	-3.8	± 0.4
BG-67*	32	0.707472	± 13	0.6050	0.70720	0.512466	± 11	0.1638	0.512432	-3.9	± 0.4
BG-59	32	0.707365	± 13	0.4647	0.707153	0.512446	± 10	0.1487	0.512414	-4.2	± 0.4
BG-82	32	0.708178	± 14	0.9233	0.707759	0.512468	± 12	0.1591	0.512435	-3.8	± 0.4
BG-52	32	0.707430	± 13	0.5982	0.707158	0.512462	± 11	0.1577	0.512429	-3.9	± 0.4
BG-92	32	0.708073	± 13	0.4486	0.707869	0.512468	± 11	0.1663	0.512433	-3.8	± 0.4
BG-117	32	0.707893	± 12	0.2994	0.707757	0.512485	± 11	0.1682	0.512449	-3.5	± 0.4
BG-107	32	0.708804	± 15	0.3559	0.708642	0.512360	± 9	0.1500	0.512328	-5.9	± 0.3
BG-61	32	0.707824	± 16	0.9118	0.707409	0.512468	± 11	0.1519	0.512436	-3.8	± 0.4
BG-64	32	0.707038	± 11	0.6778	0.706729	0.512479	± 16	0.1532	0.512447	-3.6	± 0.6
BG-64*	32	0.707040	± 11	0.6779	0.706732	0.512460	± 9	0.1532	0.512428	-3.9	± 0.3
BG-72	32	0.707227	± 13	0.4774	0.707010	0.512484	± 12	0.1674	0.512449	-3.5	± 0.5
BG-72*	32	0.707213	± 11	0.4774	0.706996	0.512489	± 13	0.1674	0.512454	-3.4	± 0.5
alkaline basalts											
BG-49	28	0.703672	± 11	0.2571	0.703570	0.512896	± 10	0.1520	0.512896	5.2	± 0.5
BG-110	28	0.703767	± 13	0.2432	0.703670	0.512897	± 7	0.1549	0.512897	5.2	± 0.5

*** replicates**

Parent daughter ratios calculated by using the trace element concentrations reported in Table 3.1.

Table 3.2: continuation

Sample	age (Ma)	Lu (ppm)[1]	Hf (ppm)[1]	$^{176}Hf/^{177}Hf$ measured	± 2σ	$^{176}Lu/^{177}Hf$	$^{176}Hf/^{177}Hf$ (i)	εHf(i)	± 2σ
absarokites									
BG-99a	32	0.2540	3.354	0.282760	± 5	0.01075	0.282753	-0.7	± 0.5
BG-102	32	0.2582	3.412	0.282767	± 5	0.01074	0.282760	-0.4	± 0.5
BG-99b	32	0.2549	3.336	0.282761	± 5	0.01084	0.282754	-0.6	± 0.5
BG-101	32	0.2139	2.820	0.282766	± 5	0.01077	0.282759	-0.4	± 0.5
BG-109a	32	0.2031	2.460	0.282857	± 7	0.01172	0.282850	2.7	± 0.5
BG-109b	32	0.2050	2.482	0.282853	± 5	0.01172	0.282846	2.6	± 0.5
BG-109b*	32	0.1925	2.329	0.282863	± 6	0.01173	0.282856	3.0	± 0.5
shoshonites									
BG-60	32	0.3642	4.482	0.282783	± 5	0.01155	0.282776	0.1	± 0.5
BG-103	32	0.3229	4.560	0.282688	± 7	0.01007	0.282682	-3.2	± 0.5
BG-103*	32	0.3018	4.279	0.282691	± 8	0.01001	0.282685	-3.1	± 0.6
BG-113	32	0.3180	3.935	0.282774	± 6	0.01111	0.282767	-0.2	± 0.5
BG-46	32	0.3498	5.692	0.282779	± 7	0.00872	0.282774	0.1	± 0.5
medium- and high-K									
BG-62	32	0.3651	4.533	0.282800	± 6	0.01143	0.282793	0.7	± 0.5
BG-58	32	0.3180	3.099	0.282798	± 6	0.01457	0.282789	0.6	± 0.5
BG-78	32	0.3392	4.771	0.282804	± 10	0.01011	0.282798	0.9	± 0.7
BG-78*	32	0.3185	4.490	0.282795	± 6	0.01007	0.282789	0.6	± 0.5
BG-56	32	0.3681	5.918	0.282768	± 7	0.00884	0.282763	-0.3	± 0.5
BG-67	32	0.3289	3.951	0.282787	± 6	0.01183	0.282780	0.3	± 0.5
BG-67*	32	0.3097	3.726	0.282781	± 6	0.01180	0.282774	0.1	± 0.5
BG-59	32	0.3292	3.835	0.282776	± 5	0.01220	0.282768	-0.1	± 0.5
BG-82	32	0.3630	4.956	0.282761	± 10	0.01041	0.282755	-0.6	± 0.7
BG-52	32	0.3445	4.714	0.282777	± 7	0.01039	0.282771	-0.1	± 0.5
BG-92	32	0.3081	3.459	0.282795	± 7	0.01264	0.282787	0.5	± 0.5
BG-117	32	0.3323	3.953	0.282810	± 6	0.01193	0.282803	1.1	± 0.5
BG-107	32	0.2999	4.612	0.282705	± 6	0.00923	0.282699	-2.6	± 0.5
BG-61	32	0.3315	4.173	0.282770	± 6	0.01129	0.282763	-0.3	± 0.5
BG-64	32	0.3619	5.920	0.282762	± 7	0.00869	0.282757	-0.5	± 0.5
BG-64*	32	0.3402	5.594	0.282771	± 7	0.00863	0.282766	-0.2	± 0.5
BG-72	32	0.3787	3.919	0.282785	± 7	0.01374	0.282776	0.2	± 0.5
BG-72*	32	0.3574	3.699	0.282792	± 6	0.01372	0.282783	0.4	± 0.5
alkaline basalts									
BG-49	28	0.3129	4.810	0.283010	± 5	0.00923	0.283005	8.2	± 0.5
BG-110	28	0.3194	4.283	0.283009	± 5	0.01058	0.283003	8.2	± 0.5

*** replicates**

[1] Isotope dilution data

Table 3.2: continuation

Sample	age (Ma)	$^{206}Pb/^{204}Pb$ measured	$^{207}Pb/^{204}Pb$ measured	$^{208}Pb/^{204}Pb$ measured	$^{238}U/^{204}Pb$	$^{235}U/^{204}Pb$	$^{232}Th/^{204}Pb$	$^{206}Pb/^{204}Pb$ (i)	$^{207}Pb/^{204}Pb$ (i)	$^{208}Pb/^{204}Pb$ (i)
absarokites										
BG-99a	32	18.707	15.668	38.927	5.53	0.0402	23.6	18.679	15.666	38.889
BG-102	32	18.715	15.669	38.930	7.90	0.0574	23.3	18.676	15.667	38.893
BG-99b	32	18.705	15.667	38.926	5.08	0.0369	22.8	18.680	15.666	38.889
BG-101	32	18.716	15.668	38.926	8.34	0.0606	23.8	18.675	15.666	38.888
BG-109a	32	18.752	15.671	38.821	11.1	0.0806	23.1	18.697	15.669	38.784
BG-109b	32	18.754	15.670	38.817	9.52	0.0692	19.6	18.707	15.668	38.786
BG-109b*	32	18.748	15.669	38.813	9.52	0.0692	19.6	18.701	15.667	38.782
shoshonites										
BG-60	32	n.d.	n.d.	n.d.						
BG-103	32	18.805	15.673	38.895	9.49	0.0690	33.9	18.758	15.671	38.841
BG-103*	32	n.d.	n.d.	n.d.						
BG-113	32	18.867	15.681	38.905	13.7	0.0996	30.4	18.799	15.677	38.857
BG-46	32	18.829	15.668	38.879	18.7	0.136	35.9	18.736	15.663	38.822
medium- and high-K										
BG-62	32	18.831	15.677	38.907	11.2	0.0814	39.2	18.775	15.674	38.845
BG-58	32	18.842	15.686	38.936	12.0	0.0875	38.9	18.782	15.684	38.874
BG-78	32	18.829	15.673	38.907	13.6	0.0988	46.9	18.761	15.670	38.833
BG-78*	32	n.d.	n.d.	n.d.						
BG-56	32	18.743	15.676	39.006	12.5	0.0910	44.5	18.681	15.674	38.935
BG-67	32	18.834	15.677	38.907	11.4	0.0831	37.6	18.777	15.674	38.847
BG-67*	32	18.832	15.676	38.903	11.4	0.0831	37.6	18.775	15.673	38.843
BG-59	32	18.829	15.681	38.926	10.3	0.0752	42.4	18.778	15.679	38.859
BG-82	32	18.807	15.681	38.928	12.1	0.0882	38.5	18.746	15.678	38.868
BG-52	32	18.829	15.666	38.868	12.4	0.0899	40.7	18.767	15.663	38.804
BG-52*	32	18.833	15.672	38.890	12.4	0.0899	40.8	18.771	15.669	38.825
BG-92	32	18.815	15.680	38.918	11.5	0.0834	32.7	18.758	15.678	38.866
BG-117	32	n.d.	n.d.	n.d.						
BG-107	32	18.745	15.676	38.964	6.85	0.0498	26.1	18.711	15.674	38.923
BG-61	32	18.842	15.678	38.941	16.1	0.117	66.1	18.762	15.674	38.836
BG-64	32	18.805	15.674	38.905	12.7	0.0921	47.2	18.742	15.672	38.830
BG-64*	32	n.d.	n.d.	n.d.						
BG-72	32	18.792	15.675	38.887	8.57	0.0623	37.5	18.750	15.673	38.828
BG-72*	32	n.d.	n.d.	n.d.						
alkaline basalts										
BG-49	28	18.988	15.636	38.893	27.459	0.200	105.866	18.869	15.631	38.746
BG-110	28	18.909	15.633	38.864	24.031	0.175	103.504	18.804	15.628	38.721

Table 3.3: Sr-Nd-Hf-Pb isotope data Santorini

Sample	$^{87}Sr/^{86}Sr$ measured	± 2σ	$^{143}Nd/^{144}Nd$ measured	± 2σ	εNd(i)	± 2σ	Lu (ppm)[1]	Hf (ppm)[1]	$^{176}Lu/^{177}Hf$	$^{176}Hf/^{177}Hf$	± 2σ	εHf(i)	± 2σ
SA-1	0.704450	± 17	0.512841	18	4.11	0.7	0.361	2.105	0.024331	0.283101	± 7	11.6	± 0.5
SA-3	0.704871	± 15	0.512684	10	1.05	0.4	n.d.	n.d.	n.d.	n.d.		n.d.	
SA-4	0.706380	± 17	0.512593	8	-0.71	0.3	0.490	4.556	0.015260	0.282823	± 8	1.80	± 0.6
SA-6	0.704596	± 17	0.512684	9	1.06	0.3	0.442	3.449	0.018184	0.282937	± 7	5.83	± 0.5
SA-9	0.704414	± 17	0.512808	8	3.47	0.3	0.665	4.985	0.018934	0.283021	± 7	8.80	± 0.5
SA-10	0.704270	± 18	0.512820	10	3.71	0.4	0.399	2.720	0.020795	0.283036	± 7	9.35	± 0.5
SA-11	0.704236	± 18	0.512812	12	3.55	0.5	0.518	3.253	0.022607	0.283027	± 9	9.03	± 0.6

[1] Isotope dilution data
Calculation of εHf using $^{176}Hf/^{177}Hf_{(CHUR)}$ of 0.282772 after Blichert-Toft and Albarède (1997)

Sample	$^{206}Pb/^{204}Pb$ measured	$^{207}Pb/^{204}Pb$ measured	$^{208}Pb/^{204}Pb$ measured
SA-1	18.917	15.669	38.901
SA-3	18.894	15.681	38.941
SA-4	18.847	15.686	38.938
SA-6	18.931	15.683	38.957
SA-9	18.908	15.671	38.907
SA-10	18.902	15.669	38.893
SA-11	18.922	15.668	38.904

3.4.2. Sr-Nd-Hf-Pb isotope compositions

Strontium-Nd-Hf-Pb isotope compositions of all analyzed samples are listed in Tables 3.2 and 3.3 and illustrated in Figs. 3.7, 3.8 and 3.9. High Rb/Sr of the samples from Bulgaria required an age correction for Sr isotope data. This was also carried out for Nd-Hf-Pb isotopes (see Table 3.2), where it was less significant. For Lu-Hf, the element concentrations obtained by isotope dilution were used for age correction, for all other isotope systems the concentrations obtained by quadrupole ICP-MS measurements were used. The larger uncertainties of these element ratios are negligible for discussion of the data in this study.

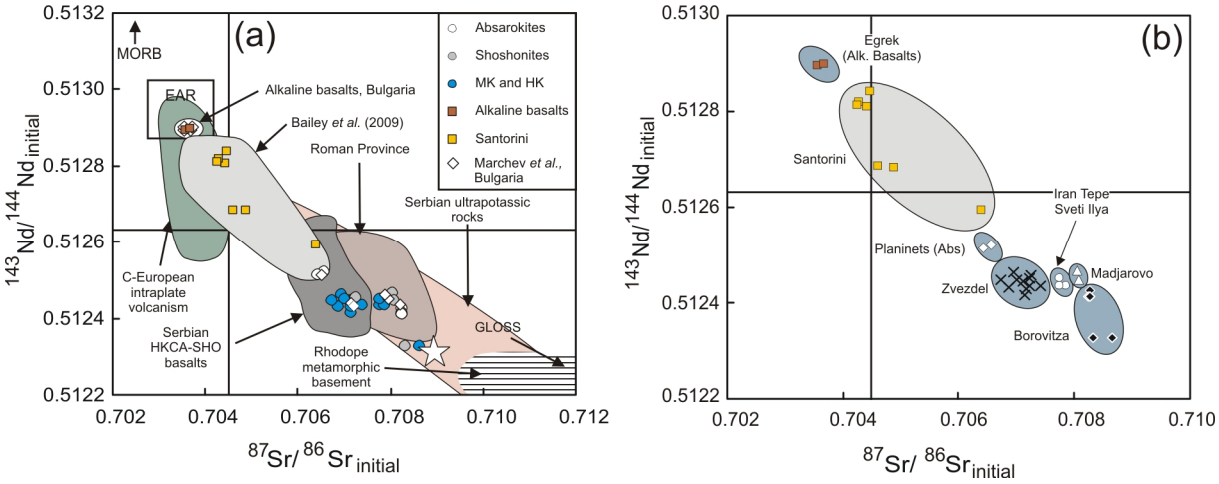

Fig. 3.7:
$^{143}Nd/^{144}Nd_{(i)}$ vs. $^{87}Sr/^{86}Sr_{(i)}$ compositions of Bulgarian and Santorini lavas illustrating the variations between compositional groups (a) and individual volcanic centres (b). Panel (a) also shows a comparison to other potassium-enriched and alkaline rock suites as well as to compositions of local metamorphic basement and previous data on Eastern Rhodope K-rich rocks by Marchev *et al.* (2004; white diamonds). Fields for E-Serbian alkaline basalts, Serbian HKCA-SHO (high-K calc-alkaline and shoshonitic basalts) and Serbian ultrapotassic rocks after Prelević *et al.* (2005) and Cvetković *et al.* (2004), Italian lavas (Neapolitan District and Roccamonfina) after Conticelli *et al.* (2002) and references within, Eastern Bulgarian metamorphic basement and alkaline basalts, Bulgaria after Marchev *et al.* (2004), Central European intraplate volcanics after the online database http://georoc.mpch-mainz.gwdg.de; EAR (=European Asthenospheric Reservoir) after Cebriá & Wilson (1995). The white asterisk represents the inferred composition of the potential source contaminant. Symbols in panel (b) are as in Fig. 3.10b, d.

The Bulgarian K-rich lavas are characterized by $^{87}Sr/^{86}Sr_{(i)}$ values of 0.7064 – 0.7086. Initial $\varepsilon Nd_{(i)}$ range from -5.8 to -1.9 with most samples scattering around a value of -3. These values are within the range reported by Marchev *et al*. (2004) for mafic rocks from the Eastern Rhodopes (see Fig. 3.7a, white diamonds). Values of $\varepsilon Hf_{(i)}$ vary from -3 to +3, the

majority of the samples exhibit $\varepsilon Hf_{(i)}$ values of ~ 0. In contrast to the high-K samples, the two alkaline basalts are characterized by almost identical isotope compositions, yielding less radiogenic $^{87}Sr/^{86}Sr_{(i)}$ (0.7036 – 0.7037) and more radiogenic $\varepsilon Nd_{(i)}$ (+5.3) and $\varepsilon Hf_{(i)}$ (+8.4). In comparison to the Bulgarian lavas, the Santorini lavas displays less radiogenic $^{87}Sr/^{86}Sr_{(i)}$ (0.7042 – 0.7064), more radiogenic Nd isotope compositions ($\varepsilon Nd_{(i)}$ = -0.71 to +4.1) and a large range in $\varepsilon Hf_{(i)}$ values (+1.8 to +11.6).

As illustrated in Fig. 3.7a, the Bulgarian K-rich samples broadly overlap the fields defined by high-K rocks from Serbia (Cvetković *et al.*, 2004; Prelević *et al.*, 2005) and Italy (Conticelli *et al.*, 2009a, and references therein), but yield by far less radiogenic $^{143}Nd/^{144}Nd_{(i)}$ and more radiogenic $^{87}Sr/^{86}Sr_{(i)}$ than average global MORB. Furthermore, the K-rich Bulgarian lavas display considerably less radiogenic Sr isotope compositions than the Rhodope metamorphic basement (Fig. 3.7a; $^{87}Sr/^{86}Sr$ = 0.709 – 0.734; Marchev *et al.*, 2004) and typical pelagic sediments (GLOSS, Global Subducting Sediment: $^{87}Sr/^{86}Sr$ = 0.717; Plank & Langmuir, 1998). Figure 3.7b illustrates the Sr-Nd isotope compositions of the samples grouped according to individual volcanic centres, which can be well distinguished in Sr-Nd space, showing an increase of $^{87}Sr/^{86}Sr_{(i)}$ from Zvezdel volcano (west) to Madjarovo (east) at near-constant $^{143}Nd/^{144}Nd_{(i)}$. However, Planinetz and Borovitza are notable exceptions in that they exhibit very similar major and trace element contents, but plot at different ends of the sample array in Sr-Nd as well as in εHf-εNd space.

The Bulgarian alkaline basalts are located in Fig. 3.7a at the upper end of a compilation of Cenozoic central European intraplate volcanics, and furthermore overlap the proposed composition of the European Asthenospheric Reservoir (EAR; after Wilson & Downes, 1992) as well as previously published Sr-Nd isotope compositions of the Bulgarian alkaline basalts by Marchev *et al*. (2004; Fig. 3.7a).

Compositions of Santorini samples are shifted towards less radiogenic Sr and more radiogenic Nd isotope compositions than those of the Bulgarian K-rich samples and the Serbian and Italian high-K rocks (Fig. 3.7a). Only one Santorini sample (SA-4, Therasia complex) yields considerably higher $^{87}Sr/^{86}Sr$ (= 0.7064). Nevertheless, the Sr-Nd isotope compositions of the Santorini samples from this study are in good agreement with those previously published by Bailey *et al*. (2009) and also cover a similarly broad range.

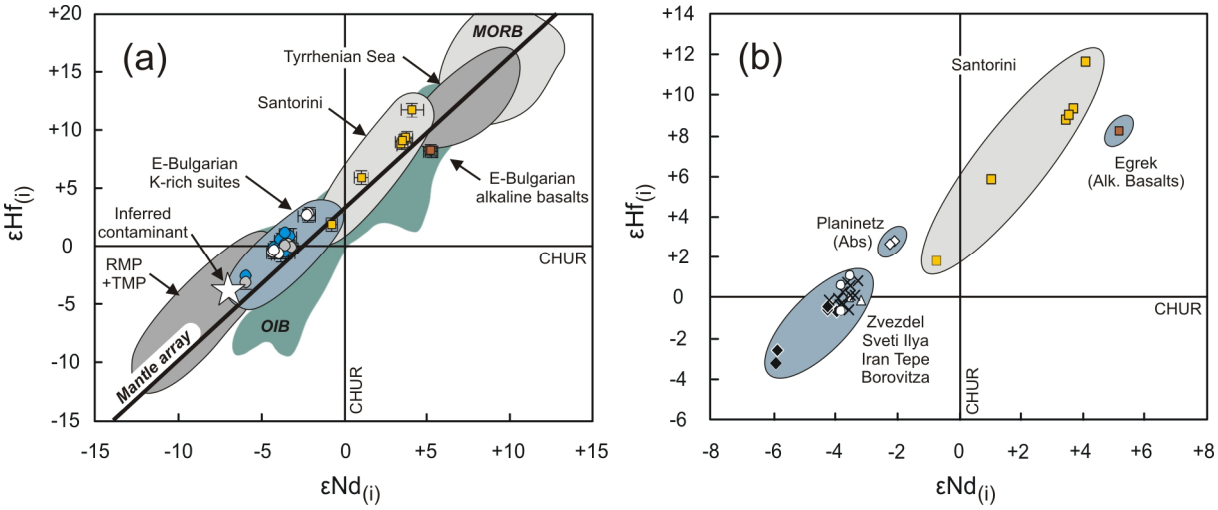

Fig. 3.8:

$\varepsilon Hf_{(i)}$ vs. $\varepsilon Nd_{(i)}$ compositions of Bulgarian and Santorini lavas illustrating the variations between compositional groups (a) and individual volcanic centres (b). Panel (a) also shows a comparison to other Mediterranean high-K and calc-alkaline rocks; MORB after Pearce *et al.* (1999), Woodhead *et al.* (2001), Chauvel & Blichert-Toft (2001), and Kempton *et al.* (2002); OIB field after Nowell *et al.* (1998), RMP+TMP (Roman Magmatic Province and Tuscan Magmatic Province) and Tyrrhenian Sea after Gasperini *et al.* (2002); Mantle array after Vervoort *et al.* (1999).

In εHf-εNd space (Fig. 3.8a), the Bulgaria-Santorini data plot well within the mantle array (after Vervoort *et al.*, 1999), but are shifted towards less radiogenic εHf and εNd compared to MORB and other arc suites as represented by lavas from the Tyrrhenian Sea (Gasperini *et al.*, 2002) and intra-oceanic arcs (e.g., Solomon Islands, Schuth *et al.*, 2004, 2009; Kamchatka, Münker *et al.*, 2004; Izu-Bonin-Mariana, Pearce *et al.*, 1999). Only the high-K rocks from the Roman and Tuscan magmatic provinces (RMP and TMP, respectively, Gasperini *et al.*, 2002) yield less radiogenic εHf and εNd than the Bulgarian lavas, whereas values of the Santorini lavas are intermediate between those of the Bulgarian lavas and those of volcanic rocks elsewhere in the Tyrrhenian Sea (Gasperini *et al.*, 2002). The Hf-Nd isotope compositions of the alkaline basalts are again less radiogenic and are similar to those of the Tyrrhenian Sea and Mt. Etna (compilation of Gasperini *et al.*, 2002). Figure 3.8b illustrates the distribution of the dataset in Hf-Nd space for individual volcanic centres. Unlike for Sr-Nd isotopes, only the absarokites from Planinetz form a discrete group by displaying the most radiogenic εHf-εNd values. The other volcanic centres overlap within error and do not define any systematic trends.

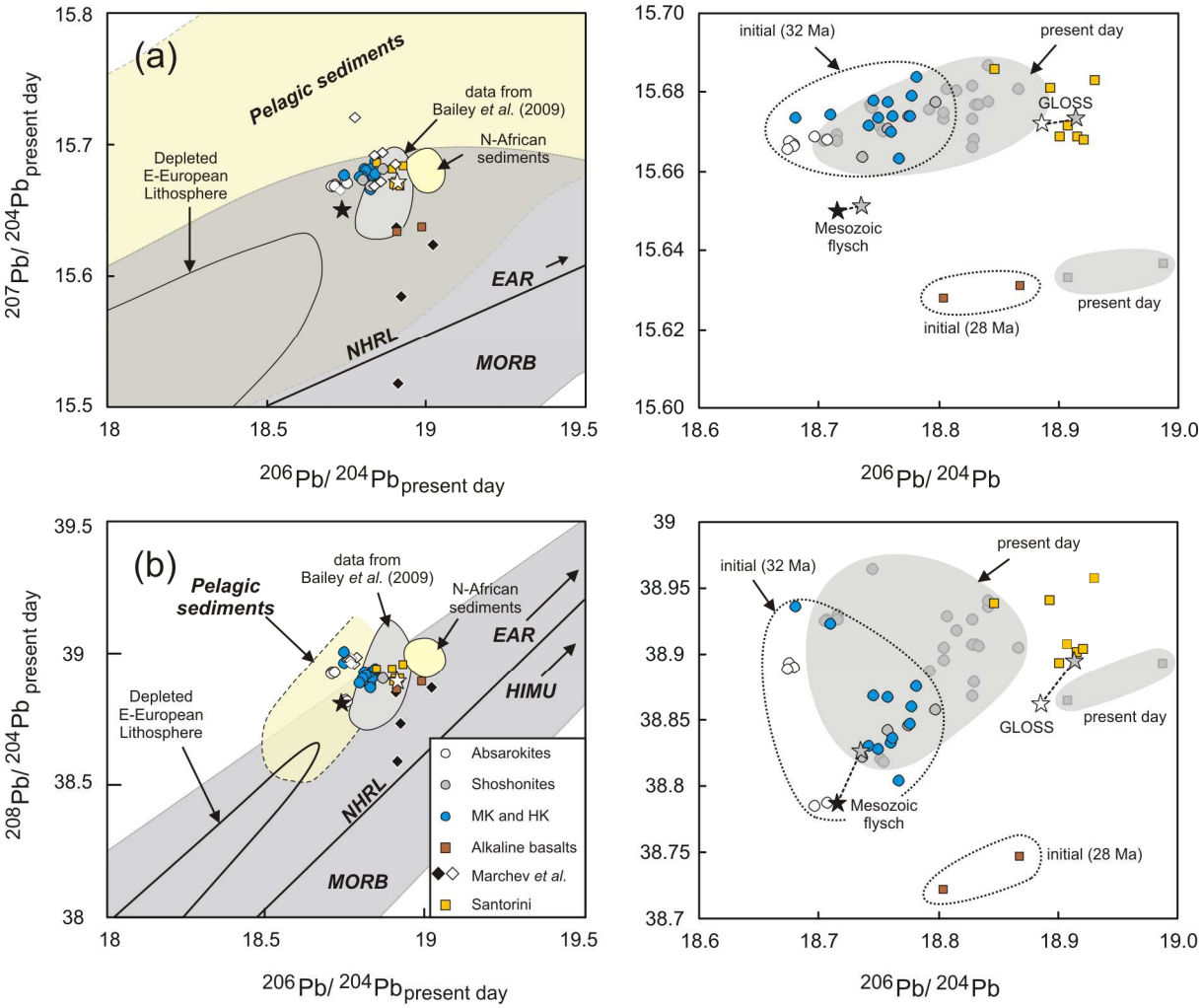

Fig. 3.9:

Lead isotope compositions of the samples from Bulgaria and Santorini in comparison to compositions of Atlantic and Pacific MORB, and pelagic sediments. Enlarged panels on the right hand side illustrate the present day (grey shaded field and grey shaded symbols) and initial Pb isotope composition of the Bulgarian samples, calculated to 32 Ma for the K-rich samples and to 28 Ma for the alkaline basalts. For comparison, compositions of GLOSS (at 32 Ma; white star; Plank and Langmuir, 1998) and a Mesozoic flysch after Prelević *et al.* (2005; at 32 Ma, black star) are shown. Fields for pelagic sediments and MORB are after Hofmann (2003) and Peate *et al.* (1997), NHRL (Northern hemisphere reference line) after Hart (1984), Depleted East European Lithosphere after Rosenbaum *et al.* (1997), North-African sediments after Pe-Piper (1994). Moreover, previously published data on the Eastern Rhodope K-rich rocks (white diamonds) and alkaline basalts (black diamonds) by Marchev *et al.* (2004) is shown as well.

Lead isotope ratios of both the Bulgarian K-rich rocks and the Santorini samples (Tables 3.2 and 3.3; Fig. 3.9) are characterized by radiogenic compositions ($^{206}Pb/^{204}Pb_{(i)}$ = 18.68 – 18.93, $^{207}Pb/^{204}Pb_{(i)}$ = 15.63 – 15.68 and $^{208}Pb/^{204}Pb_{(i)}$ = 38.72 – 39.96), overlapping both the field for pelagic sediments (Hofmann, 2003; Peate *et al.*, 1997) as well as the MORB field (Pacific and Atlantic MORB; Hofmann, 2003; Fig. 3.9). As illustrated in Figs. 3.9a and

b, both the Bulgarian K-rich rocks (this study and Marchev *et al*., 2004) and the sample suite from Santorini (this study and Bailey *et al*., 2009) display similar Pb isotope compositions as local Mesozoic flysch sediments from Serbia (data taken from Prelević *et al.*, 2005), GLOSS (Plank & Langmuir, 1998), and sediments derived from N-Africa (river Nile, Pe-Piper, 1994). The Pb isotope compositions of the Bulgarian alkaline basalts span a vertical array from the NHRL to more enriched $^{207}Pb/^{204}Pb$ and $^{208}Pb/^{204}Pb$ at low $^{206}Pb/^{204}Pb$. Compared to the EAR, the Bulgarian alkaline basalts are shifted towards lower $^{207}Pb/^{204}Pb$, $^{206}Pb/^{204}Pb$ and $^{208}Pb/^{204}Pb$.

3.5. Discussion

3.5.1. Fractional crystallization and assimilation of continental crust

In order to explain the trace element and isotope geochemistry of the volcanic rocks from Bulgaria and Santorini, the role of fractional crystallization and crustal assimilation processes needs to be assessed first. Fractional crystallization of clinopyroxene, olivine, and Fe-Ti phases controls the elemental budget of MgO, CaO, Al_2O_3, Ni, and Cr in the lavas from Bulgaria and Santorini. In Harker variation diagrams, these suites follow typical calc-alkaline fractionation trends (see Fig. 3.4, 3.5). Furthermore, the negative Ti and P anomalies of the Bulgarian shoshonites and high-K lavas (except absarokites) in multi element diagrams (Fig. 3.6b, c) indicate additional fractional crystallization of magnetite and apatite. In marked contrast to all other groups, the major element composition of the absarokites from the two localities is dominated by the fractionation of a K-Mg-rich solidus phase, possibly phlogopite (Lloyd *et al.*, 1985; Foley, 1992a, b; Conceição & Green, 2004; Fig. 3.5), whereas the strong increase of the CaO/Al_2O_3 with decreasing MgO indicates fractionation of a Mg-Al-rich phase, again being most likely phlogopite, from a parental magma with an already initially high CaO/Al_2O_3 (Fig. 3.5a and b). Such high $CaO\text{-}Al_2O_3$ ratios, i.e., >1, are also often observed for melts tapping mantle sources that were refertilized by Ca-rich components, as e.g. observed for ankaramites (e.g., Green & Wallace, 1988; Green *et al.*, 2004). Marchev *et al.* (2009) also suggested that ankaramites from the Bulgarian Srednogorie Zone (Georgiev *et al*., 2009) might represent the most primitive end-member of the shoshonitic series. Fractionation of plagioclase might play a role, as evident from the negative Eu-anomalies ($Eu/Eu^* = 0.74 – 0.87$) observed in all three Bulgarian K-rich rock suites. However, the

negative Eu-anomalies might additionally reflect source enrichment by melt-like components derived from subducted sediments (e.g., Williams *et al.*, 2004).

The Mg# and Ni and Cr contents of the Bulgarian alkaline basalts indicate that their composition has been modified by incipient crystal fractionation involving Cr-spinel, olivine, and clinopyroxene. Furthermore, the lack of Eu anomalies (Fig. 3.6d) suggests the absence of plagioclase fractionation.

Assimilation of continental crust during ascent of the magmas has long been considered as a cause for the distinct geochemical and isotope signatures of potassic magmas in continental settings and at active continental margins. However, several authors (Stolz *et al.*, 1990; Nelson, 1992b; Prelević *et al.*, 2008; Conticelli *et al.*, 2009a, b) have demonstrated that the unique isotope and geochemical features of K-rich lavas can indeed largely be attributed to source enrichment. In the case of the Bulgarian lavas, shallow-level assimilation of continental crust during magma ascent most likely has occurred to some extent as invoked by Marchev *et al.* (2004). Crustal assimilation is supported by the occurrence of Variscan, Neoproterozoic and Ordovician zircons in the Iran Tepe volcanic rocks and also in the alkaline basalts (Bonev *et al*., 2010; Marchev *et al*., in press). The zircons certainly constitute remnants of crustal material that had been assimilated during melt ascent. Hence, the Nd-Hf values measured for samples from these volcanic centres may be regarded as minimum values and the Sr-Pb compositions as maximum values with respect to pristine melt compositions. However, to explain the radiogenic Pb isotope compositions solely by assimilation of continental crust (average Pb concentration ~ 17 ppm; Rudnick & Gao, 2003), unrealistically large amounts of assimilated material (> 40%) would be required, given the high Pb concentrations of the lavas (> 13 ppm; Table 3.1). This is not in agreement with the trace element budget and the Sr-Nd isotope systematics, especially of the alkaline basalts. The alkaline basalts only show a slight displacement of their Sr-Nd isotope compositions from the narrow field defined by asthenosphere-derived basalts from the Moesian platform (P. Marchev; unpublished data) and also overlap the field for the EAR in Sr-Nd space (Fig. 3.7a). Therefore, a different model has to be developed to explain the lower Pb isotope compositions of the studied alkaline basalts with respect to EAR.

For the K-rich lavas from Bulgaria, assimilation of continental crust has previously been reported to exert some control on the isotope and trace element compositions (Marchev *et al*., 1998a, b; 2004). Inverse zonations of plagioclase, clino- and orthopyroxene have been observed in some high-K rocks and were attributed to result from mixing between mafic and evolved magmas (Marchev *et al.*, 1998a, b). From W to E, the four volcanic centres from

Zvezdel, Sveti Ilya, Iran Tepe, and Madzharovo also exhibit increasingly radiogenic Sr isotope compositions at invariant Nd isotope ratios (Figs. 3.1b, 3.7b). Most importantly, this shift is not observed for Hf and Pb isotopes, leading to the conclusion that a putative assimilation process selectively affected the Sr budget. Given the elevated Sr contents of the lavas (340 to 950 ppm; Table 3.1), however, this appears to be unlikely, as most potential contaminants have similar or even lower Sr abundances (average crustal abundance ca. 350 ppm Sr; Taylor & McLennan, 1995). The strikingly different Sr-Nd-Hf-Pb isotope compositions of the two absarokite localities (Borovitza and Planinetz) were also interpreted to indicate a variable crustal input (Shanov, 1998; Marchev *et al.*, 2004). Again this can be questioned, as lavas from both localities overlap in their Mg# that are all near primitive.

Despite the detailed observations summarised above, a significant role of shallow level crustal assimilation during the petrogenesis of the Bulgarian lavas can still be ruled out, largely on the basis of lacking correlations between isotope ratios and major elements (Fig. 3.10). In Fig. 3.10a this is illustrated for $^{87}Sr/^{86}Sr_{(i)}$ vs. SiO_2, where the expected co-variations for any of the suites are absent. These patterns also hold for $^{87}Sr/^{86}Sr_{(i)}$ if plotted versus Mg# (Fig. 3.10c), thus precluding any significant effect of crustal assimilation processes on the Sr budget of the lavas. Notably, the absarokites from Borovitza, which exhibit some of the highest $^{87}Sr/^{86}Sr_{(i)}$ of the data set, are also among the most primitive samples (see Table 3.1). Figures 3.10b and d additionally illustrate the effects of shallow level crustal assimilation within each volcanic centre, generally indicating pure fractional crystallization trends rather than co-variations expected for crustal assimilation. Collectively, the Sr-Nd-Hf budgets in the Bulgarian magmas can be expected to have been well buffered during crustal assimilation, and an unrealistically large fraction of assimilated crust would be required to generate measurable isotope effects (see also Conticelli *et al*., 2002, for high-K lavas from Italy).

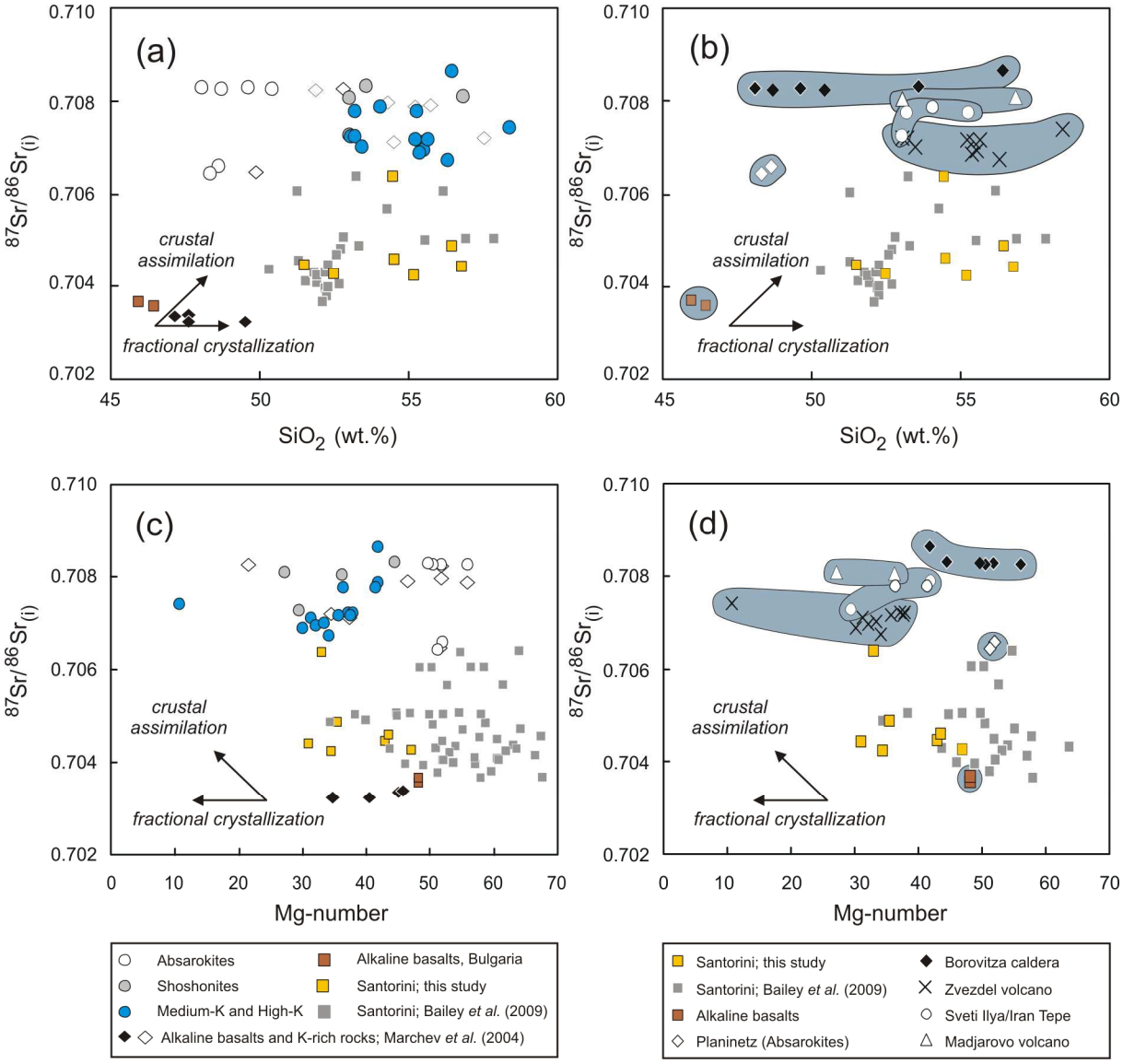

Fig. 3.10:

Diagrams illustrating variations of radiogenic $^{87}Sr/^{86}Sr_{(i)}$ with wt.-% SiO_2 and Mg-number to assess the effect of shallow level crustal assimilation on compositions of the Bulgarian and Santorini rocks. (a) $^{87}Sr/^{86}Sr_{(i)}$ isotope compositions vs.SiO_2 (wt. %) illustrate that in contrast to the Bulgarian samples some Santorini lavas (this study and Bailey *et al*., 2009) were modified to a significant degree by crustal assimilation (see arrows). (c) $^{87}Sr/^{86}Sr_{(i)}$ isotope compositions vs. Mg-number of the Bulgarian compositional groups lack co-variations expected for shallow-level bulk crustal assimilation. (b) and (d) The lack of variations of $^{87}Sr/^{86}Sr_{(i)}$ isotope compositions vs. SiO_2 (wt. %) and Mg-number of the individual volcanic centres rule out any significant effects of crustal assimilation for the Bulgarian lavas and confirm small effects of crustal assimilation for Santorini.

In marked contrast to the Bulgarian lavas, the compositions of some Santorini lavas reveal a more significant influence of shallow level crustal contamination (e.g., SA-4, Therasia Complex; SA-6, Akrotiri). The Santorini lavas exhibit a systematic increase of

$^{87}Sr/^{86}Sr_{(i)}$ with increasing SiO_2 (Fig. 3.10a) and also display correlations of $^{87}Sr/^{86}Sr_{(i)}$ with other differentiation and assimilation parameters (e.g., Mg-number, Fig. 3.10c; SiO_2 vs. $^{207}Pb/^{204}Pb$; not shown). Our inferences for the Santorini lavas are consistent with previous modelling by Druitt *et al.* (1999) and Zellmer *et al.* (2000), who postulated up to 1 - 12% of assimilation of upper crustal material. However, this estimate may vary significantly, depending on the different crustal compositions used for modelling, as pointed out by Bailey *et al.* (2009). Hence, for the discussion of source processes below, we only use Santorini lavas with MgO contents above 4 wt. % (SA-1, SA-3, SA-6, and SA-10).

3.5.2. Mantle source enrichment by subduction components vs. old lithospheric mantle components

Experimental studies demonstrated that the formation of K-rich rocks (e.g., shoshonites) requires mantle sources consisting of peridotite and hydrous, incompatible element-rich veins (e.g., Meen, 1987; Foley, 1992b; Mitchell, 1995). These domains are generated by reaction of metasomatic agents, i.e., silicic melts or fluids, with the host mantle peridotite. The mineral assemblages produced consist of mica (usually phlogopite) and clinopyroxene with varying amounts of additional apatite, spinel, titanium minerals, and amphibole (Wyllie & Sekine, 1982; Foley, 1991, 1992b; Conceição & Green, 2004). As these metasomatic mineral assemblages have a lower melting point than the surrounding wall rock, strongly incompatible element-enriched magmas may be produced at relatively low degrees of melting (Meen, 1987; Foley, 1992b).

In the absence of source enrichment by subduction fluids, partial melting of veined lithospheric mantle domains may be the response to a change in the P-T regime following asthenospheric upwelling or crustal delamination (Nelson, 1992a; Platt & England, 1994; Moore & Wiltschko, 2004). A further mechanism, particular in post-collisional settings such as Bulgaria, is the onset of extension, reflecting slab rollback, slab-break off, or crustal relaxation (Davies & von Blanckenburg, 1995; Wortel & Spakman, 2000; Faccenna *et al.*, 2003; van Hinsbergen *et al.*, 2005). The compositional spectrum of K-(Mg-) rich magmas produced in these settings could simply reflect variable proportions of melt contributions from veins and wall-rock domains (Foley, 1992a). In this context, the age of the lithospheric (veined) mantle being tapped is of crucial importance as it either reflects low-degree partial melting of old lithospheric mantle (*single-stage model* – ancient lithospheric mantle) or the

recent addition of metasomatic agents to the mantle source (*multi-stage model* – subduction-related source enrichment).

In order to assess the potential validity of *single-stage models* for the Bulgarian K-rich rocks, we carried out Sr-Nd isotope modelling of old, veined lithospheric mantle domains (see below). Furthermore, the *multi-stage model* is subsequently evaluated by comparing the Bulgarian K-rich rocks with the calc-alkaline lavas from Santorini, which are regarded as a proxy for the currently active island-arc volcanism probing the present day sub-arc mantle beneath the Aegean subduction zone.

3.5.3. Assessment of the single-stage model

As proposed for high-K suites from Indonesia and Tibet (Varne, 1985; Turner *et al.*, 1996; Williams *et al.*, 2004), ancient mantle source enrichment (*single stage model*) is a valid mechanism explaining the observed Sr-Nd isotope compositions (Fig. 3.7). In order to evaluate this hypothesis closer, we carried out Sr-Nd isotope modelling for two representative samples of the Bulgarian high-K lavas with low and high Rb/Sr, respectively. Schmidt *et al.* (1999) proposed that lamproites and shoshonites originate from previously depleted mantle sources, which were subsequently enriched by metasomatic veins dominated by clinopyroxene and > 5 % phlogopite. Due to the relatively high partition coefficients of Sm and Nd in clinopyroxene (D_{Sm} = 0.42, D_{Nd} = 0.6; Schmidt *et al.*, 1999) and Rb and Sr for phlogopite (D_{Rb} = 1.44; D_{Sr} = 0.038; Schmidt *et al.*, 1999), the abundances of Rb-Sr and Sm-Nd in the metasomatized mantle are virtually entirely dominated by this mineral assemblage (partition coefficients are shown in Table 3.4). As a result of the given D_{Sm}/D_{Nd} (clinopyroxene-controlled, 0.7) and D_{Rb}/D_{Sr} (phlogopite-controlled, 36.2), phlogopite-clinopyroxene assemblages in metasomatic veins would display high Rb/Sr at moderately elevated Sm/Nd. Hence, considering long residence times for this mineral assemblage in the mantle, the metasomatized veins should evolve towards enriched $^{87}Sr/^{86}Sr$ compositions at moderately radiogenic $^{143}Nd/^{144}Nd$ isotope signatures.

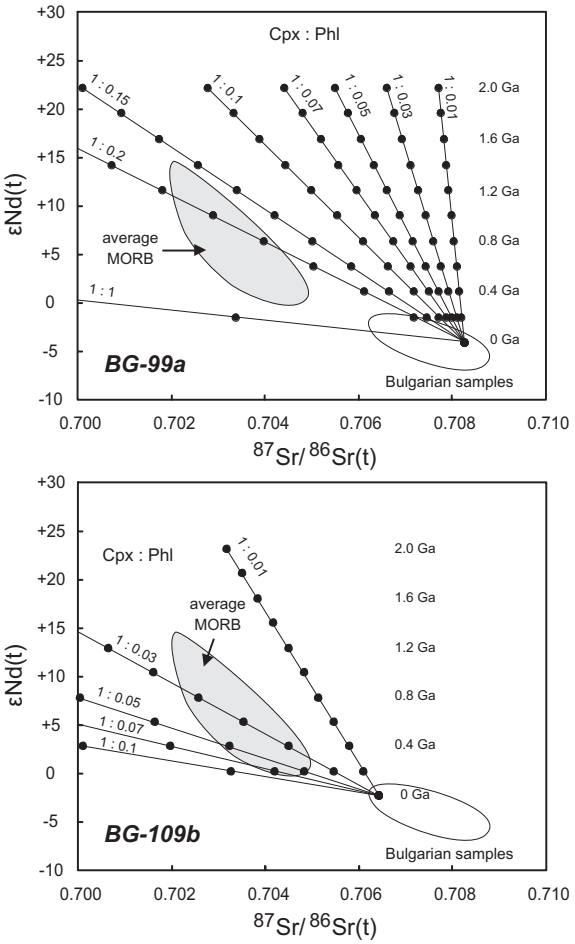

Fig. 3.11:
Sr-Nd isotope modelling illustrating the ingrowth of ^{87}Sr and ^{143}Nd in a veined lithospheric mantle with varying modal proportions of phlogopite:clinopyroxene. Calculations are made for two representative Bulgarian samples (BG-99a and BG-109b) with low and high $^{87}Sr/^{86}Sr$ as starting material. The grey shaded field corresponds to average MORB compositions after Hofmann (2003); the white field represents the compositional spread of the Bulgarian samples in Sr-Nd space. Tickmarks on isotope evolution trajectories correspond to 200 Myr steps, different tie lines correspond to cpx:phl ratios from 1:0.01 to 1:1. Input parameters are shown in Table 3.4. The back-calculation of Sr-Nd isotopes requires a minimum residence times of 250 Myr for the modelled mantle assemblages in order to evolve from average MORB compositions. Values used for calculation of εNd(t): $CHUR_{(0)}$ = 0.512638 (Jacobsen & Wasserburg, 1980); $^{147}Sm/^{144}Nd_{CHUR(0)}$ = 0.1967 (Jacobsen & Wasserburg, 1980); $\lambda^{147}Sm = 6.54\times10^{-12}$, $\lambda^{87}Rb = 1.42\times10^{-11}$.

In applying the above approach, we modelled the temporal evolution of the mantle sources of the Bulgarian lavas back through time. Two mafic samples from the Bulgarian high-K suite with different Rb/Sr of 0.151 and 0.880 (samples BG-99a and BG-109b) as well as different Sr and Nd isotope compositions (see Table 3.4) were chosen as starting compositions. In a first step, we calculated the Sr-Nd isotope compositions of residual clinopyroxene-phlogopite assemblages using the partition coefficients of Schmidt *et al.* (1999) for K-rich magmas (see Table 3.4). Assuming variable modal abundances of phlogopite (phl) and clinopyroxene (cpx) ranging from 1:0.01 to 1:1, we calculated the isotopic evolution of corresponding mantle sources. The results are illustrated in Fig. 3.11.

Table 3.4: Data used for model calculations

Sample	ppm Rb	ppm Sr	ppm Sm	ppm Nd	Rb/Sr	Sm/Nd	$^{87}Sr/^{86}Sr$ (i)	$^{143}Nd/^{144}Nd$ (i)
BG-99a	88.9	590	4.88	21.7	0.151	0.192	0.708264	0.512426
BG-109b	322	366	4.08	17.6	0.880	0.232	0.706423	0.512515

Partition coefficients after Schmidt et al. (1999)

	Phl/Lq	Cpx/Lq
Rb	1.34	0
Sr	0.037	0.304
Sm	0.00003	0.42
Nd	0.00003	0.6

Calculation of εNd(t) using $^{143}Nd/^{144}Nd_{(CHUR)}$ of 0.512630 after Bouvier et al. (2008) and $^{147}Sm/^{144}Nd_{(CHUR)}$ of 0.1967

The back-calculated $^{87}Sr/^{86}Sr$ are strongly dependant on the Rb/Sr of the starting composition, which is reflected in the slope of the tie lines for individual cpx:phl proportions. The higher the Rb/Sr in the starting composition (i.e., the composition of the two Bulgarian lavas), the stronger is the decrease in $^{87}Sr/^{86}Sr$ and the shallower the slope of the tie line. The simple conclusion is that at relatively high modal proportions of phlogopite and elevated Rb/Sr in the starting composition, a significant radiogenic ingrowth of $^{87}Sr/^{86}Sr$ in the mantle source occurs over a relatively short time span. As for Rb-Sr, the modelled Nd isotopic evolution is also dependant on the Sm/Nd of the starting composition. However, in contrast to the Rb-Sr system, the Nd isotope evolution is virtually entirely dominated by the cpx abundance. Due to the D_{Sm}/D_{Nd} of clinopyroxene (0.7; Schmidt *et al*., 1999), the back-calculated $\varepsilon Nd_{(t)}$ evolve towards radiogenic εNd values at a given time. Figure 3.11 illustrates that typical Sr-Nd isotope compositions of the depleted mantle can be achieved over a time span of > 250 Myrs. The mantle source compositions required to account for such an ingrowth of ^{87}Sr and ^{143}Nd can be highly variable and the modal amounts of phlogopite required ranges from ca. 3-7% (sample with the highest Rb/Sr) to about 50 % (sample with the lowest Rb/Sr). This range is in accord with previous studies on mantle xenoliths where reported modal abundances of phlogopite range from 1.5% - 2.5% in phlogopite-wehrlites and phlogopite-lherzolites (Grégoire *et al.*, 2002) to 20% in phlogopite-pyroxenites (Pearson & Nowell, 2002). For comparison, even higher modal amounts of phlogopite (40% and higher) are reported for MARID (mica-amphibole-rutile-ilmenite-diopside) suite of cratonic xenoliths (e.g., Pearson & Nowell, 2002).

Collectively, our modelling of Sr-Nd isotope compositions back through time highlights that residual mineral assemblages like phlogopite-clinopyroxene are capable of causing considerably enriched $^{87}Sr/^{86}Sr$ and $^{143}Nd/^{144}Nd$ compositions in the lithospheric mantle without any addition of enriched subducted material being required. For the Bulgarian setting, the time frame required to accomplish such a radiogenic ingrowth varies from ca. 250 Ma to 1.2 Ga. The lowermost end of this age range is in rough agreement with crust formation and amalgamation ages in the region (~ 300 Ma; e.g., Turpaud & Reischmann, 2010; Gaggero *et al*., 2009; Buzzi *et al*., 2010). Notably, amalgamation of the crustal fragments in the Rhodope region is of Alpine age (e.g., Jahn-Awe *et al.,* 2010, and references within), about 150 - 200 Myrs younger than the time frame required for radiogenic isotope ingrowth in the lithospheric mantle. Assuming that stabilisation of a lithospheric keel beneath the Rhodope is coupled to the final amalgamation of continental fragments, it therefore appears rather unlikely that the evolved Sr-Nd isotope signatures are derived from old lithospheric domains.

3.5.4. Assessment of the multi-stage model

(a) Mantle sources of Bulgarian K-rich lavas and alkaline basalts

As a significant role of crustal assimilation can be excluded, the compositions of the Bulgarian lavas allow a characterization of their mantle sources. The absarokites are silica-undersaturated (nepheline- and hypersthene-normative) whereas the shoshonites and medium- to high-K rocks are silica-saturated. Nevertheless, the narrow range of isotope and trace element compositions displayed by all of these groups (see Figs. 3.6 to 3.9) argue for comparatively homogeneous mantle sources of the Bulgarian K-rich lavas.

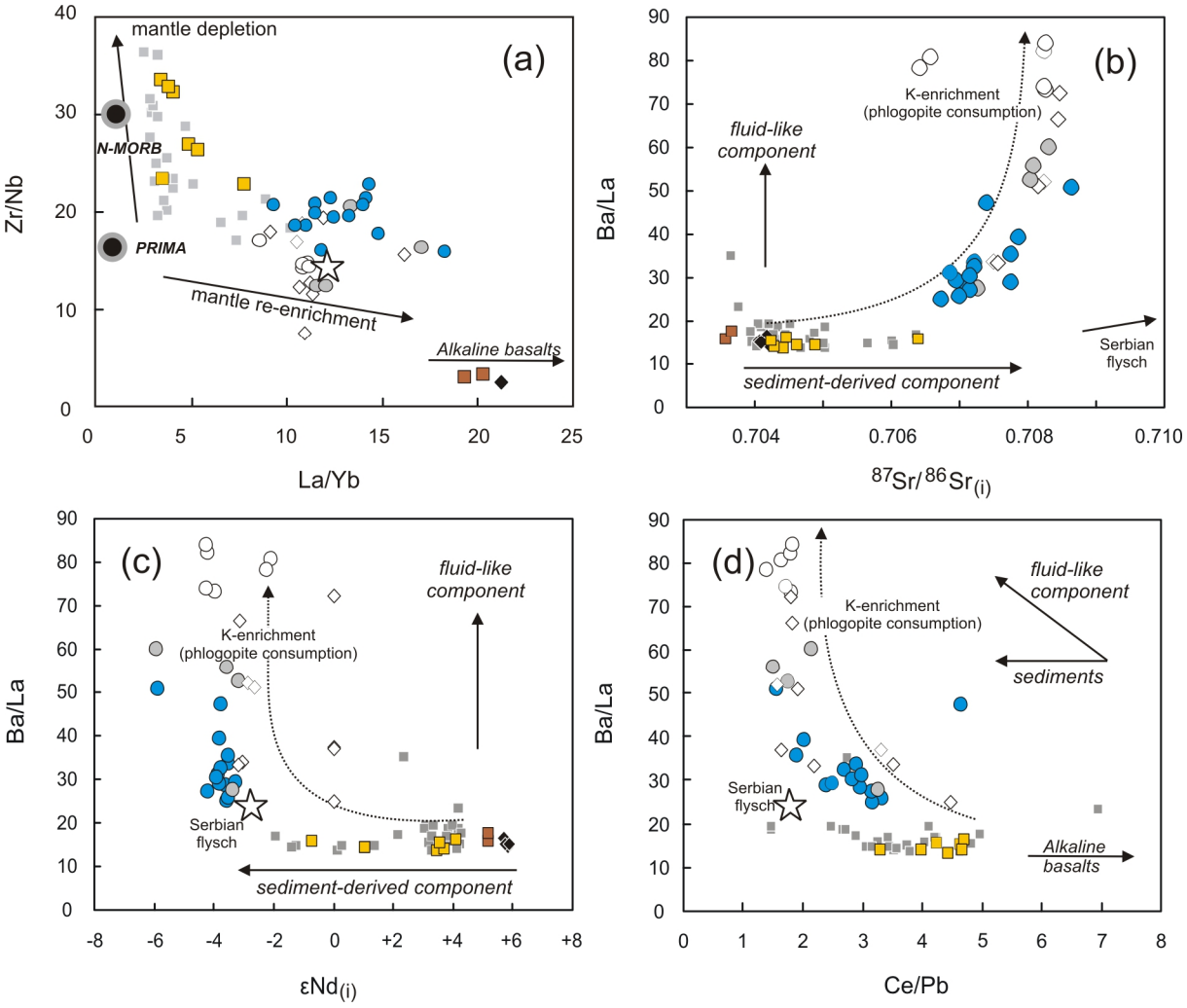

Fig. 3.12:

Trace element and isotope variation diagrams illustrating the role of fluid-like and melt-like subduction components for the lavas from Bulgaria and Santorini. (a) Zr/Nb versus La/Yb (after Münker, 2000). The variable Zr/Nb mirror different degrees of source replenishment of Bulgarian and Santorini lavas and possibly different initial mantle wedge compositions.

(b-d) Ba/La versus $^{87}Sr/^{86}Sr$, $^{143}Nd/^{144}Nd$, and Ce/Pb, confirming an important role of fluid- dominated source enrichment during *Stage 1* and phlogopite consumption during *Stage 2*. The subarc mantle sources beneath Santorini were rather fluxed by (sediment) melt-like components, resulting in nearly constant Ba/La.

The mode of mantle source enrichment of the Bulgarian lavas is best illustrated by Zr/Nb and REE patterns. Due to the higher mobility of La in fluid-like subduction components compared to Yb, Zr and Nb (e.g., Kessel *et al.*, 2005), it would be expected that a fluid-dominated source overprint increases La/Yb at largely unmodified Zr/Nb. Melt-like subduction components would not only increase La/Yb, but also decrease Zr/Nb (e.g., Münker et al., 2000). As illustrated in Fig. 3.12a, the Santorini lavas display higher Zr/Nb

(20-30) than the Bulgarian high-K lavas (Zr/Nb = 10-20). The higher Zr/Nb in the Santorini lavas either indicate a less pronounced source overprint by melt-like components or a more depleted mantle source prior to addition of subduction components. At low Zr/Nb, the Bulgarian lavas also display high La/Yb (9 – 18), pointing toward an important role of source enrichment via melt-like components (e.g., Pearce & Peate, 1995; Münker, 2000; Conticelli *et al.,* 2009a, b). Such a strong LREE enrichment may also account for the observed negative Eu-anomalies, which can either be inherited from the subducted sediments (Turner *et al.*, 1996; Williams *et al.*, 2004) or alternatively originate from the consumption of mica-rich metasomatic veins, which have been reported elsewhere to display pronounced negative Eu-anomalies (Becker *et al*., 1999). Further support for sediment-derived subduction components is also provided by the radiogenic Sr-Pb and unradiogenic Nd-Hf isotope compositions of the Bulgarian lavas that plot along mixing arrays with typical continent-derived sediments (Fig. 3.7, 3.8, 3.9).

In contrast to the K-rich rocks, trace element data and the Sr-Nd isotope compositions of the Bulgarian alkaline basalts overlap with typical asthenospheric mantle compositions such as the European Asthenospheric Reservoir (EAR, as defined by Cebriá & Wilson, 1995). Likewise, Marchev *et al.* (1998a, b) have interpreted the alkaline basalts from Bulgaria to originate from a LREE-enriched asthenospheric or lower lithospheric mantle beneath the Rhodopes. Conversely, the unradiogenic Pb isotope compositions indicate the presence of a non-asthenospheric component in the sources of the alkaline basalts. There are several possibilities to explain the origin of this component: (1) preferential incorporation of lithospheric Pb during the magma ascent without significantly shifting the Sr-Nd isotope compositions to more crustal values and (2) the presence of subducted sediments with less radiogenic $^{206}Pb/^{204}Pb$ in the mantle sources. In support of the first model, a major role of phlogopite has been proposed, as part of the source assemblage of the alkaline basalts (Marchev et al., 1998a, b). Rosenbaum (1993) showed that mantle phlogopite might represent a potential reservoir for lead, thus accounting for variable Pb isotope compositions in lithospheric melts. To account for the low $^{87}Sr/^{86}Sr$ in the alkaline basalts, a relatively young vein assemblage in the lithospheric mantle would be required. To account for the second model (source contamination), a relatively mafic subducted sediment composition (e.g., volcanogenic sediments) would be required to account for the EAR-like Sr-Nd isotope compositions.

(b) Mantle sources of Santorini lavas

The Sr-Nd-Hf isotope and incompatible element compositions of the most primitive Santorini samples (SA-1, SA-3, SA-6, and SA-10) indicate the enrichment of a depleted mantle source by subduction-derived components. A more depleted mantle source is also confirmed by Zr/Nb, which are higher than those of the Bulgarian lavas and average values for PRIMA and N-MORB (up to 30; Fig. 3.12). The high $^{207}Pb/^{204}Pb$ that are similar to those of the Bulgarian lavas resemble compositions of sediments thought to be subducted at the Hellenic Trench (N-African sediments, Fig. 3.9), confirming previous models arguing for an important role of subducted sediments (e.g., Zellmer *et al.*, 2000; Vaggelli *et al.*, 2009; Bailey *et al*., 2009).

Collectively, compositions of K-rich lavas from Bulgaria and Santorini highlight an important role of subduction-related components in their petrogenesis, in particular subducted sediments from the African plate (e.g., Pe-Piper, 1994; Weldeab *et al*., 2002). However, in contrast to uniform Pb isotope compositions, there are marked differences in Sr-Nd-Hf isotope compositions between both sample suites. These differences might reflect (1) a less efficient mobilisation of Sr-Hf-Nd compared to Pb or (2) significantly different Sr-Nd-Hf compositions of the mantle sources prior to source enrichment. Variable source compositions are also supported by variable HFSE ratios such as Zr/Nb.

(c) Subduction components

As shown above, recent addition of subduction components to the mantle sources (*multi-stage model*) appears to be the dominating process for the lavas from Bulgaria. Such fluid- or melt-like components may originate from subducted sediments and from subducted oceanic crust (e.g., Hawkesworth *et al.*, 1997; Elliott *et al.*, 1997; Woodhead *et al.*, 2001; Plank, 2005). Depending on the composition of the starting materials, pressure, and temperature, transport of subduction components may either occur as fluid- or melt-like phases (e.g., Kessel *et al.,* 2005; Klimm *et al*., 2008). As the nature of the fluid phase released from the slab and the subducted sediments is contentious (aqueous fluid – hydrous siliceous melt – supercritical liquid; Kessel *et al*., 2005; Klimm *et al*., 2008), we therefore refer to the hydrous phase as "fluid-like component" in the following discussion.

The *multi-stage model* for the generation of K-rich magmas assumes that fluid- and/or melt-like components derived from subducted sediments metasomatize the mantle wedge,

leading to the formation of metasomatic mineral assemblages often involving phlogopite (*Stage 1*). In response to tectonomagmatic events, e.g. extension, this vein-like assemblage is selectively affected by partial melting (*Stage 2*). The role of fluid- and melt-like components can be assessed by using a combination of geochemical parameters (McCulloch & Gamble, 1991; Miller *et al.*, 1994; Hawkesworth *et al.*, 1997; Elliott *et al.*, 1997; Woodhead *et al.*, 2001; Kelemen *et al.*, 2003; Plank, 2005). For example, variations of Ba/La and co-variations with K_2O, Ce/Pb and $^{87}Sr/^{86}Sr$ (see Fig. 3.12b, c, d) mirror selective addition of fluid-like components during *Stage 1* and can be inherited by arc magmas given complete consumption of residual phlogopite during partial melting throughout *Stage 2* (see Fig. 3.12b, c, d). Melt-like source enrichment, for instance, is indicated by low Ba/La and Ba/Th coupled with enrichment of HFSE and REE.

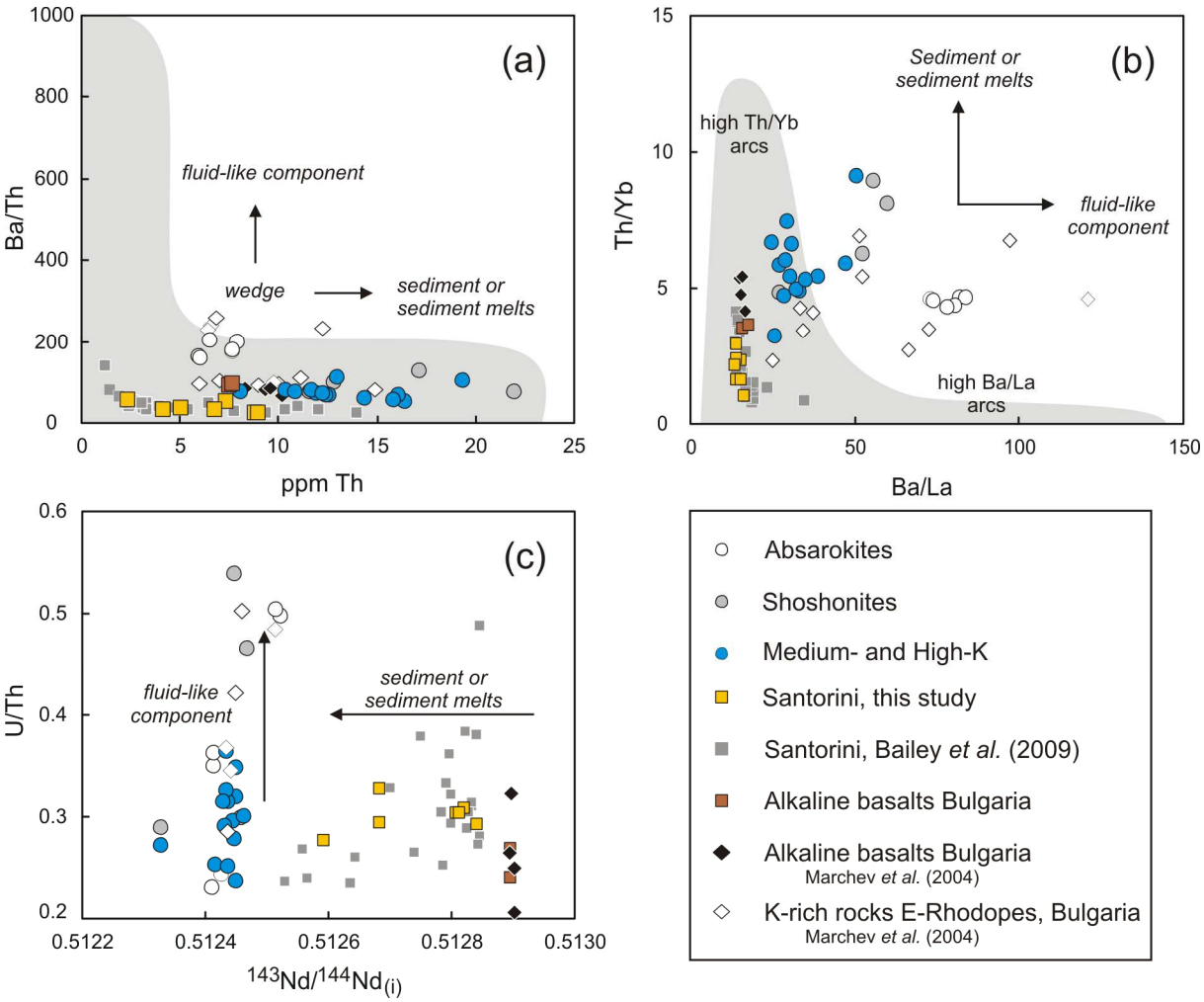

Fig. 3.13:

The role of fluids and sedimentary components in the evolution of lavas from Bulgaria and Santorini. (a) Ba/Th vs. Th concentration indicating that compositions of both sample suites are controlled by sediment-melt dominated source replenishment. The grey shaded field represents a compilation of arc basalts worldwide

(Hawkesworth *et al.,* 1997). (b) Th/Yb vs. Ba/La indicate that the compositions of Santorini lavas are controlled by sediment-melts whereas compositions of the Bulgarian lavas additionally show evidence for a fluid-controlled source overprint. The grey shaded field represents a compilation of oceanic-arc basalts (Woodhead *et al.,* 2001). (c) U/Th versus $^{143}Nd/^{144}Nd_{(i)}$ variations confirming the importance of fluid-dominated source enrichment in the sources of the Bulgarian lavas.

Bulgarian lavas. The replenishment of the sources of the Bulgarian lavas during *Stage 1* might be illustrated in a plot of Ba/Th vs. Th concentration (Fig. 3.13a). The Bulgarian samples (this study and Marchev *et al*., 2004) exhibit high Th abundances and low Ba/Th if compared to a worldwide compilation of arc lava compositions (Hawkesworth *et al.*, 1997, and references therein). Such low Ba/Th compositions are commonly interpreted as reflecting the predominance of subducted pelagic sediments in the magma sources, displaying high Th concentrations. However, if compared to the same compilation in Th/Yb vs. Ba/La space (Fig. 3.13b), it becomes obvious that the Bulgarian lavas are enriched in both Ba and Th, with a stronger relative enrichment of Th. The selective enrichment of Ba relative to La can possibly be explained by the higher mobility of Ba in fluid-like components during *Stage 1* (e.g., McCulloch & Gamble, 1991; Elliot *et al.*, 1997; Kessel *et al.*, 2005) and complete consumption of phlogopite during *Stage 2* by melting of metasomatic veins. The high Th/Yb on the other hand can only be explained by the presence of melt-like components in the magma sources. Hence, there is clear evidence for the presence of both melt- and fluid-like subduction components in the sources of the Bulgarian lavas.

Further constraints on the mode of source enrichment might be deduced from Ce/Pb systematics (Fig. 3.12d). Compared to Ce, Pb is preferentially partitioned into fluid-like slab components, resulting in low Ce/Pb (e.g., Miller *et al.*, 1994; Chauvel *et al*., 1995). Alternatively, the low Ce/Pb might alternatively been simply inherited from subducted sediments (e.g., Tatsumi, 2000; Kelemen *et al.*, 2003). The Bulgarian samples display low Ce/Pb of 1.5 – 4.7, which are comparable to arc basalts and continental crust. In a plot of Ce/Pb vs. εHf (not shown) the Bulgarian lavas yield invariant εHf with decreasing Ce/Pb, indicating that Ce/Pb is rather modified by fluid-like components due to the low mobility of Hf in shallow level subduction fluids (Pearce *et al.*, 1999; Kessel *et al.*, 2005).

Lead isotopes are a sensitive tracer for source modification by subducted sediments because of the low Pb abundances in the mantle (< 0.2 ppm), high Pb concentrations in pelagic and terrigenous sediments (ca. 20 ppm; Plank & Langmuir, 1998; White & Dupré,

1986) as well as high $^{207}Pb/^{204}Pb$ for a given $^{206}Pb/^{204}Pb$ compared to OIB and MORB. Lead isotope compositions of the Bulgarian lavas overlap the field for pelagic sediments and are similar to compositions of Mesozoic flysch from Serbia (after Prelević *et al.*, 2005), GLOSS (Plank & Langmuir, 1998), and N-African sediments (Pe-Piper, 1994; Fig. 3.9). The tight cluster of elevated $^{207}Pb/^{204}Pb$ in Pb isotope space (Fig. 3.9a) can be readily explained by flushing a depleted mantle source with subduction components derived from sediments with high $^{207}Pb/^{204}Pb$. This might also be the case for $^{87}Sr/^{86}Sr$, as Sr is also highly mobile in subduction fluids. Based on combined Th/Yb and Ba/La patterns in the Bulgarian lavas (Fig. 3.13b) the sediment-derived components must have been transported as both fluid- and melt-like components, possibly at different depths along the subducting African plate.

The comparatively low εHf – εNd values (Fig. 3.8b) support the source contamination model presented above. A more fluid-dominated source replenishment is expected to shift the εHf – εNd off the mantle array due to the higher mobility of Nd in aqueous fluids compared to Hf. As the Bulgarian samples virtually all plot on the mantle array, melt-like components exert a more pronounced influence on the Hf-Nd budget. It is furthermore important to note that the Bulgarian samples have variable Hf-Nd compositions but quite similar Pb isotope compositions, which can be explained by the much lower fluid mobility of Hf-Nd compared to Pb.

Similarly unradiogenic Hf-Nd isotope systematics as in the Bulgarian lavas were previously reported by Gasperini *et al.* (2002) for high-K rocks from the Roman Magmatic Province (RMP), the Tuscan Magmatic Province (TMP) and the Tyrrhenian Sea (see Fig. 3.8a), that are also thought to origin from sources overprinted by subducted sediments. For medium- to high-K basalts from Indonesia, Stolz *et al.* (1990) have shown that the observed radiogenic Sr and unradiogenic Nd isotope signatures can be generated by addition of less than 5 % of continent-derived sediment to the source region. This estimate might even be lower, if sediment-derived melts with higher Sr-Nd-Pb concentrations are considered (e.g., White & Dupré, 1986; Münker, 2000).

The fluid-like component in the sources of the Bulgarian lavas can be closer assessed using indicators of fluid contribution like Ba/La (e.g., Elliott *et al.*, 1997) and Ba/Th (e.g., Hawkesworth *et al.*, 1997). For the Bulgarian lavas, many of these element ratios follow hyperbolic mixing curves (Fig. 3.12b-d). Values of εNd (Fig. 3.12c) and εHf (not shown) in the Bulgarian lavas are nearly invariant with increasing Ba/La as expected from the low fluid mobilities of Nd and Hf. Hence, all of these co-variations are in accord with a preferential enrichment of K and Ba by aqueous fluids (Schmidt *et al.*, 2004; Kessel *et al.*, 2005). The

variations in Nd and Hf cannot be generated by the fluid components and require an additional source overprint by melt-like subduction components.

Santorini lavas. In Fig. 3.13a the Santorini lavas are characterized by relatively high Th concentrations at low Ba/Th compared to other arcs. However, the Th concentrations are lower than in the Bulgarian lavas. Likewise, ratios of Ba-La and Th-Yb in the Santorini samples are also lower than in the Bulgarian lavas (Fig. 3.13b). As mentioned above, the high Th concentrations reflect the preferential enrichment of Th by sediment-derived melts. For Santorini, the smaller degree of Th enrichment suggests either a less efficient enrichment by such components or, alternatively, a more depleted composition of the sub-arc mantle prior to source replenishment. Ratios of Ce-Pb are higher in the Santorini lavas (3.3 – 4.7) and combined with the invariant Ba/La compositions suggest a source overprint by siliceous melts derived from subducted sediments. These inferences are in agreement with previous studies by Druitt *et al*. (1999), Zellmer *et al*. (2000), and Bailey *et al*. (2009).

(d) Constraints on the subduction components

As explained above, the trace element inventory of both sample suites is largely controlled by fluid- and melt-like components derived from subducted sediments, which resulted in different degrees of large ion lithophile elements (LILE) enrichments, by a factor of 15 – 100 in the Santorini suite and by 100 up to 1000 in the Bulgarian lavas. The more pronounced mantle replenishment by subduction components for the Bulgarian lavas is also confirmed by the Sr-Nd-Hf isotope compositions (Figs. 3.7 and 3.8). Closer constraints on the composition of the sediment-derived contaminant might be drawn from Ba/La vs. Sr-Nd-Hf relationships. The asymptotes of the hyperbolic mixing curves shown in Fig. 3.12 approximate the composition of the possible contaminant, yielding $^{87}Sr/^{86}Sr$ of ≥ 0.709, εNd of ≤ -5, εHf of ≤ -2, and Ce/Pb of ~ 1.2. Such values are typical compositions of ocean floor sediments (e.g., Vervoort *et al.,* 1999) and are also in good agreement with reported values for Mesozoic flysch from Serbia ($^{87}Sr/^{86}Sr = 0.7119$; εNd = -8.5 and Ce/Pb = 1.9; Prelević *et al.,* 2005) and to some extent with sediments of the N-African plate ($^{87}Sr/^{86}Sr = 0.7075$; εNd = -3 to -7; Weldeab *et al*., 2002). However, detailed trace element and isotope studies concerning the presently subducted sediments at the Hellenic Trench are still lacking.

In addition to Pb, Th/La is an indicator of sediment recycling at subduction zones as Th and La are thought to mirror compositions of subducted sediments with only negligible contributions from the mantle and the subducted slab (Plank, 2005). Both suites yield

similarly high Th/La of 0.35 – 0.74 (Bulgaria; average 0.46) and 0.29 – 0.60 (Santorini; average 0.43), indicating a contaminant with comparable Th/La. This range of Th/La is also similar to Mesozoic flysch sediments (Prelević *et al.*, 2005), which have been interpreted to be involved in sources of Serbian high-K rocks. However, the additional role of allanite in the mantle has to be considered, as it represents an important host for LREE and Th with D_{La}/D_{Th} ~ 2 (Hermann, 2002; Klimm *et al.*, 2008). Hence, residual allanite would be able to increase the Th/La of the derivative partial melt.

In agreement with our model for lavas from Bulgaria and Santorini, sediment-derived components were postulated for sources of high-K lavas elsewhere (e.g., Stolz *et al.*, 1990; Wang *et al.*, 2004; Prelević *et al.*, 2005). Pelitic sediments with minor contributions from carbonates were also inferred to be the major sedimentary contaminant for Italian and Serbian high-K lavas (Conticelli *et al.*, 2002; Gasperini *et al.* 2002; Prelević *et al.* 2005). Moreover, subducted upper continental crust has been invoked by Cvetković *et al.* (2004) as a possible source contaminant for some high-K rocks from Serbia.

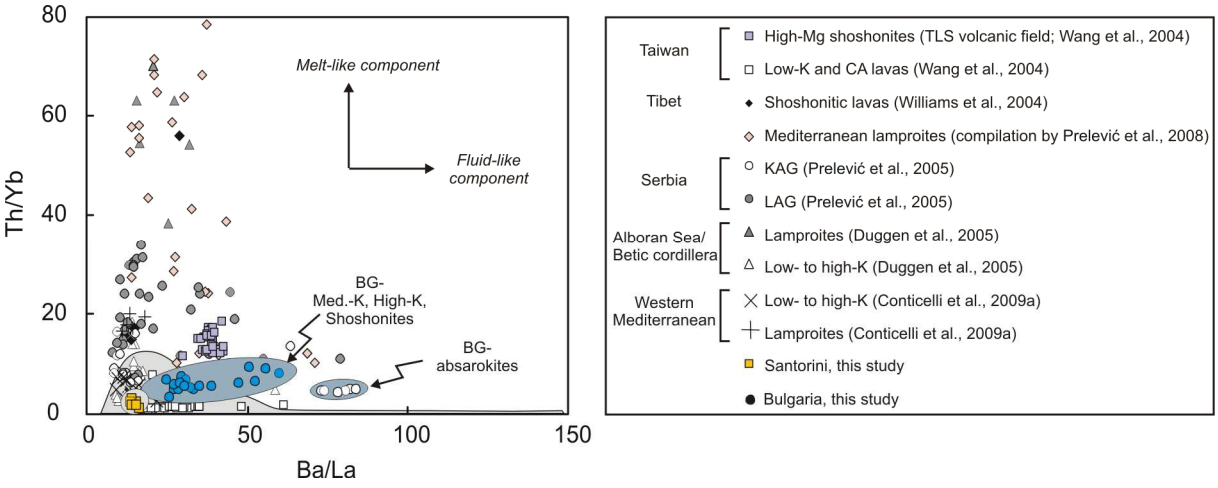

Fig. 3.14:

Th/Yb vs. Ba/La diagram showing a compilation of low-K to high-K, shoshonitic and lamproitic volcanic rocks from post-collisional tectonic settings world-wide in comparison to measured compositions of lavas from Bulgaria and Santorini (dark grey fields). Only results for samples with SiO_2 < 56 wt. % are shown. The light grey field indicates compositions of oceanic arc basalts by Woodhead *et al.* (2001). Compositions of most post-collisional rocks overlap the composition of oceanic-arcs. However, lamproites as well as high-Mg shoshonites from Taiwan exhibit much higher Th/Yb. Notably, the Bulgarian samples, especially the absarokites, exhibit higher Ba/La than most other post-collisional suites. Note that GLOSS (Ba/La = 26.6, Th/Yb = 2.5; Plank & Langmuir, 1998) and average continental crust (Ba/La = 18.3, Th/Yb = 4.9; Taylor & McLennan, 1995) show considerably lower Th/Yb than most lamproites.

3.5.5. Comparison of the Bulgarian lavas with other post-collisional high-K lavas and lamproites

Figure 3.14 shows a comparison of the high-K lavas from Bulgaria to other high-K rocks and lamproites from similar post-collisional settings (e.g., Tibet, Serbia, Taiwan, and Western Mediterranean). The comparison in Th/Yb vs. Ba/La space shows (1) that lavas in many other localities exhibit much higher Th/Yb, and (2) that many Bulgarian samples exhibit unusually high Ba/La. Except for a suite of K-rich lavas from Taiwan (TLS suite; Wang *et al.*, 2004), the Th/Yb and Ba/La of most post-collisional K-rich rocks overlap typical compositions of arc basalts world-wide (Woodhead *et al.,* 2001). The trace element inventory of other post-collisional K-rich suites seems to be rather dominated by source contamination involving subducted sediment components (Prelević *et al.*, 2005; Conticelli *et al.*, 2009a; Duggen *et al.*, 2005). Notably, the combination of both fluid- and melt-dominated source enrichments as found for the Bulgarian lavas appears not to be a typical feature of other post-collisional suites (Fig. 3.14).

The extremely high Th/Yb in particular in post-collisional lamproites (from 15 up to 80) can primarily be attributed to the extremely enriched Th concentrations (up to 130 ppm; Prelević *et al.*, 2008). Current interpretations based on major, trace elements and isotope compositions of lamproites involve a strong overprint of ultra-depleted mantle sources by melt-like crustal components, resulting in "crustal" Sr-Nd-Pb isotope compositions (e.g., Prelević *et al.*, 2008). The high Th concentrations in the lamproites may be explained by low degree melting of these enriched mantle domains. In this context, the absarokites from Bulgaria occupy an exceptional position in the compositional spectrum of post-collisional lavas, as they record some of the highest Ba/La of the compiled data sets. The high Ba/La might be attributed to the selective source replenishment by slab-derived fluids that do not significantly contribute to the Th budget. This enrichment by fluid-like components was apparently not as important in the sources of K-rich rocks elsewhere.

3.5.6. Tectonomagmatic constraints on Mediterranean volcanism

The petrogenetic model inferred for lavas from Bulgaria and Santorini can shed further light on the tectonomagmatic evolution of the eastern Mediterranean realm. Subduction in the Eastern Mediterranean was initiated in the Jurassic and continued until the

Paleogene when closure of the Vardar branch of the Tethys (Robertson & Karamata, 1994) was caused by collision of the Eurasian platform with the Pelagonian microplate (Ricou *et al.*, 1998; van Hinsbergen *et al.*, 2005). This compressional phase is constrained to have occurred between 51 and 37 Ma (Liati & Gebauer, 1999; Krohe & Mposkos, 2002; Liati, 2005). Extensional deformation and exhumation of the core complexes (Bonev *et al.*, 2006) took place contemporaneously with the onset of volcanism in the Eastern Rhodopes, at about 34 Ma (Marchev & Singer, 2002).

The triggering mechanism for volcanism in post-collisional settings is still subject of debate. Seismic tomographic imaging in the eastern Mediterranean region (Bijwaard *et al.*, 1998) enables the reconstruction of processes affecting the subducted continental and oceanic lithosphere (Wortel & Spakmann, 2000; Faccenna *et al.*, 2003; van Hinsbergen *et al.*, 2005), thus allowing insights into the processes triggering post-collisional volcanism. The tomographic models strongly suggest one single, N-vergent active subduction zone with ca. 1600 km of lithosphere being subducted since the Jurassic (see Fig. 3.2). No evidence for slab detachment or a reversal of subduction polarity since the Jurassic has been observed. In addition, the tomographic images indicate a slab-rollback towards the south by ~ 300 km, which would explain the extension of the Aegean region and trench retreat to the currently active subduction along the Hellenic Trench. In addition to slab-rollback, delamination of mantle beneath the Rhodopes might be a plausible mechanism explaining the change in tectonic regime. Replacing parts of the cold lithospheric mantle with hot asthenosphere would cause a thermal anomaly, and the increased heat flow beneath the remaining metasomatized lithospheric keel could have triggered partial melting (e.g., Wortel & Spakman, 2000). It is also inferred that the elevated heat flow and underplated hot magma might have played a significant role in the exhumation of the core complexes (Marchev *et al.*, 2006).

Our geochemical data clearly indicate a strong source overprint for the Bulgarian high-K rocks by subduction components that are similar to those presently fluxing the subarc mantle beneath Santorini. This observation is well in agreement with a long-lived subduction zone. For Bulgaria, delamination might as well explain the decrease in crustal thickness and migration of the volcanism from the western to the eastern Rhodopes (Marchev *et al.*, 1998a, b, 2004). Nevertheless, a lithospheric keel must have been stable beneath Bulgaria until the termination of high-K volcanism by 30 Ma. A delamination model could also explain the transition from post-collisional high-K to alkaline intraplate volcanism between 30 and 28 Ma. A fundamental change in the mantle regime must have occurred beneath Bulgaria during this period, leading to the upwelling of enriched asthenospheric mantle.

3.6. Conclusions

Trace element and Sr-Nd-Hf-Pb isotope compositions of mafic high-K lavas from Eastern Bulgaria provide evidence for mantle sources overprinted to variable degrees by melt- and fluid-like subduction components that largely originated from subducted sediments (*multi-stage model*). The major constraints from this study are:

1. Potassium-enriched lavas from Bulgaria cover virtually the entire spectrum of K-rich lavas worldwide, ranging from the medium-K to the shoshonite suite, and also including absarokites as the most mafic endmember.
2. Crustal contamination via AFC processes modified the inventory of some incompatible trace elements in the Bulgarian lavas. However, many isotope and trace element compositions were well buffered during crustal assimilation. Conversely, compositions of some differentiated Santorini lavas provide clear evidence for shallow-level assimilation of continental crust.
3. A test for a *single-stage model* was carried out by modelling the Sr-Nd isotope evolution of ancient lithospheric mantle. The presence of an old (> 1 Ga) trace element-enriched lithospheric mantle keel beneath the Bulgarian volcanic complexes can be excluded. Rather, it is more plausible that the lithospheric root was not stabilized until final amalgamation of continental crust in the region (Mesozoic to early Cenozoic).
4. Santorini lavas originated from a depleted spinel-lherzolitic mantle source, which was refertilized by sediment-melts during contemporaneous subduction. The sub-arc mantle beneath Santorini was mainly metasomatized by sediment-derived melts.
5. Trace element enrichment in the sources of the Bulgarian lavas was triggered by young subduction components, which originate from northward subduction of the Tethyan oceanic crust (*multi stage model*). The trace elements were transported by sediment-derived fluids and sediment-derived melts.
6. Combined extension and delamination of the lithospheric mantle may have triggered melting processes beneath the Rhodopes, thereby also explaining a progressive change in mantle composition by asthenospheric uplift. The latter is manifested by the emplacement of 28 – 26 Ma old alkaline intraplate basalts in Bulgaria.

- Chapter 4 -

The behaviour of the extended HFSE group (Nb, Ta, Zr, Hf, W, Mo, Sb) during the petrogenesis of mafic K-rich lavas from the Bulgarian Rhodopes

4.1. Introduction

The extended high-field strength element (HFSE) group comprises the elements Nb-Ta-Zr-Hf-W-Sb-Mo. They are all characterized by a small ionic size and high positive charges (4+ to 6+) and were (except for Sb and Mo) traditionally considered as being immobile in subduction zones (Brenan *et al*., 1994; Keppler, 1996; Noll *et al*., 1996 Pearce & Peate, 1995). However, this view has been challenged over the past decade, in particular by studies involving high-precision HFSE data (e.g., Weyer *et al*., 2002, 2003; Münker *et al*., 2004; König *et al*., 2008) or experimental studies (Kessel *et al*., 2005). During partial mantle melting, a relative compatibility sequence of Ba < W < Th < U < Nb < Ta < Zr, Hf < REE has been established by experimental studies (Hart & Dunn, 1993; Hill *et al*., 2000; McDade *et al*., 2003) and studies on mafic lavas (Newsom *et al*., 1996; Niu *et al*., 1996; Münker *et al*., 2004; König *et al*., 2010), confirming the incompatible behaviour of the HFSE. It has been shown that in arc lavas even the traditional HFSE (Nb, Ta, Zr, Hf) can be enriched by slab melts to a significant degree, whereas subduction fluids show only a limited transport capability for HFSE from the slab to the subarc mantle wedge (conservative behaviour; Brenan *et al*., 1994; Münker *et al*., 2004). Nevertheless, previous studies have shown that with increasing pressure and temperature silicic liquids of similar composition (aqueous fluids and silicate melts) may cross a critical endpoint, resulting in complete miscibility between the two phases (Bureau & Keppler, 1999; Kessel *et al*., 2005).

Among the extended HFSE group, special attention has been paid in the past to W, which behaves moderately siderophile under reducing conditions and as a highly incompatible lithophile element during silicate differentiation, leaving the Earth's core and the crust enriched and the mantle depleted in W (Palme & Rammensee, 1981; Newsom *et al*., 1996;

König *et al*., 2011). This is also expressed by the high crust/mantle ratio of W of ~ 60 (Palme & O'Neill, 2003). Thus, in the absence of metal and during partial melting, W behaves similar to lithophile elements like Ba, Th and U. However, W has been shown to be efficiently mobilized by fluids in subduction zones and hydrothermal fluids (Kishida *et al*., 2004; Arnórsson & Óskarsson, 2007; König *et al*., 2008; 2010), displaying a significant fractionation from the similarly incompatible elements Ba, Th, and U (König *et al*., 2008, 2010). Especially island-arc rocks record a selective enrichment of W over Th, U, and Ta when compared to MORB or OIB, leading to the conclusion that components derived from the subducted slab (fluids, melts) act as transport- and replenishment agents. In this regard, Sb and Mo are also of particular importance. Molybdenum is preferentially incorporated in mantle sulfides and is enriched in reduced environments (Crusius *et al*., 1996; Kishida *et al*., 2004). Conversely, Sb is, similar to W, moderately siderophile and behaves like an incompatible lithophile element during magmatic processes (Jochum & Hofmann, 1997). However, Sb is also highly enriched in altered oceanic crust and is preferentially mobilized by low-temperature fluids (Jochum & Verma, 1996; Rouxel *et al*., 2003; Hattori & Guillot, 2003). The different redox-susceptibilities of W, Sb, and Mo and their different mobilities in fluids with different alkalinity and temperature thus allows assertions on the redox conditions during slab dehydration and melting.

A critical evaluation of the extended HFSE also allows the identification of residual mineral phases in the magma sources of subduction-related basalts. The major hosts of HFSE are Ti-bearing phases like ilmenite or rutile, which can account for the entire Nb-Ta budget even if present in trace amounts (e.g., Zack *et al*., 2002; Klemme *et al*., 2005). Further important phases for the HFSE budget in subduction zone lavas include zircon (Zr-Hf), and possibly also mica (Nb-Ta). Furthermore, grain boundaries as well as micro-inclusions have been described as important hosts for HFSE (e.g, Bodinier *et al*., 1996; Kalfoun *et al*., 2002).

It is important to note that previous high-precision HFSE studies mainly focused on trace element depleted mafic end-members (low-K basalts and boninites) in predominantly intra-oceanic subduction zone settings with no or only limited amount of subducted sediments involved in the petrogenesis of these rocks (e.g., *Aleutians and Kamchatka*, Münker *et al*., 2004; *Solomon Islands*, *Papua New Guinea,* König *et al*., 2008; 2010). However, numerous studies have shown that subducted (terrigeneous and pelagic) sediments are, when compared to the mantle wedge and the subducted slab, the most important repository of incompatible trace elements in subduction zones (e.g., Plank & Langmuir, 1998; Hermann & Rubatto, 2009; Skora & Blundy, 2010). Hence, in subduction zones with a high flux of sediments from

the trench to sub-arc mantle depths (e.g., *Antilles*; White & Dupré, 1986; Carpentier *et al*., 2008; *Aegean Arc*; Zellmer *et al*., 2000, see also Chapter 3; Patchett *et al*., 1984), even the budgets of HFSE might be largely controlled by the sediment-derived components and may thus outbalance any contribution from the subducting slab or the mantle wedge.

So far, little high precision HFSE (+ W) data are available for incompatible element enriched end-members in subduction zones and subduction-related tectonic settings (K-rich suites after Peccerillo & Taylor, 1976), especially for those found in continental arcs where assimilation of crustal basement constitutes an additional challenge for identifying primary mantle source signatures. The HFSE have been shown to be enriched in these settings (e.g., *Indonesia*; Stolz et al., 1996), which has been attributed to a high magnitude of source enrichment by subducted sediments (Vroon *et al*., 1993; 1995).

The Eastern Mediterranean is particularly suited to study the evolution of K-rich volcanic suites because since the Tertiary several volcanic complexes including K-rich rocks were formed (e.g., *Lesbos*, Pe-Piper & Piper, 1992; *Naxos, Samos*; Pe-Piper & Piper, 2001) that are genetically linked by the same long-lasting subduction system (at least since Jurassic times; e.g., Bijwaard *et al*., 1998; Wortel & Spakman, 2000; van Hinsbergen *et al*., 2005). Thus, compositionally similar subducted sediments are involved in the replenishment of their respective mantle sources (Pe-Piper, 1994; Chapter 3). This study presents high-precision HFSE data (Nb, Ta, Zr, and W), together with Lu, Hf, Mo and Sb data to shed new light on HFSE fractionation processes in K-rich volcanic rocks. The sample suites studied include two well-characterized end-member suites of the Aegean subduction system, one being derived from metasomatized lithospheric mantle (Bulgaria) and one originating in a continental arc with a high flux of subducted sediments (Santorini).

4.2. Geological settings and source components

A detailed discussion of the petrogenetic evolution of the Santorini and Bulgarian lavas is provided in Druitt *et al*. (1999), Marchev *et al*. (2004), Bailey *et al*. (2009), and also in Chapter 3 of this thesis.

4.2.1. Rhodopes – Bulgaria

The volcanism in the Rhodopes is part of a Cenozoic magmatic belt that extends towards NW into Serbia and Macedonia and originates from the collision of the African with the Eurasian plate during the Alpine orogeny. The post-collisional volcanism was triggered by gravitational collapse/lithospheric extension of the Aegean Sea region and the rollback of the subduction zone (e.g., Jolivet *et al*., 2009). Subsequently, mafic potassium-rich lavas of the medium- to high-K and shoshonitic series were erupted during the Eo-Oligocene (34 – 30 Ma; Marchev *et al*., 2004) in several discrete volcanic centres (for details see Chapter 3, and Marchev *et al*., 2004).

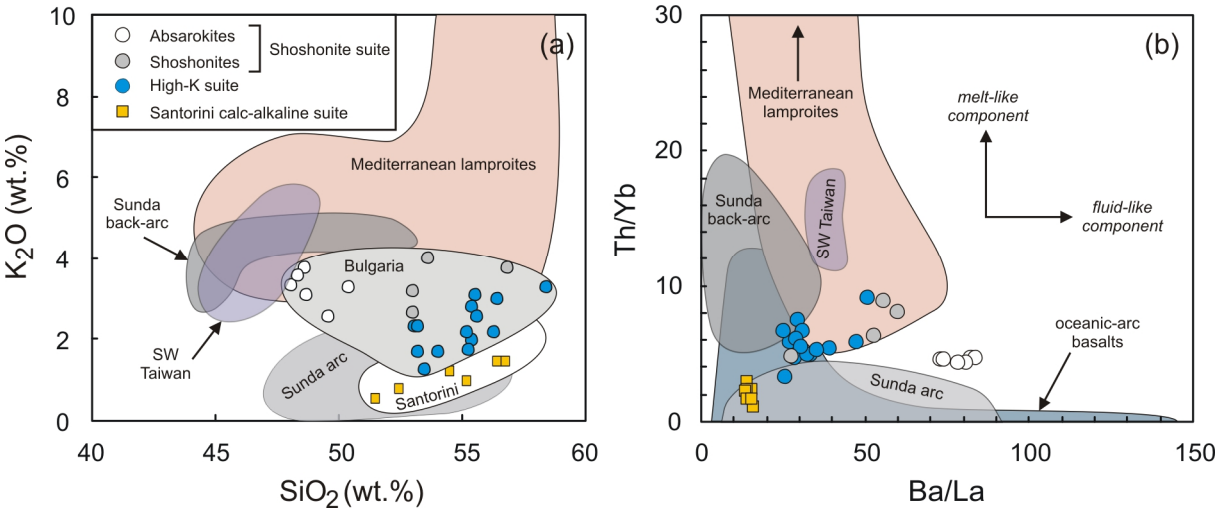

Fig. 4.1:

(a) Magnitude of K-enrichment in the Bulgarian and Santorini lavas in comparison to other (K-rich) orogenic and arc lavas.

(b) Control of melt-like or fluid-like subduction components on the incompatible element budget of K-rich lavas from different tectonic settings (orogenic lamproites, island-arc, back-arc, post-collisional).

Sunda arc and back-arc lavas after Barth *et al.* (2011) and unpublished; SW Taiwan (Tsaolingshan absarokites) after Wang *et al.* (2004); field for oceanic arc basalts after Woodhead *et al.* (2001); Mediterranean lamproites after Prelević *et al.* (2008).

The K-rich rocks from Bulgaria cover the whole spectrum from medium-K to shoshonitic (Fig. 4.1a), whereas they are less mafic than similar post-collisional rocks from Taiwan and less potassic than lamproites, which are classified as ultrapotassic ($K_2O/Na_2O > 2$). The sample suite from Bulgaria is divided here in two different K-rich suites: a medium to high-K suite and a shoshonitic suite. The most mafic end-member of the shoshonite suite are a group of samples classified as absarokites (six samples). They are of particular interest in that they reflecting small degree near-primitive melts bearing the highest contribution from a

metasomatized mantle source (see Chapter 3). This is evident from high volatile contents, higher $^{87}Sr/^{86}Sr$ than the other K-rich samples, high K_2O/Na_2O (1.2 – 2.2), relatively high MgO (5.4 – 8.8 wt.%) high compatible element contents as well as leucite phenocrysts (Ne-normative).

The geochemistry of the Bulgarian lavas involves a strong enrichment in incompatible elements, which is evident from coupled enrichment of melt-and fluid-sensitive elements like Ba/La, Ce/Pb and Th/Yb (see Fig. 4.1b). Radiogenic $^{87}Sr/^{86}Sr_{(i)}$ (0.7067 – 0.7083), unradiogenic $^{143}Nd/^{144}Nd_{(i)}$ (εNd = -5.8 to -1.9) and $^{176}Hf/^{177}Hf_{(i)}$ (εHf = -3 to +3) span a rather small range and have been interpreted to reflect homogenenous degrees of mantle metasomatism (see Chapter 3). Moreover, Pb isotope compositions ($^{206}Pb/^{204}Pb_{(i)}$ = 18.68 – 18.93, $^{207}Pb/^{204}Pb_{(i)}$ = 15.63 – 15.68 and $^{208}Pb/^{204}Pb_{(i)}$ = 38.72 – 39.96), broadly overlap values recorded for flysch sediments in Serbia, that are thought to be isotopically representative of subducted Mesozoic material (see Chapter 3; Prelević *et al*., 2005). Especially the values for Ba/La and Sr-Nd and Hf isotopes have been shown to co-vary with K-enrichment, thus providing evidence for the presence of a metasomatic (vein) component in the lithospheric mantle. Hence, it has been proposed that the post-collisional rocks from Bulgaria are most likely derived by a multi-stage process, involving decompression melting of a veined (phlogopite-bearing) lithospheric mantle that was previously metasomatized by sediment-derived subduction components (melt- and fluid-like; Chapter 3).

4.2.2. Santorini – Aegean Sea

Santorini is part of the active Aegean island arc, which is considered as the youngest magmatic belt in the Eastern Mediterranean resulting from the Africa-Eurasia convergence. Currently, subduction takes place along the Hellenic trench south of Crete with a convergence rate of ~ 3 - 4 cm/yr (Bailey *et al*., 2009, and references therein). Santorini is located on thinned continental crust of the Aegean microplate, which was extended in response to slab roll-back during re-location of the subduction zone during the Mid-Miocene (e.g., Jolivet & Brun, 2010). Volcanic rocks on Santorini are largely andesitic to rhyodacitic, however, basalts to andesites also occur in lava flows and cinder cones. The mafic rocks on Santorini belong to a calc-alkaline low- to medium-K suite (Fig. 4.1a; Zellmer *et al*., 2000; Chapter 3), similar to other continental island-arcs (e.g, Sunda arc; Barth *et al*., 2011). The sub-arc mantle source refertilization was most likely dominated by sediment-derived melts, which is evident from

low Ba/Th, elevated Th/Yb and Th concentrations as well as low and invariant Ba/La (Bailey *et al*., 2009; Chapter 3). If compared to the Bulgarian lavas, the samples are furthermore characterized by radiogenic εHf – εNd (εHf = +1.8 to +11.6; εNd = -0.71 to +4.1), unradiogenic $^{87}Sr/^{86}Sr$ (0.7042 – 0.7064) as well as radiogenic Pb isotope compositions, the latter overlapping with the values for the Bulgarian lavas.

Based on P-wave tomographic models (e.g., Bijwaard *et al*., 1998) it has been proposed that one continuous northward subduction zone is present beneath the Eastern Mediterranean since at least early Jurassic times (e.g., van Hinsbergen *et al*., 2005; Jolivet & Brun, 2010), genetically linking the volcanism on Santorini to the post-collisional rocks in Bulgaria. Geochemically this has been confirmed based on Pb isotope compositions of Santorini lavas, which are similar to locally subducted sediments and the Eo-Oligocene volcanic rocks from Bulgaria (see Chapter 3). The geochemical budget of the Santorini volcanic rocks further indicates, that they were derived from a depleted spinel-lherzolitic mantle source. A direct comparison to the lavas from Bulgaria (see Chapter 3) provides evidence for a more pronounced source replenishment of the Bulgarian lavas by both melt- and fluid-like components, whereas the Santorini mantle source overprint was clearly dominated by sediment-derived melts. The higher magnitude of incompatible trace element enrichment of the Bulgarian lavas might either argue for a more depleted mantle prior to source overprint or a more efficient source metasomatism.

Collectively, Santorini lavas are well suited to study the contribution of sediment-melt dominated subduction components to the extended HFSE budget of continental arc lavas. Furthermore, the Bulgarian post-collisional high-K rocks enable to constrain the behaviour of HFSE in lavas derived from a multi-stage process in older, enriched lithosphere. The previously shown covariations of K-enrichment with those of other incompatible elements like Ba and Th provide a good opportunity to test for the relationship between HFSE+W enrichment and the magnitude of K-enrichment. This also might allow insights into the role of metasomatic mineral phases being responsible for the incompatible element budget in metasomatized lithospheric mantle assemblages.

Table 4.1.:

Sample	Locality	Description	Zr (ppm)	Nb (ppm)	Ta (ppm)	W (ppm)	Lu[1] (ppm)	Hf[1] (ppm)	Nb/Ta	Zr/Hf	Zr/Nb	Ta/W	$^{176}Lu/^{177}Hf$	W/Th[1]	W/Mo[1]	Sb/Ce[1]	Ba/La[1]
SA-1	Santorini	calc-alkaline	73.87	3.41	0.228	0.172	0.361	2.105	14.9	35.1	21.6	1.33	0.02433	0.0736	0.334	0.00382	16.2
SA-3	Santorini	calc-alkaline	131.2	5.43	0.440	0.658	n.d.	n.d.	12.3	n.d.	24.2	0.669	n.d.	0.0745	0.536	0.00451	14.2
SA-4	Santorini	calc-alkaline	175.8	8.80	0.548	0.512	0.490	4.556	16.0	38.6	20.0	1.07	0.01526	0.0692	0.500	0.00154	15.6
SA-5	Santorini	calc-alkaline	202.1	11.0	0.768	0.920	0.583	5.356	14.3	37.7	18.5	0.835	0.01546	0.0595	0.658	0.00208	14.4
SA-6	Santorini	calc-alkaline	128.0	5.50	0.384	0.482	0.442	3.449	14.3	37.1	23.3	0.798	0.01818	0.0711	0.525	0.00304	14.2
SA-9	Santorini	calc-alkaline	178.9	6.39	0.466	0.642	0.665	4.985	13.7	35.9	28.0	0.726	0.01893	0.0713	0.391	0.00477	13.4
SA-10	Santorini	calc-alkaline	96.07	3.26	0.231	0.305	0.399	2.720	14.1	35.3	29.4	0.757	0.02080	0.0739	0.395	0.00435	14.1
SA-11	Santorini	calc-alkaline	115.1	4.02	0.285	0.356	0.518	3.253	14.1	35.4	28.6	0.801	0.02261	0.0701	0.382	0.00372	15.4
BG-99a	Bulgaria	Absarokite	124.3	9.13	0.476	1.67	0.254	3.354	19.2	37.0	13.6	0.284	0.01075	0.218	1.65	0.03359	73.1
BG-99b	Bulgaria	Absarokite	123.3	9.04	0.473	2.20	0.255	3.336	19.1	36.9	13.6	0.215	0.01084	0.288	1.93	0.05107	73.9
BG-101	Bulgaria	Absarokite	104.3	7.53	0.381	1.96	0.214	2.820	19.8	37.0	13.9	0.194	0.01077	0.300	2.44	0.00951	83.9
BG-102	Bulgaria	Absarokite	125.9	9.27	0.461	0.958	0.258	3.412	20.1	36.9	13.6	0.481	0.01074	0.121	1.48	0.00242	82.2
BG-109a	Bulgaria	Absarokite	85.20	5.33	0.330	1.31	0.203	2.460	16.2	34.6	16.0	0.252	0.01172	0.219	0.94	0.00198	80.6
BG-109b	Bulgaria	Absarokite	86.01	5.35	0.324	1.26	0.205	2.482	16.5	34.7	16.1	0.256	0.01172	0.210	0.915	0.00303	78.3
BG-109b*	Bulgaria	Absarokite	84.98	5.15	0.331	1.13	0.205	2.472	15.6	34.4	16.5	0.292	0.01173				
BG-46	Bulgaria	Shoshonite	226.1	19.6	1.35	4.63	0.372	6.041	14.5	37.4	11.5	0.292	0.00872	0.211	1.86	0.01288	55.9
BG-60	Bulgaria	Shoshonite	165.3	8.89	0.610	0.933	0.364	4.482	14.6	36.9	18.6	0.654	0.01155	0.0806	1.37	0.00284	27.4
BG-103	Bulgaria	Shoshonite	167.1	10.9	0.731	1.55	0.323	4.560	14.9	36.6	15.3	0.473	0.01007	0.0900	1.85	0.00473	60.1
BG-103*	Bulgaria	Shoshonite	165.8	10.7	0.730	1.54	0.321	4.541	14.6	36.5	15.5	0.475	0.01001				
BG-113	Bulgaria	Shoshonite	143.5	12.7	0.849	2.45	0.308	3.935	14.9	36.5	11.3	0.346	0.01111	0.191	1.63	0.00238	52.7
BG-52	Bulgaria	high-K	174.4	8.99	0.612	1.18	0.344	4.714	14.7	37.0	19.4	0.520	0.01039				30.3
BG-56	Bulgaria	high-K	221.3	11.5	0.775	1.15	0.368	5.918	14.8	37.4	19.3	0.677	0.00884	0.0713	0.559	0.00208	31.1
BG-58	Bulgaria	high-K	114.3	7.81	0.532	1.07	0.318	3.099	14.7	36.9	14.6	0.495	0.01457	0.103	0.797	0.00180	33.5
BG-59	Bulgaria	high-K	136.8	8.81	0.618	n.d.	0.329	3.835	14.2	35.7	15.5	n.d.	0.01220			0.00329	27.1
BG-61	Bulgaria	high-K	153.0	8.38	0.586	0.918	0.332	4.173	14.3	36.7	18.3	0.639	0.01129	0.0708	1.04	0.00270	47.2
BG-62	Bulgaria	high-K	178.4	9.03	0.636	1.09	0.388	4.810	14.2	37.1	19.8	0.583	0.01143	0.0914	0.640	0.00178	28.4
BG-64	Bulgaria	high-K	223.2	11.2	0.720	1.29	0.362	5.920	15.5	37.7	20.0	0.559	0.00869	0.0811	0.652	0.00176	25.0
BG-64*	Bulgaria	high-K	223.0	10.4	0.721	n.d.	0.362	5.937	14.4	37.6	21.4	n.d.	0.00863				
BG-67	Bulgaria	high-K	140.8	7.62	0.545	1.08	0.329	3.951	14.0	35.6	18.5	0.506	0.01183	0.0988	0.826	0.00173	32.5
BG-67*	Bulgaria	high-K	141.6	7.56	0.544	1.08	0.330	3.955	13.9	35.8	18.7	0.503	0.01180				
BG-72	Bulgaria	medium-K	142.7	7.34	0.498	0.728	0.379	3.919	14.8	36.4	19.4	0.684	0.01374	0.0896	0.603	0.00178	25.8
BG-72*	Bulgaria	medium-K	142.3	7.25	0.498	0.677	0.380	3.925	14.5	36.2	19.6	0.736	0.01372				
BG-78	Bulgaria	high-K	174.7	9.54	0.690	1.53	0.339	4.771	13.8	36.6	18.3	0.451	0.01011	0.0931	1.01	0.00195	29.4
BG-78*	Bulgaria	high-K	174.5	9.20	0.691	1.53	0.339	4.765	13.3	36.6	19.0	0.452	0.01007				
BG-82	Bulgaria	high-K	184.0	10.1	0.768	1.31	0.363	4.956	13.1	37.1	18.2	0.589	0.01041	0.0906	0.943	0.00162	29.0
BG-92	Bulgaria	high-K	131.8	7.52	0.565	1.19	0.328	3.671	13.3	35.9	17.5	0.473	0.01264	0.102	1.08	0.00225	39.1
BG-107	Bulgaria	high-K	179.1	11.9	0.912	2.31	0.319	4.895	13.0	36.6	15.1	0.394	0.00923	0.120	1.37	0.00130	50.6
BG-117	Bulgaria	high-K	151.8	8.68	0.669	1.28	0.354	4.195	13.0	36.2	17.5	0.523	0.01193	0.104	1.08	0.00217	35.3
BHVO-II		Whole-rock standard	166.6	18.3	1.1097	0.220	0.295	4.513	16.5	36.9	9.1	5.04					
BHVO-II		Whole-rock standard	165.8	17.9	1.1000	0.232	0.281	4.494	16.3	36.9	9.2	4.75					

* Replicates; Samples highlighted in bold characters represent samples with < 55 wt. SiO_2 and > 4 wt.% MgO.
[1] Isotope dilution data for Lu and Hf and ICP-MS data for Th, Mo, Sb, Ce, Ba, and La in Chapter 3.

4.3. Analytical techniques and results

Major and trace element concentrations, Sr-Nd-Hf-Pb isotope compositions, and Lu and Hf isotope dilution data of the volcanic rock suites from Bulgaria and Santorini are given in Chapter 3. The HFSE concentration data reported in this study (see Table 4.1) were measured on the same sample splits (ca. 100 mg) as the Sr-Nd-Hf isotopes and the Lu-Hf ID data reported in Chapter 3. Prior to digestion, all sample splits were spiked with a mixed ^{183}W-^{180}Ta-^{180}Hf-^{176}Lu-^{94}Zr tracer that was calibrated against > 99.9% pure Ames Laboratory metals. Tabletop digestion was carried out in a 1:1 HNO_3 – HF mixture for 48 h at 120 °C. Following digestion, the samples were dried down and evaporated to dryness three times with 1 ml concentrated HNO_3. Subsequent solution in 6 N HCl-0.06 N HF was carried out to ensure full sample-spike equilibrium. An aliquot of this solution was employed for W separation, as described in detail in Münker (2011; and references within). Separation of Nb, Ta, and Zr was carried out according to the procedures described by Münker *et al*. (2001) and Weyer *et al*. (2002). Procedural blanks were lower than < 50 pg for Nb, < 180 pg for Ta, < 10 ng for Zr, and < 120 pg for W.

The HFSE (Nb, Ta, Zr) and W concentration data reported in this study were obtained by isotope dilution and were measured using a Thermo-Finnigan Neptune MC-ICP-MS at Universität Bonn, operated in static mode. The results are shown in Table 4.1.
Mass bias correction for Ta and Zr was carried out by Re-doping (for Ta and W) and Sr-doping (for Zr). As niobium is monoisotopic its concentrations were measured as Zr/Nb against a Zr/Nb standard prepared from > 99.9 % pure Ames Laboratory metals. The Nb concentrations were subsequently calculated from the measured Zr/Nb using the Zr concentrations obtained by isotope dilution (Weyer *et al*., 2002). The external precision for Zr/Hf, Nb/Ta, Zr/Nb, and Ta/W corresponds to ± 0.5 % (Zr/Hf), ± 4 % (Zr/Nb, NbTa), and ± 0.5 % (Ta/W), respectively (all 2σ r.s.d.). Using Th data obtained by conventional quadrupole ICPMS, the reproducibility for W/Th was ± 8 %. External reproducibility and accuracy were checked by digestion of reference standard material BHVO-II, and multiple digestion of six samples (replicates, see Table 4.1). Results for all 34 analyzed samples as well as the six replicates and two rock standards BHVO-II are reported in Table 4.1.

The Sb and Mo concentrations discussed in this study are reported in Chapter 3 and were obtained by conventional quadrupole ICP-MS using an Agilent 7500cs mass spectrometer at CAU Kiel. Analytical procedures follow Garbe-Schönberg (1993). The analytical precision was estimated to be better than 3 % (2σ r.s.d) for Mo and better than 15 % (2σ r.s.d) for Sb.

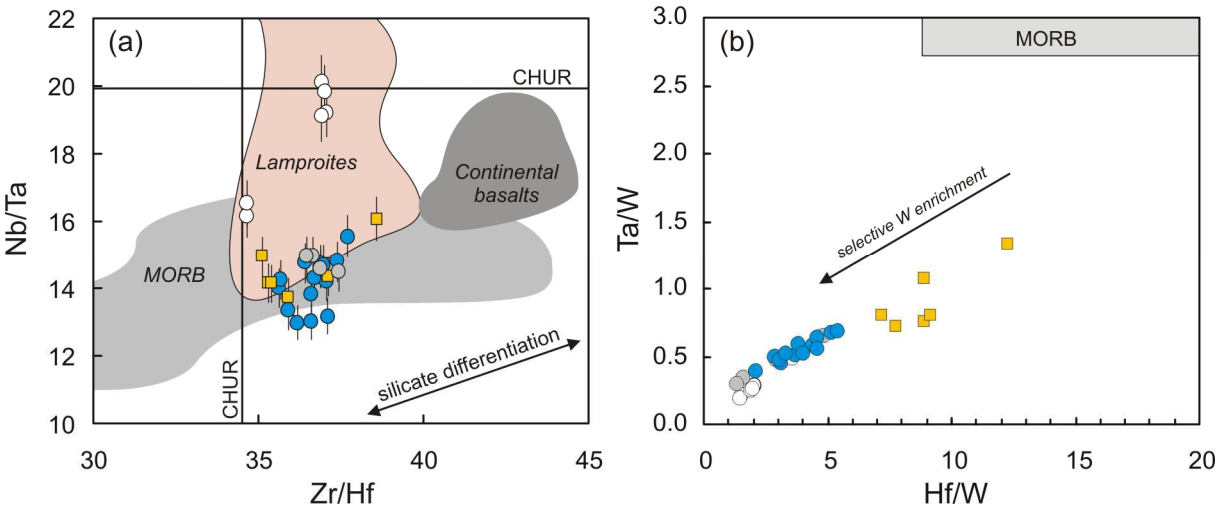

Fig. 4.2:

(a) Nb/Ta vs. Zr/Hf space with Bulgarian and Santorini lavas in comparison to a compilation of MORB, continental basalts and Mediterranean lamproites. Fields for MORB and continental basalts after Münker *et al*. (2003) and references within; lamproites after Prelević *et al*. (2008).

(b) Both sample suites in Ta/W vs. Hf/W space, illustrating the selective enrichment of W compared to other incompatible lithophile elements like Hf or Ta. MORB after König *et al*. (2011).

Symbols as in Fig. 4.1.

HFSE systematics

Both Santorini and Bulgarian suites display high Nb and Ta concentrations ($Nb_{(Santorini)}$ = 3.27 – 11.0 ppm; $Nb_{(Bulgaria)}$ = 5.10 – 19.6 ppm; $Ta_{(Santorini)}$ = 0.228 – 0.768 ppm; $Ta_{(Bulgaria)}$ = 0.324 – 1.35 ppm), exceeding values recorded for intraoceanic arc basalts like Cyprus and the Solomon Islands (0.228 – 5.71 ppm Nb, and 0.0130 – 0.272 ppm Ta).

In Nb/Ta – Zr/Hf space the sample suites from Bulgaria and Santorini broadly cover the array previously defined for MORB (Büchl *et al*., 2002), with values ranging from 12.3 – 15.5 for Nb/Ta and 35.1 – 38.6 for Zr/Hf (see Fig. 4.2a). The absarokites form a distinct group with higher, near chondritic Nb/Ta of 16.2 – 20.1, at Zr/Hf that overlap with the other suites of 34.6 – 37.0. Except for the absarokites, the Bulgarian and the Santorini suites lack correlations of

either Nb/Ta or Zr/Hf with degree of K-enrichment. In contrast to Nb/Ta and Zr/Hf, the $^{176}Lu/^{177}Hf$ of the Bulgarian and Santorini suite do not overlap, with the Bulgarian lavas (0.00863 – 0.0146) displaying lower Lu-Hf ratios than the Santorini lavas (0.0153 – 0.0243). Additionally, both suites are considerably lower than values defined for MORB (Büchl *et al*., 2002) and for intraoceanic arc basalts (0.0224 – 0.102; König *et al*., 2008; 2010).

W, Sb, Mo systematics

The Santorini suites displays W concentrations of 0.172 – 0.920 ppm, exceeding values reported for intraoceanic arc basalts, for which a maximum W concentration of 0.477 ppm is reported (König *et al*., 2008; 2010; 2011). Ratios of W-Th are relatively uniform, ranging from 0.060 – 0.074, which is lower than MORB (W/Th_{MORB} = 0.087 – 0.24; Babechuk *et al*., 2010; König *et al*., 2011) and estimated values for primitive mantle (W/Th_{PM} = 0.14; König *et al*., 2011). This also account for Ta/W that range from 0.73 to 1.33 (Ta/W_{MORB} = 2.84 – 11.8; Ta/W_{PM} = 3.4; Babechuk *et al*., 2010; König *et al*., 2011), and except for two samples also for Hf/W (5.82 – 12.3, see Fig. 4.2b; Hf/W_{MORB} = 8.9 – 304; Hf/W_{PM} = 25.8; Babechuk *et al*., 2010; König *et al*., 2011).

The Bulgarian suite spans a range of high tungsten concentrations of 0.730 to 4.63 ppm, even exceeding average values reported for the continental crust (1.9 ppm; Rudnick & Gao, 2003). Ratios of W/Th range from 0.047 – 0.30, trending to higher values than estimates for PM and MORB. From Fig. 4.2b it is evident that Ta/W (0.19 – 0.68) and Hf/W (1.30 – 5.38) of the Bulgarian suite are considerably lower than both MORB and PM, resulting from selective enrichment of W. This is similar to intra-oceanic arc basalts reported by König *et al*. (2008; 2011) that broadly overlap in Ta/W (0.170 – 4.84), and Hf/W (5.60 – 119) with the samples from Bulgaria and Santorini.

The Mo concentrations in the Santorini and Bulgarian suites overlap with concentrations from 0.514 – 2.49 ppm. Conversely, Sb concentrations of the Santorini lavas are systematically lower (65.8 – 178 ppb) compared to the Bulgarian lavas (0.0562 – 2.00 ppm). Intraoceanic arc basalts reported by König *et al*. (2008, 2010) display high Mo concentrations (0.115 – 2.82 ppm) similar to the Bulgarian lavas while Sb concentrations tend to be as low as 0.658 – 103 ppb.

4.4. Discussion

4.4.1. Assessment of assimilation and fractional crystallization

In order to constrain magmatic source signatures and to characterise the influence of different subduction components on the HFSE budget, it is important to discriminate between crustal assimilation and source contamination.

As pointed out in detail in Chapter 3, assimilation of continental crust is negligible in the lavas from Bulgaria, which can be tested using differentiation parameters such as SiO_2 or MgO together with Sr-Nd-Hf isotope compositions. The Bulgarian lavas are devoid of any such correlations. Moreover, the Bulgarian data set is considered as well-buffered against shallow-level assimilation owing to the high degree of trace element enrichment that by far exceeds average values for crustal contaminants (e.g., Rudnick & Gao, 2003; for details see Chapter 3). This is supported by the trace and major element geochemistry of the group of absarokites, which represent the most mafic samples of the sample set (highest MgO and compatible element contents like Cr, Ni, Co), yet display the highest degree of incompatible trace element enrichment as well as the most radiogenic $^{87}Sr/^{86}Sr$ isotope compositions of the Bulgarian lavas. Conversely, the Santorini lavas record effects of assimilation in the more evolved lavas, which is especially critical for the here investigated HFSE. The Bulgarian K-rich rocks are devoid of any correlations between HFSE concentrations and MgO or SiO_2 whereas the concentrations of Nb, Ta, Zr, Hf, and W of the Santorini lavas tend to increase with decreasing MgO and increasing SiO_2 (not shown). Hence, the data set was screened and only samples with < 55 wt.% SiO_2 and > 4 wt.% MgO were selected from the data set and highlighted in Table 4.1 (17 samples). This selection criteria was also applied for the Bulgarian samples in order to provide a common basis for better comparability of the sample suites. Additionally, critical ratios of HFSE (Nb/Ta and W/Th) might provide further insight into AFC processes and are thus depicted in Fig. 4.3 to test for any fractionations of these ratios with increasing degree of differentiation. Fig. 4.3 shows that Nb/Ta as well as W/Th largely remain constant with decreasing MgO and increasing K_2O contents in the Santorini and the Bulgarian high-K suite. Considering the lack of correlation between, for instance W/Th and MgO (Fig. 4.3c), which would be expected to tend to higher ('crustal') W/Th (> 0.2; Rudnick & Gao, 2003) with increasing degree of differentiation, effects of assimilation can be regarded as negligible.

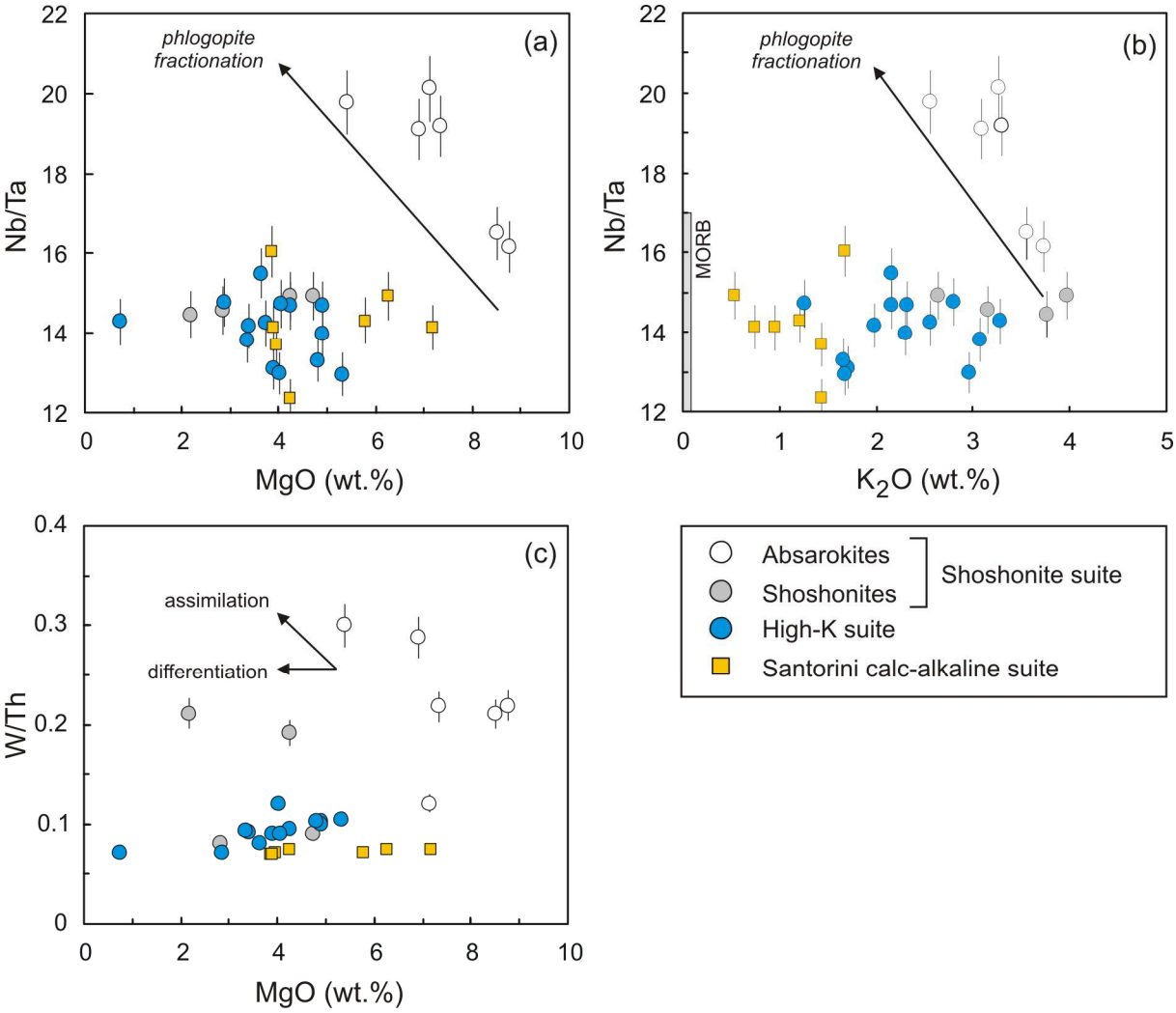

Fig. 4.3:

Effects of assimilation and fractional crystallization illustrated based on Nb/Ta and W/Th ratios in conjunction with major elements. (a) Nb/Ta vs. MgO (wt.%); (b) Nb/Ta vs. K_2O (wt.%); and (c) W/Th vs. MgO (wt.%).

As illustrated in Fig. 4.3a and b, the Nb-Ta ratios of the Santorini lavas as well as of the Bulgarian high-K series remain constant with decreasing MgO and increasing K_2O. The absarokite group of the Bulgarian shoshonite series, however, provides an exception in that it shows an increase of Nb/Ta with decreasing MgO and K_2O. Fractional crystallization of phlogopite is assumed to dominate the Nb-Ta budget in the absarokite group, owing to inverse correlations of Nb/Ta with MgO and K_2O (Fig. 4.3b, c). The importance of phlogopite for the HFSE budget in metasomatized lithospheric mantle samples has previously been emphasized by Ionov & Hofmann (1995) and Ionov *et al*. (1997), who reported phlogopites from mantle xenoliths that span a wide range of superchondritic Nb/Ta (20 – 54) at high Nb concentrations (up to 700 ppm). Moreover, in experimental studies Nb and Ta have been shown to be mildly incompatible in phlogopite (D_{Nb} = 0.047 - 0.085; D_{Ta} = 0.047 – 0.11), with a D_{Nb}/D_{Ta} of 0.77

– 1; (phl/melt; Foley *et al*., 1996; Adam & Green, 2006). The slightly higher compatibility of Ta in phlogopite might explain the fractionation trends defined by the absarokites shown here in Fig. 4.3a, b; however, the overlap of $D^{phl/melt}$ values for Nb and Ta within error and the highly variable HFSE concentrations in metasomatic phlogopites still leave it ambiguous as to whether phlogopite is indeed capable of fractionating Nb from Ta. Hence, as the Nb-Ta ratios of the absarokites are unlikely to represent source processes, this group is excluded from the discussion below.

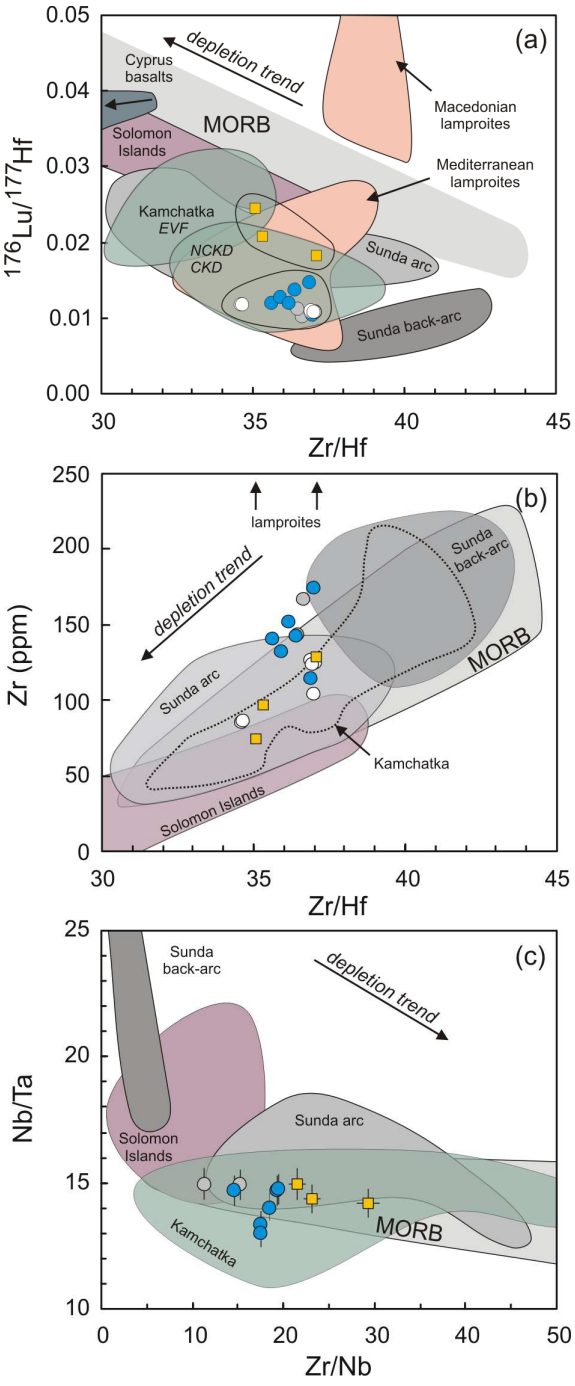

Fig. 4.4:
Characterization of the Bulgarian and Santorini mantle sources based on HFSE ratios.
(a) $^{176}Lu/^{177}Hf$ vs. Zr/Hf;
(b) Zr concentration (ppm) vs. Zr/Hf;
(c) Nb/Ta vs. Zr/Nb.
MORB after Büchl *et a*l. (2002); Kamchatka after Münker *et al*. (2004), Sunda arc and back-arc after Barth *et al*. (2011) and unpublished; Solomon Island and Cyprus basalts after König *et al*. (2008).
Symbols as in Fig. 4.1.

4.2. Behaviour of Nb-Ta and Zr-Hf in the mantle sources

The isovalent element pairs Nb-Ta and Zr-Hf possess virtually similar compatibilities during partial mantle melting, with a relative compatibility order of Nb < Ta << Zr < Hf << Lu, which has been confirmed by both experimental and geochemical studies (Weyer *et al*., 2003; McDade *et al*., 2003, Büchl *et al*., 2002). These expected variations (inverse correlations of Lu/Hf with Zr/Hf and Nb/Ta with Zr/Nb) are indeed observed in MORB (Büchl *et al*., 2002, Münker *et al*., 2004), and are also broadly observed in both the Santorini and Bulgarian sample suites (Fig. 4.4a, c). However, at given Zr/Hf values both suites are displaced towards lower $^{176}Lu/^{177}Hf$ than MORB (Fig. 4.4a), similar to other subduction-related high-K rocks (*Sunda arc*; Barth *et al*., 2011; unpublished), adakitic melts (*Kamchatka/Aleutians*; Münker *et al*., 2004) and some Mediterranean lamproites (except for Macedonian lamproites that tend towards higher $^{176}Lu/^{177}Hf$). Notably, Santorini lavas display higher $^{176}Lu/^{177}Hf$ as well as $^{176}Hf/^{177}Hf$ at a given Zr/Hf compared to the Bulgarian samples. This is, however, not the case for Zr/Hf vs. Zr concentration (Fig. 4.4b) where Santorini samples broadly overlap with the Bulgarian absarokites and also with fields for MORB, adakites from Kamchatka and Sunda arc basalts, while the Bulgarian high-K suite is displaced to slightly higher Zr concentrations. Furthermore, the Bulgarian samples are displaced to lower Zr/Nb than the Santorini samples (Fig. 4.4c) at similar Nb/Ta, whereas only the absarokite group tends to higher Nb/Ta, which however does not reflect source processes and is excluded from the following discussion.

Although both sample suites overlap the fields defined for MORB in Zr vs. Zr/Hf, Nb/Ta vs. Zr/Nb, and Nb/Ta vs. Zr/Hf spaces (Fig. 4.2a; 4.4b, c), they form two distinct groups in all diagrams shown in Fig. 4.4. Hence, a successful petrogenetic model needs to explain the contrasting HFSE fractionation trends of the sample suites, that only in some cases (Zr/Hf, Nb/Ta) broadly overlap with MORB compositions, but are depleted in $^{176}Lu/^{177}Hf$.

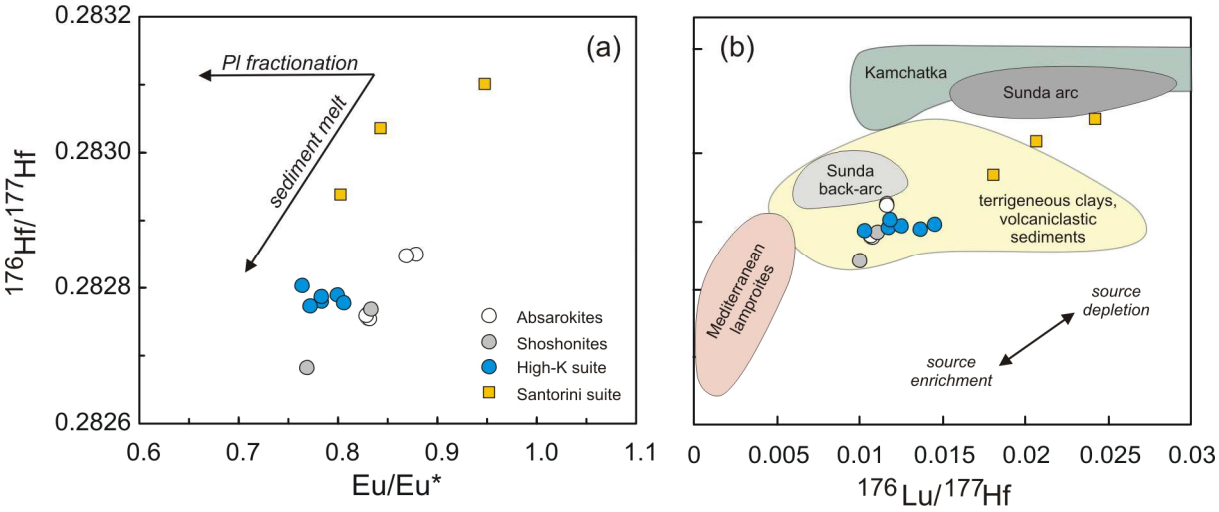

Fig. 4.5:

Inferred influence of a sediment melt-like component on the Hf isotope and incompatible element budget of Santorini and Bulgarian lavas. Only samples < 4 wt.% MgO and > 55 wt.% SiO_2 are shown. (a) $^{176}Hf/^{177}Hf$ vs. Eu-anomaly, (b) $^{176}Hf/^{177}Hf$ vs. $^{176}Lu/^{177}Hf$.

Mediterranean lamproites after Prelevic *et al*. (2010); Terrigeneous clays and volcaniclastic sediments after Vervoort *et al*. (2011); Sunda arc and back-arc after Barth *et al*. (2011) and unpublished; Kamchatka after Münker *et al*. (2004); Serbian flysch after Prelević *et al*. (2005); GLOSS after Plank & Langmuir (1998).

Zr-Hf pairs

As shown in Chapter 3, the trace element and Sr-Nd-Hf-Pb isotope inventory of both sample suites is largely dominated by components derived from subducted sediments (fluids and melts), that are assumed to be compositionally similar to currently subducted sediments at the Hellenic trench as well as Mesozoic flysch sediments from Serbia (see Chapter 3; Weldeab *et al*., 2002; Prelević *et al*., 2005). For the Santorini suite is has been shown that the incompatible trace element budget as well as the Sr-Nd-Hf-Pb isotope compositions reflect the preferential enrichment by sediment-derived melts, overprinting a depleted spinel-lherzolitic mantle (e.g., Druitt *et al*., 1999; Zellmer *et al*., 2000; Bailey *et al*., 2009; Chapter 3). Fluid-like components were ruled out to play a major role in their trace element budget, in contrast to the K-rich lavas from Bulgaria. Based on trace element systematics, for instance shown here in Fig. 4.1b, the influence of both fluid-like and melt-like components in the sources of the Bulgarian lavas could be assessed. The significant higher magnitude of trace element enrichment in the Bulgarian lavas might either reflect a more pronounced and efficient source replenishment in the Bulgarian lavas or, alternatively, might mirror a more depleted Santorini sub-arc mantle wedge prior to source hybridization. These two different processes might also explain the systematically different Zr/Nb and $^{176}Lu/^{177}Hf$ (Fig. 4.4a, c),

which are higher in the Santorini lavas compared to the Bulgarian K-rich lavas. The offset from the MORB array in Fig. 4.4a might reflect the selective addition of subduction components, as it is confirmed by e.g., negative covariation of Zr/Hf with εHf of the Santorini lavas (not shown). The importance of a metasomatizing sediment-melt in the sources of both Santorini and Bulgarian rock suites can be furthermore illustrated in Fig. 4.5, employing Hf isotopes as well as trace element systematics. Hafnium isotope compositions are a valuable tool to identify sediment-melt derived signatures in arc lavas (Pearce *et al*., 1999; Woodhead *et al*., 2001) owing to the conservative behaviour of Hf in subduction zone fluids and its selective mobility in hydrous melts (Hermann & Rubatto, 2009) or high-temperature (supercritical) fluids (Kessel *et al*., 2005). This can be illustrated for the most mafic rocks from Santorini, that follow trends predicted for source overprint by sediment-melts, e.g., increasing Eu-anomalies with decreasing Hf isotope composition (Fig. 4.5a), which is attributed to the inheritance of a negative Eu-anomaly by felsic sediment-melts overprinting an initially depleted mantle wedge to varying degrees. This is, to a lesser degree, also evident for some Bulgarian lavas. Figure 4.5b furthermore shows the Bulgarian and Santorini sample suites in $^{176}Lu/^{177}Hf$ vs. $^{176}Hf/^{177}Hf$ space in comparison to Kamchatka adakites (Münker *et al*., 2004), Sunda-arc and back-arc basalts (Barth *et al*., 2011, and unpublished), Mediterranean lamproites (Prelević *et al*., 2008) and a compilation of terrigeneous clays and volcaniclastic sediments (Vervoort *et al*., 2011). Notably, the Santorini suite defines a positive slope, trending from both high $^{176}Lu/^{177}Hf$ and $^{176}Hf/^{177}Hf$ similar to Kamchatka and Sunda-arc basalts to lower values, overlapping with the field defined for terrigeneous clays and volcaniclastic sediments. This trend once more emphasizes the role of sediment-melts during source enrichment of the Santorini suite. This trend is less pronounced for the Bulgarian suite, which defines a narrow field at slightly less radiogenic $^{176}Hf/^{177}Hf$ as the high-K rocks from the Sunda back-arc. Nevertheless, both sample suites broadly overlap the field defined for terrigeneous clays and volcaniclastic sediments (e.g., Fig. 4.5b).

Nb-Ta pairs

The broad overlap of Nb/Ta with MORB of the Santorini and the Bulgarian sample suite (Fig. 4.2a, 4.4c) implies that Nb and Ta were not significantly fractionated during the respective source enrichment. As shown above, the budget of Zr/Hf was strongly replenished in both sample suites by sediment-derived components. Depending on the degree of mantle source depletion prior to source enrichment, it is also assumed that silicic melts dominate the Nb-Ta budget of the metasomatized (hybrid) mantle sources (e.g., Stolz *et al*., 1996). These

melts tend to exhibit very low Zr/Nb, which would explain the systematically lower Zr/Nb and higher Nb/Ta with increasing enrichment.

In order to provide constraints on the possible mechanisms active during HFSE fractionation in subducted sediments, the experimental data set of Hermann & Rubatto (2009) might offer further insight. The authors studied the trace element distribution in hydrous sediment melts as a function of residual accessory phases present on the solidus. Phases relevant to HFSE frationation include zircon, phengite or apatite. Hermann & Rubatto (2009) also showed that in hydrous sediment-melts trace amounts of zircon (< 0.04%) constitute the major phase hosting Zr and Hf. Consequently, in the presence of residual zircon, hydrous pelitic melt is able to fractionate Zr and Hf, whereas Hf is preferentially enriched in the melt compared to Zr (Linnen & Keppler, 2002; Rubatto & Hermann, 2007), thus decreasing the Zr-Hf ratio in the melt. Fractionation of Zr from Hf furthermore gets more pronounced with decreasing temperature (Hermann & Rubatto, 2009). This implies that in order to reproduce the observed Zr-Hf ratios in the two volcanic suites by sediment-melt dominated source enrichment, a precursor sediment with initially high Zr-Hf ratios is required. This is consistent with data for subducted sediments that range in their Zr/Hf between 30 – 43 (Plank & Langmuir, 1998; Barth *et al*., 2000).

According to Hermann & Rubatto (2009), low-degree partial melting of hydrous sediment is also able to cause significant fractionation of Nb from Ta owing to the presence of residual rutile, in agreement with previous studies (e.g., Klimm *et al*., 2008). An overlap of Nb-Ta ratios with the MORB array in both the Santorini and Bulgarian high-K basalts and shoshonites, however, implies that any addition of Nb-Ta to the mantle wedge by subduction-components caused a barely detectable change in the Nb/Ta ratios. This can either be explained by the absence of rutile in the subducted sediment due to low bulk TiO_2 contents or by complete consumption of rutile during sediment melting. Alternatively, if compared to continental sediments (Barth *et al*., 2000), it is evident that these rocks possess lower Nb/Ta (10.1 – 16.0) at a wide range of Zr/Nb (7.10 – 46.1) or Zr/Hf (32.8 – 43.0). This might indeed argue for small amounts of residual rutile in the subducted sediments, resulting in slightly elevated Nb/Ta in the Santorini and Bulgarian lavas compared to continental sediments.

Curiously, as noted by Hermann & Rubatto (2009), their experimentally produced hydrous sediment-melt is devoid of a pronounced negative Nb-Ta anomaly, although residual rutile was present in all of their experimental charges. Similar observations have additionally been made by other partitioning studies involving fluid-basalt or fluid-metapelite systems (Green & Adam, 2003; Spandler *et al*., 2007; Klimm *et al*., 2008). Hermann & Rubatto

(2009) therefore proposed that either in addition to rutile a further phase might be required to effectively retain Nb and Ta or that the negative Nb-Ta anomaly in arc lavas is simply inherited from subducted sediments with an initially negative Nb-Ta anomaly.

Collectively, although some HFSE ratios (Zr/Nb, Nb/Ta, Zr/Hf) broadly overlap with MORB compositions, it is especially evident from lower $^{176}Lu/^{177}Hf$ than MORB, coupled variations of HFSE ratios with Hf isotope compositions (e.g., Fig. 4.5b), and experimental constraints on sediment-melting (Hermann & Rubatto, 2009) that sediment-derived components largely control the concentrations and ratios of the HFSE in both the Santorini and Bulgarian mantle sources.

4.4.3. Behaviour of W-Sb-Mo during source replenishment

General behaviour of W, Sb, Mo in subduction zone melts and fluids

Following the pioneering study of Noll *et al*. (1996), Newsom *et al*. (1996) argued for an immobile behaviour of W in subduction zone fluids, attributing the enrichment of W in the crust to its highly incompatible behaviour. Therefore, W should not be significantly fractionated from elements like Th or U during mantle melting and crust formation. Owing to improved analytical techniques, now allowing for high-precision measurements of low-concentration samples, König *et al*. (2008; 2010) could reveal a quite mobile behaviour of W in subduction zone fluids in a study on intra-oceanic island-arc basalts. This finding results in a significant enrichment of W over Th and U, which are considered as similar incompatible. Ensuing W/Th and W/U are significantly higher than MORB in the studied arc rocks by König *et al*. (2008; 2010). Conversely, Ba has been shown to be more mobile than W, Th, and U, resulting in a relative mobility trend of Ba > W > Th, U in subduction zone fluids. Moreover, high-grade W enrichment as in the Erzgebirge (Förster *et al*., 1999) or the Panasqueira ore district in Portugal (Noronha *et al*., 1992) commonly occur as magmatic-hydrothermal deposits in association with granitic intrusion, where the ore-grade W-enrichment is attributed to late-stage hydrothermal fluids (Förster & Tischendorf, 1992; Hedenquist & Lowenstern, 1994; Webster *et al*., 1997).

Nevertheless, mechanisms controlling the fluid-melt partitioning of W are not straightforward and depend on several factors, e.g., chlorinity, pH, as well as oxygen fugacity and the peraluminosity of the melt (e.g., Hedenquist & Lowenstern, 1994; Kishida *et al*., 2004; Zajacz

et al., 2008; MacKenzie & Canil, 2011). Keppler & Wyllie (1991) and Newsom *et al*. (1996) constrained that W is transported as an hydroxide species ($WO_3(OH)^-$) with highest $K_D^{fluid/melt}$ in pure H_2O and decreasing $K_D^{fluid/melt}$ with increasing concentration of HCl and HF. However, more recent studies indicate a larger influence of chlorine and fluorine on the solubility of W in aqueous fluids (Zajacz *et al*., 2008; MacKenzie & Canil, 2011). Whereas Zajacz *et al*. (2008) rather favour tungstate (WO_4^{2-}) as dissolved W-species, MacKenzie & Canil (2011) showed for the system haplobasaltic melt - fluid that W might dissolve as an oxide-hydroxide complex even in low chlorinity fluids. However, W might be rather present as a chloride species in fluids with a high chlorinity (threshold Cl molarity > 17). This discrepancy in existing experimental data sets and the observations in natural samples was attributed by Zajacs *et al*. (2008) to a combined effect of different oxygen fugacities, pH, or different fluid chlorinities in the respective studies.

Molybdenum shares many geochemical properties with W, for example almost identical ionic radii (0.4 – 0.7 Å depending on coordination; Shannon, 1976) and a preferred 6+ oxidation state (O'Neill *et al*., 2008). Hence, in oxidized low-temperature aquatic environments Mo occurs as 6+ oxy-anion (molybdate, MoO_4^{2-}), similar to W (tungstate, WO_4^{2-}; Johannesson *et al*., 2000; Arnórsson & Óskarsson, 2007). Molybdenum is furthermore assumed to be rather immobile in low-temperature fluids (Hattori & Guillot, 2003), which is also supported by the formation of most Mo deposits at T > 500 °C (Hedenquist & Lowenstern, 1994). The solubility of Mo in aqueous solutions increases with increasing pH (Rempel *et al*., 2009), however, its speciation additionally exerts control on the solubility in high chlorine fluids (MacKenzie & Canil, 2011). However, Mo is enriched in reducing sedimentary environments with free H_2S (e.g., shales; Crusius *et al*., 1996) where it is precipitated as sulfide, thus showing higher chalcophile tendencies as W. Hence, the higher redox-sensitivity of Mo compared to W leads to enrichment of Mo over W in suboxic sediments (pelagic shales; Crusius *et al*., 1996) and thus enables assertions on their redox state during subduction zone processes.

Antimony is classified as chalcophile and moderately siderophile element and behaves like an incompatible lithophile element during silicate melting processes in the mantle (Jochum & Hofmann, 1997; Rouxel *et al*., 2003). In the presence of sulfur, Sb would be expected to be retained in the mantle sulfide (9 – 146 ppm Sb; Hattori *et al*., 2002). Antimony is furthermore particularly mobile in low-temperature fluids (Jochum & Verma, 1996; Hattori & Guillot, 2003), in H_2S-rich fluids and Cl-rich and –poor solutions where it dissolves as Sb(OH) (Wood *et al*., 1987). Hence, similar to W, Sb may be transported as OH-complex. In

arc rocks, Sb has been shown to be enriched (0.01 – 1.5 ppm; Noll *et al*., 1996) compared to MORB (0.01 – 0.05; Jochum & Hofmann, 1994; Jochum & Verma, 1996), which is attributed to efficient scavenging of Sb by fluids derived from the slab or the mantle wedge (Hattori *et al*., 2002; Hattori & Guillot, 2003). Hence, Sb concentrations and ratios to similar mobile elements like Pb can provide constraints on redox and temperature conditions in the mantle source.

The composition of any subduction fluid involved in the petrogenesis of the studied rock suites is especially important in that it might allow conclusions on the partition behaviour of incompatible trace elements and explain the high enrichment of the latter in enriched arc magmas. Following Konzett *et al*. (2011) any Cl-rich fluid (brine) released from, e.g., subducted serpentinites (e.g., Scambelluri & Phillippot, 2001; John *et al*., 2011) might efficiently strip any K from the mantle column and from subducted sediments, with Cl being similarly incompatible as K and Nb (Workman *et al*., 2006; Sun *et al*., 2007). Subsequently, Cl and F are preferentially partitioned into hydrous minerals like apatite, amphibole and some sheet minerals (owing to the similar ionic radius of F and OH^-) in the lithospheric mantle. Whereas the presence of F stabilizes phlogopite (e.g., Foley *et al*., 1986), metasomatic mantle apatite has previously been identified to be rich in Cl in contrast to magmatic apatites, which are rich in F (O'Reilly & Griffin, 2000; Patiño Douce *et al*., 2011). This might argue for a concurrent transport of P, K and other similarly incompatible elements in Cl-rich fluids (Konzett *et al*., 2011). However, this is not straightforward for W. The alkalinity of a fluid has been shown to exert some control on the partitioning of W (Zajacs *et al*., 2008), but no clear dependance of chlorinity has been observed so far. It is likely that W, which is thought to be mostly present as WO_4^{2-} (tungstate) in oxidized systems forms compounds with 2+ cations (preferably $CaWO_4$ = scheelite), however, the stability and behaviour of these phases at mantle and subduction zone conditions as well as in hydrothermal systems are unknown.

Arc lavas with high Ba/La are usually considered to mirror the addition of an aqueous fluid phase to their source as Ba is considered highly fluid-mobile (Elliott *et al*., 1997; Pearce *et al*., 2005). Thus, the comparison of ratios of incompatible elements with ratios of Ba-La allows placing constraints on relative fluid mobilities during subduction-related source replenishment. However, residual epidote-group minerals like allanite potentially fractionate Ba-La ratios owing to their high $D_{La}^{allanite\text{-}melt}$ (> 700; Hermann, 2002; Klimm *et al*., 2008).

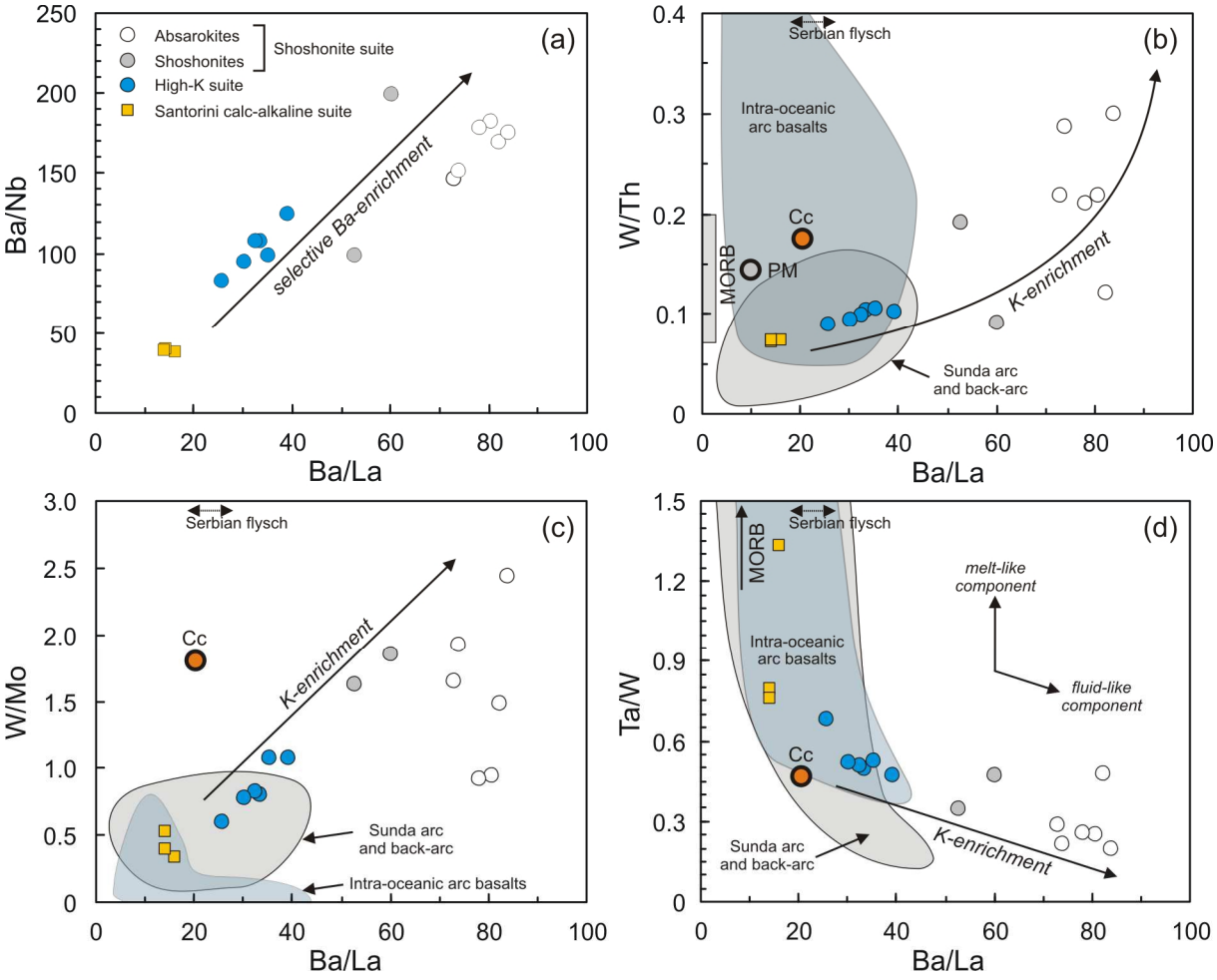

Fig. 4.6:

(a) Ba/Nb vs. Ba/La illustrating the selective enrichment of Ba compared to Nb and La, with Ba enrichment covarying with K-enrichment in the Bulgarian suite.

(b), (c), (d) Ba/La vs. ratios of W with incompatible elements, emphasizing the concurrent W and K enrichment in the Bulgarian suite whereas the W budget in the Santorini suite is controlled by melt-like source enrichment.

Values for PM (Primitive mantle) and MORB after König *et al*. (2011; W-Th ratios) and Sun & McDonough (1989; Ba-La ratios), average values for continental crust after Rudnick & Gao (2003), Serbian flysch after Prelevic *et al*. (2005), Sunda arc and back-arc after Barth *et al*. (2011) and unpublished, intra-oceanic arc basalts after König *et al*. (2008; 2010).

Figure 4.6a illustrates a positive co-variation between Ba/La and Ba/Nb for both the Santorini as well as the Bulgarian sample suite, inverse to a trend expected if La was buffered by residual allanite. Thus, it can be confidently assumed that Ba is selectively enriched by fluid-like components relative to both La and Nb, excluding a major role of residual allanite. However, the fractionation of Ba-La ratios has recently also been documented for low-temperature hydrous melts owing to the control of Ba by phengite with allanite or monazite controlling the budget of LREE including La. This is not the case for higher temperatures

(1050 °C; Hermann & Rubatto, 2009) where these phases are not stable in the respectively investigated bulk compositions (Hermann & Rubatto, 2009). During partial melting Ba is considered as similarly incompatible as W or Th (Newsom *et al*., 1996). However, Ba was shown elsewhere to be more mobile in subduction zone fluids than both W or Th (König *et al*., 2008). Hence, the mobility of W-Mo-Sb in the sub-arc mantle can be tested by comparing ratios such as W/Th, W/Mo, Ta/W with Ba/La ratios (Fig. 4.6).

Figure 4.6b, c, and d illustrates incompatible element ratios (W/Th, W/Mo, Ta/W) together with Ba/La. Generally, the Santorini and Bulgarian suites can be distinguished in all diagrams. The Bulgarian lavas show a broad range of W-Th ratios that both co-vary with increasing Ba/La as well as K-enrichment (Fig. 4.6b), i.e., the most primitive samples (absarokites) display the highest K-contents, highest Ba/La as well as highest W/Th. Conversely, the Santorini samples show invariant W/Th ratios for a small range of Ba/La (14.1 – 16.2). Whereas the Santorini suite and the Bulgarian high-K suite broadly overlap with compositions for other arc basalts (Fig. 4.6b; Sunda arc, intra-oceanic arcs like Cyprus or Tonga; references see figure caption), the shoshonite suite displays considerably higher Ba/La at similar W/Th than intra-oceanic arc basalts. Likewise, in W/Mo vs. Ba/La space (Fig. 4.6c) the Santorini and the Bulgarian high-K suite well overlap with fields defined for arc basalts, whereas the Bulgarian shoshonite series tends to high W/Mo at high Ba/La. The K-enrichment again increases with increasing W/Mo and Ba/La. A similar trend can be shown for Ta/W (Fig. 4.6d) that decreases with increasing Ba/La and K-enrichment. Conversely, the Santorini lavas display higher Ta/W than the Bulgarian lavas at invariant Ba/La, overlapping with fields for other arc-basalts.

Bulgarian lavas - For the post-collisional Bulgarian lavas where multi-stage source enrichment and melting processes are involved, Ba-La ratios serve as a proxy for fluid-related K-enrichment in the sources of the post-collisional lavas. In addition, however, Ba/La represent a proxy for the presence of metasomatic phases in lithopheric veins (see Chapter 3). For instance, Ba/La might be lowered by residual phlogopite (Schmidt *et al*., 1999; Adam & Green, 2003) and increased by residual allanite or monazite (Hermann, 2002; Klimm *et al*., 2008). This implies that a distinction between melt-like and fluid-like source enrichment is not straightforward for the Bulgarian suite, as the observed geochemical signatures may rather reflect trace element fractionation during partial melting processes in the metasomatized mantle controlled by volatile-rich hydrous minerals and a peridotitic wall rock (e.g., Foley, 1992; Ionov *et al*., 1997).

In the Bulgarian lavas, W is strongly enriched with high concentrations (up to 4.63 ppm) and W/Th ratios exceeding MORB values, however, lower than values observed for arcs dominated by sediment-derived fluids like Cyprus (W/Th up to 0.96; König *et al*., 2008). With respect to the diagrams shown in Fig. 4.6, this implies that although strongly enriched in W (and Ta, see section 4.3), ratios of W/Th or Ta/W do not show higher W-Th or Ta-W fractionations when compared to other island-arcs. W/Th, W/Mo, and Ta/W covary with K-enrichment and Ba/La, confirming a selective enrichment of W (see also Fig. 4.2b) as well as a coupled selective mobilization of K together with W. This implies that no residual phase is present in the lithospheric mantle that selectively retains W. Furthermore, the primary coupled high enrichment of W, Th, K, and Ba during mantle metasomatism emphasizes the importance of both a melt-like and a fluid-like component, which is most likely derived from subducted terrigeneous sediments. This is furthermore supported by the selective enrichment of W over Ta (not shown), that results in decreasing Ta/W with K-enrichment and increasing Ba/La (Fig. 4.6d). This implies that Ta is probably retained by small amounts of residual rutile in either the subducted sediment or the lithospheric mantle. However, Ti-phases like rutile are usually not stable in the mantle wedge due to their high solubility in basaltic melts. Notably, some exceptions have been recorded, for example the MARID suite of cratonic xenoliths (e.g., Pearson & Nowell, 2002; Grégoire *et al*., 2002). In metasomatized lithospheric mantle, those Ti-phases can be shielded in metasomatic veins, as inclusions or during the unusual conditions related to the origin of K-rich rocks (Stolz *et al*., 1996 and references within). The presence of a residual Ti-phase in lithospheric veins could account for the negative Nb-Ta anomaly observed in all post-collisional rocks from this study. Conversely, these features could also be inherited from the primordial enrichment of the lithospheric mantle by sediment-melts with initial negative Nb-Ta anomalies, which could also account for the slightly elevated Nb/Ta compared to terrigeneous sediments (see section 4.2; Barth *et al*., 2000). Such a model is furthermore supported by the fact, that negative Nb-Ta anomalies have been observed in cratonic phlogopite-bearing mantle xenoliths (e.g., Grégoire *et al*., 2002).

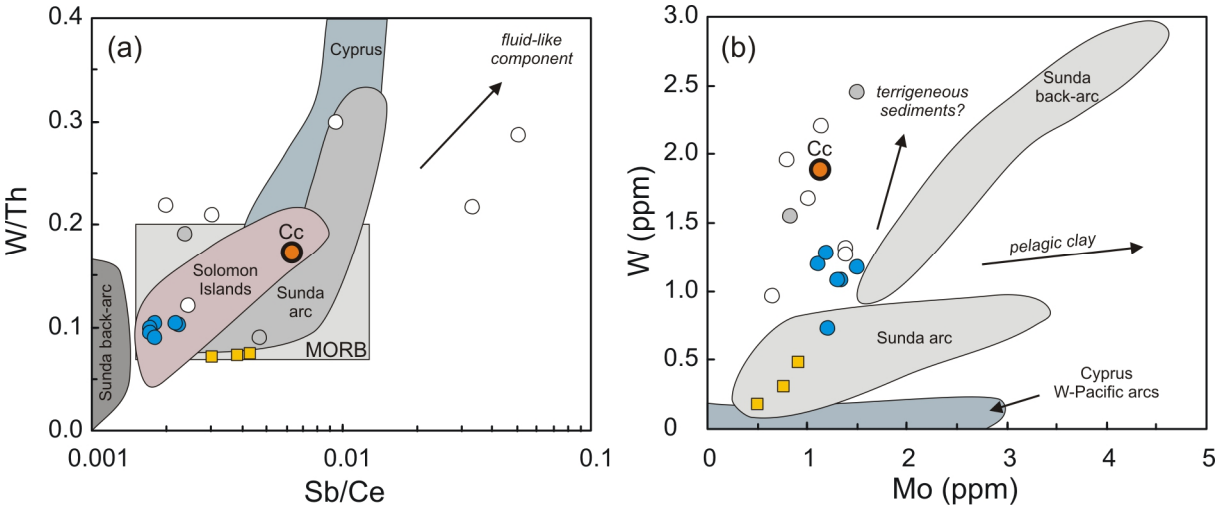

Fig. 4.7:

Variations of the extended HFSE W, Sb, and Mo in comparison to MORB, other island-arc (W-Pacific arcs, Sunda-arc and back-arc), and average values for the continental crust (Cc; Rudnick & Gao, 2003). Pelagic clay after Li (1991; Mo = 27 ppm, W = 4 ppm); values for MORB after König *et al*. (2011; W-Th ratios) and Sun & McDonough (1989; Sb-Ce ratios); Sunda arc and back-arc after Barth *et al*. (2011) and unpublished; Cyprus, Solomon Islands, and W-Pacific arcs after König *et al*. (2008; 2010); values for average continental crust (Cc) after Rudnick & Gao (2003).

That a sediment-derived component dominates the budget of W and Mo is furthermore evident by the high W/Mo in the Bulgarian lavas (0.56 - 2.4, Figs. 4.6c, 4.7b), that rather argue for the involvement of terrigenous sediments than pelagic clays. The latter are characterized by low W/Mo (~ 0.1; e.g, Li, 1991) owing to the high concentration of Mo in reducing environments (e.g., Crusius *et al*., 1996). The selective enrichment of W relative to Mo in the Bulgarian suite is furthermore illustrated in Fig. 4.7b, in comparison to a compilation of W-Pacific arcs, as well as the Sunda arc and back-arc (references see figure caption). At similar Mo concentrations as in intra-oceanic arc and Sunda arc lavas, W is highly enriched in K-rich rocks from Bulgaria and Santorini, but also in K-rich rocks elsewhere such as in the Sunda back-arc (Barth *et al*., 2011; unpublished). These rocks additionally have higher Mo concentrations (Fig. 4.7b), possibly reflecting a different composition of the subducted sediments. The fact that W appears to be more efficiently replenished than Mo in the Bulgarian lavas might have several reasons. (1) Presence of a residual phase with low W/Mo, which might account for residual sulfides. However, arc rocks generally form under quite oxidized conditions (Ballhaus, 1993), where sulfides are oxidized and thus not stable as residual phases (fO_2 as low as ΔFMQ = + 1.85; Jugo *et al*., 2005); (2) changing alkalinity of the hydrous melt, or (3) initially different element ratios in the

subducted sediment, i.e., terrigeneous sediments with initial high W/Mo (average crust W/Mo ~ 1.7; Rudnick & Gao, 2003) as opposed to pelagic clays with low W/Mo (0.1; Li, 1991). Given the compositional similarities of flysch sediments from Serbia (Prelević *et al*., 2005), presently subducted sediments at the Hellenic trench (Weldeab *et al*., 2002), and the inferred composition of the subducted sediments for the Bulgarian lavas (see Chapter 3), it seems highly likely that fluids and melts derived from terrigeneous sediments dominate the W and Mo bugdet of the post-collisional K-rich lavas from Bulgaria.

The Bulgarian lavas furthermore display a high enrichment in Sb (up to 2 ppm), exceeding values for average continental crust (0.4 ppm; Rudnick & Gao, 2003) and MORB (0.01 – 0.05 ppm; Jochum & Hofmann, 1994; Jochum & Verma, 1996). However, ratios of Sb/Ce overlap with MORB and arc lavas worldwide (Fig. 4.7a and Hattori & Guillot, 2003), which is owing to concomitant high concentrations of Sb and Ce (up to 78 ppm). Additionally, Sb/Pb of the shoshonite suite are similar to arc basalts like Cyprus, the Solomon Islands or Papua New Guinea (Ce < 36 ppm; Pb < 6.6 ppm; König *et al*., 2008; 2010), the high-K suite on the contrary tends to lower Sb/Pb (not shown) owing to the high Pb concentrations (up to 49 ppm). As suggested by Jochum & Verma (1996), Hattori *et al*. (2002), and Hattori & Guillot (2003), high Sb concentrations in arc rocks can be attributed to the dehydration of altered oceanic crust, the overlying sediments as well as serpentinites, which all have been shown to yield high concentrations in chalcophile elements like Sb or As (up to 40 ppm Sb in MORB; Jochum & Verma, 1996; up to 12 ppm Sb in serpentinites; Hattori *et al*., 2002; Hattori & Guillot, 2003). The budget of Sb in the Bulgarian rocks can thus be attributed to efficient fluid-induced scavenging of Sb from the more or less altered slab and the mantle wedge at low-T in the absence of any residual mantle sulfides retaining Sb. Importantly, during partial melting of the metasomatized (veined) mantle residual phases buffering Sb were absent.

Of particular interest for the Bulgarian lavas are also the identification of potential minerals hosting the extended HFSE in the metasomatized lithospheric mantle. Metasomatic hydrous and volatile-rich minerals like phlogopite, amphibole, and apatite can be considered as the major hosts of LILE and incompatible elements in a veined mantle (e.g., Foley, 1992; Ionov & Hofmann, 1995; Ionov *et al*., 1997). Metasomatic phlogopite is a major host for elements like Ba, Nb, Sr, and Rb (e.g., Ionov & Hofmann, 1995), whereas apatite hosts the LREE-MREE, Th, U, and Pb (O'Reilly & Griffin, 2000). From the high concentrations of all of these elements in the Bulgarian samples as well as from the correlations shown in Fig. 4.6 it is evident that none of these minerals was present as a residual phase and were most likely

gradually consumed during partial mantle melting, as proposed by e.g., Foley (1992). This is confirmed by experimental studies by Conceição & Green (2004) on the decompression melting of metasomatized peridotite. These authors showed that phlogopite and amphibole (pargasite) disappear close to the solidus and are completely transferred to the melt, which forms at 1050 – 1150 °C at 10 – 15 kbar, leaving a residual lherzolite (ol + opx + cpx + sp).

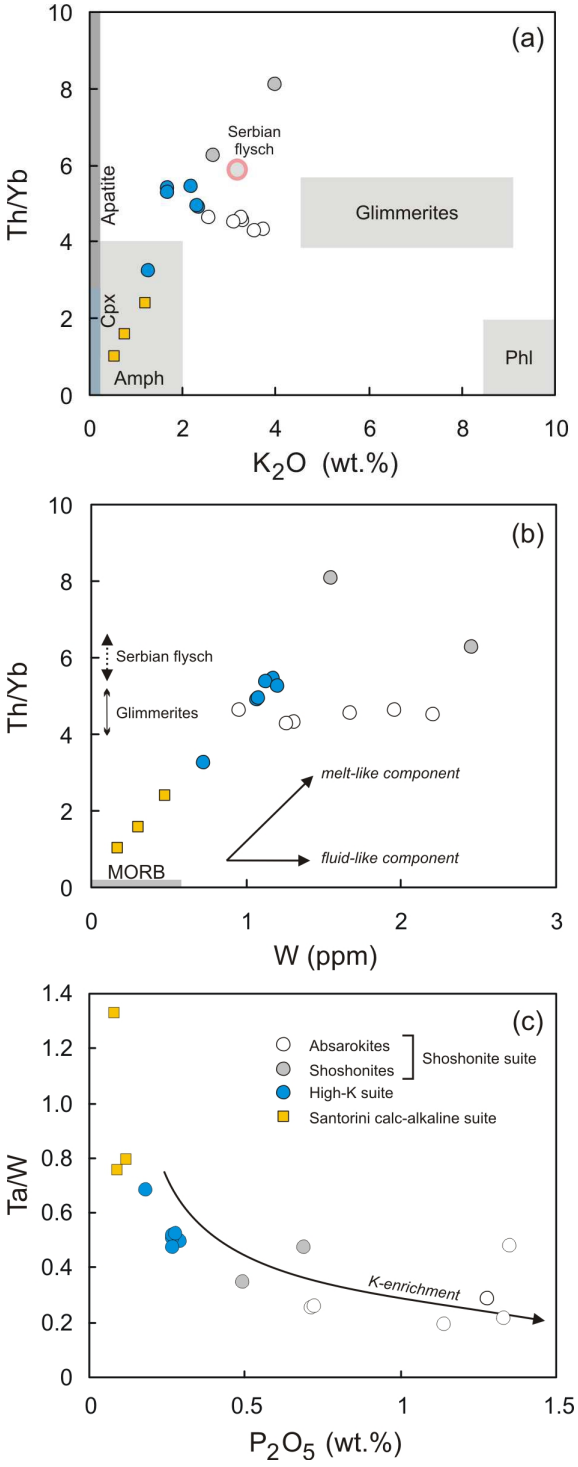

Fig. 4.8:

Relative mobility of incompatible elements illustrated by (a) Th/Yb vs. K_2O (wt.%), and (b) Th/Yb vs. W (ppm), furthermore showing the influence of potential metasomatic mineral on the incompatible trace element budget on the Bulgarian lavas.

Glimmerites after Becker *et al*. (1999); fields for cpx, amph, phl, and apatite after a compilation of mantle xenoliths via the http://georoc.mpch-mainz.gwdg.de database. Tungsten data for MORB after König *et al*. (2011).

(c) Ta/W vs. P_2O_5 (wt.%) space illustrating W and K enrichment with increasing P – content, emphasizing a possible role for metasomatic apatite.

The major volatile-rich metasomatic minerals are illustrated in Fig. 4.8a in Th/Yb vs. K_2O space together with the studied sample suites. The inverse correlation shown for the Bulgarian lavas is attributed to different contributions of phlogopite (dominating the K-budget), apatite (control on Th-budget), and possibly also amphibole, which is less well constrained. For the source of the absarokites it seems that Th is selectively retained by a residual phase, due to invariant Th/Yb, Th/La, and Th concentrations with increasing W concentrations (see Fig. 4.8b). This feature also differs from the high-K group, where Th is similarly enriched compared to W. As the absarokites represent small-degree melts with the highest contribution from the metasomatized mantle, the phase controlling the Th budget might only get exhausted at higher degrees of partial melting as found for the other Bulgarian suites. Scarce partitioning data for W suggests that it is incompatible in grt, ol, cpx, opx, mica, and amphibole with $D_W < 0.004$ in all minerals between mica-amphibole bearing garnet lherzolite and hydrous basanitic melt (Adam & Green, 2006). In contrast, for felsic systems W has been shown to be highly compatible in apatite ($D_W = 16$; INA data by Luhr *et al*., 1984). However, as W is a redox sensitive element (O'Neill *et al*., 2008), and because melt composition (e.g., SiO_2 saturation and melt polymerization; O'Neill & Eggins, 2002) may affect the crystal-melt partitioning of W, it is possible that these data are not suited for mafic systems. Nevertheless, a detailed study of the behaviour of P, W, K, and other incompatible elements might give further insight into a possible role of apatite for the sources of the Bulgarian lavas. Apatite has previously been shown to be an important phase in metasomatic mineral assemblages (O'Reilly & Griffin, 2000; Patiño Douce *et al*., 2011), while apatite-bearing mantle assemblages, associated with calcite, ilmenite and phlogopite, have also been shown to be highly enriched in volatiles, P and REE (Grégoire *et al*., 2002). In Fig. 4.8c variations of Ta/W vs. P_2O_5 (wt.%) are shown. It is striking that Ta/W decreases with increasing P-content and with K-enrichment. This might suggest a possible influence of a phosphate phase hosting W, that is getting gradually consumed during increasing degrees of partial melting. The absarokites yield the highest contribution from the metasomatized lithospheric mantle, thus also having the highest P, K and W concentrations. The positive P-anomaly of the absarokite group in primitive mantle normalized multi-element diagrams (see Chapter 3, Fig. 3.6a) provides additional evidence that apatite was completely consumed during partial melting. Altogether, this might eventually argue for apatite as a possible host for W in the metasomatic mineral assemblage, however more detailed studies on the partitioning behaviour of W in hydrous, volatile-rich phases is required to confirm this assertion.

Collectively, the above shown W, Mo, and Sb systematics show that these elements are highly enriched in the Bulgarian post-collisional K-rich lavas, which is evident from comparisons with other arc basalts. Nevertheless, some ratios of these elements (e.g., Sb/Ce, W/Th, Ta/W) broadly overlap with other arc basalts, whereas others (e.g., W/Mo, Sb/Pb) show a greater range of fractionations. These are ascribed to a higher magnitude, i.e., more efficient source enrichment, probably over a longer period of time. This is in agreement with geophysical and geochronological data inferring that subduction underneath the Rhodopes occurred for several tens of Myrs before the refertilized mantle sources were tapped (see Chapter 2 and 3 and references therein). Moreover, the major budget of incompatible elements is concentrated in the metasomatic portion of the lithospheric mantle. During partial melting, the metasomatic mineral assemblage is gradually consumed, leading to the high incompatible element enrichments found in the Bulgarian K-rich lavas. As major important hosts for the extended HFSE, phlogopite, apatite, and possibly also amphibole could be identified, whereas apatite might eventually represent a major host for W in the lithospheric mantle.

Santorini lavas – In contrast to the sample suite from Bulgaria, the Santorini lavas lack evidence for the involvement of subduction-derived fluids in their source enrichment, which is for instance illustrated by invariant Ba/La and Ba/Nb (Fig. 4.6a). As illustrated in Chapter 3 and section 4.2, the trace element and Nb-Ta and Zr-Hf budget is largely controlled by hydrous sediment-melts, which is subsequently also tested for W, Mo, and Sb.

Ratios of W-Th in the Santorini lavas (0.060 – 0.074; Fig. 4.6b) are slightly lower than MORB (0.09 – 0.24; Babechuk *et al*., 2010; König *et al*., 2011). Compared to other island-arcs both W and Th concentrations are strongly elevated. Both elements additionally show similar compatibilies as K in the Santorini lavas (Fig. 4.8a, b). The systematically lower W/Th than MORB hint towards a potential phase in the magma source that selectively retains W with respect to Th. In this context, small amounts of rutile in the subducted sediments have been proposed to control the Nb-Ta budget of the Santorini lavas (section 4.2) and might also buffer W to a certain degree, as proposed by Klemme *et al*. (2005). These authors showed that rutile/silicate melt partition coefficients are high for W (0.5 – 14.5) and low for Th (< 0.0011). Hence, fractionation of W-Th by residual rutile might be possible, but probably only occurred to a small degree in the Santorini lavas.

As shown in Fig. 4.2b, W is selectively enriched compared to Ta (and Hf), thus implying that the decreasing Ta/W at invariant Ba/La (Fig. 4.6d) can be attributed to melt-like source enrichment, otherwise a stronger increase in Ba/La with decreasing Ta/W would be expected.

Thus, both W-Th and Ta-W ratios are controlled by the selective replenishment of W, which for the Santorini samples has been attributed to a sediment-melt that had left W/Th unfractionated but had strongly decreased Ta/W at invariant Ba/La (Fig. 4.6b, d). However, W has been replenished more efficiently by silicic sediment melts than Ba as evident from W-Ba ratios, which are controlled by the more pronounced enrichment of W over Ba. This might be due to Ba being preferentially buffered by residual phengite with $D_{Ba}^{mica/melt}$ of 3 – 4 (Adam & Green, 2006), in which W has been shown to be incompatible ($D_{W}^{mica/melt} < 0.001$; Adam & Green, 2006). Altogether, this establishes a relative mobility order of Th > W > Ba > Nb for the Santorini suite, which is furthermore supported by invariant W/Th at increasing W/Nb (not shown).

Tungsten-Mo systematics shown in Fig. 4.6c illustrate the lower W/Mo at invariant Ba/La of the Santorini lavas compared to the Bulgarian suite. Nevertheless, the Santorini lavas are similar to other island-arc basalts like Cyprus and the Sunda arc in W/Mo – Ba/La space. Tungsten and Mo concentrations display a positive covariation (Fig. 4.7b), overlapping with the field for Sunda arc basalts. However, W is relatively enriched compared to Mo, which is evident from a comparison of W/Mo vs. W concentrations and W/Mo vs. Mo concentrations where the W budget dominates the increase of W-Mo ratios. The selective enrichment of W over Mo furthermore hints towards subducted sediments with high W/Mo, which accounts for terrigeneous sediments rather than pelagic clays (e.g, Li, 1991; Rudnick & Gao, 2003). Hence, W-Mo systematics support the assertion that, the Santorini source enrichment was accomplished rather by sediment-melts than by fluids, in contrast to the Bulgarian lavas.

A more important role for sediment-melts can also be confirmed by Sb systematics in the Santorini lavas. Concentrations of Sb (66 – 180 ppb) are significantly lower than in the Bulgarian lavas, but only slightly higher than values found in MORB (0.01 – 0.05; Jochum & Hofmann, 1994; Jochum & Verma, 1996). Ratios of Sb/Ce and Sb/Pb (not shown) are similar to the Bularian lavas and plot within the MORB array (Fig. 4.7a). This emphasizes the fact that the Bulgarian lavas are significantly more enriched than the Santorini lavas, however, ratios of incompatible elements like Sb/Ce and Sb/Pb are not significantly fractionated compared to the Bulgarian lavas. As the bulk portion of Sb in arc lavas is most likely derived from the dehydration of the oceanic crust (Jochum & Verma, 1996; Hattori & Guillot, 2003) the Sb systematics in the Santorini lavas might be explained by: (1) dehydration of the slab was not as important as for the Bulgarian lavas; (2) a higher T regime hampering the mobilization of Sb from the slab; (3) a more depleted mantle source for the Santorini lavas,

(4) different alkalinity of the hydrous melts.

Considering the findings reported above and in Chapter 3 it is rather likely that in the Santorini lavas, whose geochemical budget is largely dominated by sediment-derived melts, Sb is less efficiently mobilized by silicic melts than by fluids, probably at higher T than in the Bulgarian lavas.

Combining the findings of König *et al*. (2008; 2010) with the results of this study it becomes obvious that care has to be taken when interpreting W data for island-arcs. If present, W abundances in subduction zone lavas might be largely controlled by hydrous sediment melts (e.g., Santorini) in agreement with findings of Spandler *et al*. (2007) and Hermann & Rubatto (2009) who showed that hydrous melts are capable of transporting traditionally "fluid-mobile" elements like Ba more efficiently (up to 2 magnitudes). Collectively, W is highly enriched in both suites from Santorini and Bulgaria. The W enrichment in the Santorini mantle source is assumed to have been accomplished by hydrous sediment-derived melts, which is supported by Sb-Mo systematics. For the Bulgarian lavas fluid-like components play a large role, accounting for significant fractionations of W from less fluid-mobile elements. However, the distinct phases hosting W and the other HFS elements in the metasomatic mantle assemblage have to be further characterised. From the composition of the Bulgarian lavas, however, it appears that in accord with petrological observations these phases were largely consumed during melting, although some diagnostic trends appear to be more obscured than in the Santorini lavas .

4.5. Conclusions

New extended HFSE data (Nb, Ta, Zr, Hf, W, Mo, Sb) for lavas from Bulgaria and Santorini are the first high precision HFSE dataset for K-rich lavas in continental subduction zone and post-collisional settings. In conjunction with previously published Sr-Nd-Hf-Pb and trace element data, the new HFSE data provide important insights into trace element mobility and the behaviour of W-Sb-Mo and the "traditional" HFSE in continental arcs and in K-rich rocks from post-collisional settings.

(1) No significant fractionation of the HFSE ratios (Nb/Ta, Zr/Hf, Zr/Nb) compared to MORB were observed in the Santorini lavas and in the Bulgarian high-K rocks. Elevated Nb/Ta in the absarokite group can be largely attributed to the fractionation of phlogopite. An

influence on the HFSE budget by residual phases like allanite, zircon, or phengite can be largely ruled out, whereas trace amounts of residual rutile in the source might account for slightly lower Nb/Ta than expected for bulk sediment addition.

(2) Hafnium isotope compositions in combination with HFSE ratios highlight the role of hydrous sediment-melts in refertilizing the Bulgarian and Santorini sub-arc mantle wedges.

(3) The W, Sb, and Mo budgets in the Bulgarian lavas are primarily controlled by dehydration of the slab and sediments (Sb) and mobilization from subducted terrigenous sediments by partial melts (W, Mo). Tungsten enrichment covaries with K, Ba, and P enrichment, which highlights the role of a metasomatic mantle domain hosting the bulk of the incompatible elements. These hydrous, volatile-rich metasomatic mineral assemblages get virtually entirely consumed during partial melting and thus result in the high enrichment observed in the Bulgarian lavas.

(4) The W budget in the Santorini lavas is dominated by hydrous sediment-melts, in which a relative mobility order of Th > W > Ba > Nb was established. This is in contrast to fluid-dominated intra-oceanic island-arcs, where Ba has been shown to be more mobile than W. The difference is possibly caused by residual phengite in the subducted sediments. Furthermore, the higher incompatibility of Th compared to W results in W/Th lower than MORB, which is most likely caused by trace amounts of residual rutile that selectively retains W during partial melting.

(5) The Sb and Mo budget in the Santorini lavas is primarily controlled by the sediment-derived melts, which is less efficient than fluid-mobilization as recorded for the Bulgarian lavas, resulting in the mobility order W > Mo > Sb.

- References -

Adam, J. & Green, T. (2006). Trace element partitioning between mica- and amphibole-bearing garnet lherzolite and hydrous basanitic melt: 1. Experimental results and the investigation of controls on partitioning behaviour. *Contributions to Mineralogy and Petrology* **152**, 1-17.

Albarède, F., Telouk, P., Blichert-Toft, J., Boyet, M., Agranier, A. & Nelson, B. (2004). Precise and accurate isotopic measurements using multiple-collector ICPMS. *Geochimica et Cosmochimica Acta* **68**, 2725-2744.

Amato, J.M., Johnson, C.M., Baumgartner, L.P. & Beard, B.L. (1999). Rapid exhumation of the Zermatt-Saas ophiolite deduced from high-precision Sm-Nd and Rb-Sr geochronology. *Earth and Planetary Science Letters* **171**, 425-438.

Arnórsson, S. & Óskarsson, N. (2007). Molybdenum and tungsten in volcanic rocks and in surface and < 100 °C ground waters in Iceland. *Geochimica et Cosmochimica Acta* **71**, 284-304.

Babechuk, M.G., Kamber, B.S., Greig, A., Canil, D. & Kodolányi, J. (2010). The behaviour of tungsten during mantle melting revisited with implications for planetary differentiation time scales. *Geochimica et Cosmochimica Acta* **74**, 1448-1470.

Bailey, J.C., Jensen, E.S., Hansen, A., Kann, A.D.J. & Kann, K. (2009). Formation of heterogeneous magmatic series beneath North Santorini, South Aegean island arc. *Lithos* **110**, 20-36.

Ballhaus, C. (1993). Redox states of lithospheric and asthenospheric upper mantle. *Contributions to Mineralogy and Petrology* **114**, 331-348.

Barr, S.R., Temperley, S. & Tarney, J. (1999). Lateral growth of the continental crust through deep level subduction-accretion: a re-evaluation of central Greek Rhodope. *Lithos* **46**, 69-94.

Barth, M.G., McDonough, W.F. & Rudnick, R.L. (2000). Tracking the budget of Nb and Ta in the continental crust. *Chemical Geology* **165**, 197-213.

Barth, A.R., Kirchenbaur, M., König, S., Schuth, S., Luguet, A., Idrus, A. & Münker, C. (2011). The cause of high Nb/Ta in K-rich lavas from the Sunda arc system. *Mineralogical Magazine* **75**, 494.

Bauer, C., Rubatto, D., Krenn, K., Proyer, A. & Hoinkes, G. (2007). A zircon study from the Rhodope metamorphic complex, N-Greece: Time record of a multistage evolution. *Lithos* **99**, 207-228.

Baziotis, I., Mposkos, E. & Asimow, P.D. (2008). Petrogenesis of ultramafic rocks from the ultrahigh-pressure metamorphic Kimi Complex in Eastern Rhodope (NE Greece). *Journal of Petrology* **49**, 885-909.

Becker, H., Wenzel, T. & Volker, F. (1999). Geochemistry of glimmerite veins in peridotites from Lower Austria – Implications for the origin of K-rich magmas in collision zones. *Journal of Petrology* **40(2)**, 315-338.

Becker, H., Jochum, K.P. & Carlson, R.W. (2000). Trace element fractionation during dehydration of eclogites from high-pressure terranes and the implications for element fluxes in subduction zones. *Chemical Geology* **163**,

65-99.

Beinlich, A., Klemd, R., John, T. & Gao, J. (2010). Trace-element mobilization during Ca-metasomatism along a major fluid conduit: Eclogitization of blueschist as a consequence of fluid-rock interaction. *Geochimica et Cosmochimica Acta* **74**, 1892-1922.

Berman, R.G. (1988). Internally-consistent thermodynamic data for minerals in the system Na2O-K2O-CaO-MgO-Fe2O3-Al2O3-SiO2-TiO2-H2O-CO2. *Journal of Petrology* **29**, 445-522.

Berman, R.G. (1990). Mixing properties of Ca-Mg-Fe-Mn garnets. *American Mineralogist* **75**, 328-344.

Bijwaard, H., Spakman, W. & Engdahl, E.R. (1998). Closing the gap between regional and global travel time tomography. *Journal of Geophysical Research* **103**, 30,055-30,078.

Bizzarro, M., Baker, J.A., Haack, H., Ulfbeck, D. & Rosing, M. (2003). Early history of Earth's crust-mantle system inferred from hafnium isotopes in chondrites. *Nature* **421,** 931-933.

Black, R., Caby, R., Moussine-Pouchkine, A., Bayer, R., Bertrand, J.M.L., Boullier, A.M., Fabre, J. & Lesquer, A. (1979). Evidence for late Precambrian plate tectonics in West Africa. *Nature* **278**, 223-227.

Blasband, B., White, S., Brooijmans, P., de Boorder, H. & Visser, W. (2000). Late Proterozoic extensional collapse in the Arabian-Nubian Shield. *Journal of the Geological Society* **157**, 615-628.

Blichert-Toft, J. & Albarède, F. (1997). The Lu-Hf isotope geochemistry of chondrites and the evolution of the mantle-crust system. *Earth and Planetary Science Letters* **148**, 243-258.

Blichert-Toft, J., Albarède, F., Rosing, M., Frei, R. & Bridgwater, D. (1999). The Nd and Hf isotopic evolution of the mantle through the Archean. Results from the Isua supracrustals, West Greenland, and from the Birimian terranes of West Africa. *Geochimica et Cosmochimica Acta* **63,** 3901-3914.

Blichert-Toft, J. & Frei, R. (2001). Complex Sm-Nd and Lu-Hf isotope systematics in metamorphic garnets from the Isua supracrustal belt, West Greenland. *Geochimica et Cosmochimica Acta* **65,** 3177-3187.

Bodinier, J.-L., Merlet, C., Bedini, R.M., Simien, F., Remaidi, M. & Garrido, C.J. (1996). Distribution of niobium, tantalum, and other highly incompatible trace elements in the lithospheric mantle: The spinel paradox. *Geochimica et Cosmochimica Acta* **60,** 545-550.

Bonev, N., Burg, J.-P. & Ivanov, Z. (2006). Mesozoic-Tertiary structural evolution of an extensional gneiss dome – the Kesebir-Kardamos dome, eastern Rhodope (Bulgaria-Greece). *International Journal of Earth Sciences* **95**, 318-340.

Bonev, N. & Stampfli, G. (2003). New structural and petrologic data on Mesozoic schists in the Rhodope (Bulgaria): geodynamic implications. *Compte Rendu Geosciences* **335**, 691-699.

Bonev, N. & Stampfli, G. (2008). Petrology, geochemistry and geodynamic implications of Jurassic island arc magmatism as revealed by mafic volcanic rocks in the Mesozoic low-grade sequence, Eastern Rhodope,

Bulgaria. *Lithos* **100**, 210-233.

Bonev, N., Spikings, R., Moritz, R. & Marchev, P. (2010). The effect of early Alpine thrusting in late-stage extensional tectonics: Evidence from the Kulidzhik nappe and the Pelevun extensional allochthon in the Rhodope Massif, Bulgaria. *Tectonophysics* **488**, 256-281.

Bosse, V., Boulvais, P., Gautier, P., Tiepolo, M., Ruffet, G., Devidal, J.L., Cherneva, Z., Gerdjikov, I. & Paquette, J.L. (2009). Fluid-induced disturbance of the monazite Th-Pb chronometer: In situ dating and element mapping in pegmatites from the Rhodope (Greece, Bulgaria). *Chemical Geology* **261**, 286-302.

Bott, M.H.P. (1976). Formation of sedimentary basins of graben type by extension of the continental crust. *Tectonophysics* **36**, 77-86.

Bouvier, A., Vervoort, J.D. & Patchett, P.J. (2008). The Lu-Hf and Sm-Nd isotopic composition of CHUR: Constraints from unequilibrated chondrites and implications for the bulk composition of terrestrial planets. *Earth and Planetary Science Letters* **273**, 48-57.

Boyanov I. & Goranov A. (2001). Late Alpine (Paleogene) superimposed depressions in parts of Southeast Bulgaria. *Geologica Balcanica* **34(3-4)**, 3-36.

Brenan, J.M., Shaw, H.J., Phinney, D.L. & Ryerson, F.J. (1994). Rutile-aqueous fluid partitioning of Nb, Ta, Hf, Zr, U and Th: implications for high field strength element depletions in island-arc basalts. *Earth and Planetary Science Letters* **128**, 327-339.

Brueckner, H.K. & van Roermund, H.L.M. (2004). Dunk tectonics: A multiple subduction/eduction model for the evolution of the Scandinavian Caledonides. *Tectonics* **23**, TC2004.

Büchl, A., Münker, C., Mezger, K. & Hofmann, A.W. (2002). High-precision Nb/Ta and Zr/Hf ratios in global MORB. *Geochimica et Cosmochimica Acta* **66(15A),** A108-A108.

Bureau, H. & Keppler, H. (1999). Complete miscibility between silicate melts and hydrous fluids in the upper mantle: experimental evidence and geochemical implications. *Earth and Planetary Science Letters* **165**, 187-196.

Burg, J.-P., Ivanov, Z., Ricou, L.-E., Dimor, D. & Klain, L. (1990). Implications of shear-sense criteria for the tectonic evolution of the Central Rhodope massif, southern Bulgaria. *Geology* **18,** 451-454.

Burg, J.-P., Ricou, L.E., Ivanov, Z., Godfriaux, I., Dimov, D. & Klain, L. (1996). Syn-metamorphic nappe complex in the Rhodope massif: Structure and kinematics. *Terra Nova* **8**, 6-15.

Buzzi, L., Gaggero, L., Grozdanov, L., Yanev, S. & Slejko, F. (2010). High-Mg potassic rocks in the Balkan segment of the Variscan belt (Bulgaria): implications for the genesis of orogenic lamproite magmas. *Geological Magazine* **147**(3), 434-450.

Caddick, M.J., Konopásek, J. & Thompson, A.B. (2010). Preservation of garnet growth zoning and the duration of prograde metamorphism. *Journal of Petrology* **51**, 2327-2347.

Carpentier, M., Chauvel, C. & Mattielli, N. (2008). Pb-Nd isotopic constraints on sedimentary input into the Lesser Antilles arc system. *Earth and Planetary Science Letters* **272**, 199-211.

Carrigan, C.W., Essene, E.J., Mukasa, S.B., Kolcheva, K., Haydoutov, I. & Carpenter, C.M. (2002). Thermobarometric constraints on the formation of sapphirine-spinel-plagioclase symplectites in kyanite eclogites, and the prograde and retrograde P-T path, central Rhodope massif, Bulgaria. *GSA Ann Meeting*, 220-10.

Cebriá, J.M. & Wilson, M. (1995). Cenozoic mafic magmatism in western/central Europe: a common European asthenospheric reservoir? *Terra Abstr., EUG 8, Suppl. Terra Nova* **7**, 162.

Chakraborty, S. & Rubie, D.C. (1996). Mg tracer diffusion in aluminosilicate garnets at 750-850 °C, 1 atm and 1,300 °C, 8.5 GPa. *Contributions to Mineralogy and Petrology* **122**, 406-414.

Chauvel, C., Goldstein, S.L. & Hofmann, A.W. (1995). Hydration and dehydration of oceanic-crust controls Pb evolution in the mantle. *Chemical Geology* **126**(1), 65-75.

Chauvel, C. & Blichert-Toft, J. (2001). A hafnium isotope and trace element perspective on melting of the depleted mantle. *Earth and Planetary Science Letters* **190**, 137-151.

Cherneva, Z., Ovtcharova, M., von Quadt, A., Kolcheva, K., Stancheva, E., Sarov, S. & Peytcheva, I. (2002). Monazite and zircon U–Pb ages of migmatites from Arda River Valley, Central Rhodopian Dome, Bulgaria. *Proceedings of the annual scientific conference of BGS*, Sofia, pp. 20– 22.

Chopin, C. (1984). Coesite and pure pyrope in high-grade blueschists of the Western Alps: a first record and some consequences. *Contribution to Mineralogy and Petrology* **86**, 107–118.

Clift, P. & Vannucchi, P. (2003). Controls on tectonic accretion versus erosion in subduction zones: Implications for the origin and recycling of the continental crust. *Reviews of Geophysics* **42**, RG2001.

Coleman, R.G. (1981). Tectonic setting for ophiolite obduction in Oman. *Journal of Geophysical Research* **86**, 2497-2508.

Coltorti, M., Bonadiman, C., Faccini, B., Grégoire, M., O'Reilly, S.Y. & Powell, W. (2007). Amphiboles from suprasubduction and intraplate lithospheric mantle. *Lithos* **99**, 68-84.

Conceição, R.V. & Green, D.H. (2004). Derivation of potassic (shoshonitic) magmas by decompression melting of phlogopite+pargasite lherzolite. *Lithos* **72**, 209-229.

Conticelli, S., D'Antonio, M., Pinarelli, L. & Civetta, L. (2002). Source contamination and mantle heterogeneity in the genesis of Italian potassic and ultrapotassic volcanic rocks: Sr-Nd-Pb isotope data from Roman Province and Southern Tuscany. *Mineralogy and Petrology* **74**, 189-222.

Conticelli, S., Marchionni, S., Rosa, D., Giordano, G., Boari, E. & Avanzinelli, R. (2009a). Shoshonite and sub-alkaline magmas from an ultrapotassic volcano: Sr-Nd-Pb isotope data on the Roccamonfina volcanic rocks,

Roman Magmatic Province, Southern Italy. *Contributions to Mineralogy and Petrology* **157**, 41-63.

Conticelli, S., Guarnieri, L., Farinelli, A., Mattei, M., Avanzinelli, R., Bianchini, G., Boari, E., Tommasini, S., Tiepolo, M., Prelević, D. & Venturelli, G. (2009b). Trace elements and Sr-Nd-Pb isotopes of K-rich, shoshonitic, and calc-alkaline magmatism of the Western Mediterranean Region: Genesis of ultrapotassic to calc-alkaline magmatic associations in a post-collisional geodynamic setting. *Lithos* **107**, 68-92.

Cornelius, N.K. (2008). UHP metamorphic rocks of the Eastern Rhodope Massif, NE Greece: new constraints from petrology, geochemistry and zircon ages. *Dissertation*, Johannes Gutenberg-Universität Mainz.

Crawford, A.J., Stevens, B.P.J. & Fanning, M. (1997). Geochemistry and tectonic setting of some Neoproterozoic and early Cambrian volcanics in western New South Wales. *Australian Journal of Earth Sciences* **44**, 831-852.

Crusius, J., Calvert, S., Pedersen, T. & Sage, D. (1996). Rhenium and molybdenum enrichments in sediments as indicators of oxic, suboxic and sulfidic conditions of deposition. *Earth and Planetary Science Letters* **145**, 65-78.

Cvetković, V., Prelević, D., Downes, H., Jovanović, M., Vaselli, O. & Pécskay, Z. (2004). Origin and geodynamic significance of Tertiary postcollisional basaltic magmatism in Serbia (central Balkan Peninsula). *Lithos* **73,** 161-186.

Davies, H.L. & Warren, R.G. (1988). Origin of eclogite-bearing, domed, layered metamorphic complexes (core complexes) in the D'Entrecasteaux Islands, Papua-New-Guinea. *Tectonics* **7**, 1-21.

Davies, J.H. & von Blanckenburg, F. (1995). Slab breakoff: A model of lithosphere detachment and its test in the magmatism and deformation of collisional orogens. *Earth and Planetary Science Letters* **129**, 85-102.

De Capitani, C. & Petrakakis, K. (2010). The computation of equilibrium assemblage diagrams with Theriak/Domino software. *American Mineralogist* **95**, 1006-1016.

Dercourt, J., Zonenshain, L.P. & Ricou, L.E. (1986). Geological evolution of the Tethys belt from the Atlantic to the Pamirs since the Lias. *Tectonophysics* **123**, 241-315.

Dewey, J.F. & Bird, J.M. (1971). Origin and emplacement of ophiolite suite – Appalachian ophiolites in Newfoundland. *Journal of Geophysical Research* **76**, 3179-3206.

Dewey, J.F., Pitman, W.C., Ryan, W.B.F. & Bonnin, J. (1973). Plate tectonics and evolution of alpine system. *Geological Society of America Bulletin* **84**, 3137-3180.

Dhont, D., Yanev, Y., Bardintzeff, J.-M. & Chorowicz, J. (2008). Evolution and relationships between volcanism and tectonics in the central-eastern part of the Oligocene Borovitsa caldera (Eastern Rhodopes, Bulgaria). *Journal of Volcanology and Geothermal Research* **171**, 269-286.

Dickinson, W.R. & Hatherton, T. (1967). Andesitic volcanism and seismicity around the Pacific. *Science* **157**, 801–803.

Dinter, D.A. & Royden, L. (1993). Late Cenozoic extension in northeastern Greece: Strymon Valley detachment and Rhodope metamorphic core complex. *Geology* **21**, 45-48.

Dinter, D.A. (1998). Late Cenozoic extension of the Alpine collisional orogen, northeastern Greece: Origin of the north Aegean basin. *Geological Society of America Bulletin* **110***,* 1208–1226.

Druitt, T.H., Edwards, L., Mellors, R.M., Pyle, D.M., Sparks, R.S.J., Lanphere, M., Davies, M. & Barriero, B. (1999). *Santorini Volcano*. Geological Society Memoir, vol. 19. Geological Society, London. 165 pp.

Duchêne, S., Blichert-Toft, J., Luais, B., Telouk, P., Lardeaux, J.M. & Albarède, F. (1997). The Lu-Hf dating of garnets and the ages of the Alpine high-pressure metamorphism. *Nature* **387**, 586-589.

Duggen, S., Hoernle, K., van den Bogaard, P. & Garbe-Schönberg, D. (2005). Post-collisional transition from subduction- to intraplate magmatism in the westernmost Mediterranean: evidence for continental-edge delamination of subcontinental lithosphere. *Journal of Petrology* **46**, 1155-1201.

Dutch, R. & Hand, M. (2010). Retention of Sm-Nd isotopic ages in garnets subjected to high-grade thermal reworking: implications for diffusion rates of major and rare earth elements and the Sm-Nd closure temperature in garnet. *Contributions to Mineralogy and Petrology* **159**, 93-112.

Edwards, C., Menzies, M. & Thirlwall, M. (1991). Evidence from Muriah, Indonesia, for the interplay of supra-subduction zone and intraplate processes in the genesis of potassic alkaline magmas. *Journal of Petrology* **32**, 555-592.

Elliott, T., Plank, T., Zindler, A., White, W. & Bourdon, B. (1997). Element transport from slab to volcanic front at the Mariana arc. *Journal of Geophysical Research* **102**, 14991-15019.

Faccenna, C., Jolivet, L., Piromallo, C. & Morelli, A. (2003). Subduction and the depth of convection in the Mediterranean mantle. *Journal of Geophysical Research* **108**, doi:10.1029/2001JB001690.

Foley, S. (1991). High-pressure stability of the fluor- and hydroxy-endmembers of pargasite and K-richterite. *Geochimica et Cosmochimica Acta* **55**, 2689-2694.

Foley, S. (1992a). Petrological characterization of the source components of potassic magmas: geochemical and experimental constraints. *Lithos* **28**, 187-204.

Foley, S. (1992b). Vein-plus-wall-rock melting mechanisms in the lithosphere and the origin of potassic alkaline magmas. *Lithos* **28**, 435-453.

Foley, S.F., Jackson, S.E., Fryer, B.J., Greenough, J.D. & Jenner, G.A. (1996). Trace element partition coefficients for clinopyroxene and phlogopite in an alkaline lamprophyre from Newfoundland by LAM-ICP-MS. *Geochimica et Cosmochimica Acta* **60**, 629-638.

Förster, H.-J. & Tischendorf, G. (1992). Volatile signatures of the Hercynian postkinematic granites of the Erzgebirge: implications to related tin-tungsten-molybdenum metallogenesis. *Chemie der Erde* **52**, 47-61.

Förster, H.-J., Tischendorf, G., Trumbull, R.B. & Gottesmann, B. (1999). Late-collisional granites in the Variscan Erzgebirge, Germany. *Journal of Petrology* **40**, 1613-1645.

Francalanci, L., Vougioukalakis, G.E., Perini, G. & Manetti, P. (2005). *A west-east traverse along the magmatism of the South Aegean volcanic arc in the light of volcanological, chemical and isotope data*. In: Fytikas M., Vougioukalakis G. E. (Eds.) *The South Aegean Active Volcanic Arc, Present Knowledge and Future Perspectives*, Developments in Volcanology 7, Elsevier, 65-111.

Fuhrman, M.L. & Lindsley, D.H. (1988). Ternary feldspar modeling and thermometry. *American Mineralogist* **73**, 201-215.

Furnes, H., de Wit, M., Staudigel, H., Rosing, M. & Muehlenbachs, K. (2007). A vestige of Earth's oldest ophiolite. *Science* **315**, 1704-1707.

Gaggero, L., Buzzi, L., Haydoutov, I. & Cortesogno, L. (2009). Eclogite relics in the Variscan orogenic belt of Bulgaria (SE Europe). *International Journal of Earth Sciences* **98(8)**, 1853-1877.

Galer, S.J.G. & Abouchami, W. (1998). Practical application of lead triple spiking for correction of instrumental mass discrimination. *Mineralogical Magazine* **62**, 491-492.

Ganguly, J., Tirone, M. & Hervig, R.L. (1998). Diffusion kinetics of samarium and neodymium in garnet, and a method for determining cooling rates of rocks. *Science* **281**, 805-807.

Gao, Y., Wei, R., Ma, P., Hou, Z. & Yang, Z. (2009). Post-collisional ultrapotassic volcanism in the Tangra Yumco-Xuruco graben, south Tibet: Constraints from geochemistry and Sr-Nd-Pb isotope. *Lithos* **110**, 129-139.

Garbe-Schönberg, C.-D. (1993). Simultaneous determination of thirty-seven trace elements in twenty-eight international rock standards by ICP-MS. *Geostandards and Geoanalytical Research* **17**, 81-97.

Gasperini, D., Blichert-Toft, J., Bosch, D., Del Moro, A., Macera, P. & Albarède, F. (2002). Upwelling of deep mantle material through a plate window: Evidence from the geochemistry of Italian basaltic volcanics. *Journal of Geophysical Research* **107**, doi: 10.1029/2001JB000418,2002.

Gealey, W.K. (1988). Plate tectonic evolution of the Mediterranean – Middle East region. *Tectonophysics* **155**, 285-306.

Gebauer, D., Schertl, H.-P., Brix, M. & Schreyer, W. (1997). 35 Ma old ultrahigh-pressure metamorphism and evidence for very rapid exhumation in the Dora Maira Massif, Western Alps. *Lithos* **41**, 5-24.

Gebauer, D (1999). Alpine geochronology of the Central and Western Alps: new constraints for a complex geodynamic evolution. *Schweizerische Mineralogische und Petrographische Mitteilungen* **79**, 191-208.

Georgiev, N., Pleuger, J., Froitzheim, N., Sarov, S., Jahn-Awe, S. & Nagel, T.J. (2010). Separate Eocene-Early Oligocene and Miocene stages of extension and core complex formation in the Western Rhodopes, Mesta Basin,

and Pirin Mountains (Bulgaria). *Tectonophysics* **487**, 59-84.

Georgiev, S., Marchev, P., Heinrich, C.A., von Quadt, A., Peytcheva, I. & Manetti, P. (2009). Origin of nepheline-normative high-K ankaramites and the evolution of Eastern Srednogorie arc in SE Europe. *Journal of Petrology* **50**, 1899-1933.

Georgieva, M., Cherneva, Z., Kolcheva, K., Sarov, S., Gerdjikov, I. & Voinova, E. (2002). P-T metamorphic path of silimanite-bearing schists in an extensional shear zone, Central Rhodopes, Bulgaria. *Geochemistry Mineralogy Petrology* **39**, 95-106.

Gerdjikov, I., Gautier, P., Cherneva, Z., Bosse, V. & Ruffet, G. (2010). Late Eocene synmetamorphic thrusting and synorogenic extenison across the metamorphic pile of the Bulgarian Central Rhodope. *Geologica Balcanica CBGA*, 132-133.

Govindaraju, K. (1994). 1994 complication of working values and sample description for 383 geostandards. *Geostandards Newsletter* **18** Special Issue.

Green, D.H. & Wallace, M.E. (1988). Mantle metasomatism by ephemeral carbonatite melts. *Nature* **336**, 459–462.

Green, D.H., Schmidt, M.W. & Hibberson, W.O. (2004). Island-arc ankaramites: Primitive melts from fluxed refractory lherzolitic mantle. *Journal of Petrology* **45**, 391-403.

Green, T.H. & Adam, J. (2003). Experimentally-determined trace element characteristics of aqueous fluid from partially dehydrated mafic oceanic crust at 3.0 Gpa, 650-700 degrees C. *European Journal of Mineralogy* **15**, 815-830.

Grégoire, M., Bell, D.R. & Le Roex, A.P. (2002). Trace element geochemistry of phlogopite-rich mafic mantle xenoliths: their classification and their relationship to phlogopite-bearing peridotites and kimberlites revisited. *Contributions to Mineralogy and Petrology* **142**, 603-625.

Grégoire, M., Jego, S., Maury, R.C., Polve, M., Payot, B., Tamayo Jr., R.A. & Yumul Jr., G.P. (2008). Metasomatic interactions between slab-derived melts and depleted mantle: Insights from xenoliths within Monglo adakite (Luzon arc, Philippines). *Lithos* **103**, 415-430.

Groves, D.I., Goldfarb, R.J., Gebre-Mariam, M., Hagemann, S.G. & Robert, F. (1998). Orogenic gold deposits: A proposed classification in the context of their crustal distribution and relationship to other gold deposit types. Ore Geology Reviews 13, 7-27.

Hacker, B.R. (1994). Rapid emplacement of young oceanic lithosphere – Argon geochronology of the Oman ophiolite. *Science* **265**, 1563-1565.

Hart, S.R. (1984). A large-scale isotope anomaly in the southern-hemisphere mantle. *Nature* **309**, 753-757.

Hart, S.R. & Dunn, T. (1993). Experimental cpx/melt partitioning of 24 trace elements. *Contributions to Mineralogy and Petrology* **113**, 1-8.

Hattori, K.H., Arai, S. & Clarke, D.B. (2002). Selenium, tellurium, arsenic and antimony contents of primary mantle sulfides. *The Canadian Mineralogist* **40**, 637-650.

Hattori, K.H. & Guillot, S. (2003). Volcanic fronts from as a consequence of serpentinite dehydration in the forearc mantle wedge. *Geology* **31**, 525-528.

Hawkesworth, C.J. & Vollmer, R. (1979). Crustal contamination versus enriched mantle: 143Nd/144Nd and 87Sr/86Sr evidence from Italian volcanics. *Contributions to Mineralogy and Petrology* **69**, 151-165.

Hawkesworth, C., Turner, S., Peate, D., McDermott, F. & van Calsteren, P. (1997). Elemental U and Th variations in Island arc rocks: implications for U-series isotopes. *Chemical Geology* **139**, 207-221.

Hermann, J. (2002). Allanite: thorium and light rare earth element carrier in subducted crust. *Chemical Geology* **192**, 289 – 306.

Hermann, J. & Rubatto, D. (2009). Accessory phase control on the trace element signature of sediment melts in subduction zones. *Chemical Geology* **265**, 512-526.

Herwartz, D., Münker, C., Scherer, E.E., Nagel, T.J., Pleuger, J. & Froitzheim, N. (2008). Lu-Hf garnet geochronology of eclogites from the Balma Unit (Pennine Alps): implications for Alpine paleotectonic reconstructions. *Swiss Journal of Geosciences* **101**, S173-S189.

Herwartz, D., Nagel, T.J., Münker, C., Scherer, E.E. & Froitzheim, N. (2011). Tracing two orogenic cycles in one eclogite sample by Lu-Hf garnet chronometry. *Nature Geoscience*. doi:10.1038/ngeo1060.

Himmerkus, F., Reischmann, T. & Kostopoulos, D. (2009a). Triassic rift-related meta-granites in the Internal Hellenides, Greece. *Geological Magazine* **146**, 252-265.

Himmerkus, F., Reischmann, T. & Kostopoulos, D. (2009b). Serbo-Macedonian revisited: A Silurian basement terrane from northern Gondwana in the Internal Hellenides, Greece. *Tectonophysics* **473**, 20-35.

Hirata, T. (1996). Lead isotopic analysis of NIST standard reference materials using multiple-collector-inductively coupled plasma mass spectrometry coupled with modified external correction method for mass discrimination effect. *Analyst* **121**, 1407-1411.

Hofmann, A.W. (2003). *Sampling mantle heterogeneity through oceanic basalts: isotopes and trace elements*. In: Carlson, R.W. (ed.) *Treatise on Geochemistry, vol. 2*. Elsevier, 61–101.

Holland, T.J.B. & Powell, R. (1998). An internally consistent thermodynamic data set for phases of petrological interest. *Journal of Metamorphic Geology* **16**, 309-343.

Iddings, J.P. (1895). Absarokite-shoshonite-banakite series. *The Journal of Geology* **3**, 935-959.

Ionov, D.A. & Hofmann, A.W. (1995). Nb-Ta-rich mantle amphiboles and micas: Implications for subduction-related metasomatic trace element fractionations. *Earth and Planetary Science Letters* **131**, 341-356.

Ionov, D.A., Griffin, W.L., O'Reilly, S.Y. (1997). Volatile-bearing minerals and lithophile trace elements in the upper mantle. *Chemical Geology* **141**, 153-184.

Jacobsen, S.B. & Wasserburg, G.J. (1980). Sm-Nd isotopic evolution of chondrites. *Earth and Planetary Science Letters* **50**, 139-155.

Jacobshagen, J. (1986). Geologie von Griechenland. *Berlin-Stuttgart, Borntraeger*, 279 p.

Jahn-Awe, S., Froitzheim, N., Nagel, T.J., Frei, D., Georgiev, N. & Pleuger, J. (2010). Structural and geochronological evidence for Paleogene thrusting in the western Rhodopes, SW Bulgaria: Elements for a new tectonic model of the Rhodope Metamorphic Province. *Tectonics* **29**, TC3008, doi:10.1029/2009TC002558.

Jahn-Awe, S., Pleuger, J., Frei, D., Georgiev, N., Froitzheim, N. & Nagel, T.J. (2011). Time constraints for low-angle shear zones in the Central Rhodopes (Bulgaria) and their significance for the exhumation of high-pressure rocks. *International Journal of Earth Science,* in revision.

Janák, M., Froitzheim, N., Georgiev, N., Nagel, T.J. & Sarov, S. (2011). P-T evolution of kyanite eclogite from the Pirin Mountains (SW Bulgaria): implications for the Rhodope UHP Metamorphic Complex. *Journal of Metamorphic Geology* **29**, 317-332.

Jochum, K.P. & Hofmann, A.W. (1994). Antimony in mantle-derived rocks: constraints on Earth evolution from moderately siderophile elements. *Mineralogical Magazine* **58A**, 452-453.

Jochum, K.P. & Verma, S.P. (1996). Extreme enrichment of Sb, Tl and other trace elements in altered MORB. *Chemical Geology* **130**, 289-299.

Johannesson, K.H., Lyons, W.B., Graham, E.Y. & Welch, K.A. (2000). Oxyanion concentrations in eastern Sierra Nevada rivers – 3. Boron, molybdenum, vanadium, and tungsten. *Aquatic Geochemistry* **6**, 19-46.

John, T., Scherer, E.E., Haase, K. & Schenk, V. (2004). Trace element fractionation during fluid-induced eclogitization in a subducting slab: trace element and Lu-Hf-Sm-Nd isotope systematics. *Earth and Planetary Science Letters* **227**, 441-456.

John, T., Klemd, R., Gao, J. & Garbe-Schönberg, C.D. (2008). Trace-element mobilization in slabs due to non steady-state fluid-rock interaction: Constraints from an eclogite-facies transport vein in blueschist (Tianshan, China). *Lithos* **103**, 1-24.

John, T., Scambelluri, M., Frische, M., Barnes, J.D. & Bach, W. (2011). Dehydration of subducting serpentinite: Implications for halogen mobility in subduction zones and the deep halogen cycle. *Earth and Planetary Science Letters* **308**, 65-76.

Jolivet, L., Faccenna, C. & Piromallo, C. (2009). From mantle to crust: Stretching the Mediterranean. *Earth and Planetary Science Letters* **285**, 198-209.

Jolivet, L. & Brun, J.-P. (2010). Cenozoic geodynamic evolution of the Aegean. *International Journal of Earth Sciences* **99**, 109-138.

Jugo, P.J., Luth, R.W. & Richards, J.P. (2005). An experimental study of the sulfur content in basaltic melts saturated with immiscible sulfide or sulfate liquids at 1300°C and 1.0 GPa. *Journal of Petrology* **46**, 783-798.

Kalfoun, F., Ionov, D. & Merlet, C. (2002). HFSE residence and Nb/Ta ratios in metasomatised, rutile-bearing mantle peridotites. *Earth and Planetary Science Letters* **199**, 49-65.

Kamber, B.S. & Collerson, K.D. (2000). Role of hidden deeply subducted slabs in mantle depletion. *Chemical* Geology **166**,241-254.

Kelemen, P.B., Yogodzinski, G.M. & Scholl, D.W. (2003). *Along-strike variation in the Aleutian island arc: genesis of high-Mg# andesites and implications for continental crust*. In: Eiler J. (ed.) *Inside the Subduction Factory*. Geophysical Monograph, American Geophysical Union **138**, 223-276.

Kelly, E.D., Carlson, W.D. & Connelly, J.N. (2011). Implications of garnet resorption for the Lu-Hf garnet geochronometer: an example from the contact aureole of the Makhavinekh Lake Pluton, Labrador. *Journal of Metamorphic Geology*, DOI: 10.1111/j.1525-1314.2011.00946.x.

Kempton, P.D., Pearce, J.A., Barry, T.L., Godfrey Fitton, J., Langmuir, C. & Christie, D.M. (2002). Sr-Nd-Pb-Hf isotope results from ODP Leg 187: Evidence for mantle dynamics of the Australian-Antarctic discordance and origin of the Indian MORB source. *Geochemistry Geophysics Geosystems* **3**, doi:10.1029/2002GC000320.

Keppler, H. (1996). Constraints from partitioning experiments on the composition of subduction-zone fluids. *Nature* **380**, 237- 240.

Kessel, R., Schmidt, M.W., Ulmer, P. & Pettke, T. (2005). Trace element signature of subduction-zone fluids, melts and supercritical liquids at 120-180 km depth. *Nature* **437**, 724-727.

Kilias, A., Falalakis, G. & Mountrakis, D. (1999). Cretaceous-Tertiary structures and kinematics of the Serbomacedonian metamorphic rocks and their relation to the exhumation of the Hellenic Hinterland (Macedonia, Greece). *International Journal of Earth Sciences* **88**, 513-531.

Kishida, K., Sohrin, Y., Okamura, K. & Ishibash, J. (2004). Tungsten enriched in submarine hydrothermal fluids. *Earth and Planetary Science Letters* **222**, 819-827.

Klimm, K., Blundy, J.D. & Green, T.H. (2008). Trace element partitioning and accessory phase saturation during H_2O-saturated melting of basalt with implications for subduction zone chemical fluxes. *Journal of Petrology* **49**, 523-553.

Kogiso, T., Tatsumi, Y. & Nakano, S. (1997). Trace element transport during dehydration processes in the subducted oceanic crust. 1. Experiments and implications for the origin of ocean island basalts. *Earth and Planetary Science Letters* **148**, 193-205.

Kohn, M.J. (2003). Geochemical zoning in metamorphic mineral. *In: Rudnick RL (ed) The Crust, Treatise of Geochemistry*, Vol 3, pp. 229-258.

Kohn, M.J. (2009). Models of garnet differential geochronology. *Geochimica et Cosmochimica Acta* **73**, 170-182.

Kolčeva, K., Željažkova-Panajotova, M., Dobrecov, N.L. & Stojanova, V. (1986). Eclogites in the Rhodope Metamorphic group and their retrograde metamorphism. *Geochemistry Mineralogy Petrology* **20-21**, 130-144.

König, S., Münker, C., Schuth, S. & Garbe-Schönberg, D. (2008). Mobility of tungsten in subduction zones. *Earth and Planetary Science Letters* **274**, 82- 92.

König, S., Münker, C., Schuth, S., Luguet, A., Hoffmann, J. E. & Kuduon, J. (2010). Boninites as windows into trace element mobility in subduction zones. *Geochimica et Cosmochimica Acta* **74**, 684-704.

König, S., Münker, C., Hohl, S., Paulick, H., Barth, A.R., Lagos, M., Pfänder, J. & Büchl, A. (2011). The Earth's tungsten budget during mantle melting and crust formation. *Geochimica et Cosmochimica Acta* **75**, 2119-2136.

Konzett, J., Rhede, D. & Frost, D.J. (2011). The high PT stability of apatite and Cl partitioning between apatite and hydrous potassic phases in peridotite: an experimental study to 19 Gpa with implications for the transport of P, Cl and K in the upper mantle. *Contributions to Mineralogy and Petrology*, DOI 10.1007/s00410-011-0672-x.

Korkisch, J. & Hazan, I. (1965). Anion exchange separations in hydrobromic acid-organic solvent media. *Analytical Chemistry* **37**, 707-710.

Krenn, K., Bauer, C., Proyer, C., Klötzli, U. & Hoinkes, G. (2010). Tectonometamorphic evolution of the Rhodope orogen. *Tectonics* **29**, TC4001.

Krohe, A. & Mposkos, E. (2002). *Multiple generations of extensional detachments in the Rhodope Mountain (Northern Greece): evidence of episodic exhumation of high-pressure rocks*. In: Blundell, D., Neubauer, F. & von Quadt, A. (eds.) *The Timing and Location of Major Ore Deposits in an Evolving Orogen*. Geological Society of London Special Publications **206**, 151-178.

Lagos, M., Scherer, E.E., Tomaschek, F., Münker, C., Keiter, M., Berndt, J. & Ballhaus, C. (2007). High precision Lu-Hf geochronology of Eocene eclogite-facies rocks from Syros, Cyclades, Greece. *Chemical Geology* **243**, 16-35.

Lapen, T.J., Johnson, C.M., Baumgartner, L.P., Mahlen, N.J., Beard, B.L. & Amato, J.M. (2003). Burial rates during prograde metamorphism of an ultra-high-pressure terrane: an example from Lago di Cignana, western Alps, Italy. *Earth and Planetary Science Letters* **215**, 57-72.

Lepichon, X. & Angelier, J. (1979). Hellenic arc and trench system – key to the neotectonic evolution of the Eastern Mediterranean area. *Tectonophysics* **60**, 1-42.

Li, Y-H. (1991). Distribution patterns of the elements in the ocean: A synthesis. *Geochimica et Cosmochimica Acta* **55**, 3223-3240.

Liati, A. & Mposkos, E. (1990). Evolution of the eclogites in the Rhodope Zone of northern Greece. *Lithos* **25,** 89-99.

Liati, A. & Seidel, E. (1996). Metamorphic evolution and geochemistry of kyanite eclogites in central Rhodope, northern Greece. *Contribution to Mineralogy and Petrology* **123**, 293-307.

Liati, A. & Gebauer, D. (1999). Constraining the prograde and retrograde P-T-t path of Eocene HP rocks by SHRIMP dating of different zircon domains: inferred rates of heating, burial, cooling and exhumation for central Rhodope, northern Greece. *Contribution to Mineralogy and Petrology* **135**, 340-354.

Liati, A., Gebauer, D. & Wysoczanski, R. (2002). U-Pb SHRIMP-dating of zircon domains from UHP garnet-rich mafic rocks and late pegmatoids in the Rhodope zone (N Greece); evidence for early Cretaceous crystallization and Late Cretaceous metamorphism. *Chemical Geology* **184**, 281-299.

Liati, A. (2005). Identification of repeated Alpine (ultra) high-pressure metamorphic events by U-Pb SHRIMP geochronology and REE geochemistry of zircon: the Rhodope zone of Northern Greece. *Contributions to Mineralogy and Petrology* **150**, 608-630.

Lips, A.L.W., White, S.H. & Wijbrans, J.R. (2000). Middle-Late Alpine thermotectonic evolution of the southern Rhodope massif, Greece. *Geodinamica Acta* **13**, 281-292.

Lister, G.S. & Davis, G.A. (1989). The origin of metamorphic core complexes and detachment faults formed during Tertiary continental extension in the northern Colorado River region, U.S.A. *Journal of Structural Geology* **11**, 65–94.

Lister, G.S., Etheridge, M.A. & Symonds, P.A. (1986). Detachment faulting and the evolution of passive continental margins. *Geology* **14**, 246-250.

Lloyd, F.E., Arima, M. & Edgar, A.D. (1985). Partial melting of a metasomatized mantle assemblage; an experimental study bearing on the origin of highly potassic continental rift volcanics. *Contributions to Mineralogy and Petrology* **91**, 321-329.

Longerich, H.P., Jackson, S.E. & Günther, D. (1996). Laser ablation inductively coupled plasma mass spectrometric transient signal data acquisition and analyte concentration calculation. *Journal of Analytical Atomic Spectrometry* **11**, 899-904.

Ludwig, K.R. (2001). Isoplot/Ex version 2.49, Geochronological Toolkit for Microsoft Excel. *Berkeley Geochronology Center Special Publications* **1a**.

Luhr, J.F., Carmichael, I.S.E. & Varekamp, J.C. (1984). The 1982 eruptions of El Chichón volcano, Chiapas, Mexico: Mineralogy and petrology of the anhydrite-bearing pumices. *Journal of Volcanology and Geothermal Research* **23**, 69-108.

Lustrino, M. & Wilson, M. (2007). The circum-Mediterranean anorogenic Cenozoic igneous province. *Earth-Science Reviews* **81**, 1-65.

MacKenzie, J.M. & Canil, D. (2011). Fluid/melt partitioning of Re, Mo, W, Tl and Pb in the system haplobasalt-H2O-Cl and the volcanic degassing of trace metals. *Journal of Volcanology and Geothermal Research* **204**, 57-

65.

Marchev, P. (in press). $^{40}Ar/^{39}Ar$ and U-Pb geochronology of the Iran Tepe volcanic complex, Eastern Rhodopes. *Geologica Balkanica*, in press.

Marchev, P., Rogers, G., Conrey, R., Quick, J., Vaselli, O. & Raicheva, R. (1998a). Paleogene orogenic and alkaline basic magmas in the Rhodope zone: relationship, nature of magma sources, and role of crustal contamination. *Acta Vulcanologica* **10**, 217-232.

Marchev, P., Vaselli, O., Downes, H., Pinarelli, L., Ingram, G., Rogers, G. & Raicheva, R. (1998b). Petrology and geochemistry of alkaline basalts and lamprophyres: implications for the chemical composition of the upper mantle beneath the Eastern Rhodopes (Bulgaria). *Acta Vulcanologica* **10**, 233-242.

Marchev, P. & Singer, B. (2002). *40Ar/39Ar geochronology of magmatism and hydrothermal activity of the Madjarovo base-precious metal ore district, eastern Rhodopes, Bulgaria*. In: Blundell D., Neubauer F., von Quadt A. (Eds.). *The Timing and Location of Major Ore Deposits in an Evolving Orogen*. Geological Society of London Special Publications **204**, 137-150.

Marchev, P., Raicheva, R., Downes, H., Vaselli, O., Chiaradia, M. & Moritz, R. (2004). Compositional diversity of Eocene-Oligocene basaltic magmatism in the Eastern Rhodopes, SE Bulgaria: implications for genesis and tectonic setting. *Tectonophysics* **393**, 301-328.

Marchev, P., Kaiser-Rohrmeier, M., Heinrich, C.A., Ovtcharova, M., von Quadt, A. & Raicheva, R. (2005). Hydrothermal ore deposits related to post-orogenic extensional magmatism and core complex formation: the Rhodope massif of Bulgaria and Greece. *Ore Geology Reviews* 27, 53-89.

Marchev, P., Arai, S. & Vaselli, O. (2006). Cumulate xenoliths in Oligocene alkaline basaltic and lamprophyric dikes from the eastern Rhodopes, Bulgaria: Evidence for the existence of layered plutons under the metamorphic core complexes. *Geological Society of America Special Paper* **409**, 237-258.

Marchev, P., Georgiev, S., Zajacz, Z., Manetti, P., Raicheva, R., von Quadt, A. & Tommasini, S. (2009). High-K ankaramitic melt inclusions and lavas in the Upper Cretaceous Eastern Srednogorie continental arc, Bulgaria: Implications for the genesis of arc shoshonites. *Lithos* **113**, 228-245.

Massonne, H.J. (2001). First find of coesite in ultrahighpressure metamorphic region of the Central Erzegebirge,Germany. *European Journal of Mineralogy* **13**, 565–570.

Massonne, H.J. & Szpurka, Z. (1997). Thermodynamic properties of white mica on the basis of high-pressure experiments in the system K2O-MgO-Al2O3-SiO2-H2O and K2O-FeO-Al2O3-SiO2-H2O. *Lithos* **41**, 229-250.

McCulloch, M.T. & Gamble, J.A. (1991). Geochemical and geodynamical constraints on subduction zone magmatism. *Earth and Planetary Science Letters* **102**, 358-374.

McDade, P., Blundy, J.D. & Wood, B.J. (2003). Trace element partitioning on the Tinaquillo Lherzolite solidus at 1.5 Gpa. *Physics of the Earth and Planetary Interiors* **139**, 129-147.

McKenzie, D. (1978). Active tectonics of Alpine-Himalayan belt – Aegean Sea and surrounding regions. *Geophysical Journal of the Royal Astronomical Society* **55**, 217-254.

McKenzie, D. (1989). Some remarks on the movement of small melt fractions in the mantle. *Earth and Planetary Science Letters* **95**, 53-72.

Meen, J.K. (1987). Formation of shoshonites from calc-alkaline basalt magmas – Geochemical and experimental constraints from the type locality. *Contributions to Mineralogy and Petrology* **97**, 333-351.

Miller, D.M., Goldstein, S.L. & Langmuir, C.H. (1994). Cerium/lead and lead isotope ratios in arc magmas and the enrichment of lead in the continents. *Nature* **368**, 514-520.

Mitchell, R.H. (1995). Melting experiments on a sanidine phlogopite lamproites at 4-7 GPa and their bearing on the sources of lamproitic magmas. *Journal of Petrology* **36**, 1455-1474.

Mitchell, R.H. & Edgar, A.D. (2002). Melting experiments on SiO_2 – rich lamproites to 6.4 GPa and their bearing on the sources of lamproites magmas. *Mineralogy and Petrology* **74**, 115-128.

Moore, V.M. & Wiltschko, D.V. (2004). Syncollisional delamination and tectonic wedge development in convergent orogens. *Tectonics* **23**, TC2005.

Mposkos, E. & Krohe, A. (2000). *Petrological and structural evolution of continental high pressure (HP) metamorphic rocks in the Alpine Rhodope Domain (N. Greece)*. In: Panayides, I., Xenophontos, C. & Malpas, J. (Eds). *Proceedings of the 3rd International Conference on the Geology of the Eastern Mediterranean, Nicosia, Cyprus, 1999*. Geological Survey, Nicosia, Cyprus, 221-232.

Mposkos, E.D. & Kostopoulos, D.K. (2001). Diamond, former coesite and supersilicic garnet in metasedimentary rocks from the Greek Rhodope: a new ultrahigh-pressure metamorphic province established. *Earth and Planetary Science Letters* **192**, 497-506.

Münker, C. (2000). The isotope and trace element budget of the Cambrian Devil River Arc System, New Zealand: Identification of four source components. *Journal of Petrology* **41**, 759-788.

Münker C., Weyer S., Scherer E. & Mezger, K. (2001). Separation of high field strength elements (Nb, Ta, Zr, Hf) and Lu from rock samples for MC-ICPMS measurements. *Geochemistry Geophysics Geosystems* **2**: paper no. 10.1029/2001GC000183.

Münker, C., Pfänder, J.A., Weyer, S., Büchl, A., Kleine, T. & Mezger, K. (2003). Evolution of planetary cores and the Earth-Moon system from Nb/Ta systematics. *Science* **301**, 84-87.
Münker, C., Wörner, G., Yogodzinski, G. & Churikova, T. (2004). Behaviour of high field strength elements in subduction zones: constraints from Kamchatka-Aleutian arc lavas. *Earth and Planetary Science Letters* **224**, 275-293.

Münker, C. (2011). A high field strength element perspective on early lunar differentiation. *Geochimica et Cosmochimica* Acta **74**, 7340-7361.

Nagel, T.J., Schmidt, S., Janák, M., Froitzheim, N., Jahn-Awe, S. & Georgiev, N. (2011). The exposed base of a collapsing wedge – the Nestos Shear Zone (Rhodope Metamorphic Province, Greece). *Tectonics*. doi:10.1029/2010TC002815.

Nelson, K.D. (1992a). Are crustal thickness variations in old mountain belts like the Appalachians a consequence of lithospheric delamination? *Geology* **20**, 498-502.

Nelson, D.R. (1992b). Isotopic characteristics of potassic rocks: evidence for the involvement of subducted sediments in magma genesis. *Lithos* **28**, 403-420.

Newsom, H.E., Sims, K.W.W., Noll Jr., P.D., Jaeger, W.L., Maehr, S.A. & Beserra, T.B. (1996). The depletion of tungsten in the bulk silicate earth: Constraints on core formation. *Geochimica et Cosmochimica Acta* **60**, 1155-1169.

Nicholls, I.A. (1971). Petrology of Santorini volcano, Cyclades, Greece. *Journal of Petrology* **12**, 67–119.

Ninkovich, D. & Hays, J.D. (1972). Mediterranean island arcs and origin of high potash volcanoes. *Earth and Planetary Science Letters* **16**, 331-345.

Niu, Y., Waggoner, J.M., Sinton, J.M. & Mahoney, J.J. (1996). Mantle source heterogeneity and melting processes beneath seafloor spreading centers: the East Pacific Rise, 18° - 19°S. *Journal of Geophysical Research* **101**, 27711-27733.

Noll Jr., P.D., Newsom, H.E., Leeman, W.P. & Ryan, J.G. (1996). The role of hydrothermal fluids in the production of subduction zone magmas: Evidence from siderophile and chalcophile trace elements and boron. *Geochimica et Cosmochimica Acta* **60(4)**, 587-611.

Noronha, F., Doria, A., Dubessy, J. & Charoy, B. (1992). Characterization and timing of the different types of fluids present in the barren and ore-veins of the W-Sn deposit of Panasqueira, Central Portugal. *Mineralium Deposita* **27**, 72-79.

Nowell, G.M., Kempton, P.D., Noble, S.R., Fitton, J.G., Saunders, A.D., Mahoney, J.J. & Taylor, R.N. (1998). High precision Hf isotope measurements of MORB and OIB by thermal ionisation mass spectrometry: insights into the depleted mantle. *Chemical Geology* **149**, 211-233.

O'Neill, H.St.C. & Eggins, S.M. (2002). The effect of melt composition on trace element partitioning: an experimental investigation of the activity coefficients of FeO, NiO, CoO, MoO_2 and MoO_3 in silicate melts. *Chemical Geology* **186**, 151-181.

O'Neill, H.St.C. & Palme, H. (2008). Collisional erosion and the non-chondritic composition of the terrestrial planets. *Philosophical Transactions of the Royal Society A – Mathematical Physical and Engineering Sciences* **366**, 4205-4238.

O'Reilly, S.Y. & Griffin, W.L. (2000). Apatite in the mantle: implications for metasomatic processes and high heat production in Phanerozoic mantle. *Lithos* **53**, 217-232.

Ovtcharova, M., von Quadt, A.V., Cherneva, Z., Sarov, S., Heinrich, C. & Peytcheva, I. (2004). U-Pb dating of zircon and monazite from granitoids and migmatites in the core and eastern periphery of the Central Rhodopean Dome, Bulgaria. *Geochimica et Cosmochimica Acta* **68**, A664.

Palme, H. & Rammensee, W. (1981). Tungsten and some other siderophile elements in meteoritic and terrestrial basalts. *Lunar and Planetary Science* **XII**, 796-798.

Palme, H. & O'Neill, H.St. (2003). Cosmochemical estimates of mantle composition. In: Holland, H.D. & Turekian, K.K. (eds.). *Treatise on Geochemistry* **2**. Elsevier, pp. 1-38.

Papanikolaou, D. (2009). Timing of tectonic emplacement of the ophiolites and terrane paleogeography in the Hellenides. *Lithos* **108**, 262-280.

Patchett, P.J., White, W.M., Feldmann, H., Kielinczuk, S. & Hofmann, A.W. (1984). Hafnium/rare earth element fractionation in the sedimentary system and crustal recycling into the Earth's mantle. *Earth and Planetary Science Letters* **69**, 365-378.

Patiño Douce, A.E., Roden, M.F., Chaumba, J., Fleisher, C. & Yogodzinski, G. (2011). Compositional variability of terrestrial mantle apatites, thermodynamic modeling of apatite volatile contents, and the halogen and water budgets of planetary mantles. *Chemical Geology* **288**, 14-31.

Pearce, J.W. & Peate, D.W. (1995). Tectonic implications of the composition of volcanic arc magmas. *Annual Review of Earth and Planetary Sciences* **23**, 251–285.

Pearce J.A., Kempton P.D., Nowell G.M. & Noble, S.R. (1999). Hf-Nd element and isotope perspective on the nature and provenance of mantle and subduction components in Western Pacific arc-basin systems. *Jounal of Petrology* **40**, 1579-1611.

Pearce, N.J.G., Perkins, W.T., Westgate, J.A., Gorton, M.P., Jackson, S.E., Neal, C.R. & Chenery, S.P. (1997). A compilation of new and published major and trace element data for NIST SRM 610 and NIST SRM 612 glass reference materials. *Geostandard Newsletter* **21**, 115-144.

Pearce, J.A., Stern, R.J., Bloomer, S.H. & Fryer, P. (2005). Geochemical mapping of the Mariana arc-basin system: Implications for the nature and distribution of subduction components. Geochemistry Geophysics Geosystems 6, Q07006.

Pearson, D.G. & Nowell, G.M. (2002). The continental lithospheric mantle: characteristics and significance as a mantle reservoir. *Philosophical Transactions of the Royal Society of London* **360**, 2383-2410.

Peate, D.W., Pearce, J.A., Hawkesworth, C.J., Colley, H., Edwards, C.M.H. & Hirose, K. (1997). Geochemical variations in Vanuatu Arc Lavas: the Role of Subducted Material and a Variable Mantle Wedge Composition. *Journal of Petrology* **38**, 1331-1358.

Peccerillo, A. & Taylor, S.R. (1976). Geochemistry of Eocene calc-alkaline volcanic rocks from Kastamonu area, Northern Turkey. *Contributions to Mineralogy and Petrology* **58**, 63-81.

Pe-Piper, G. & Piper, D.J.W. (1992). Geochemical variation with time in the Cenozoic high-K volcanic rocks of the island of Lesbos, Greece: significance for shoshonite petrogenesis. *Journal of Volcanology and Geothermal Research* **53**, 371-387.

Pe-Piper, G. (1994). Lead isotopic compositions of Neogene volcanic rocks from the Aegean extensional area. *Chemical Geology* **118**, 27-41.

Pe-Piper, G. (1998). The nature of Triassic extension-related magmatism in Greece: evidence from Nd and Pb isotope geochemistry. *Geological Magazine* **135**, 331-348.

Pe-Piper, G. & Piper, D.J.W. (2001). Late Cenozoic, post-collisional Aegean igneous rocks: Nd, Pb and Sr isotopic constraints on petrogenetic and tectonic models. *Geological Magazine* **138(6)**, 653-668.

Pe-Piper, G. & Moulton, B. (2008). Magma evolution in the Pliocene-Pleistocene succession of Kos, South Aegean arc (Greece). *Lithos* **106**, 110-124.

Perraki, M., Proyer, A., Mposkos, E., Kaindl, R. & Hoinkes, G. (2006). Raman micro-spectroscopy on diamond, graphite and other carbon polymorphs from the ultrahigh-pressure metamorphic Kimi Complex of the Rhodope Metamorphic Province, NE Greece. *Earth and Planetary Science Letters* **241**, 672-685.

Peytcheva, I., von Quadt, A., Ovtcharova, M., Handler, R., Neubauer, F., Salnikova, E., Kostitsyn, Y., Sarov, S. & Kolcheva, K. (2004). Metagranitoids from the eastern part of the Central Rhodopean Dome (Bulgaria): U-Pb, Rb-Sr and $^{40}Ar/^{39}Ar$ timing of emplacement and exhumation and isotope-geochemical features. *Mineralogy and Petrology* **82**, 1-31.

Pfänder, J.A., Münker, C., Stracke, A. & Mezger, K. (2007). Nb/Ta and Zr/Hf in ocean island basalts – Implications for crust-mantle differentiation and the fate of Niobium. *Earth and Planetary Science Letters* **254**, 158-172.

Pfänder, J.A., Jung, S., Münker, C., Stracke, A. & Mezger, K. (2011). A possible high Nb/Ta reservoir in the continental lithospheric mantle and consequences on the global Nb budget – evidence from continental basalts from Germany. *Geochimica et Cosmochimica Acta*, doi: 10.1016/j.gca.2011.11.017.

Pin, C. & Zalduegui, J.F.S. (1997). Sequential separation of light rare-earth elements, thorium and uranium by miniaturized extraction chromatography: Application to isotopic analyses of silicate rocks. *Analytica Chimica Acta* **339**, 79-89.

Plank, T. & Langmuir, C.H. (1998). The chemical composition of subducting sediment and its consequences for the crust and mantle. *Chemical Geology* **145**, 325-394.
Plank, T. (2005). Constraints from thorium/lanthanum on sediment recycling at subduction zones and the evolution of the continents. *Journal of Petrology* **46**, 921-944.

Platt, J.P. & England, P.C. (1994). Convective removal of lithosphere beneath mountain belts – thermal and mechanical consequences. *American Journal of Science* **294**, 307-336.

Pleuger, J., Georgiev, N., Jahn-Awe, S., Froitzheim, N. & Valkanov, N. (2011). Kinematics of Palaeogene low-angle extensional faults and basin formation along the eastern border of the Central Rhodopes (Bulgaria). *Zeitschrift der deutschen Gesellschaft für Geowissenschaften* **162**, 171-192.

Polat, A., Hofmann, A.W., Münker, C., Regelous, M. & Appel, P.W.U. (2003). Contrasting geochemical patterns in the 3.7-3.8 Ga pillow basalt cores and rims, Isua greenstone belt, Southwest Greenland: Implications for postmagmatic alteration processes. *Geochimica et Cosmochimica Acta* **67**, 441-457.

Prelević, D., Foley, S.F., Romer, R.L., Cvetković, V. & Downes, H. (2005). Tertiary ultrapotassic volcanism in Serbia: Constraints on Petrogenesis and Mantle Source Characteristics. *Journal of Petrology* **46,** 1443-1487.

Prelević, D., Foley, S.F., Romer, R. & Conticelli, S. (2008). Mediterranean Tertiary lamproites derived from multiple source components in postcollisional geodynamics. *Geochimica et Cosmochimica Acta* **72**, 2125-2156.

Rehkämper, M. & Mezger, K. (2000). Investigation of matrix effects for Pb isotope ratio measurements by multiple collector ICP-MS: verification and application of optimized analytical protocols. *Journal of Analytical Atomic Spectrometry* **15**, 1451-1460.

Rempel, K.U., Williams-Jones, A.E. & Migdisov, A.A. (2009). The partitioning of molybdenum(VI) between aqueous liquid and vapour at temperatures up to 370 degrees C. *Geochimica et Cosmochimica Acta* **73**, 3381-3392.

Ricou, L.-E., Burg, J.-P., Godfriaux, I. & Ivanov, Z. (1998). Rhodope and Vardar: the metamorphic and the olistostromic paired belts related to the Cretaceous subduction under Europe. *Geodinamica Acta* **11**, 285-309.

Robertson, A.H.F. & Karamata, S. (1994). The role of subduction accretion processes in the tectonic evolution of the Mesozoic Tethys in Serbia. *Tectonophysics* **234**, 73-94.

Rosenbaum, J.M. (1993). Mantle phlogopite: a significant lead repository? *Chemical Geology* **106**, 475-483.

Rosenbaum, J.M., Wilson, M. & Downes, H. (1997). Multiple enrichment of the Carpathian-Pannonian mantle: Pb-Sr-Nd isotope and trace element constraints. *Journal of Geophysical Research* **102**, 14.947-14.961.

Rosenthal, A., Foley, S.F., Pearson, D.G., Nowell, G.M. & Tappe, S. (2009). Petrogenesis of strongly alkaline primitive volcanic rocks at the propagating tip of the western branch of the East African Rift. *Earth and Planetary Science Letters* **284**, 236-248.

Rouxel, O., Ludden, J. & Fouquet, Y. (2003). Antimony isotope variations in natural systems and implications for their use as geochemical tracers. *Chemical Geology* **200**, 25-40.

Rudnick, R.L., Barth, M., Horn, I. & McDonough, W.F. (2000). Rutile-bearing refractory eclogites: Missing link between continents and depleted mantle. *Science* **287**, 278-281.

Rudnick, R.L. & Gao, S. (2003). *The composition of the continental crust*. In: Holland, H.D. & Turekian, K.K. (eds) *Treatise on Geochemistry, vol. 3*. Elsevier, 1-64.

Scambelluri, M. & Philippot, P. (2001). Deep fluids in subduction zones. *Lithos* **55**, 213-227.

Scherer, E.E., Cameron, K.L., Johnson, C.M., Beard, B.L., Barovich, K.M. & Collerson, K.D. (1997). Lu-Hf geochronology applied to dating Cenozoic events affecting lower crustal xenoliths from Kilbourne Hole, New Mexico. *Chemical Geology* **142**, 63-78.

Scherer, E.E., Cameron, K.L. & Blichert-Toft, J. (2000). Lu-Hf garnet geochronology: Closure temperature relative to the Sm-Nd system and the effects of trace mineral inclusions. *Geochimica et Cosmochimica Acta* **64**, 3413-3432.

Scherer, E.E., Münker, C. & Mezger, K. (2001). Calibration of the Lutetium-Hafnium clock. *Science* **293**, 683-687.

Schmid, S.M., Pfiffner, O.A., Froitzheim, N., Schonborn, G. & Kissling, E. (1996). Geophysical-geological transect and tectonic evolution of the Swiss-Italian Alps. *Tectonics* **15**, 1036-1064.

Schmid, S.M., Fügenschuh, B., Kissling, E. & Schuster, R. (2004). Tectonic map and overall architecture of the Alpine orogen. *Eclogae geologicae Helvetiae* **97**, 93-117.

Schmidt, A., Weyer, S., John, T. & Brey, G.P. (2009). HFSE systematics of rutile-bearing eclogites: New insights into subduction zone processes and implications for the earth's HFSE budget. *Geochimica et Cosmochimica Acta* **73**, 455-468.

Schmidt, K.H., Bottazzi, P., Vannucci, R. & Mengel, K. (1999). Trace element partitioning between phlogopite, clinopyroxene and leucite lamproite melt. *Earth and Planetary Science Letters* **168**, 287-299.

Schmidt, S., Nagel, T.J. & Froitzheim, N. (2010). A new occurrence of microdiamond-bearing metamorphic rocks, SW Rhodopes, Greece. *European Journal of Mineralogy* **22**, 189-198.

Schuth, S., Rohrbach, A., Münker, C., Ballhaus, C., Garbe-Schönberg, D. & Qopoto, C. (2004). Geochemical constraints on the petrogenesis of arc picrites and basalts, New Georgia Group, Solomon Islands. *Contributions to Mineralogy and Petrology* **148**, 288-304.

Schuth, S., Münker, C., König, S., Qopoto, C., Basi, S., Garbe-Schönberg, D. & Ballhaus, C. (2009). Petrogenesis of Lavas along the Solomon Island arc, SW Pacific: Coupling of compositional variations and subduction zone geometry. *Journal of Petrology* **50**, 781-811.

Shannon, R. (1976). Revised effective ionic radii and systematic studies of interatomic distances in halides and chalcogenides. *Crystal Physics, Diffraction, Theoretical and General Crystallography* **32**, 751-767.

Shanov, S. (1998). Deep structures in the crust and the upper mantle beneath the Rhodopes from geophysical data. *Acta Vulcanologica* **10**, 347-352.

Siemes, A., McCann, T., Fischer, A. (2009). Paleogene alluvial – volcaniclastic deposits in the Mesta Basin (SW Bulgaria): depositional setting and basin evolution. *Geological Magazine* **147**, 321-338.

Singer, B. & Marchev, P. (2000). Temporal evolution of arc magmatism and hydrothermal activity, including epithermal gold veins, Borovitsa caldera, southern Bulgaria. *Economic Geology* **95**, 1155-1164.
Skora, S., Baumgartner, L.P., Mahlen, N.J., Johnson, C.M., Pilet, S. & Hellebrand, E. (2006). Diffusion-limited REE uptake by eclogite garnets and its consequences for Lu-Hf and Sm-Nd geochronology. *Contributions to Mineralogy and Petrology* **152**, 703-720.

Skora, S., Lapen, T.J., Baumgartner, L.P., Johnson, C.M., Hellebrand, E. & Mahlen, N.J. (2009). The duration of prograde garnet crystallization in the UHP eclogites at Lago di Cignana, Italy. *Earth and Planetary Science Letters* **287**, 402-411.

Skora, S. & Blundy, J. (2010). High-pressure hydrous phase relations of radiolarian clay and implications for the involvement of subducted sediment in arc magmatism. *Journal of Petrology* **51**, 2211-2243.

Smit, M.A., Scherer, E.E., Bröcker, M. & van Roermund, H.L.M. (2010). Timing of eclogite facies metamorphism in the southernmost Scandinavian Caledonides by Lu-Hf and Sm-Nd geochronology. *Contributions to Mineralogy and Petrology* **159**, 521-539.

Smith, D.C. (1984). Coesite in clinopyroxene in the Caledonides and its implications for geodynamics. *Nature* **310**, 641-644.

Sobolev, N.V. & Shatsky, V.S. (1990). Diamond inclusions in garnets from metamorphic rocks: a new environment for diamond formation. *Nature* **343**, 742–746.

Söderlund, U., Patchett, P.J., Vervoort, J.D. & Isachsen, C.E. (2004). The 176Lu decay constant determined by Lu-Hf and U-Pb isotope systematics of Precambrian mafic intrusions. *Earth and Planetary Science Letters* **219**, 311-324.

Sokoutis, D., Brun, J.-P., Van Den Driessche, J. & Pavlides, S. (1993), A major Oligo-Miocene detachment in southern Rhodope controlling north Aegean extension, *Journal of the Geological Society of London* **150**, 243 – 246.

Spandler, C., Hermann, J., Arculus, R. & Mavrogenes, J. (2003). Redistribution of trace elements during prograde metamorphism from lawsonite blueschist to eclogite facies; implications for deep subduction-zone processes. *Contributions to Mineralogy and Petrology* **146**, 205-222.

Spandler, C., Hermann, J., Arculus, R. & Mavrogenes, J. (2004). Geochemical heterogeneity and element mobility in deeply subducted oceanic crust; insights from high-pressure mafic rocks from New Caledonia. *Chemical Geology* **206**, 21-42.

Spandler, C., Mavrogenes, J. & Hermann, J. (2007). Experimental constraints on element mobility from subducted sediments using high-P synthetic fluid/melt inclusions. *Chemical Geology* **239**, 228-249.

Stampfli, G.M. & Borel, G.D. (2002). A plate tectonic model for the Paleozoic and Mesozoic constrained by dynamic plate boundaries and restored synthetic oceanic isochrons. *Earth and Planetary Science Letters* **196**, 17-33.

Stolz, A.J., Varne, R., Davies, G.R., Wheller, G.E. & Foden, J.D. (1990). Magma source components in an arc-continent collision zone: the Flores-Lembata sector, Sunda arc, Indonesia. *Contributions to Mineralogy and Petrology* **105**, 585-60.

Stolz, A.J., Jochum, K.P., Spettel, B. & Hofmann, A.W. (1996). Fluid- and melt-related enrichment in the subarc mantle: Evidence from Nb/Ta variations in island-arc basalts. *Geology* **24**, 587-590.

Sun, S.-s. & McDonough, W.F. (1989). *Chemical and isotopic systematics of oceanic basalts: implications for mantle composition and processes*. In Saunders A.D. & Norry M.J. (eds) *Magmatism in the Ocean Basins*. Geological Society Special Publications **42**, 313-345.

Sun, W.D., Binns, R.A., Fan, A.C., Kamenetsky, V.S., Wysoczanski, R., Wei, G.J., Hu, Y.H. & Arculus, R.J. (2007). Chlorine in submarine volcanic glasses from the eastern Manus basin. *Geochimica et Cosmochimica Acta* **71**, 1542-1552.

Tait, J.A., Bachtadse, V., Franke, W. & Soffel, H.C. (1997). Geodynamic evolution of the European Variscan fold belt: palaeomagnetic and geological constraints. *Geologische Rundschau* **86**, 585-596.

Tani, K., Dunkley, D.J., Kimura, J-I., Wysoczanski, R.J., Yamada, K. & Tatsumi, Y. (2010). Syncollisional rapid granitic magma formation in an arc-arc collision zone: Evidence from the Tanzawa plutonic complex, Japan. *Geology* **38**, 215-218.

Tatsumi, Y. (2000). Slab melting: its role in continental crust formation and mantle evolution. *Geophysical Research Letters* **27**, 3941–3944.

Taylor, S.R. & McLennan, S.M. (1995) The geochemical evolution of the continental crust. *Reviews of Geophysics* **33**, 241–265.

Teng, L.S. (1990). Geotectonic evolution of late Cenozoic arc-continent collision in Taiwan. *Tectonophysics* **183**, 57-76.

Thöni, M. (2002). Sm-Nd isotope systematics in garnet from different lithologies (Eastern Alps): age results, and an evaluation of potential problems for garnet Sm-Nd chronometry. *Chemical Geology* **185**, 255-281.

Tomaschek, F., Kennedy, A.K., Villa, I.M., Lagos, M. & Ballhaus, C. (2003). Zircons from Syros, Cyclades, Greece – Recrystallization and Mobilization of Zircon during High-Pressure Metamorphism. *Journal of Petrology* **44**, 1977-2002.

Tueckmantel, C., Schmidt, S., Neisen, M., Georgiev, N., Nagel, T.J. & Froitzheim, N. (2008). The Rila-Pastra Normal Fault and multi-stage extensional unroofing in the Rila Mountains (SW Bulgaria). *Swiss Journal of Geosciences* **101**, S295-S310.

Turner, S., Arnaud, N., Liu, J., Rogers, N., Hawkesworth, C., Harris, N., Kelley, S., van Calsteren, P. & Deng, W. (1996). Post-collision, Shoshonitic Volcanism on the Tibetan Plateau: Implications for Convective Thinning of the Lithosphere and the Source of Ocean Island Basalts. *Journal of Petrology* **37**, 45-71.

Turpaud, P. & Reischmann, T. (2010). Characterisation of igneous terranes by zircon dating: implications for UHP occurrences and suture identification in the Central Rhodope, northern Greece, *International Journal of Earth Sciences* **99**, 567-591.

Vaggelli, G., Pellegrini, M., Vougioukalakis, G., Innocenti, S. & Francalanci, L. (2009). Highly Sr radiogenic tholeiitic magmas in the latest inter-Plinian activity of Santorini volcano, Greece. *Journal of Geophysical Research* **114**, B06201.

Vance, D. & O'Nions, R.K. (1990). Isotopic chronometry of zoned garnets: growth kinetics and metamorphic histories. *Earth and Planetary Science Letters* **97**, 227-240.

van Hinsbergen, D.J.J., Hafkenscheid, E., Spakman, W., Meulenkamp, J.E. & Wortel, R. (2005). Nappe stacking resulting from subduction of oceanic and continental lithosphere below Greece. *Geology* **33**, 325-328.

van Hinsbergen, D.J.J., Dupont-Nivet, G., Nakov, R., Oud, K. & Panaiotu, C. (2008). No significant post-Eocene rotation of the Moesian Platform and Rhodope (Bulgaria): Implications for the kinematic evolution of the Carpathian and Aegean arcs. *Earth and Planetary Science Letters* **273**, 345-358.

van Orman, J.A., Grove, T.L., Shimizu, N. & Layne, G.D. (2002). Rare earth element diffusion in a natural pyrope single crystal at 2.8 GPa. *Contributions to Mineralogy and Petrology* **142**, 416-424.

Varne, R. (1985). Ancient subcontinental mantle: A source for K-rich orogenic volcanics. *Geology* **13**, 405-408.

Vervoort, J.D., Patchett, P.J., Blichert-Toft, J. & Albarède, F. (1999). Relationships between Lu-Hf and Sm-Nd isotopic systems in the global sedimentary system. *Earth and Planetary Science Letters* **168**, 79-99.

Vervoort, J.D., Plank, T. & Prytulak, J. (2011). The Hf-Nd isotopic composition of marine sediments. *Geochimica et Cosmochimica Acta* **75**, 5903-5926.

von Huene, R. & Scholl, D.W. (1991). Observations at convergent margins concerning sediment subduction, subduction erosion, and the growth of continental crust. *Reviews of Geophysics* **29**, 279-316.

von Quadt, A., Moritz, R., Peytcheva, I. & Heinrich, C.A. (2005). Geochronology and geodynamics of Late Cretaceous magmatism and Cu-Au minerlization in the Panagyurishte region of the Apuseni-Banat-Timok-Srednogorie belt, Bulgaria. *Ore Geology Reviews* **27**, 95-126.

Vroon, P.Z., van Bergen M.J., White, W.M. & Varekamp, J.P. (1993). Sr-Nd-Pb isotope systematics of the Banda Arc, Indonesia – combined subduction and assimilation of continental material. *Journal of Geophysical Research – Solid Earth* ***98***, 22349-22366.

Vroon, P.Z., van Bergen, M.J., Klaver, G.J. & White, W.M. (1995). Strontium, neodymium, and lead isotopic and trace-element signatures of the East Indonesian sediments – Provenance and implications for Banda Arc magma genesis. *Geochimica et Cosmochimica Acta* **59**, 2573-2598.

Wade, J. & Wood, B.J. (2001). The Earth's missing niobium may be in the core. *Nature* **409**, 75-78.

Wang, K.-L., Chung, S.-L., O'Reilly, S.Y., Sun, S.-S., Shinjo, R. & Chen, C.-H. (2004). Geochemical constraints for the genesis of post-collisional magmatism and the geodynamic evolution of the Northern Taiwan region. *Journal of Petrology* **45**, 975-1011.

Warwzenitz, N. & Mposkos, E. (1997). First evidence for Lower Cretaceous HP/HT-metamorphism in NE Greece. *European Journal of Mineralogy* **9**, 659-664.

Weldeab, S., Emeis, K.-C., Hemleben, C. & Siebel, W. (2002). Provenance of lithogenic surface sediments and pathways of riverine suspended matter in the Eastern Mediterranean Sea: evidence from $^{143}Nd/^{144}Nd$ and $^{87}Sr/^{86}Sr$ ratios. *Chemical Geology* **186**, 139-149.

Weyer, S., Münker, C., Rehkämper, M. & Mezger, K. (2002). Determination of ultra-low Nb, Ta, Zr and Hf concentrations and the chondritic Zr/Hf and Nb/Ta ratios by isotope dilution analyses with multiple collector ICP-MS. *Chemical Geology* **187**, 295-313.

Weyer, S., Münker, C. & Mezger, K. (2003). Nb/Ta, Zr/Hf and REE in the depleted mantle: implications for the differentiation history of the crust-mantle system. *Earth and Planetary Science Letters* **205**, 309-324.

White, W.M. & Dupré, B. (1986). Sediment subduction and magma genesis in the Lesser Antilles: Isotopic and trace element constraints. *Journal of Geophysical Research* **91**, 5927-5941.

Williams, H.M., Turner, S.P., Pearce, J.A., Kelley, S.P. & Harris, N.B.W. (2004). Nature of the source regions for post-collisional, potassic magmatism in Southern and Northern Tibet from geochemical variations and inverse trace element modelling. *Journal of Petrology* **45**, 555-607.

Wilson, J.T. (1966). Did the Atlantic close and then re-open? *Nature* **211**, 676-681.

Wilson, M. & Downes, H. (1992). Mafic alkaline magmatism associated with the European Cenozoic rift system. *Tectonophysics* **208**, 173-182.

Witt-Eickschen, G., Seck, H.A., Mezger, K., Eggins, S.M. & Altherr, R. (2003). Lithospheric mantle evolution beneath the Eifel (Germany): Constraints from Sr-Nd-Pb isotopes and trace element abundances in spinel peridotite and pyroxenite xenoliths. *Journal of Petrology* **44(6)**, 1077-1095.

Wood, S.A., Crerar, D.A. & Borcsik, M.P. (1987). Solubility of the assemblage pyrite-pyrrhotite-magnetite-sphalerite-galena-gold-stibnite-bismuthinite-argenite-molybdenite in H_2O-NaCl-CO_2 solutions from 200 to 350°C. *Economic Geology* **82**, 1864-1887.

Woodhead, J.D., Hergt, J.M., Davidson, J.P. & Eggins, S.M. (2001). Hafnium isotope evidence for 'conservative' element mobility during subduction zone processes. *Earth and Planetary Science Letters* **192**, 331– 346.

Wortel, M.J.R. & Spakman, W. (2000). Subduction and slab detachment in the Mediterranean-Carpathian region. *Science* **290**, 1910-1917.

Wyllie, P.J. & Sekine, T. (1982). The formation of mantle phlogopite in subduction zone hybridization. *Contributions to Mineralogy and Petrology* **79**, 375-380.

Xu, S., Okay, A.I., Ji, S., Sengor, A.M.C., Su, W., Liu, Y., & Jiang, L. (1992). Diamond from the Dabie Shan met-morphic rocks and its implication for tectonic setting. *Science* **256**, 80–82.

Yanev, Y., Innocenti, F., Manetti, P. & Serri, G. (1998). Upper Eocene-Oligocene collision-related volcanism in Eastern Rhodopes (Bulgaria) – Western Thrace (Greece): Petrogenetic affinity and geodynamic significance. *Acta Vulcanologica* **10**, 279 –291.

Yordanov, B., Sarov, S., Georgiev, S., Dobrev, G., Grozdev, V., Balkanska, E. & Moskovska, L. (2007). Geological map of Bulgaria 1:50000, Map sheet K-35-75-B Komuniga, with explanatory notes. *Geology and Geophysics Ltd*, Sofia.

Zack, T., Kronz, A., Foley, S.F. & Rivers, T. (2002). Trace element abundances in rutiles from eclogites and associated garnet mica schists. *Chemical Geology* **184**, 97-122.

Zack, T. & John, T. (2007). An evaluation of reactive fluid flow and trace element mobility in subducting slabs. *Chemical Geology* **239**, 199-246.

Zellmer, G., Turner, S. & Hawkesworth, C. (2000). Timescales of destructive plate margin magmatism: new insights from Santorini, Aegean volcanic arc. *Earth and Planetary Science Letters* **174**, 265-281.

Zhao, Z-F., Zheng, Y-F., Chen, R-X., Xia, Q-X. & Wu, W-B. (2007). Element mobility in mafic and felsic ultrahigh-pressure metamorphic rocks during continental collision. *Geochimica et Cosmochimica Acta* **71**, 5244-5266.

- Acknowledgments -

This dissertation was funded by the German National Science Foundation (DFG) grants BR 1909/8-1 and Mu 1490/9-2, which was highly appreciated.

I am particularly grateful to my supervisor, Prof. Carsten Münker, for providing me the opportunity of carrying out this dissertation. His steady support, scientifically and financially, during field and lab work, helped shaping this thesis from the very beginning.

Furthermore, I thank all people that contributed to this dissertation scientifically, above all the structural geology group of Prof. Nikolaus Froitzheim including Dr. Thorsten Nagel, Silke Jahn-Awe and Dr. Jan Pleuger as well as our Bulgarian cooperation partner Prof. Peter Marchev from the Bulgarian Academy of Sciences in Sofia.

I am thankful to the scientific and technical staff in both Bonn and Köln that keep the lab and the mass specs up and running, fix computers, prepare thin sections and XRF discs, and all the other little things that keep the institutes functioning.

I would also like to thank the Postdocs, PhD and diploma students in Bonn for discussions, lab assistance, barbecues and beer!

An meine Familie: die mich nicht nur während der letzten vier Jahre immer unterstützt hat, sondern während der letzten 30 Jahre und solange ich denken kann immer Inspiration und Ansporn waren!

- Erklärung -

Ich versichere, dass ich die von mir vorgelegte Dissertation selbständig angefertigt, die benutzten Quellen und Hilfsmittel vollständig angegeben und die Stellen der Arbeit – einschließlich Tabellen, Karten und Abbildungen, die anderen Werken im Wortlaut oder dem Sinn nach entnommen sind, in jedem Einzelfall als Entlehnung kenntlich gemacht habe; dass diese Dissertation noch keiner anderen Fakultät oder Universität zur Prüfung vorgelegen hat; dass sie – abgesehen von unten angegebenen Teilpublikationen – noch nicht veröffentlicht worden ist sowie, dass ich eine solche Veröffentlichung vor Abschluss des Promotionsverfahrens nicht vornehmen werde. Die Bestimmungen der Promotionsordnung sind mir bekannt. Die von mir vorgelegte Dissertation ist von Prof. Dr. Carsten Münker betreut worden.

---------- ----------

(Ort, Datum) (Maria Kirchenbaur)